TESTING AND MODELING OF SOIL - NAILED SLOPES

Thesis submitted in fulfillment of the requirements for the Degree of

DOCTOR OF PHILOSOPHY

By

SAURABH RAWAT

Department of Civil Engineering

JAYPEE UNIVERSITY OF INFORMATION TECHNOLOGY
WAKNAGHAT, DISTRICT SOLAN, H.P., INDIA

December, 2017

TABLE OF CONTENTS

CHAPTER 2

CHAPTER 3

DECLARATION BY THE SCHOLAR

I hereby declare that the work reported in the Ph.D. thesis entitled **"Testing and Modeling of Soil – Nailed Slopes"** submitted at **Jaypee University of Information Technology, Waknaghat, Himachal Pradesh, India,** is an authentic record of my work carried out under the supervision of **Prof. Ashok Kumar Gupta.** I have not submitted this work elsewhere for any degree or diploma. I am fully responsible for the contents of my Ph.D. Thesis.

(Saurabh Rawat)
Department of Civil Engineering
Jaypee University of Information Technology, Waknaghat, India
Date:

SUPERVISOR'S CERTIFICATE

This is to certify that the work reported in the Ph.D. thesis entitled **"Testing and Modeling of Soil – Nailed Slopes"** submitted by **Saurabh Rawat** at **Jaypee University of Information Technology, Waknaghat, Himachal Pradesh, India,** is a bonafide record of his/her original work carried out under my supervision. This work has not been submitted elsewhere for any other degree or diploma.

(Prof. Ashok Kumar Gupta)
Head of Department
Department of Civil Engineering
Jaypee University of Information Technology, Waknaghat, India
Date:

Dedicated to my mother USHA RAWAT

and

my father Late Mr. B. L. RAWAT

ACKNOWLEDGEMENT

I would like to express my immense sense of gratitude to my supervisor **Prof. Ashok Kumar Gupta,** Head of Department, Department of Civil Engineering, Jaypee University of Information Technology, Waknaghat, Himachal Pradesh, India, for providing me his enlightened guidance, valuable suggestions, encouragement, inspiration and unflinching support throughout the duration of this work. His timely help, constructive criticism and painstaking efforts made it possible for me to present the work embodied in this thesis in its present form.

I am extremely grateful to all DPMC members and faculty of Department of Civil Engineering, Jaypee University of Information Technology, Waknaghat, India for their assistance from time to time.

I would like to express my deep sense of gratitude and reverence to my mother Mrs. Usha Rawat, sisters Shilpi and Shivani for their kind blessings and always being a constant source of inspiration. A special thanks to my father Late. Mr. B. L. Rawat for his blessings and unsaid support which gave me confidence, whenever I was down and low.

Last but not the least, I would like to express my sincere thanks to all my friends for their endeavour to keep my moral high throughout the period of my work and all those who helped me directly or indirectly at various stages of this research work.

(Saurabh Rawat)

ABSTRACT

Soil nailing is a technique to facilitate the stabilization of an existing or a newly constructed excavation/slope. With the development in field of infrastructure, transportation and other man – made structures, available land has become scarce. Hence, the urge of utilizing weak and unstable ground is inevitable. Accordingly, numerous methods have been developed in the past with soil nailing being one such solution to counter this problem.

The present research work is an investigation in understanding soil nailing mechanism in slopes with different types of soil nails against the conventional soil nails that have been used in the past. To achieve that three different types of soil nail have been fabricated namely smooth soil nail, screw soil nail and helical soil nail. To comprehend the response of slopes towards reinforcement due to soil nails, 36 small - scale laboratory testing of soil – nailed slopes has been conducted. The soil slopes are constructed at three different slope angles of 45°, 60° and vertical cut of 90° with horizontal. Each type of 6 soil nails are used to reinforce the soil slope at four different nail inclinations of 0°, 15°, 20° and 30° with horizontal. Thus, effect of slope angle and nail inclination on soil nailing mechanism is studied. The optimum inclination of soil nail to corresponding slope is angle determined. The variation in soil nailing mechanism with change in nail type from conventional smooth nail to screw nail and similarly to helical nail is also examined. This enable to assess the behavior of soil slopes to change in nail geometry and nail installation method. A gradual increasing surcharge load is also applied at slope crest to study load – deformation of soil - nailed slopes in comparison to unreinforced soil slopes for all slope angles.

The failure mechanism, failure surface and nail forces generated along nail length during slope failure are also determined from model testing. To validate the model testing, numerical modeling has been carried out using Limit Equilibrium Method and Finite Element method. The Limit Equilibrium Analysis has been done using subroutine Slope/W and Finite Element Analysis is carried out by Plaxis 2D code. The numerical modeling with both these methods has been done for all slope angle of 45°, 60° and 90° with nail inclinations of 0°, 15°, 20° and 30° for smooth, screw and helical nails. The factor of safety, slope deformation with surcharge loading, soil – nailed slope failure mechanism, failure slip surfaces and nail forces along nail length are predicted. A comparative study is also carried out between results obtained from model testing and numerical modeling of soil – nailed slopes. The pullout behavior of helical soil nail has also been investigated through two - dimensional and three – dimensional finite element analysis. Plaxis 2D has been used for two - dimensional analysis and Abaqus/Explicit is used for three – dimensional analysis. The pullout mechanism of helical soil nail has been optimized by studying variations of non - dimensional factors with different combination helical plate spacing, helical plate diameter, embedment ratios, anchorage length ratios and number of helical plates. The validation of results of model testing, numerical modeling of soil – nailed slopes and helical nail pullout behavior is also done by published results from literature.

The model testing results have revealed an increase in load carrying capacity of reinforced slopes as compared to unreinforced slopes. The maximum load carrying capacity is obtained for slope angle of 45° with nail inclination of 15°. However, nail inclined at 0° is found to give best results for 90° vertical cut. It is found that load carrying capacity of slopes is not increased beyond nail inclinations of 15°. It is also depicted that helical nails provide the best reinforcement followed by screw nails and then smooth nails. The slope crest is observed to undergo settlement with outward horizontal slope movement under gradual increasing surcharge load. The failure slip surface as given by model testing accounts for a circular slip surface for 45° and 60° slope and complex unpredictable slip surface for 90° vertical cut. However, for 90° slope, the slip surface is characterized by overturning of slope about its toe for all nail inclinations. The nail forces are found maximum at intermediate nail length and approaching zero at nail end. These observations are similar for all different types of soil nails used.

Results from numerical modeling further validate the results of model testing with maximum factor of safety greater than 2 obtained for helical nails. The predicted slip surfaces, slope deformations and nail forces are similar to model testing with slight variations. The numerical modeling of pullout of helical nail presents that failure mechanism can be well predicted by both two dimensional and three – dimensional finite element analysis. However, variation in magnitude is observed in pullout capacity from both analyses. There lies a critical relative helical plate spacing, diameter and number of plates beyond which failure mechanism shows transition between deep global to shallow local failure.

Keywords: soil nails, model testing, limit equilibrium method, finite element method, pullout behavior

LIST OF ACRONYMS AND ABBREVIATIONS

CD	Consolidated drained
CDG	Completely decomposed granite
CH	Highly compressible inorganic clay
CIP	Cast – in - place
CR	Covering ratio
FEA	Finite Element Analysis
FEM	Finite Element Method
FHWA	Federal Highway Administration
FRP	Fibre Reinforced Plastic
GF	Gauge Factor
IRC	Indian Road Congress
LEA	Limit Equilibrium Analysis
LEM	Limit Equilibrium Method
LVDT	Linear Variable Differential Transformer
MSE	Mechanically Stabilized Earth
NAT	New Austrian Tunnelling
PIV	Particle Image Velocimetry
PMMA	Polymethyl Methacrylate
SFRS	Steel Fibre Reinforced Shotcrete
SKW	Sand, Kaolin and Water
SRM	Strength Reduction Method
UTM	Universal Testing Machine
WMM	Welded-Wire Mesh

LIST OF SYMBOLS

γ	Unit weight
ϕ	Angle of internal friction
D_{50}	Mean diameter of soil
H	Maximum height of structure in project
T_{ij}	Tensile resistance
T_{tj1}	Maximum tensile resistance force applied to the reinforced material by a moving soil mass
T_{tj2}	Maximum tensile resistance force applied to the reinforced material from an unmoved natural ground
T_{ta}	Allowable tensile force of each individual reinforced material
T_{sj}	shear resistance
T_{sj1}	Maximum lateral resistance force applied to reinforced material by a moving soil mass
T_{sj2}	Maximum lateral resistance force applied to reinforced material from an unmoved soil mass
T_{sa}	Allowable shear resistance force of individual reinforced material composed of steel bar and grouting mortar
G	Specific gravity
D_{10}	Effective size of soil
C_u	Coefficient of uniformity
C_c	Coefficient of curvature
$\gamma_{d(max)}$	Maximum dry unit weight of soil
$\gamma_{d(min)}$	Minimum dry unit weight of soil
$\gamma_{(max)}$	Maximum unit weight of soil
$\gamma_{(min)}$	Minimum unit weight of soil
c	Cohesion of soil
R_D	Relative density of soil
e_{max}	Maximum void ratio
e_{min}	Minimum void ratio

w_L	Liquid limit of soil
w_P	Plastic limit of soil
OMC	Optimum moisture content of soil
$\phi_{(Peak)}$	Peak angle of internal friction of soil
$\phi_{(Critical)}$	Critical angle of internal friction of soil
ε_1	Maximum principle strain (compressive)
ε_3	Minimum principle strain (tensile)
α	Inclination of loading
d	Vertical spacing of reinforcement strips
B	Width of footing
Q	Surcharge
T_{max}	Maximum tension resistance
S_v	Vertical spacing of nails
S_h	Horizontal spacing of nails
K	Equivalent earth pressure
K_0	Earth pressure at – rest condition
R_t	Non – dimensional parameter
N_{head}	Nail head
X_{max}	Distance from facing
D_{nail}	Nail diameter
D_{grout}	Grout hole diameter
$\beta°$	Wall face inclination with horizontal
$i°$	Nail inclination with horizontal
L	Maximum nail length in project
δ_{max}	Maximum lateral wall displacement
f^*	Apparent friction coefficient
F_p	Pullout force
p	Nail perimeter
σ_v	Normal stress
P_R	Limiting nail force
A_s	Plan area of sand
A_r	Total surface area of nail
θ	Angle of nail from vertical

ϕ_{ps}	Plain strain friction angle of sand
τ_{EXT}	Extra shearing resistance due to nail
$\theta_{m\theta}$	Average normal stress on nail at an angle θ
k_{20}	Coefficient of permeability at 20°c
μ^*	Apparent friction coefficient
τ_s	Interface shear strength
$\Delta\sigma'_n$	Change in effective normal stress
τ	Shear stress
υ	Poisson's ratio
ψ	Dilatancy of soil
D_r	Relative density of soil
σ_3	Confining pressure
P_a	Reference atmospheric pressure
D_0	External diameter
D_{in}	Internal diameter
T_d	Thread depth
S_p	Screw pitch of the nail
R	Roughness factor
σ_h	Horizontal stress on the nail
σ_m	Mean normal stress
τ_{max}	Maximum shear stress
a^*	Apparent interface parameters for interface adhesion
δ^*	Apparent interface parameters for interface friction angle
f_δ	Apparent friction
f_a	Interface adhesion
c'_a	Soil adhesion
q_s	Pullout resistance
C^*	Damping coefficient
F_r	'Net' rapid soil response
F_s	Quasi – static pullout load
v	Pullout velocity
$\bar{\tau}$	Soil – nail interface shear resistance
c'_G	Interception value of the initial vertical stress (overburden)

μ'_G	Slope of fitting line
p_G	Grouting pressure
E_n	Modulus of elasticity of nail
A_n	Cross – sectional area of nail
I_0, I_1	Interaction factors
μ	Coefficient of interface friction in 3d
σ_{av}	Average overburden pressure at nail height
P_{3D}	Pullout capacity of soil – nail interface under uniform normal pressure
M_{3D}	Mobilization factor of 3d nail forces at soil – nail interface corresponding to pullout capacity
M_{2D}	Mobilization factor of 2d plate for nail forces at soil – nail interface corresponding to pullout capacity
μ_R	Reduced coefficient of friction
A_f	Contact surface area factor
K_T	Torque correlation factor
q_u	Terzaghi or Meyerhof bearing capacity
A_n	Area of n^{th} helical plate
V_{in}	Input voltage
V_{out}	Measured output voltage
$R1, R2, R3$	Arms of wheatstone bridge
Rg	Resistance from strain gauge attached on respective nail
ε	Nail strain
ΔR	Change in resistance
R	Initial resistance of foil strain gauge
E_{sn}	Modulus of elasticity of screw nail
υ_{sn}	Poisson's ratio of screw nail
f	Coefficient of friction from direct shear test
u	Pore water pressure
W, P and N	Slice weight, concentrated point load and slice base normal force
α	Slice base inclination with horizontal
β, f, d, ω	Geometric parameters
X	Inter-slice shear force
E	Inter-slice normal force

$f(x)$	Inter-slice function (half – sine function default slope/w)
λ	Percentage of function used
γ_{bulk}	Bulk unit weight of soil
S_m	Mobilized shear
S_{soil}	Shear resistance of soil
$S_{reinforcement}$	Shear resistance of reinforcement
z	Depth of nail from ground
T_a	Tensile capacity for screw nails
V	Shear force for screw nails
A_c	Cross – sectional area of screw nails
f_y	Yield strength of screw nails
RF	Reduction factor
A_b	Cross – sectional area of bolt
F_v	Ultimate shear stress of steel
M_{sf}	Incremental multiplier in PLAXIS 2D
E_{eq}	Equivalent modulus of elasticity
Eg	Elastic modulus of grout
EA	Equivalent axial stiffness
d_{eq}	Equivalent plate diameter of the nail
EI	Equivalent bending stiffness
I	Moment of inertia of circular nails
R_{inter}	Interface strength reduction factor in PLAXIS 2D
t_f	Interface of virtual thickness factor
D_s	Diameter of the nail shaft
s	Spacing of helical plates
D_h	Helical plate diameter
H	Depth of embedment of top helical plate
E_{50}^{ref}	Reference stiffness modulus corresponding to reference confining pressure $p^{ref} = 100$ kN/m^2
E_{oed}^{ref}	Oedometer loading modulus
E_{ur}^{ref}	Elastic unloading modulus
$\sum -M_{weight}$	M_{weight} is the soil weight

$\sum M_{load}$	Load incremental factor in PLAXIS 2D
Q_0	Characteristic pullout load
1-H	Helical nail with single helical plate
2-H	Helical nail with double helical plates
3-H	Helical nail with multi-helical plates
D_c	Circular discs diameter
N	Number of circular discs
q	Mobilized shear stress acting at the perimeter of nail – soil interface
N_{qi}	Bearing capacity factor at disc i
A_i	Area of circular disc i

LIST OF FIGURES

LIST OF TABLES

CHAPTER 1
INTRODUCTION

1.1 General

Large scale construction work such as housing projects, extensive expansion of road networks and other man - made activities such as deforestation have resulted in disturbing the fragile eco – system. This exploitation of natural ground conditions renders instability and leads to hazards such as landslides. An unstable slope always creates difficulties not only in development of that area but also poses threat to human life. For example, creating an uninterrupted communication between far off areas requires the expansion of roads, which in turn depends on the excavation and construction through weak and unstable grounds. Similarly, ever increasing population has created scarcity of land. Since infrastructural development signifies the development of nation, construction of buildings never ceases to grow. To meet this never ending demand for buildings and road networks, stabilization of unstable ground conditions serves as the best suited remedial measure. Development of hilly and remote areas, construction of dams and hydropower projects on difficult terrains, utilization of weak ground conditions and even increasing defense of the country all require stabilization of unstable ground conditions in some way or the other. Many stabilization techniques have been developed in the past to combat these situations. Ground stabilization techniques like mechanical and chemical ground stabilization, grouting, earth retaining structures, anchors and soil nailing have all proved beneficial in providing structural and serviceable stability. This chapter provides the details of one such ground improvement technique for unstable slopes called as soil nailing. The chapter also outlines the organization of the thesis.

1.2 Soil Nailing

Soil is a heterogeneous material which is strong in compression but weak in tension. The overall strength of soil can therefore be enhanced by using a material having significant tensile strength such as steel. The term ‘soil nailing’ as developed by Jewel [1] thus derives its fundamental concept of reinforcement of existing ground conditions (natural slopes/cuts) by inserting closely spaced passive inclusions called as ‘nails’ directly into ground or through drilling and grouting to increase the in – situ soil shear strength and provide stability. The term ‘passive’ is mainly used to distinguish soil anchors from soil nails. Soil anchors are pre

– tensioned before installation whereas no pre-tensioning is done for soil nails prior to installation. However, as the ground deforms laterally, tension is developed in soil nails. Soil nailing technique is used to provide reinforcement to both in – situ natural and steep cut slopes. In case, support is required for an unstable existing ground with buildings in the vicinity that are sensitive to deformation, method of soil nailing is used to provide stability by temporary constructions or permanent retaining structures with appropriate measures to reduce ground movements.

1.3 Evolution of Soil Nailing Technique

Soil nailing evolved as an efficient technique in the form of a rock bolting system of underground excavation referred to as the New Austrian Tunneling (NAT) Method in 1960 [2], which incorporated a combination of shotcrete and fully bonded steel inclusions to render efficient excavation stability. After the inception of soil nailing in hard rock stratum, its use was extended in less competent materials like silt, gravels and sands with application in metro tunnels in Frankfurt in 1970 and in construction of a double tube of a subway station in Nuremberg. Based on the experiences and observations from NAT, idea of in – situ reinforced soil was adopted by Germany in 1975 by researchers like Stocker et al. [3], Gassler and Gudehus [4]. Germany initiated research to develop the new technique for slope stabilization and excavation cuts under a project called 'Boden – Vernagelung' with 'Boden' meaning soil and 'Vernagelung' meaning nailing. Thus, the technical term soil nailing was coined. In France, the first recorded application of soil nailing was carried out by French contractor Bouygues for railway widening scheme near Versailles. With the successful onset of Versailles contract, many fundamental research and development programmes were carried out in France by Plumelle [5] and many others which lead to the national project known as 'Programme Clouterre' in 1986 [6]. The project title was derived from 'Clou' meaning nail and 'Terre' meaning soil. Meanwhile, independent development of the new technique of soil nailing began in North America [7], USA under the name of 'lateral earth support system' [8, 9], United Kingdom [10], Brazil [11], Japan [12], Australia [13] and Hong Kong [14]. In India, soil nailing technique is also rapidly increasing with Indian Institute of Science, Bangalore and Indian Road Congress (IRC) working together to form its design guidelines [15] wherein till date guidelines given by FHWA is adopted.

1.4 Components of a Soil – Nail System

Soil nail: A composite structure comprising of a tendon, grout and corrosion protection put together forms a typical soil nail. The tendon is generally a steel bar or can be any other element having significant resistance against tensile stresses. An ideal tendon is one which is able to resist both shear stresses and bending moments in addition to tensile stresses also. Soil movement can occur as natural slopes tend to fail under surcharge load, man – made cut deforms during excavation or time – dependent deformation in the absence of external load. With the deformation of ground, tensile stresses are mobilized in the tendon. These tendons can be hollow or solid bars depending upon the in – situ soil conditions available. If the in – situ conditions are stable for drill hole and grouting, solid bars are preferred, whereas for unstable soil conditions which are unable to withstand drilling hollow bars are used as drilling and grouting can be carried out simultaneously. The recent development in field of soil nailing has also led to use of innovative tendon known as fiber reinforced plastic (FRP) soil nails obtained by combining glass fiber with different types of resins [16]. Tendons have also been made up of renewable resource like Moso bamboo, which have high tensile strength for short period but is cost effective [17].

Once the tendons are placed in drill hole aligned through the centralizers which ensures the bar is centered in the grout column [18], grouting using tremie method is carried out under gravity. The centralizers are provided for necessary separation between tendon and surrounding soil and thus help achieve effective penetration of grout. The grout usually consists of a mixture of Portland cement and water. Grouting is usually done to increase the soil – tendon (nail) bond and to enhance the corrosion protection. By increasing the soil – nail interaction, grouting leads to proper transfer of shear stresses between the deforming ground and the tendons. Moreover, it also transfers tensile stresses from the tendons to surrounding stable soil. However, the latest development in field of soil nail tendons is the use of soil nail with the advantage of no drilling and grouting of tendon and still deriving considerable interaction between surrounding soil and nail. This is achieved by using screw type steel tendons with equal spaced helical plates attached along tendon length. Such nail tendons are installed by applying torque.

The tendons are exposed to corrosion depending on the corrosion potential of surrounding soil. The tendons are thus required to be made corrosion protected for increasing its serviceability. As mentioned earlier, grouting serves as the lowest level of corrosion protection. In order to use soil nails in permanent applications more suitable and subtle protection against corrosion is attained by encapsulating the tendon in a corrugated outer sheath of PVC with an inner cement annulus [19, 20]. Other methods of corrosion protection of soil nail tendons include cathodic protection method, epoxy coating, galvanization and sacrificial steel method.

The composite form of grouted, corrosion protected tendon is highly dependent on the in – situ conditions. The residing soil condition in turn governs the installation process for these soil nails. Hence based on different installation techniques, soil nails can be divided into the following types:

Grouted soil nails are solid bar nails with smooth or threaded surface. Low pressure grouting or grouting under gravity is carried out in a pre – drilled hole having diameter ranging from 100 mm to 150 mm. Based on the available ground conditions, drilling of holes can be carried out through down–the–hole hammer, rotary and rotary percussive drilling techniques. The diameter of a typical steel tendon used as soil nail is between 15 mm to 46 mm. The space between steel tendon and drill hole is chosen so as to accommodate a grout cover of 30 mm to 80 mm around soil nail. Centralizers are placed at intervals of 1.5 – 2.0 m along the nail to ensure uniform grout cover. Grouting of soil nail increases the surface area of nail and renders it significant roughness. Thus, an enhanced soil - nail interaction and consequently, significant bond strength is achieved for grouted soil nails. In addition to this increased pullout resistance, grouting also provides corrosion protection to soil nail. A spacing of 1 m to 3 m in vertical and horizontal direction is adopted depending on the type of in - situ soil such that one grouted nail per 4 m^2 is achieved.

Self – drilling soil nails consists of hollow bars which are installed using drilling and grouting technique as a single operation. The hollow tendon which serves both as drill rod and grout pipe is directly drilled into the ground using a sacrificial drill bit. This makes installation process rapid, with drilling and grouting being carried out simultaneously. Instead of using air or water, cement grout is used as the flushing medium. The added benefit of using cement grout is maintaining the drill hole stability. As the grout comes out of drill bit, it leads to grouting of annular space between the tendon and drill hole. With the permeation of grout into surrounding soil, bond strength between soil and tendon is increased, thereby enhancing the capacity of soil nail. This grouting method also provides a better corrosion resistance to tendons. Moreover, without use of casing and centralizers, self drilling soil nails can easily be installed in loose granular soils [21]. In addition to above advantages, self drilling soil nails are more cost effective and less time consuming during construction as compared to conventional grouted soil nails.

Jet-grouted soil nails are nails that differ from grouted nails and self drilling nails based on grouting pressure and installation technique. Jet-grouting technique employs percussion driving with high pressure grouting jets greater than 20MPa for creating drill holes in the slope surface [22]. The high grouting pressure causes hydraulic fracturing and re-compaction of the surrounding soil. This increases the soil – nail interface strength and thus enhances pullout resistance of soil nail. This composite inclusion made of a grouted soil with a central steel rod can be as thick as 30 to 40 cm. Similar to self drilling nails, pre-drilling and high pressure grouting is carried out simultaneously.

Driven nails are composed of ordinary steel bars or angle bars having a nominal diameter of 20 mm to 50 mm [23]. The length of tendons to be used as driven nails is limited to a maximum of 20 m with smaller contact area of 2 to 4 bars per m^2. The tendons used as driven nails are required to have perfectly ductile properties rather than brittle [24] to avoid brittle failure of soil nail. The driving mechanism for tendons is achieved by methods such as percussive method using hammering equipment or by vibratory method using a vibrator which require no pre - drilling. With the advantage of rapid installation, driven nails are the only viable alternative for retaining collapsible soils. If the steel bars are forced into soil by ballistic method using a compressed air launcher, then they are termed as launched nails [25]. The advantage of these nails also lies in their rapid installation which can be completed within 4 to 6 per hour and also causes fewer disturbances to surrounding soil. However, driven or launched nails are difficult to install with soil containing boulders and driving action mobilizes low soil – nail interface friction.

Screw soil nails are made up of high strength steel alloy because of large stresses associated with the high torque applied during installation. The tendon consists of 38 mm solid square or circular shafts with welded steel bearing plates or helices at regular intervals. The spacing of the bearing plates depends on the bearing plate diameter and is generally adopted as 3.6 times the plate diameter. The spacing of bearing plates also ensures that each plate is contributing individually in bearing without overlapping the influence zone of adjacent plates. The helical shape of bearing plate promotes easy soil cutting during installation without the necessity of prior drilling and later grouting. Hence Screw soil nails can be easily be screwed into the soil and develop soil – nail bond through plate bearing of helices against the soil and shaft friction [26].

Facing: Facing of a soil – nailed system serves the purpose of providing local stability between soil and soil nail. It also provides an additional resistance to outward deformation of a soil – nailed system. Moreover, facing enables surface erosion, weathering effect and moisture loss from the face of the soil – nail system. In order to improve the aesthetic appearance of the nailed structure, facing is an obvious aid. The thickness of facing varies between 150 mm to 200 mm with thinner facing being employed for inclined slopes and thicker facing is generally adopted for vertical permanent cuts. The facing component of soil - nailed structure consists of an initial and final component. The initial component comprises of welded – wire mesh (WWM) which is fixed against the entire excavation face using appropriate lap splices. To provide bending resistance in horizontal and vertical directions, horizontal (waler bars) and vertical bars are also provide around the nail head. With this reinforcement intact, shotcreting is carried out to complete the initial facing.

Shotcrete methods used for soil nail facing can be of two types: dry mix and wet mix. In dry mix method water is added at the nozzle of shotcrete gun which is fed with a blend of dry aggregates and cement. If a mixture of aggregate, cement and water is conveyed to the nozzle after mixing them in a batch plant, it is termed as wet shotcrete method. In order to attain high strength with significant durability and correspondingly low permeability, the water/cement of less than 0.45 is desirable. Wet shotcrete method is usually preferred over dry mix method owing to its higher rate of production of fresh shotcrete which lies between 1.68 m^3/hour to 3 m^3/hour and high tendency of sticking without significant loss due to rebound.

The final facing generally consists of cast – in – place (CIP) reinforced concrete, reinforced shotcrete or precast concrete panels. Recently, steel fiber reinforced shotcrete (SFRS) is also utilized instead of mesh reinforcement. The SFRS consists of high tensile strength steel elements with hooked ends having a diameter of 0.5 mm with length of 30 mm to 50 mm. Theses steel fibres are mixed in concrete as an aggregate having unit weight ranging between 350 to 600 N/m^3 and used with dry or wet sprayed concrete mix [11]. Headed studs welded to the bearing plates are used to connect the final facing to the soil nails. The total thickness of a reinforced shotcrete final facing is often between 150 and 300 mm, excluding the thickness of the initial facing. The thickness of the final facing is created by applying successive layers of shotcrete in bottom - up manner as opposed to initial facing which is carried out in top – down method. Waler bars are not required for final facing constructed by reinforced shotcrete.

Drainage: To satisfy the serviceability of a soil – nailed system, it is necessary to provide a drainage system behind initial facing or adjacent excavation face. The drainage system helps in regulating the pore water pressure developed behind a soil – nail system. It also serves the purpose of protecting the facing from deterioration due to adverse affect of water when in contact and sustaining the bond between soil and nail which can be damaged severely due to generation of excessive hydrostatic pressure. Thus, a proper drainage system helps in maintaining the structural performance and stability of soil – nail system during and after excavation. Bruce and Jewel [27] suggests the use of shallow and deep to reduce water accumulation and prevent wall saturation. Collector drains provided at top and bottom of soil – nailed wall or slope for regulating drainage was also given by Raju [28]. However, now – a –days the drainage system mainly consists of vertical strip drains. In cases of large volumes of groundwater behind soil – nail structure, horizontal pipe drains are also used. The strip drains are composed of drainage core manufactured from synthetic polymer which wrapped around by a geotextile to accompany filtration. A typical cross – section of a soil nail with all its components is shown in Fig. 1.1.

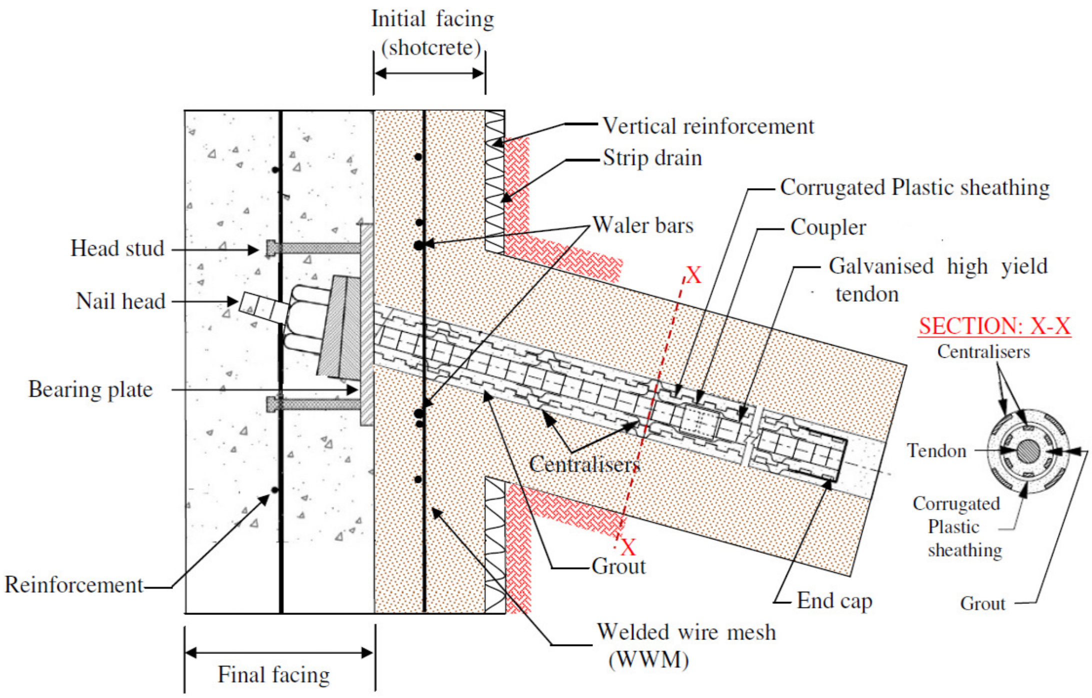

Fig. 1.1: Typical cross – section of a complete soil nail

1.5 Construction Procedure of a Soil – Nail System

As shown in Fig 1.2, the procedure adopted to carry out soil nailing can be divided into the following steps:

Step 1 – Excavation: The reinforcement of in – situ soil by soil nails is carried out by excavation in top – down sequence. To install the first row of nails, an initial excavation lift is made with an excavator having a depth of 0.9 m to 1.5 m. The depth of initial excavation depends on the prevailing in – situ ground conditions. Since the unsupported cut has to withstand a period of 1 to 2 days for complete nail installation, feasibility of depth of initial lift thus becomes critical. The ground or soil conditions which are favourable for soil nailing are mainly dense granular soils with certain apparent cohesion, weather rocks with adverse weakness planes and stiff fined - grained soils.

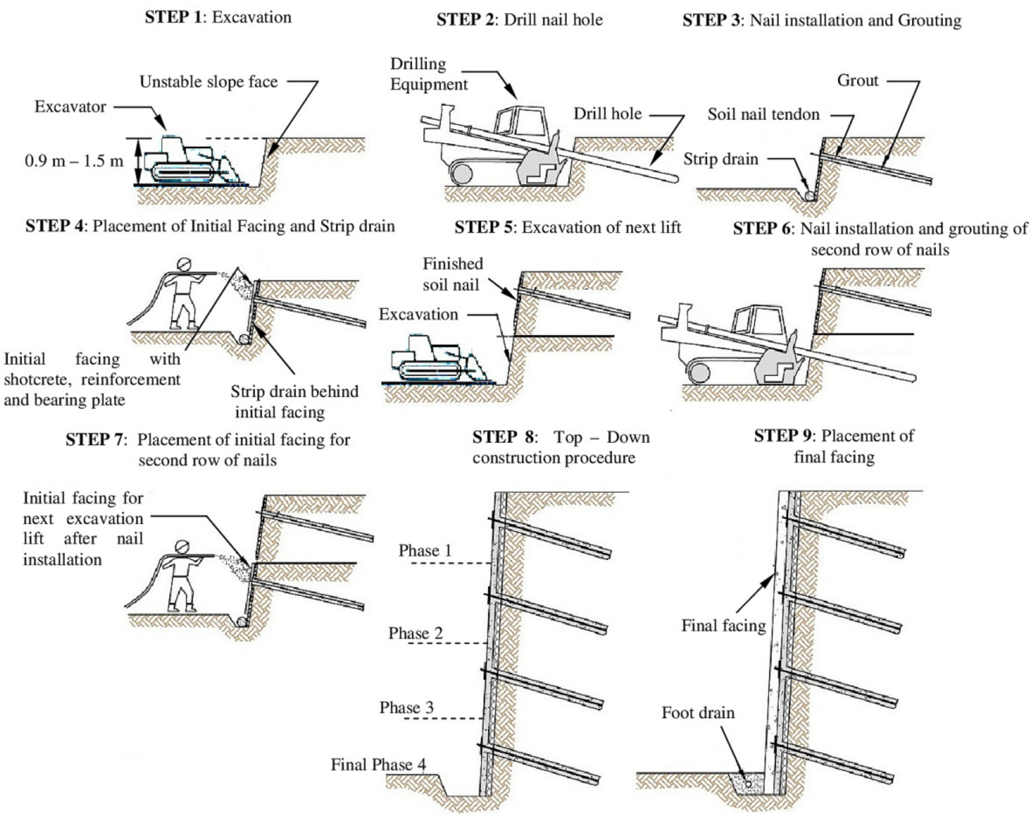

Fig. 1.2: Construction procedure of a soil - nail system

Step 2 – Drill holes: For installation of soil nails, drill holes are created with the help of exclusive drilling machinery which can be rotary, percussion or auger drilling. In case stable ground conditions prevail, drilling is carried out without casing. Otherwise, casing is used for executing bore hole drilling in weak soil conditions of dry poorly graded cohesionless soil, soft fine – grained soils, collapsible soils or granular soils with high water table. All these in – situ conditions are unfavourable for soil nailing technique.

Step 3 – Nail installation and Grouting: As the drilling is carried out, soil nail tendons are oriented in the desired location utilizing the centralisers fixed along the nail length.

Grouting of the drill hole along with the tendon is done using a tremie grout pipe. The centralisers also help in proper flow of grout by maintaining required space between the tendon and drill hole walls. The pipe is inserted in the drill hole and grout is allowed to flow under gravity or at low pressures of less than 35 – 69 kN/m^2. If the ground condition is unable to withstand drilling, then drilling and grouting is carried out as a single operation with the help of hollow soil nail tendons. During the installation of nails, strip drains are also placed between adjacent nails. The strip drains are rolled down as the excavation progresses from initial excavation lift to next lift. In this manner continuous installation of drains is attained from the top of excavation face till the bottom of excavation.

Step 4 – Initial facing: The soil nail tendon after grouting is maintained at desired orientation with the help of initial facing. The initial facing also imparts structural stability to the installed soil nail. It is applied to the excavation face before proceeding to the next excavation phase. Welded - wire mesh (WWM) is placed at the respective excavated face along with horizontal and vertical bars situated around nail head to resist bending. With this reinforcement intact, shotcreting is done. Once the shotcrete partially sets steel bearing plate is placed at the nail head and proper connection is achieved by wrench - tightened hexagonal nuts and washers. The hexagonal nuts and washers are tightened within 24 hours of shotcreting. Horizontal and vertical bars are also placed around the nail heads for bending resistance. As the shotcrete starts to cure, a steel bearing plate is placed over the tendon that is protruding from the drill hole. The bearing plate is lightly pressed into the fresh shotcrete. Hex nuts and washers are then installed to engage the nail head against the bearing plate. The hex nut is wrench-tightened within 24 hours of placement of shotcrete which applies a load of 5 kN on the corresponding tendon due to torque applied. In situations where small diameter (< 20 mm) nails are used, the tendons are laterally bent at right angles to anchor the mesh and shotcrete.

Step 5 – Excavation of next lift: By completing one sequence of construction, the next excavation phase is carried out in a similar manner as Step 1.

Step 6, 7 and 8 – Similar to Steps 2, 3 and 4, installation of second row of nails is done through the grouted drill hole. The strip drains placed between adjacent soil nails of first row are rolled down to the second row of nails. Initial facing is carried out using reinforced shotcrete.

Step 9 – Final facing: The final facing is not necessarily done after initial facing of the last excavation phase is completed. It can also be carried out in a bottom up manner for each excavation phase with the completion of its initial facing. In order to safely execute bottom - up final facing, precautions are taken to check that significant support is available bear the weight of facing during the subsequent excavation lift. The final facing is connected to soil nail tendon by welding headed studs to the bearing plates.

1.6 Advantages and Disadvantages of Soil Nailing

In comparison to other top – down construction methods and ground anchors, soil nailing beholds several advantages as enlisted below:

1) Soil nails can be installed relatively faster using smaller equipments even in areas of remote access. Due to low requirement of construction materials and easy installation, soil nails causes minimum environmental impact.
2) Since soil nails are shorter and do not use soldiers beams as in case of ground anchors, hence overhead construction costs are small. With respect to tieback walls, soil nails offer a cost saving of 10 – 30 percent [29]. Soil nails offers less expenses due to low field adjustments when obstructions like cobbles, boulders, piles and underground utilities are encountered during construction owing to installation.
3) When compared to braced excavations soil nails do not provide congested bottom. An obstruction free working environment can easily be associated with soil nailing technique.
4) Due to flexibility of soil – nail walls, significant large total and differential settlements can be accommodated. The maximum horizontal displacement of a soil – nailed wall at the end of construction is not more than 0.3% of excavation depth [27]. Owing to its low stiffness, soil nail walls perform well in seismically active regions [4].

Some of the potential disadvantages of soil nails can be described as follows:

1) Soil nailing is not recommended for soils which cannot withstand unsupported excavation depths of 1.2 m to 1.8 m for a period of 2 to 3 days to facilitate placement of soil nail into the drill hole without casing and later grouting. To render this condition favourable, certain cohesion or apparent cohesion is desirable.
2) Deformation sensitive structures pose problems for soil nailing as soil – nail system requires soil deformation to mobilize resistance. Hence soil nailing is not recommended for applications where very strict deformation control is required. However, post tensioning of soil nails can overcome this shortcoming but at the expense of increasing the project cost. Grounds with high water table also render

unfavourable conditions for soil nailing. A high ground water table not only creates construction difficulties for drilling and excavation but also increases the possibility of corrosion of soil nail tendon. The high water table also leads to seepage problem which causes the drill holes to collapse. Due to this movement of water in to the drill hole, water – cement ratio of grout is adversely affected.

3) In case of loose dry cohesionless soils, drill hole for soil nail can collapse due to weak nature of the soil. In such cases drilling and grouting is carried out as a single process. Moreover, if corrosive nature of soft cohesive soil exists, it leads durability issues of a soil – nail system. In such conditions, pullout capacity of soil nail is not economically mobilized [30].
4) Soil nails cannot be used in regions having buried water pipes, underground cables and drainage systems in or around the vicinity as it creates difficulty in drilling operation. Therefore, change in soil nail orientation or length or spacing becomes necessary so as to maintain sufficient clearance from other systems. This requires specialized and experienced contractors.

1.7 Mechanism of Soil Nail in Soil – Nailed Structures

Soil is a material which is weak in tension. Addition of a material having significant tensile strength not only increases the tensile strength of soil but also provides it stability against shear strength failures. In order to achieve that closely spaced passive inclusions in the form of steel bars or rods are inserted into soil mass. The failure of slopes is generally a shear failure occurring at a potential slip surface which divides the soil mass into two states [31].

The soil mass in front of the failure surface tends to move outwards and is in an active state of earth pressure. The soil mass behind the failure surface is subjected to passive earth pressure condition. The reasons for soil nail to be referred as 'passive inclusions' depends on the fact that soil nails are not pre - tensioned like anchors and have a length such that it extends deep into the passive zone of soil mass. The passive inclusion now acts as a tie fastening the active and passive soil mass during failure. The outward movement of soil mass during failure induces tensile forces in the soil domain which are resisted by these inclusions called soil nails. Thus soil nails are subjected to tensile forces during slope failure. The tensile strength of soil nails is thus mobilized due to outward movement of soil mass as given in Fig. 1.3.

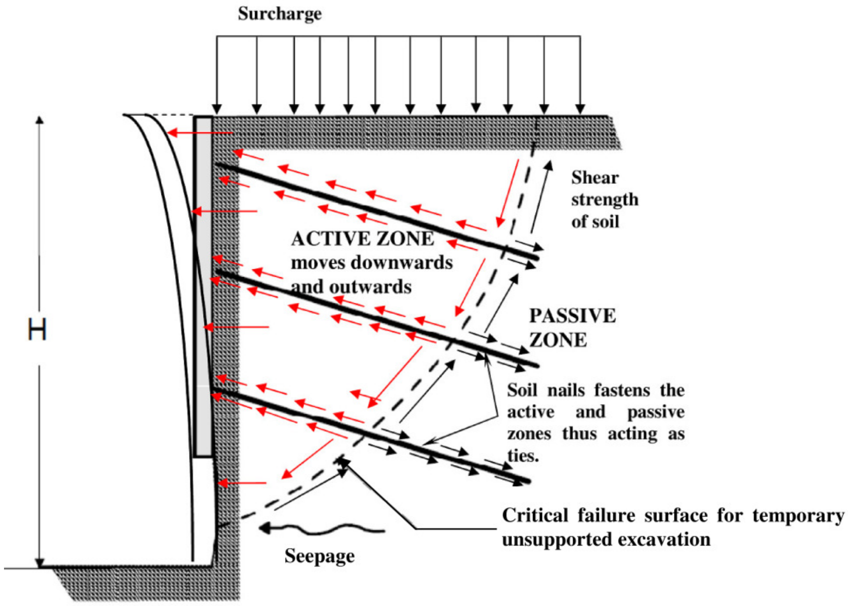

Fig. 1.3: Load transfer mechanism in soil – nailed system

Consequently, soil nails are under a constant pullout which is resisted by nail length in passive soil zone and is termed as soil nail pullout resistance. Moreover, to further restrain the slope and nail movement, soil - nailed structures are provided with a permanent or temporary facing panel. This facing also helps resist the tensile forces of soil mass and provides an additional tensile resistance to soil nails. Hence, during failure of soil – nailed structures, the forces mobilized along the soil nail length are nail tensile capacity, nail pullout capacity and facing capacity (Fig. 1.4). Moreover, it has also been found by researchers in the past that though soil nails work predominantly in tension, but shear and bending stresses are also mobilized at the intersection of the slip surface and soil nails [32 – 35]. However, the contribution of shear and bending is considered negligible under service load condition [34 and 36].

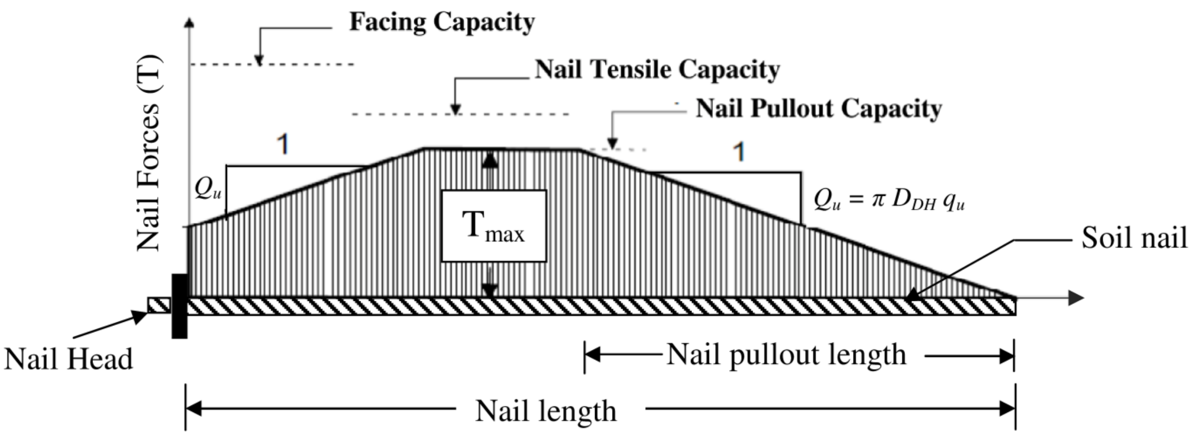

Fig. 1.4: Forces mobilized along soil nail length during failure

The potential failure modes for a soil – nailed system can be classified as external failure mode, internal failure mode and facing failure mode. The occurrence of these failure modes governs the limiting conditions for soil – nailed slopes. If a soil – nail system collapses under induced stresses from surcharge which is greater than the soil shear strength, then it refers to strength limit state. A service limit state is one in which soil – nailed wall deforms excessively hampering safe and normal operation of structure. For optimum design of a soil – nail structure, the above mentioned limit states must be satisfied, hence safety check against three different failure modes becomes necessary. The external failure mode is concerned with the condition that potential failure surface may or may not intersect the soil nails. In such a case the soil mass undergoes a block failure and will result in global stability failure, sliding failure and base failure as depicted in Fig. 1.5.

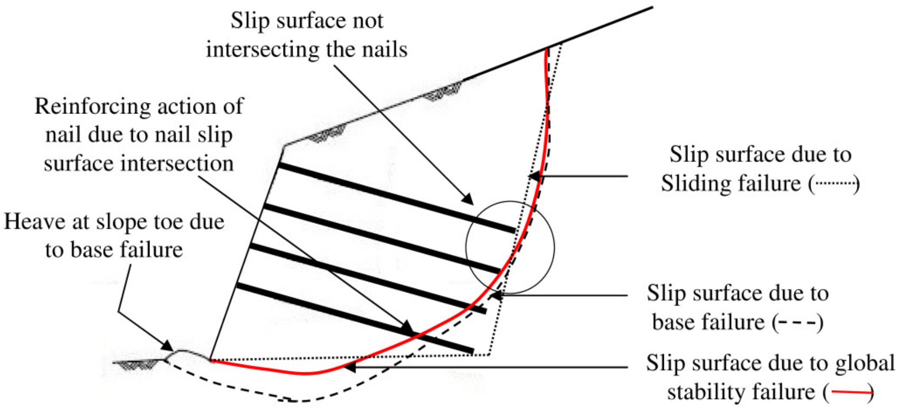

Fig. 1.5: External modes of failure

The load transfer mechanism between soil nail and surrounding soil determines the internal failure mode of soil – nailed structure. As the reinforced system deforms, bond strength between soil nail embedded grout column and surrounding soil is mobilized progressively along grout - surrounding soil interface. The tensile forces are thus mobilized and bond stresses are distributed along the soil nail length. The distribution of bond stress and tensile strength of soil nail governs the internal failure modes of system. As can be seen from Fig. 1.6, internal failure modes of soil – nailed system includes nail pullout failure, tensile failure of nail, bending and shear of nails and slippage of nail – grout interface. The facing failure mode is related to flexure failure, punching shear failure and headed – stud tensile failure of connection between nail head and facing.

The external and internal stability of a soil – nailed system can be evaluated using limit equilibrium method (LEM). The limit equilibrium method is based on the concept of finding the most critical surface along which the destabilizing forces causes failure. Other factors on which the external stability analysis depends are the structure height, nail lengths and the soil type of nailed system. The external stability analysis is used to find the critical factor of safety by considering a number of failure surfaces such as planar, bi – linear, circular, parabolic and log – spiral. Since the analysis involves large error and trial data, computer programs like SNAIL and SLOPE/W are commonly used.

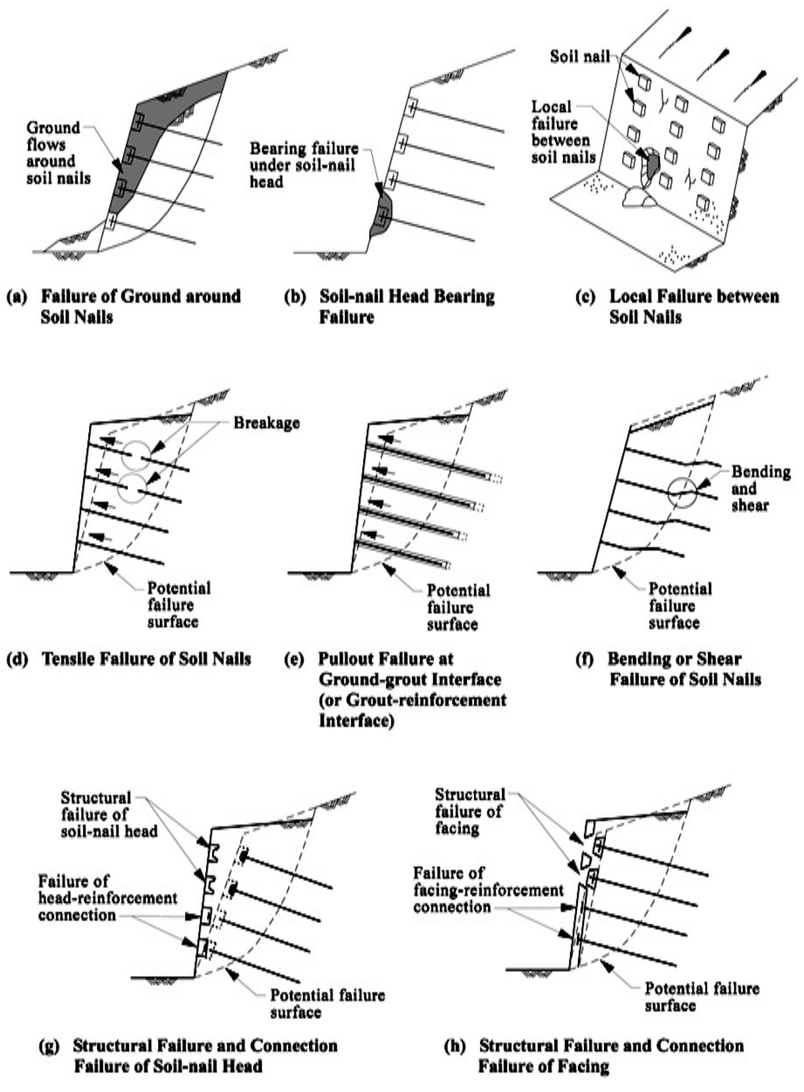

Fig. 1.6: Types of internal failure modes of soil – nailed system (After Geoguide, 2008)

However, finite element method (FEM) based computer programmes are also employed for external and internal stability analysis of soil – nailed slopes. PLAXIS 2D and FLAC 2D has always been common choices for finite element analysis of soil nail structures. The advantage of studying non – linear stress strain behavior of soil during failure and load - deformation of reinforced slope failure are well predicted by finite element method. LEM uses different slip circles and predicts slip circle with minimum factor of safety as critical.

The convergence of force equilibrium and moment equilibrium governs the FOS and hence critical slip surface. Moreover, the local factor of safety is constant throughout the analysis in LEM, thus eliminating the cases of local slip failure. On the other hand, the slip surface obtained from FEM is based on stress distribution within the continuum. The stress distribution in more realistic in FEM as local factor of safety is not constant and thus convergence of results is achieved.

1.8 Concept of Soil and Nail Interaction

The soil – nail interaction plays an important role in load transfer mechanism of a soil – nailed system. The tensile forces developed in nails are result of frictional forces due to soil – nail interaction. This interaction reduces the imposed shear force in soil by increasing the normal stresses in soil along potential failure surface, thus allowing higher shear resistance to be mobilised by the bearing soil. The soil mass above the nail act as an overburden and in addition to surcharge it increases the normal stress on the nail [37]. The outward movement of soil mass is also a consequence of soil mass loading. The outward movement causes a pull on the anchorage length of the nail i.e. nail length behind the failure surface. Alternatively, pullout resistance of nail is mobilized by apparent coefficient of friction at soil – nail interface which is a function of the normal stress around the nail. The tensile forces are mobilized by axial stress, whereas lateral strains mobilize shear and bending forces in the soil nail. The soil - nail interaction is influenced by factors such as nail stiffness, nail inclination, nail bending strength, soil stiffness and soil shear strength. The nail thus resists the soil deformation by its mobilized tensile capacity, pullout capacity, shear stress at soil nail interface and facing capacity. The facing capacity is generally a fraction of ultimate nail capacity and is primarily caused due to nail and facing interaction.

The nail force is found to vary from zero at the nail end to a maximum value at intermediate length and a reduced value at slope/wall facing. However, maximum tensile capacity does not necessarily occur at nail - slip surface intersection. The distribution of shear stress along nail length is not uniform but changes from positive to negative at the intersection of nail and failure surface. Due to improper soil – nail interaction, significant reduction in radial stresses during nail installation around the drill hole is also observed due to a phenomenon known as soil arching. However, pressure grouting is usually employed to counter this reduction in radial stress. Moreover, a soil – nailed system develops a significant portion of bond resistance from drill hole roughness and soil grout interlocking.

1.9 Development of Screw Soil Nail

The conventional soil nail holds many benefits above other earth retaining construction techniques. However, performance of conventional soil nails i.e. grouted soil nails are significantly influenced by in – situ soil type and construction processes. Conventional soil nails have always posed difficulties in construction with soil conditions consisting of silt, sand, gravels, cobbles, and boulders. The pullout mechanism of a conventional soil nail is also affected by factors such as soil saturation, soil dilation, grout pressure, overburden pressure, nail roughness and nail bending. Further, unfavourable ground conditions can make the construction processes rather uneconomical and often difficult. The process of drilling during grouted soil nail installation often results in soil disturbances and release of stresses in the surrounding soil. This stress relief in surrounding soil affects the pullout resistance of soil nail by making it independent of surcharge pressure, thereby making the pullout resistance reach only a limiting value. The stress release is further enhanced as grouting of drill hole is carried out. As the grouting is carried out at low pressure and is allowed to flow under gravity, air from the voids is replaced by grout which increases the soil disturbance. This compromises the structural integrity of nail and its compressive strength.

Subsequently, if cracking of grout occurs, it can lead to reduced interaction between soil nail tendon and surrounding soil. Moreover, cracking of grout can ultimately lead to breakage of soil nail. Another installation difficulty related with conventional soil nails is the placement of centralisers along nail length. The centralisers maintain orientation of soil nail and also easy the grout flow to fill up spaces between the tendon and drill wall. Thus, poorly placed centralisers often results in non – uniform grouting around soil nail tendon which causes bending of soil nail and hampers the stability of soil – nailed system.

The shortcomings of conventional soil nail installation can be rectified by a soil nail which can be installed without any pre – drilling and grouting to bond the soil nail tendon with surrounding soil. Another remedial measure can be a soil nail which can be installed in unfavourable ground conditions and still develop significant interaction between nail and soil. To achieve such interaction from weak soils, nail installation should produce minimum disturbances so that no bridging occurs. Reduced soil remoulding during installation will also ensure that in – situ shear strength properties of soil has not been altered. Since remoulding of soil reduces its shear strength, soil nails installed without causing significant disturbance can be realised to mobilize higher bond strength between soil and nail. Without drilling and grouting, installation of nail will also produce fewer soil spoils.

The above listed concerns eventually lead to the development of screw soil nails which can be installed easily by applying torque at nail head, even in weak soils with minimum ground disturbances. The application of torque further enhances the surrounding soil properties by densification and consequently mobilizing maximum soil strength parameters. The idea of screw soil nail generated from helical anchors. With the advantages of rapid installation, immediate loading capability and resistance to both uplift and bearing loads, helical anchors were used beyond their traditional application in electrical power industries. Helical anchors are already used as tie - downs for structures subject to uplift and tiebacks for the retention of slopes and walls. Adopting a similar design philosophy, screw soil nails are developed to stabilize slopes and cuts. The screw nails provided added advantages over conventional grouted nails as given below:

1) Quicker installation and immediate reinforcement – Screw soil nails can be drilled into ground within a short period of time and soil reinforcement is available immediately upon installation.
2) No requirement of specific equipment – Screw soil nails can be installed using simple drill motor with sufficient torque output attached to a backhoe, skid loader or track hoe.
3) The capacity of screw soil nails can be estimated directly from torque required to install the soil nail [38]. This helps in monitoring that design requirements are fulfilled during installation and hence eliminates the need of carrying out expensive and time - consuming load tests.
4) Soil nailing using screw nails is more economical than conventional soil nails because stable soil condition which can withstand unsupported cut for 1 to 2 days is not required as screw nails are able to penetrate the ground at a rate compatible to the pitch of the helices.
5) Screw nails can be used in soil conditions consisting of naturally cemented or dense sand, gravel, residual soils, weathered rock without unfavourable oriented joints or low shear strength, sand with some apparent cohesion due to capillary effects, stiff cohesive soils such as clayey or sandy silts and low plasticity clays that are not susceptible to creep.
6) Screw soil nails eliminate building – up of pore water pressures, hence are also beneficial for construction in soil conditions below groundwater table.

7) Screw soil nails are well suited for applications in rehabilitation of distressed retaining structures.

1.10 Organization of Thesis

The first chapter of the thesis provides a brief introduction on application of soil nailing and evolution of soil nailing technique with time. It also elaborates the components of a soil – nailed system, its construction procedure along with the mechanism and concept of soil – nail interaction. The chapter also enlists the advantages and disadvantages of soil nailing and describes the development of screw nails. The chapter also gives an overview on the organization of thesis.

The second chapter deals with the review of available literature on small scale laboratory model testing and large scale field testing. It also gives insight on previous experimental, theoretical and analytical studies conducted to understand the soil – nail interaction through different types of soil nail pullout tests. The chapter also provides the summary of literature review with the investigated research gaps. The objectives of the present research work are also provided in this chapter.

The third chapter elaborates the material testing and model testing of unreinforced and reinforced slopes at different slope angles (β) of 45°, 60° and 90° with nail inclinations (i) of 0°, 15°, 20° and 30°. The chapter provides a detailed description of model testing of different slope angles and nail inclinations using smooth soil nails, screw soil nails and helical soil nails.

The fourth chapter presents complete limit equilibrium method (LEM) and finite element method (FEM) based numerical modeling procedure adopted for simulation of different unreinforced and reinforced slopes using different types of soil nails. It also provides two – dimensional (2D) and three – dimensional (3D) numerical modeling of helical soil nail pullout for various combinations of parameters.

The fifth chapter includes all the results obtained from material testing, model testing and numerical modeling using LEM and FEM. Comparison and discussions on critical observations from results between model testing and numerical modeling are also presented here. This chapter also provides validation of model testing and numerical modeling with past literatures.

The sixth chapter deals with the conclusions derived from model testing and numerical modeling of different soil – nailed slopes using smooth, screw and helical soil nails.

CHAPTER 2
LITERATURE REVIEW

2.1 General

The chapter reviews the published literature on model testing of soil – nailed structures to understand and estimate the failure mechanism of slopes or cuts. Large scale or field testing studies has also been reviewed for better understanding of failure mechanism and ground deformations in actual soil conditions. The chapter reviews different methods adopted by previous researchers for better comprehension of mechanism of soil – nail structure interaction through direct shear tests, interface shear tests and pullout tests. Review of innovative developments to overcome shortcomings of conventional soil nailing is also provided in the chapter.

2.2 Small - Scale Model Tests of Soil - Nailed Structures

The detailed study of primary design parameters of soil – nailed structure is expensive through full – scale testing, though actual construction procedures can be simulated more accurately in field. Thus, earliest attempts to investigate the effects of main design parameters on failure mechanism by soil – nailed model testing were carried out by Juran et al. [39], Juran and Elias [40]. The authors demonstrated that the observed model behavior and field observations on instrumented full - scale structures were found consistent. They also concluded that evaluation of design assumptions and performance assessment of soil – nailed structures can well be predicted by laboratory model study.

The stability analysis of soil – nailed structures involve the study of assumed geometry of failure surface, forces in the active zone and corresponding factor of safety. Various methods have been developed at different countries based on the concerned parameters listed above through model test of reinforced slopes. Gassler and Gudehus [41] conducted three small model tests on granular soil under two different conditions. Two model tests were carried out with freely moving Perspex sheets walls to represent shotcrete. In the third test rigid Perspex sheet wall acting as an irrotational guided wall was used. The model box size was 1100 mm in length with 720 mm of width and 560 mm of height. The moving Perspex sheet walls had dimensions of 750 mm width and 350 mm height whereas 450 mm of height was designed for guided wall. The granular soil used in testing mainly consisted of dense dry sand having properties of unit weight (γ) = 17 kN/m^3, angle of internal friction (ϕ) = 44° and D_{50} = 0.33 mm. The dry sand was filled in the model box in layers with colored sand bands sandwiched between every two sand layers with each having a thickness of 40 mm. With the assurance of desired density of fill due to filling in layers, sand slope was also loaded with water filled cushions to act as uniformly distributed surcharge on slope crest. After failure under surcharge load, the sand model was submerged in water and drained. This method was used to create apparent cohesion due to capillarity, so that a vertical cut can be made to study failure mechanism of sand slope model.

The first test on sand slope was found to reach failure at a surcharge load of 0.75 γH, whereas for second test, failure surcharge was found to be 2.5 γH. 'H' represents the model height of sand slope. The authors also observed failure surface to be nearly a circular slip surface of radius 5H such that it intersected all the nails used for the slope. However, for second test the failure of slope was observed to have occurred along two slip blocks thus developing two curved slip surfaces as shown in Fig. 2.1.

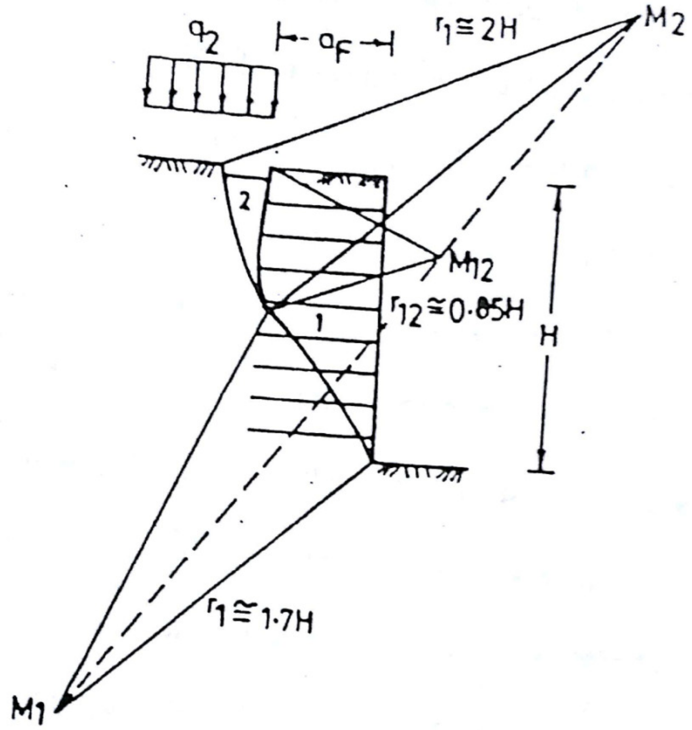

Fig. 2.1: Curved slip surfaces (After Gassler and Gudehus [41])

However, the authors also concluded that the slip surface radius (5H) found during model testing was far less than 11H as computed from analytical study. In the third test with irrotational guide walls, no surcharge was applied but failure was initiated using horizontal traction force. The failure surface observed during the third test was found to be inclined at 43° with the horizontal. However, the analytical study has revealed to produce a minimum factor of safety when failure surface was inclined at 40° with horizontal.

A similar model test on dense dry sand using 1 mm thick steel nails of length 100 mm was also conducted by Schwing and Gudehus [42]. The sand model was constructed by using colored sand bands between every two layers of thickness 40 mm till the model height of 260 mm was reached. The sand model was reinforced using nails in two rows. Similar to Gassler and Gudehus [41], the model was submerged and drained vertical cut at the centre for failure mechanism investigation. The authors observed that combined failure mechanism at 54° with horizontal is found to occur instead of an inclination of 52.5° as determined for minimum factor of safety using limit equilibrium method.

Kitamura et al. [43] carried out model tests on sandy slopes having dimensions of 200 mm width x 2100 mm length x 750 mm height. In this steel frame sandy soil was filled by compacting layers in thickness of 15 cm each. The soil nails were fabricated as aluminium strip plates. The reinforcing elements were oriented at inclination to horizontal such that a variation of 20° on either side upward and downward is obtained. The aluminium plates are pre – buried in the model slope during compaction. In order to study the effect of aluminium bar as reinforcement for sandy slope, vertical loading tests are conducted. The gradual increasing vertical load in form of a surcharge load 49 kN/m^2 was applied on reinforced slope by 27 x 105 cm load plate. The failure of reinforced slope was considered until the rate of slope settlement of 0.5% per minute at each loading step was attained. As the slope began to yield, the loading steps were reduced to $25 kN/m^2$. The authors made an observation regarding the load plate and slope deformation. The reinforcement stresses were also measured. From the observations made during model testing, the authors concluded that maximum reinforcing action is obtained when aluminium plates are inclined downwards at an angle of 20° with horizontal. Minimum reinforcing action is achieved when reinforcement orientation is in upwards direction. During the testing, bending and shearing resistance did not significantly affect the reinforcing action of aluminium plate. Moreover, maximum axial stresses are observed between slip surfaces of reinforced and unreinforced slopes.

Using phosphor bronze strips of dimensions 30 x 50 x 300 mm, Gutierrez and Tatsuoka [44] carried out a series of small model tests and developed a new stability analysis method. The sand models were constructed using air dried Toyoura sand using three 1.5 mm thick acrylic plates acting as slope facing. A bellofram cylinder was used to simulate load from footing. Displacement rates were kept at 0.1 mm per minute and the load direction was fixed at 30 degrees to the vertical. 11 small load cells having two components were used to measure footing load at its middle one – third. Pictures of the lateral surfaces of the model slopes at appropriate displacements of footing were captured so that displacement and strain fields could be determined and slope failure mechanism can be studied. The authors obtained a relationship between average axial stress and footing displacement. The tensile forces developed along the reinforcement were also found out. Fellenius method was employed to carry out the stability analysis of model slope using the ordinary method of slices. The authors proposed a new analytical method called Directional Slicing Fellenius method which is a modified Fellenius method to calculate factor of safety for a soil – nailed system comprising of inclined reinforcement with tension forces and the inclined footing pressure to vertical. The critical slip surfaces can also be predicted using the new method by taking into account the progressive failure of model slopes.

In order to investigate the mechanism of soil reinforcement of cut-off slopes with steel bar, Hayashi et al. [45] conducted a series of model tests which simulated sliding force acting on a cut-off slope. A modified Bishop's design method was also developed by considering the tensile force and the shear resistance mobilized in individual reinforcement. A numerical study of various reinforced soil cases was carried out using the proposed method. More than 100 cases of soil – reservoir – model were studied to correctly understand the mechanism of steel bars in reinforced soil. The design of soil reinforcement with steel bars was simplified by carrying out constructing nomographs from the numerical study results. The proposed method was based on rigid plasticity theory with the concept that mechanical function of individual reinforcement can be understood from angle of intersection of hypothetical sliding surface and individual reinforcements.

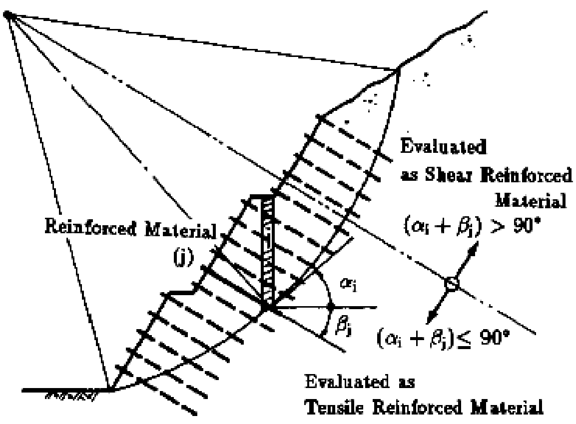

Fig. 2.2: Evaluation of function of Individual Reinforced Material (After Hayashi et al. [45])

According to the authors, reinforcement material can be categorized based on the mechanism by which they derive their reinforcing function. Some reinforcing materials derive shearing resistance and tensile resistance with respect to the angles of intersection between hypothetical sliding surface and individual reinforced material (Fig. 2.2) while others can be treated as tensile reinforced materials and shear reinforce materials. The tensile resistance (T_{ij}) developed by tensile reinforced materials on the moving soil mass is evaluated based on minimum value obtained from the following three types of tensile forces (Fig. 2.3):

1) The maximum tensile resistance force (T_{tj1}) applied to the reinforced material by a moving soil mass.
2) The maximum tensile resistance force (T_{tj2}) applied to the reinforced material from an unmoved natural ground.
3) Allowable tensile force (T_{ta}) of each individual reinforced material.

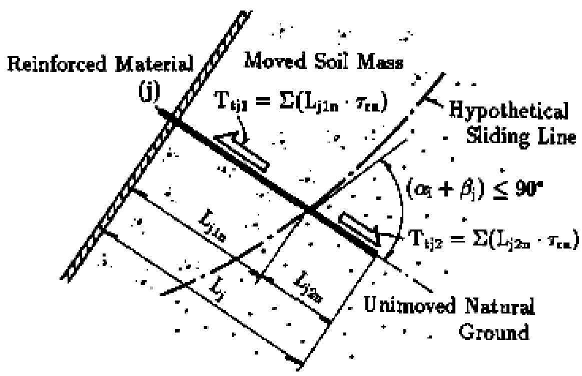

Fig. 2.3: Evaluation as Tensile Reinforced Material (After Hayashi et al. [45])

Similarly, if the reinforced material is treated as shear reinforced material, its evaluation of shear resistance (T_{sj}) force applied by it to a moving soil mass is based on the minimum of three resistance forces (Fig. 2.4) given as:

1) The maximum lateral resistance force (T_{sj1}) applied to reinforced material by a moving soil mass.
2) The maximum lateral resistance force (T_{sj2}) applied to reinforced material from an unmoved soil mass.
3) Allowable shear resistance force (T_{sa}) of individual reinforced material composed of steel bar and grouting mortar.

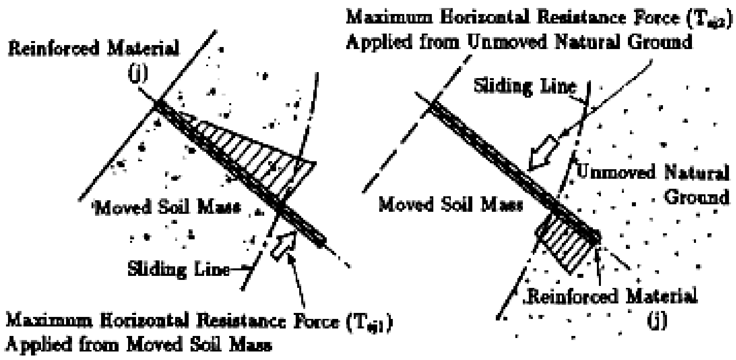

Fig. 2.4: Evaluation as Shear Reinforced Material (After Hayashi et al. [45])

Utilizing the resistance forces (T_{tj}) as shown in Fig. 2.3, (T_{sj}) in Fig. 2.4 and correlative relation with a hypothetical sliding surface given in Fig. 2.2, the margin of safety can be obtained in accordance with the individual reinforced material. By modifying and expanding the Bishop's method and employing the repetitive approximation, the factor of safety can be calculated from equation (2.1):

$$F_{st} = \frac{\sum \frac{1}{\cos\alpha_i} \frac{c_i l_i \cos\alpha_i \{W_i - u_i l_i \cos\alpha_i - 1/F_{st}(T_{sj}\sin\alpha_i - T_{tj}\sin\beta_i)\}\tan\emptyset_i}{1 + 1/F_{st}\tan\alpha_i\,\emptyset_i}}{\sum\left[W_i \sin\alpha_i - \frac{1}{F_{st}} - \{T_{sj} - T_{tj}\cos(\alpha_i - \beta_j)\}\right]} \tag{2.1}$$

Nomograph is a sketch in a graphical style so as to provide calculations in accordance to the design method of soil reinforcement with the following design conditions (Fig. 2.5):

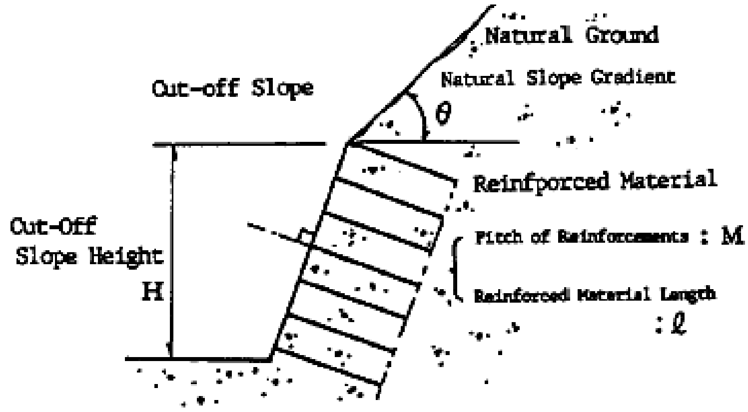

Fig. 2.5: Simplified slope shape for nomograph (After Hayashi et al. [45])

1) The natural ground should be isotropic, homogeneous with no underground water and infinite slope having uniform gradient on the shoulder of cut – off slope.
2) The height of maximum cut - off slope should be one step 7.0 m. A berm of width 1.5 m should be applied if height greater than maximum height is required.
3) With uniform length and spacing equal to M = 1.0 m or 1.5 m, insertion angles for reinforced materials should be in a direction perpendicular to the cut-off slope surface.
4) The connection between reinforced materials and surface protection should be sufficient with perfect slope surface protection of the cut-off soil.

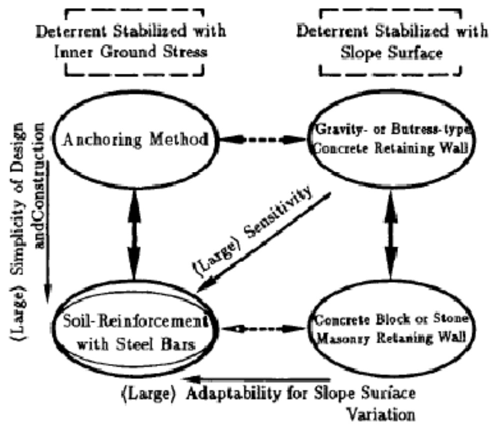

Fig. 2.6: Comparison of slope stabilizing method (After Hayashi et al. [45])

The authors concluded that based on the design and nomographs, soil reinforcement with steel bars is sensitive (Fig. 2.6) as compared to conventional slope stabilizing methods and hence not only the local design but also soil reinforcement mechanism should be carefully executed for it effective use.

A series of plain - strain model tests of footing on unreinforced and reinforced sand slopes were carried out using fine quartz – rich sand called as Toyoura sand by Huang et al. [46]. The construction of model Toyoura sand slopes had dimensions of 182.7 cm (length) x 40.0 cm (width) x 67.7 cm (height) with a dip angle of 30°. Toyoura sand consisted of sub – angular to angular particles with G = 2.64, D_{10} = 0.16 mm, C_u = 1.46, $\gamma_{d(max)}$ = 16.11 kN/m^3, $\gamma_{d(min)}$ = 13.09 kN/m^3 and residual friction angle for plane - strain condition as 35°. The proper simulation of plain – strain condition was achieved by using two transparent acrylic sidewalls, steel end plates and steel stiffeners for sand box fabrication. To attain minimum wall friction, 0.05 mm thick layer of silicon grease and a rubber membrane sheet having thickness of 0.2 mm was used along the tank sidewalls. This measure helped in achieving a small friction angle of 0.5° to 1° between sidewalls and sand. Moreover, to further minimize the effect of wall friction on load – settlement characteristics of footing, load cells used for measuring footing load were installed at central third of strip footing. A total of eleven load cells were used for footing load measurement. The footing load on the slope crest was generated by using 39.8 cm long and 10 cm wide rigid strip footing which was positioned at a off – set distance of 0.3 cm from slope crest. To ensure non – eccentric loading condition, a two hinge set at both sides of footing was used for footing load application. The inclination of footing load was controlled through a double – action air cylinder. The loading system also included a low friction roller at top of loading piston which was guided by bearing house and high – precision linear guide ways for regulating the loading piston both in horizontal and vertical directions (Fig. 2.7).

During the observation for load eccentricity against settlement ratio of footing, it was recorded that an eccentricity within 5% had negligible effects on the load – settlement response of modeled slopes. The modeled Toyoura sand slopes were reinforced using 3 mm wide and 0.5 mm thick high linear - elastic phosphor bronze strips with length varying from 10 cm to 40 cm. The tensile stresses are measured by four strain gauges attached to each strip in such a manner that strain due to bending is self – compensated. To acquire rough nail surface, sand was glued on to it. The strain fields developed during loading of slopes was recorded by photogrammetric method. The images taken during various stages of loading were numerically processed to obtain maximum shear strain (ε_1 - ε_3) distribution through principle strains i.e. maximum principle strain (compressive) (ε_1) and minimum principle strain (tensile) (ε_3). To study the bearing capacity behavior of unreinforced and reinforced sand slopes, grouping of model tests for various configurations was done. The model tests were divided into 5 groups as reinforced slopes

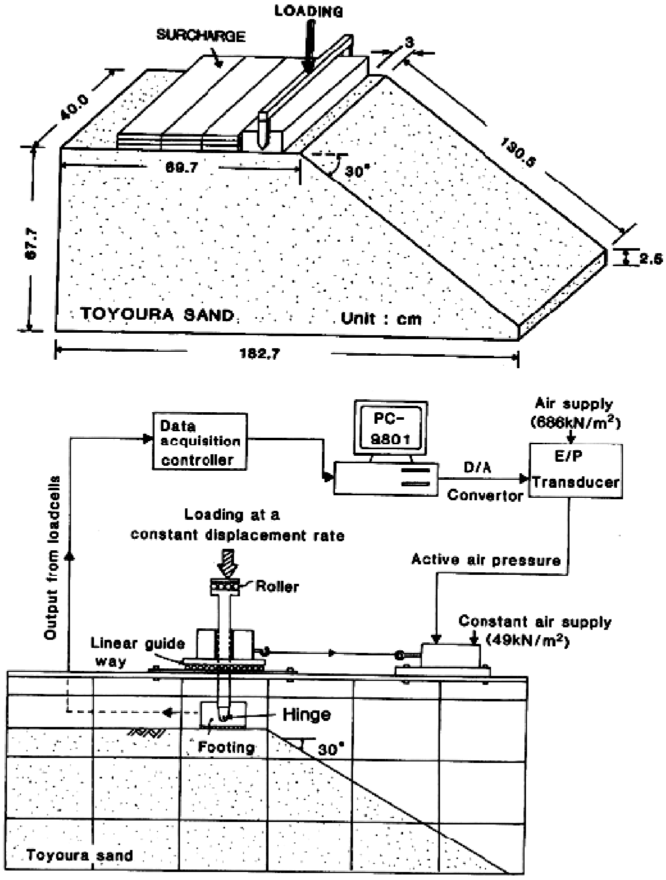

Fig. 2.7: Geometry of model sand slope with schematic diagram of loading system (After Huang et al. [46])

(Group 1), with changed vertical spacing of reinforcement (Group 2), with changed length and position of reinforcement (Group 3), covering ratio (Group 4) and with different reinforcement orientation (Group 5).

The findings from model testing of unreinforced sand slopes classified as group 1 indicated that as the inclination of loading changed to $\alpha = 5°$, the bearing capacity reduced to one – fourth of bearing capacity for horizontal ground level. Moreover, it was also observed that normalized contact pressure of footing becomes significantly susceptible as the loading inclination (α) changes between $\pm 5°$. The strain contours depicted that as footing load reaches it maximum value, intense strains are generated at toe of footing. However, at post – peak footing load, maximum strains are observed to have developed rapidly at heel of footing and sheared band gets propagated towards the slope face. The failure of sand slopes can thus be classified as progressive in nature since maximum angel of internal friction of sand is never mobilized along the potential failure surface.

The experimental findings from group 2 revealed that an increase in bearing capacity can be achieved if three reinforcement strips at vertical spacing (d) of 0.3B are placed under the footing for $\alpha = 0°$. The width of footing is denoted by 'B'. It is also reported that reinforced slopes show an increased bearing capacity which is greater than the bearing capacity of unreinforced slopes even on horizontal ground. For $\alpha = 5°$, bearing capacity increase can be observed for three reinforcement strips with $d = 0.5B$. Similar to unreinforced slopes, variation of $\alpha = 0°$ to $\alpha = 5°$ lead to a decrease in bearing capacity of reinforced slopes also. It was also investigated that vertical spacing of 0.5B yielded larger bearing capacity than 0.3B for both vertical and inclined loading inclination. With 0.5B vertical spacing, shallow failure surface was found to develop at second layer of reinforcement due to significant post – peak softening.

From observation carried out for model tests with different length and position of reinforcement signifies that as the length is increased from B to 4B, an increase in bearing capacity is achieved (Fig. 2.8).

Moreover, the position of reinforcement within the active zone without intersection of slip surface with reinforcement length produced higher bearing capacity than an unreinforced slope. When the length of reinforcement is equal to width of footing and is positioned below the footing, the bearing capacity recorded was found to be the maximum among all other testing conditions such as longer length reinforcement placed within the active zone intersecting the failure surface developed from heel of footing or reinforcement within the active zone. The reason for this increase was attributed to the fact that maximum bearing capacity will always be observed if reinforcement intersects both the failure surfaces generated from toe as well as heel of footing. The increase in bearing capacity of footing can also be attributed to load dispersion over a slab formed by soil and reinforcement acting as a single unit.

As given in Fig. 2.9, it was also deduced that strains are concentrated around long reinforcement when placed beneath the footing as compared to small length of reinforcement for similar position. This mechanism depicts that significant pullout is developed during loading of slopes and reinforced slopes with significant pullout length will definitely have higher bearing capacity owing to this minor contribution of pullout resistance.

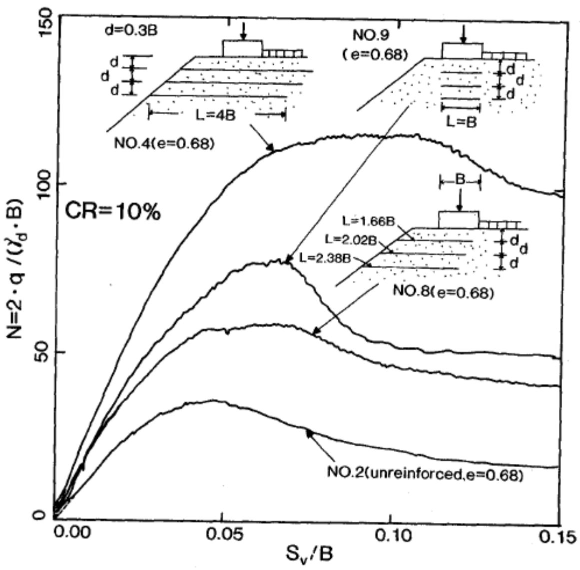

Fig. 2.8: Effect of length and position characteristics on bearing capacity of reinforced slopes (After Huang et al. [46])

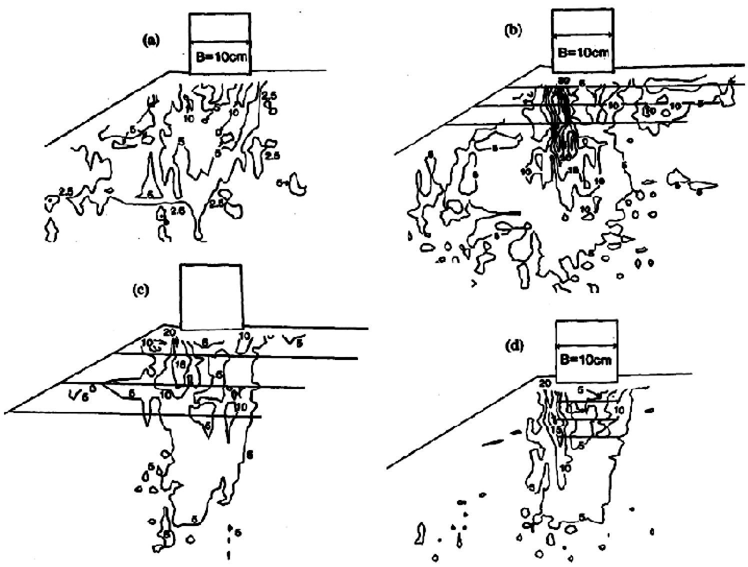

Fig. 2.9: Contours for maximum shear strains (a) Unreinforced slope (b) reinforced slope with long reinforcement and small vertical spacing (c) reinforced slope with long reinforcement and large vertical spacing (d) reinforced slope with short reinforcement and small vertical spacing (After Huang et al. [46])

The effect of covering ratio (CR) as studied from group 4 indicated that as covering ratio is increased to 10%, an increase in initial stiffness of load – settlement curves for model reinforced slopes is observed. Beyond 10%, its effect is not significant. Moreover, CR variation is found to affect the failure surface of reinforced slopes as shown in Fig. 2.10. It was also investigated that as CR value increases from 20% to 100%, similar failure surfaces are observed. This can be accounted for the fact that increasing covering ratio brings about an increase in group effect. This minimizes the development of shear band around the reinforcement zone due to restrained soil nature but consequently, reduces the efficiency of individual reinforcement. However, progressive failure is mainly observed for slopes which are reinforced heavily.

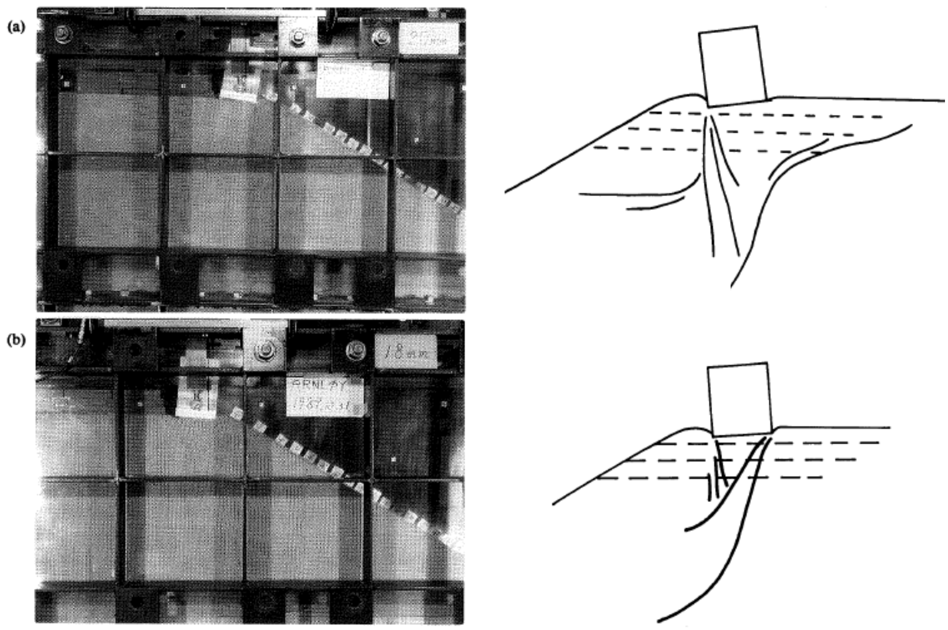

Fig. 2.10: Actual slope deformation of model slopes with simplified failure pattern for slope with (a) CR = 20% and (b) CR = 5% (After Huang et al. [46])

The optimum orientation as suggested by authors primarily depict that maximum reinforcing effect is achieved when deep footing effect is maximized in such a manner that failure does not occur within the reinforced zone and in the zone between the upper reinforcement layer and footing base. It was also concluded that model test failure mechanism can be classified under four types as triangular wedge failure where two defined shear bands develop under the footing base, failure wedge which is deeper than the triangular wedge mainly attributed to slope reinforced by small length reinforcements, punching failure comprised of two or more major failure surface accompanied by many minor failure surfaces observed mainly in reinforced zones of slopes reinforced with larger length of reinforcements and a compressive local failure due to minimum restrainment to soil observed at reinforcement zone.

A series of 6 model tests as given in Table 2.1, under unreinforced and reinforced conditions with and without facing panel were tested to understand the failure mechanism, settlement characteristics of slope under footing load and axial strains developed along reinforcement during failure. The dimensions of model test slopes were adopted as 500 mm (length) x 900 mm (width) with height depending upon the slope required for the slope. Two slope angles of 1: 0.5 (mild slope) and the other as 1: 0.2 (steep) were adopted for construction of slopes. Based on the slopes angles, the maximum height attained for test slope was 941 mm.

However, the authors endured that the top horizontal surface and loading position remains unaltered for all the tests. The slope construction was carried out in a tank consisting of four rigid concrete walls of thickness 400 mm each. The walls were connected with Teflon sheets with thickness of 1 mm fastened by fourteen steel bolts each. Greasing of these sheets was also done in order to achieve a frictionless surface during slope construction. In addition to greasing, another soft silicon mixed paper sheet was also attached so that under small stresses these paper sheets can tear. With this arrangement of reducing friction between soil and concrete walls, plane strain conditions were simulated. The tank was filled with silty sand (SM) having properties of G = 2.716, c = 0 kN/m^2, ϕ = 35°, C_u = 27.1 and C_c = 3.48.

Table 2.1: Model test scheme (After Kodaka et al. [46])

<table>
<tr><th>Model</th><th>Face slope</th><th>Reinforcements</th><th>Facing panels</th><th>Length of reinforcement</th></tr>
<tr><td>A</td><td rowspan="3">Mild slope 1V:0.5H</td><td>Non - reinforced</td><td rowspan="2">No facing</td><td>-</td></tr>
<tr><td>B</td><td rowspan="2">Reinforced</td><td rowspan="2">500 mm</td></tr>
<tr><td>C</td><td>5 mm thick panel</td></tr>
<tr><td>D</td><td rowspan="3">Steep slope 1V:0.2H</td><td>Non – reinforced</td><td rowspan="2">No facing</td><td>-</td></tr>
<tr><td>E</td><td rowspan="2">Reinforced</td><td rowspan="2">500 mm</td></tr>
<tr><td>F</td><td>5 mm thick panel</td></tr>
</table>

The homogeneous soil mixture having water content of 10% was placed in layers; 3 for base; 9 for mild slope and 8 for steep slope construction. The soil layers were compacted with a wooden tamper having weight of 98.1 N to attain desired height and unit weight of 18.13kN/m^3. For construction of slope face with desired slope angles, a rigid wedge shaped form composed of expanded polystyrene was also used. The reinforcement comprised of five to six, 3 mm diameter and 500 mm long steel bars with sand glued on its surface. The facing panel consisted of 5 mm acrylic resin board with sufficient rigidity against lateral earth pressure. The reinforcements are fixed centrally at each facing panel which are arranged in overlapping manner. A loading cell is also installed at centre of the load plate to apply the footing load. The load is applied till failure of reinforced slopes is found to occur. The complete reinforced slope used by Kodaka et al. [46] is shown in Fig. 2.11.

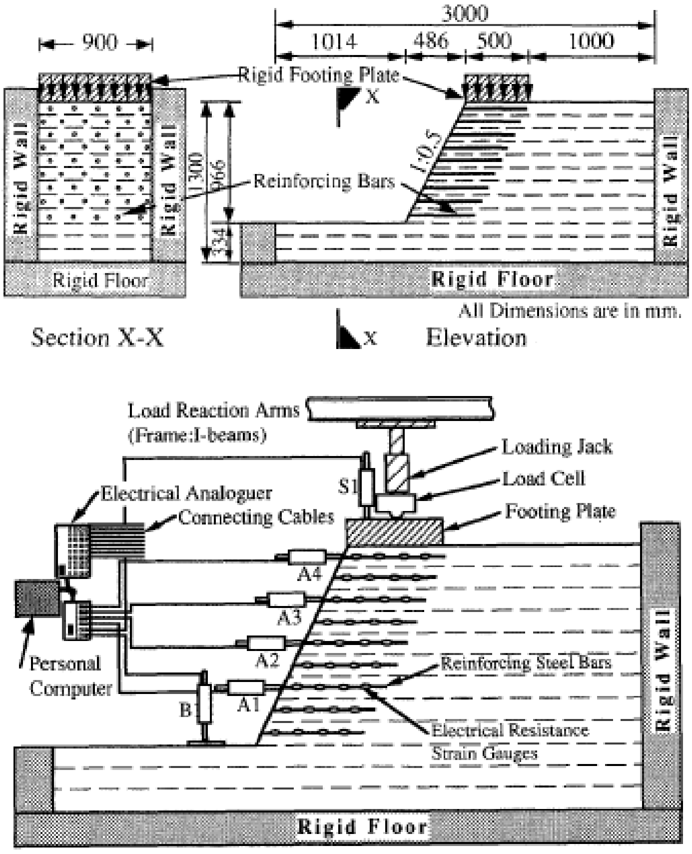

Fig. 2.11: Details of model testing with instruments and measurements (After Kodaka et al. [47])

From the observations made during model testing, authors found that different failure mechanism is observed for plain (unreinforced), reinforced slope with facing and reinforced slope without facing setup. For plain model test, failure surface was found to initiate at top slope face with inclination of loading plate towards slope face. As the load was increased another failure surface developed at the lower part of model slope. However, the authors classified this failure surface as a shallow because of its location near slope face for the entire slope height. For reinforced slope without facing, failure mechanism was observed to have occurred in three phases. As the gradual increasing footing load reached 170kPa, crack was found to initiate at the second layer from top of slope and a horizontal crack developed at mid height of slope. Subsequently, loading plate inclined towards the slope face similar to plain model test, as the load reached value of 270kPa. At this moment, the top layer began to crack. The third phase of cracking appeared when load value reached 290kPa. At 290kPa, a new horizontal crack developed at the inner of footing and reached the toe or bottom of slope.

It was also observed that the first and second phases primarily involved shallow failure surface generation with many local failure surfaces. As the third phase was reached, deep failure surface was initiated from slope toe towards base of footing. The model test of reinforced slopes with facing panel did not show any local failures like plain slope and reinforced slope without facing. Moreover, an entire different failure surface was observed for reinforced slope with facing panels. The failure surface passed through the end of each reinforcement bar in a direction parallel to slope face. Such a failure surface was classified as ‘block failure’ by the authors.

The failure surface observed for model tests of steep slopes further confirmed shallow failure surface for plain slopes and deep failures for reinforced slopes. However, for reinforced slopes without facing the crack was found to end above the bottom or slope toe in case of steep slopes. Also, for reinforced slopes with facing, block failure was observed for even steep slopes. Based on the observations from model tests, authors concluded that reinforcement and facing panels are effective in preventing collapse of mild and steep slope by local failures. The failure surfaces of all the model tests as observed by Kodaka et al. [47] are given in Fig. 2.12.

The load – settlement studies carried out by authors further signified the advantage of using reinforcement and facing panels for soil slopes. It was found from load – settlement curves that reinforced slopes with facing panels depicted the maximum failure loads with considerable settlement in comparison to plain slope for both mild and steep slopes. Moreover, reinforced slopes without facing showed failure load greater than plain slope but smaller than reinforced slope with facing panel. However, in all cases the significant vertical settlement for slopes is found.

The axial strain measurements for various reinforcements corresponding to mild and steep slopes signified that maximum outward movement is observed at middle height of slope. For mild and steep slope with facing demonstrated maximum axial strains as compared to similar slopes without facing. It was also observed that axial strain was found to maximum at slope faces for upper steel bars. As the depth of reinforcement increases from the slope top, maximum axial strains are found to occur near the reinforcement inner end. It was also investigated that there might be cases where two strain peaks may occur along reinforcement. The axial strain distribution further demonstrated that reinforcements are effective against slope failure and restrains slope deformation.

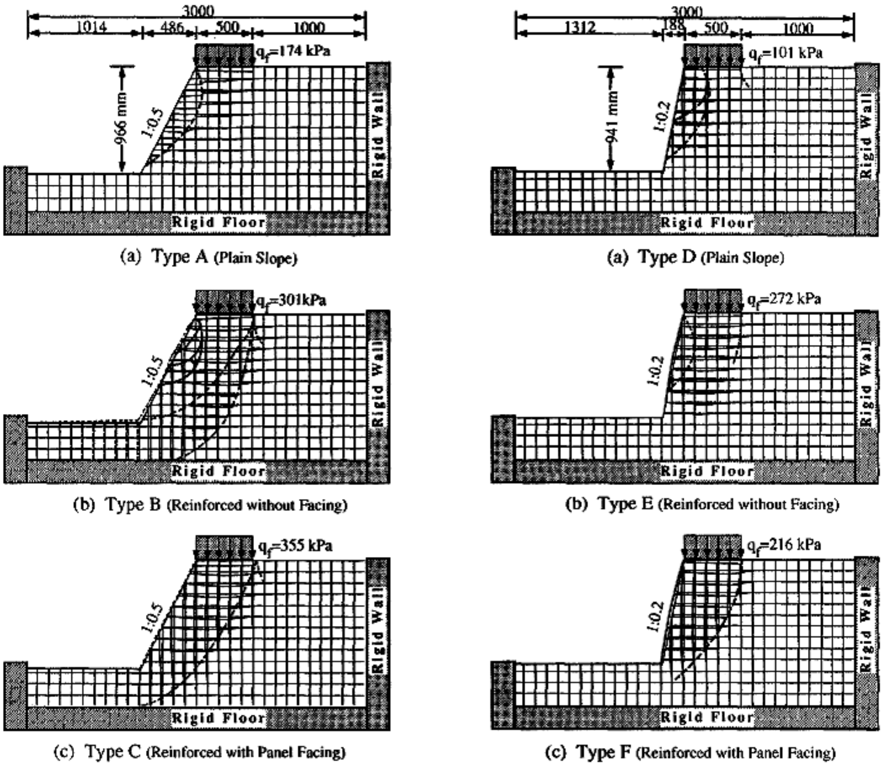

Fig. 2.12: Failure surfaces and deformations observed for mild slopes as Type A, B and C and steep slope as Type D, E and F (After Kodaka et al. [47])

Kim et al. [48] conducted model test studies by carrying out 14 model tests on soil – nailed slopes using two construction sequences of excavation followed by loading for simulating new construction and loading followed by excavation for simulation of in – situ rehabilitation. The general configuration of model box used box was 1.22 m high x 1.22 m wide x 2.44 m long. The box was restrained to an allowable lateral deflection of 0.5 mm by attaching steel angles at 0.3 m centre – to – centre vertical spacing. Scratch – resistant plexiglass was used on both sides of model box to render it frictionless. The effective height of the model soil slope was 1.22 m to accommodate the loading mechanism which comprised of an air bag placed into a channel -

shaped steel frame. To simulate the phase construction of approach embankment, wooden strips were stacked at front and rear of model box to support backfill (Fig. 2.13). For simulating excavation, layer by layer removal of wooden strips is done.

The backfill material consisted of uniformly graded sand with maximum and minimum dry density of 16.8kN/m^3 and 14.1kN/m^3 respectively. The effective size (D_{10}) of backfill is 0.3 mm. The angle of internal friction is 40° determined by drained triaxial tests. The backfill material is filled in layers of 100 mm thickness such that maximum dry density is maintained for the entire soil model. In order to have constant unit weight for each layer, predetermined weight of backfill is poured into a known volume. The load is applied on 0.3 m wide and 1.12 m long area using an air bag inflated with compressed air to apply a pressure of 104kPa. For soil – nail system to deform vertically, a steel frame was bolted to the model box which prevented the upward movement of air bag. The air bag was so designed that it allowed a vertical deformation of 38 mm. The nails made up of Polystyrene and installed without driving at inclination angle of 15° to the horizontal with horizontal spacing of 300 mm between the nails. The use of polystyrene as a material for nail was accounted for its ease of handling, homogeneous and breakable nature under tension, shear and bending. Two types of polystyrene specimen were used by the authors (1) low - density polystyrene for tests without loading and (2) high - density polystyrene for tests with loading condition. The tension resistance for polystyrene nails was determined from direct tension test and bending stiffness was calculated from deflection tests. The Young's modulus of 27.6MPa for both low – density and high - density polystyrene nails was determined by beam deflection test.

The nails were arranged in three columns by dividing the model in three independent sections. Each section was separated from the other by sheets of negligible strength placed between cut facings. This was done in order to minimize the effect of friction between soil – nailed system and plexiglass from affecting the middle independent section of nails. Since the facing panel was not designated to play any significant structural role, it was made up of double folded flexible aluminium foil so as to perfectly fit the irregularities of cut slope and be continuous in nature. The whole sole aim for facing was to restrain the backfill flow during failure and account for any local failures that might persist during failure. With the use of 100 mm high elements, the facing of model slopes was carried out with proper connection with nails being maintained using double cardboard paper and pins. The complete set – up of model soil nailed slope is shown in Fig. 2.14.

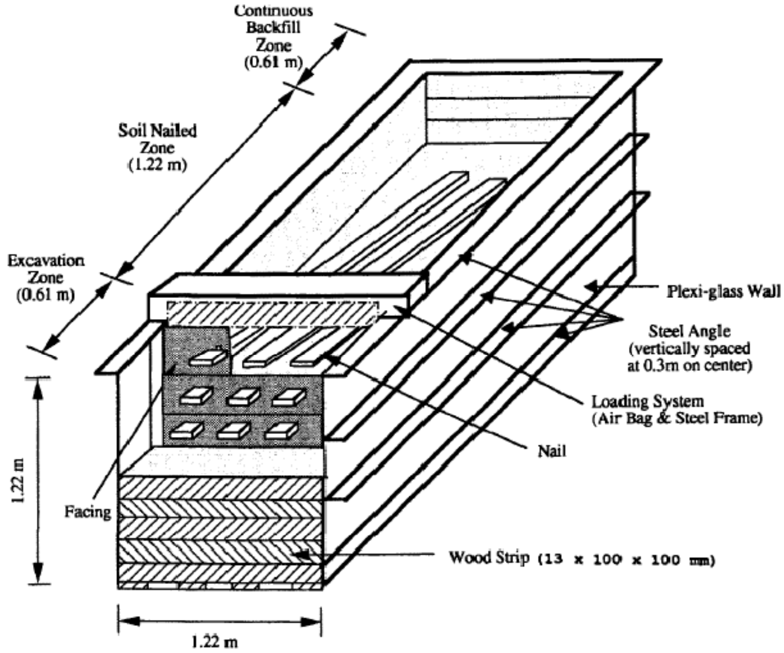

Fig. 2.13: Schematic diagram of soil – nailed model structure (After Kim et al. [48])

The use of cardboard paper served two purposes (1) Enabled nail and facing to function as a single unit and (2) Minimized local tear around nail cut hole by uniformly distributing the mobilized tension force in nails. The observations made during model testing primarily involved the vertical and horizontal displacements of slope with gradual increasing surcharge load and tension resistance of nails with increasing surcharge. For test sequence of excavation followed by loading, it was investigated that vertical settlement and horizontal displacement of facing increases with increase in surcharge load.

However at failure, both displacements were found to increase while an abrupt decrease in surcharge load was observed. On the other hand for loading followed by excavation test, surcharge load remained constant throughout the excavation sequence while horizontal displacement was observed to increase suddenly at failure. The observed variations of vertical and horizontal displacements with time are given in Fig. 2.15.

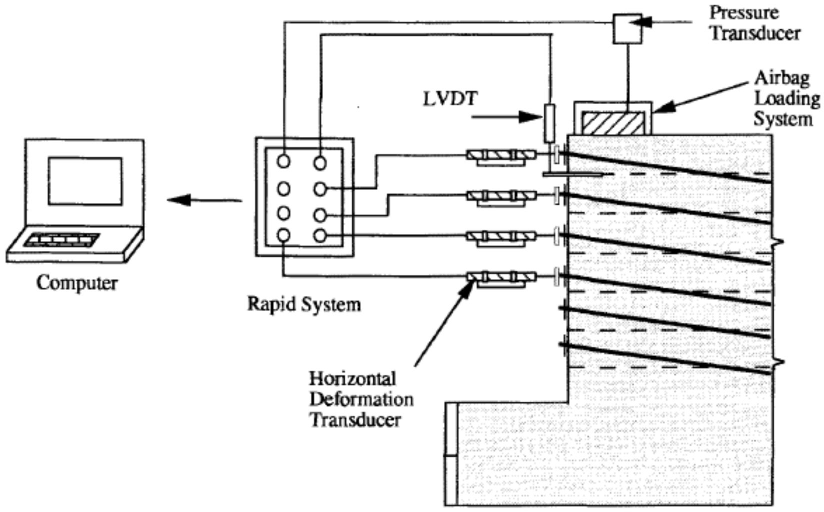

Fig. 2.14: Schematic diagram of instrumentation scheme for excavation followed by loading test (After Kim et al. [48])

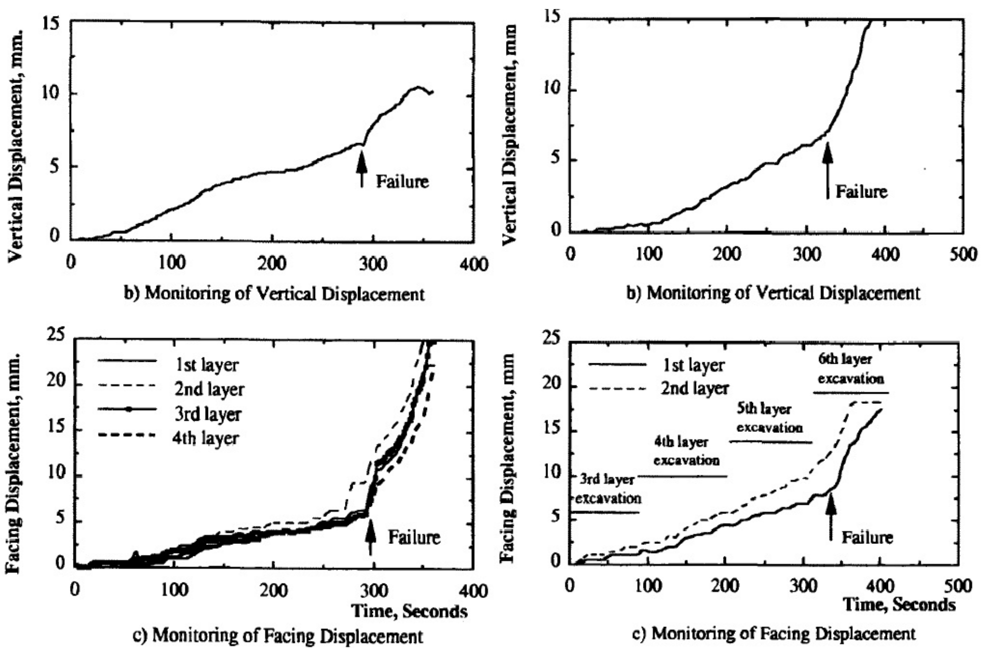

(A) (B)

Fig. 2.15: Typical instrumented data for (A) Excavation followed by loading scheme (B) Loading followed by excavation scheme (After Kim et al. [48])

Moreover, for both tests scheme, the authors observed that breakage of nails occurred during failure. The effect of tension resistance on the nails with surcharge was found to increase with increase in surcharge. It was also determined that the tensile strength of nails can be increased by increasing the cross – sectional area of nails. In order to study tension resistance of nails with change in cross – sectional area, variation of surcharge and overburden ($Q + \gamma H$) with maximum tension resistance per unit surface area ($T_{max}/S_v S_h$) was plotted (Fig. 2.16). It was observed from the plot that a non – dimensionless parameter (TN) can be calculated having value of 0.15 which was similar to theoretical value obtained from kinematical limit analysis and other model tests conducted by previous researchers.

An equivalent earth pressure (K) was also determined and can be calculated as given in Equation (2.2):

$$K = \frac{T_{max}/S_v S_h}{Q + \gamma H} \tag{2.2}$$

The equivalent earth pressure was found to yield the same value as TN for without surcharge condition. It was also noticed that due to interaction of surcharge and soil – nailed slope, top nails were restrained from outward movement.

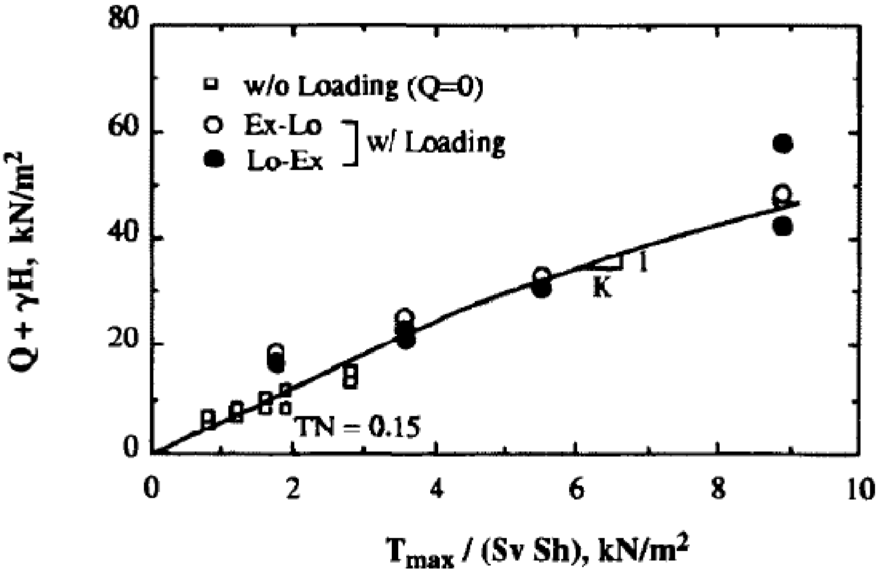

Fig. 2.16: Variation of vertical pressure ($Q + \gamma H$) at failure with maximum tension resistance ($T_{max}/S_v S_h$) from model testing both for with and without surcharge condition (After Kim et al. [48])

The state of stress in the upper part of soil – nail structure mainly resembled earth pressure at – rest condition (K_0). This further signified that top nails will primarily govern the failure or undergo breakage at failure in contrast to soil – nailed slope without surcharge where nails at mid- height of slope were found to break under failure. Thus, to understand the variation of maximum tension in nails with surcharge, a non – dimensional parameter (R_t) was developed.

The variation of normalized surcharge (Q/γH) with R_t under a linear variation of K from TN to K_0 was determined theoretically by Equation (2.3) and compared to values obtained from model testing.

$$\frac{Q}{\gamma H} = \frac{\frac{R_t}{TN} - 1}{1 + \frac{1}{TN}\left(1 - \frac{TN}{K_0}\right)\frac{R_t}{X_0}} \tag{2.3}$$

Where,

$X_0 = Q/gH$

$R_t = \dfrac{T_{max}}{S_v S_h \gamma H}$

It was found from the plot (Fig. 2.17) that model testing and theoretical results are in good agreement for X_0 variation of 5 to 10. With X_0 evaluated as 10, the equivalent earth pressure was found to vary from TN to K_0 with normalized surcharge. This suggested that as surcharge is applied on a soil – nailed system, state of stress in the upper regions tends to approach earth pressure at - rest condition which was also observed from field testing.

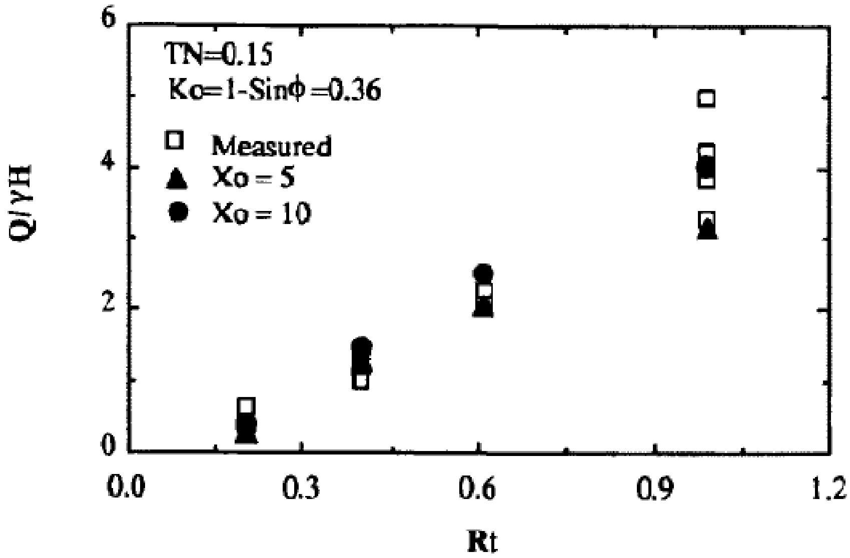

Fig. 2.17: Comparison between measured and estimated variation in non – dimensional surcharge (Q/γH) with non – dimensional maximum tension resistance (R_t) (After Kim et al. [48])

In order to assess the locus of breakage of nails during failure, the authors classified the nails as rigid and flexible. The locus of breakage of nails for without surcharge condition was taken as reference. It was observed that both testing schemes revealed the same locus as the reference conditions. Moreover, locus of breakage of nails was found to be unaffected by the loading of slopes. Based on the observations of model testing, the authors concluded that at top of slope under surcharge condition for both schemes, stresses are similar to earth pressure at rest. The maximum horizontal displacement of slope facing is only significant up to 0.25 to 0.4 times the height of slope and locus of breakage of nails is independent of nail rigidity and surcharge.

Soil – nailed model tests using phosphate – bronze nails of 5 mm diameter and 750 mm long round bars in iron ore backfill was conducted by Nishida and Nishigada [49] (Fig. 2.18). The properties of iron ore backfill used in the study were given as γ = 29.5 kN/m^3; D_{50} = 0.55 mm; c = 4.8 kN/m^2 and ϕ = 42.8°. The density of iron ore backfill was found to be 45kN/m^3, which was the only difference between iron ore backfill and sandy soil.

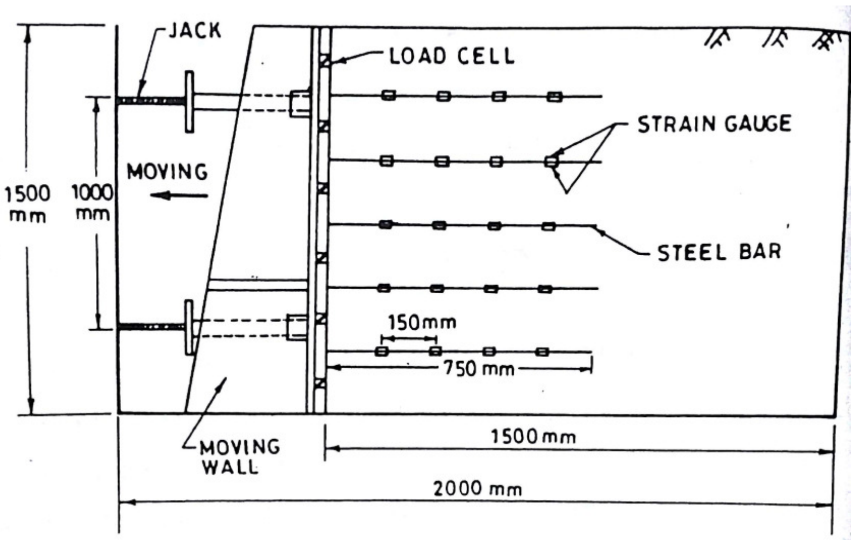

Fig. 2.18: Model set up of soil – nailed cut (After Nishida and Nishigata [49])

The failure of nailed cut was caused by the wall movement which was fixed with a rigid facing consisting of 200 mm wide and 50 mm thick aluminium bars. The phosphate – bronze nails were varied in vertical spacing and number of bars used. Two strains gauges were fixed on the upper and lower portion of nails to study the bending strains generated along nail during failure. The horizontal spacing of 75 mm was kept constant for all nails. The variation in vertical spacing and corresponding number of bars used were determined as 6 bars when S_v = 50 cm; 9 bars when S_v = 37.5 cm; 15 bars when S_v = 25 cm; 27 bars when S_v = 15 cm and 57 bars when S_v = 7.5 cm with nail arrangements as shown in Table 2.2.

Through the model set up of reinforced cut, the authors investigated nail forces by measuring strains along nail length, effect of nail spacing by conducting with and without reinforcement model tests and reinforcing mechanism of nails.

Table 2.2: Arrangement of reinforcing bars in model tests (Nishida and Nishigata [49])

Number of reinforcement	0	6	9	15	27	57
Space	-	50.0 cm	37.5 cm	25.0 cm	15.0 cm	7.5 cm
Arrangement	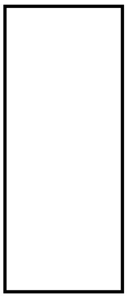	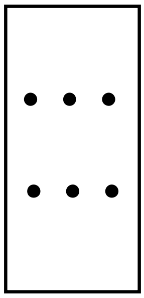	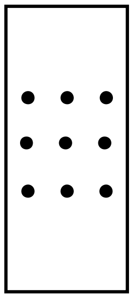	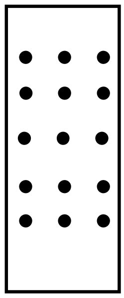	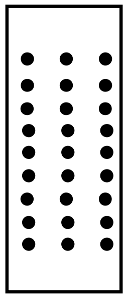	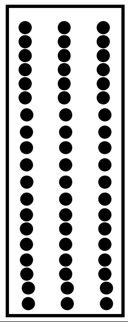

The authors observed that strain distribution along nail axis is symmetrical in pattern with maximum strains observed at intersection of nails and active zone. As observed from the plot between strain of reinforcement bar against installation ratio i.e. ratio of total sectional area of nail to area of reinforced slope surface (Fig. 2.19), it can be seen that small strains are generated when 9 bars are used. However, as the numbers of bars are increased to 15 maximum strain value of 1.4×10^{-3} is found for installation ratio of 0.065%. With further increase in number of bars to 27, decrease in strain value is observed with increasing installation ratio.

The variation was accounted for the fact that as fewer bars are used for reinforcement, the effect of peripheral soil confinement is minimum with small strain development. The reinforcing action of bars is not sufficient to with hold the soil around it during failure and hence soil passes through without any restriction. Now, as the number of bars is increased to more than 15, large soil restrainment is attained. Consequently, soil movement under failure is restricted which lowers the strains generated in subsequent nails. Thus, reinforcing force of nails is found to decrease with restrained soil movement in reinforced area of soil – nailed cut.

Another finding from experimental study for model tests was observed from plotting the variation of coefficient of earth pressure against moving wall displacement (Fig. 2.20). The earth pressure was reported to have been measured using load cells fixed on to the moving wall surface. The earth pressure is found to decrease as the number of nails is increased from 6 to 27 from earth pressure at rest condition corresponding to wall movement of 0 mm to active earth pressure condition at 30 mm displacement. Moreover, it was observed that earth pressure decrease is found to be significant from 6 bars to 27 bars beyond which earth pressure variation is approximately constant. This signifies that for achieving maximum soil restrainment over reinforced area, optimum number of nails should be 27.

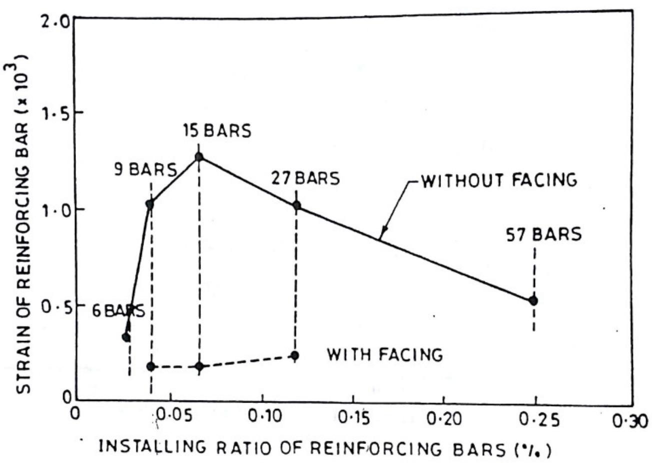

Fig. 2.19: Strain against installation ratio (After Nishida and Nishigata [49])

This was however against the optimum number of bars determined for maximum reinforcing force over reinforced area which was reported as 15. The difference in number of bars for attaining maximum reinforcing force and maximum restrainment of soil was concluded to have developed from two different reinforcing mechanisms. The authors also concluded that using a rigid facing significantly reduces the strains on reinforcing bars and should be treated as a secondary parameter in design of soil – nailed cuts.

In the same year for better understanding of effect of nail length, nail inclination, nail installation method and facing rigidity on performance of soil – nailed model was studied by Raju [28]. The test model tank of dimensions 1500 mm (length) x 600 mm (width) x 1000 mm (height) was fitted with 12 mm thick Perspex sheet on two sides with rear side consisting of 20 mm thick plywood. The backfill soil comprised of poorly graded medium fine sand with properties of G = 2.61; R_D = 50% and ϕ = 45°. The sand was filled in layers and unit weight of each layer was kept constant at 15 .5 kN/m^3. For achieving uniform unit weight throughout the sand layer, rainfall technique was employed by dropping sand from a fixed height of 150 cm. The nails were fabricated using 10 mm x 10 mm x 1.0 mm hollow aluminum square pipes of lengths adopted as 0.8H, 1H and 1.25H, where H is the slope height. The nails were installed by driving or pre – buried at inclinations of 0° and 10° with horizontal.

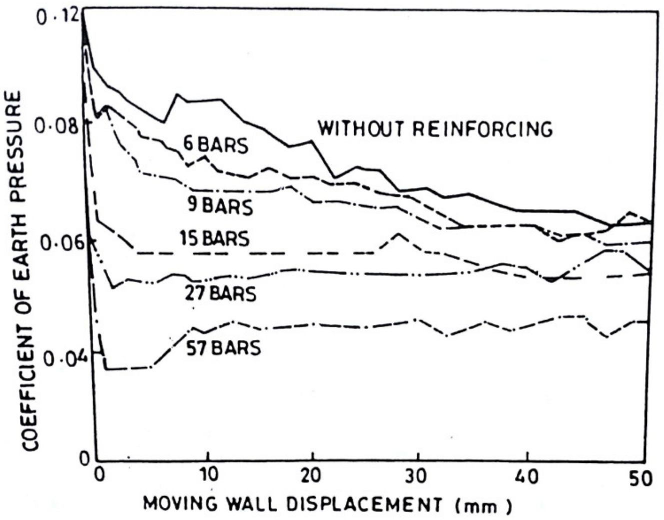

Fig. 2.20: Earth pressure variation with moving wall displacement (After Nishida and Nishigata [49])

A total of 6 model tests (Fig. 2.21) were carried out with same configuration using a pre – buried 1.0 mm thick aluminium sheet facing. The failure of model slope was generated using uniform surcharge pressure at the horizontal surface of retained soil. The observation carried out during model testing primarily involved horizontal displacement of model wall, vertical settlement of model top surface, nail forces generated during excavation and application of surcharge. To study the effect of rigidity of facing development of earth pressure behind facing was also investigated.

The authors observed that during model testing the horizontal displacement was maximum not near the crest but at a distance of 300 mm from top surface. The lateral displacement was governed by wall rotation about the model toe. It was reported by the authors that such a trend can be attributed to the 2:1 vertical stress distribution taken into consideration due to strip loading. The stress distribution signifies that no increase in lateral pressure under surcharge loading acts up to the depth of 200 mm from top. However, model test no. 5 showed variation from this common trend. For model test no. 5, rigid facing was used. Due to the rigid facing, a linear horizontal displacement is observed due to cantilever rotation of rigid facing about toe.

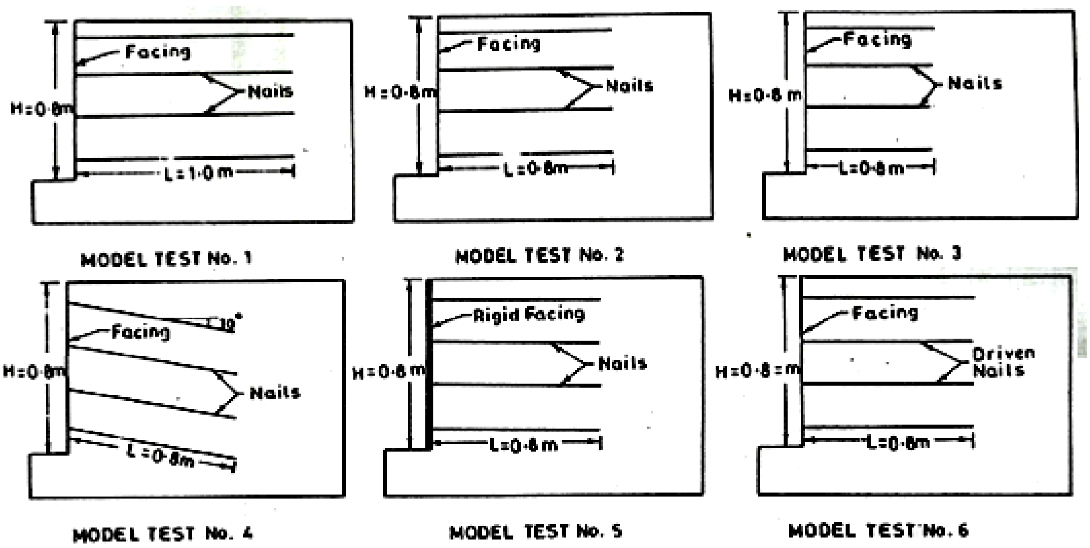

Fig. 2.21: Model tests set – up with different nail lengths and nail inclinations (After Raju [28])

Raju [28] described a term as deflection ratio which was ratio of maximum horizontal displacement at crest to total height of cut. It was observed that model tests constructed with factor of safety smaller than 1.2 depicted higher deflection ratios. Such observations were reported for model test no. 3 and model test no. 5.

The vertical settlement as observed from model testing showed that vertical deformation of nailed walls is higher than the corresponding lateral displacements. The maximum nail forces generated in nails was influenced by the adopted method of installation. For driven nails, higher nails forces were reported as compared to pre – buried nails for same surcharge loading. Moreover, the installation method also affects the location of maximum nail force. For driven nails as used in model no. 6, maximum nail forces were recorded at 300 mm depth whereas for pre – buried nails as used in model test no. 1, 2, 3, 4 and 5, maximum nail forces were achieved at 500 mm depth. The variations in nail forces due to installation was accounted for earth pressure envelopes generated in model tests with buried nails as compared to model tests with driven nails.

The length of nails was also reported to affect the failure load for model tests. The model tests which included smaller nail length depicted reduced failure load values as compared to model tests with larger nail lengths. It was also investigated that as the nail inclination is varied from 0° to 10°, an increase in failure load is achieved. The experimental investigation also revealed that slip failure surface for different mode tests was found to be a curved failure surface.

The failure surface passed through the model toe and intersected the top surface at right angles. Hence, the authors concluded that failure surface can be approximated as an arc of log – spiral curve.

In order to further enhance the understanding of effect of nail length, spacing and nail inclination, model tests on soil - nailed retaining wall was performed by Rajagopal and Ramesh [50]. Using a poorly graded sand with properties of C_u = 1.96, C_c = 1.05, D_{10} = 0.25 mm, γ_{min} = 14.97 kN/m^3, γ_{max} = 18.5 kN/m^3 and ϕ = 41°, a soil – nailed model retaining wall was constructed in a tank with dimensions of 200 cm (length) x 74 cm (width) x 200 cm (height). The backfill relative density was maintained at 70% with individual facing blocks used as facing to attain a height of 180 cm. the model retaining wall was reinforced using mild steel rods of diameter 12.5 mm with length varying from 600 mm to 1600 mm. the number of nails used in mode testing were also varied between 9 to 24. Each nail was fixed with four strain gauges to measure the nail forces along nail lengths, two LVDTs were attached to wall facing to measure horizontal displacement, soil pressure and vertical displacement was measured by pressure cells and to measure load at facing, load rings were used. The complete instrumented soil – nailed retaining wall is given in Fig. 2.22. The failure was achieved by applying a surcharge load through an inflated air bag.

The observations reported by authors included that failure surface for model retaining walls can be obtained by plotting the locus of maximum strains along the wall height. The maximum strain points are often reflected by the points where failure surface intersects the nail. The failure surface meets the top surface of wall at right angles. The inclination of nail from horizontal is found to increase the failure load and decrease the slope facing deformation. The measurements recorded from LVDTs indicated that large horizontal displacements occur at the wall top and tend to decrease towards the wall toe. The load rings indicated that loads in the upper row of nails was constant throughout testing procedure but was found to drop abruptly as failure was achieved. The variation in load signifies the pullout of top row of nails at failure leading to sudden decrease in nail load. The measurements from pressure cells depicted that lateral soil pressure behind the wall facing increased linearly and decreased suddenly at failure. Moreover, it was concluded by the authors that friction between tank walls and soil affected the factor of safety calculation for modeled soil – nailed retaining wall.

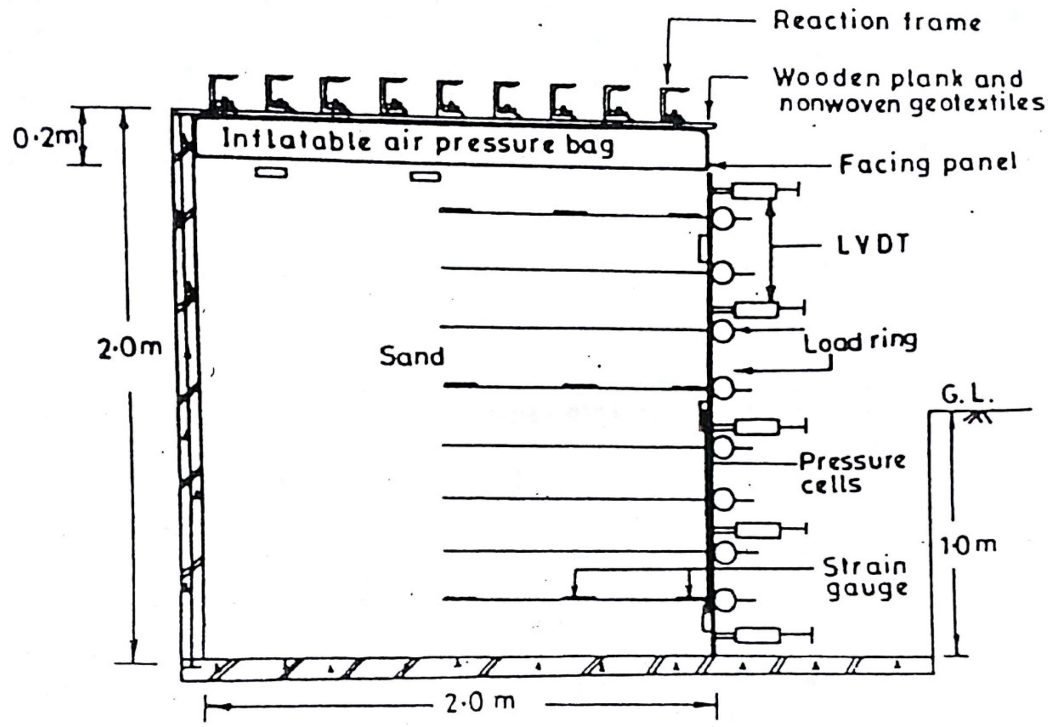

Fig. 2.22: Soil – nailed retaining model tests set – up (After Rajagopal and Ramesh [50])

Gosavi et al. [51] developed a pseudo – static analysis method for soil – nailed cuts and used two model tests to validate the proposed method. The dimensions of model tank used were (length) 2000 mm x (width) 870mm x (height) 1100 mm. The sides of the tank were made by 6 mm thick mild steel sheets covering one complete side, the rear end of tank and a length of 800 mm on the other side of tank. The remaining length of 1200 mm was covered with 12 mm thick Perspex sheet (Fig. 2.23). The connection between mild steel sheets and tank was made rigid by welding whereas Perspex sheet was bolted to the tank. The front side of tank was to serve as the facing of nailed wall. In order to facilitate the measurement of lateral displacement, wall facing was hinged at its bottom. The entire tank was placed on a base of steel channels which was rested on concrete floor. A 19 mm thick plywood board of size 100 mm x 865 mm was used as facing. The rigid facing served as replacement of shotcreting carried out at site due to unstable nature of cuts in sandy soil.

The facing were provided with circular holes for installation of nails at respective locations. Two different configurations of vertical spacing and constant centre – to centre horizontal spacing of 300 mm with edge distance of 135 mm were used. The facing consisted of holes in square (3 x 3) and rectangular (2 x 3) patterns with 25 mm x 25 mm aluminium flaps to protect leakage of sand. The material testing of sand locally obtained from river Solani revealed that soil consisted of poorly graded sand with e_{max} = 0.79, e_{min} = 0.45, C_u = 5, G = 2.54, D_{10} = 0.16 mm, γ = 16.5 kN/m^3, R_D = 70% and ϕ = 38°. To achieve a model height of 1000 mm, sand was compacted in layers using rainfall technique to ensure that unit weight of 16.5 kN/m^3 is maintained at all places. This unit weight reflected to a relative density of 70%. The soil nails used in experimental study comprised of tor steel bars of diameter 10 mm and 12 mm with length of 0.75 H. The installation of nails was carried out by filling the sand up to centre of holes of facing. The nails were positioned through the holes and filling of sand was continued till the next row of nails. After installation of last row of nails, sand filling was done to achieve the desired height of 1000 mm. Another model test was constructed using the same construction procedure but with nail length of 0.8 H.

The surcharge was applied on nailed slope with the help of known weight of bags filled with sand. The increase in surcharge load was also achieved by using cast iron weights on 8 mm thick mild steel plate placed directly over wall crest. The lateral deflection of nailed wall was measured using dial gauges and factor of safety calculation for test1 and test 2 was carried out using the theoretical formulation derived by the authors earlier. The failure surface was also observed and recorded with investigation of failure wedge done by inspecting the colored band deformations occurred during wall failure.

From the model testing carried out using two different configurations of soil nail pattern, it was observed that nailed wall depicts higher failure surcharge with nails installed at vertical distance of 170 mm for first row of nails, 500 mm for second row of nails and 830 mm for third row of nails. For wall with first row of nails at 250 mm and next row at 750 mm from top surface of wall, smaller failure surcharge load are recorded for same lateral wall deflection. Moreover, factor of safety of 1.12 and 1.10 was calculated for test1 and test2 respectively. This clearly signified that higher reinforcing action is achieved by using more soil nails at small vertical spacing.

The use of flexible facing for soil nailed wall was investigated by Pokharel et al. [51] with the help of finite element analysis method. In order to validate the numerical modelling and understand the actual behaviour of flexible facing, physical model test was conducted in a steel tank of size 2.2 m (length) x 2 m (width) x 2 m (height). The backfill material consisted of clay obtained from Lawrence, Kansas area. The soil testing revealed backfill as highly compressible inorganic clay (*CH*) with $G = 2.71$, $w_L = 55$, $w_P = 25$, $OMC = 24\%$, $\gamma_d = 15.44$ kN/m^3.

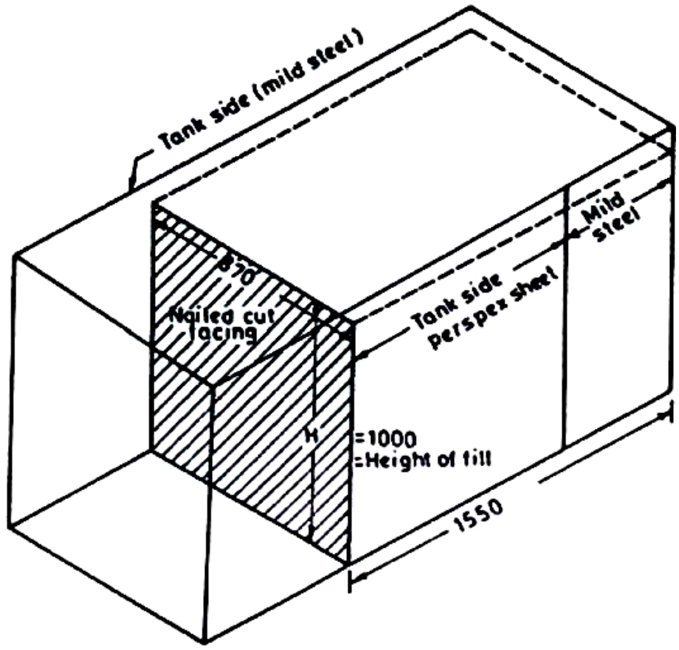

Fig. 2.23: Model set up of soil – nailed wall (After Gosavi et al. [51])

The model test wall was reinforced using four threaded steel soil nail bars of diameter 24.35 mm having an elastic modulus of 199.94GPa. The nails were installed at spacing of 1.5 m x 1.5 m. Similar to actual soil nail installation using grouting; the steel bars were covered by 152.4 mm diameter cement concrete layer before installation. For proper orientation of nails, an arrangement of connecting chain links was fixed at rear interior of model steel tank. The clay is filled in steel tank with lifts of 15 cm after compacting it with jackhammer. The density of fill is carefully monitored by regular measuring after every three layers using drive tubes. The first row of nails was placed above 15 cm of base layer. Similarly, next row of soil nails were installed after the next lift of 15 cm. The procedure was continued till desired height is achieved. Each nail is fixed with a strain gauge at top surface of nail with connection to a smart dynamic strain recorder (DC-204R) for strain measurements. The specifications of strain gauges used are given as grid resistance of 120.0 ± 0.6 ohm, grid length of 6.35 mm and grid width of 3.18 mm. The top surface of model wall is provided with a geosynthetic drainage layer with permeable side in downward direction. To simulated rainfall in case failure was not achieved after initial loading, a set of water supply tubes were also attached to this drainage layer. The surcharge load is applied using geofoam layer and 245kN capacity load actuator to apply pressure in steps of 18.3kN/m^2. The flexible facing is comprises of galvanized wire mesh, a 99.65 g non - woven geotextile and 330 mm x 190 mm x 10 mm dimension spike plates. The competed model test wall with flexible facing is shown in Fig. 2.24.

The horizontal wall facing displacement was measured using string potentiometer while failure surfaces, settlement of wall and breakage of anchor connections was inspected thoroughly by excavating sections. The results recorded from model testing revealed that under first surcharge pressure application of 13.8kN/m^2, no wall deformation is observed. However, wall deformation at a distance of 305 mm from bottom of tank occurs as the surcharge value reaches 27.5kN/m^2. The breakage of connection link chains occurred with 46 kN/m^2 of surcharge pressure.

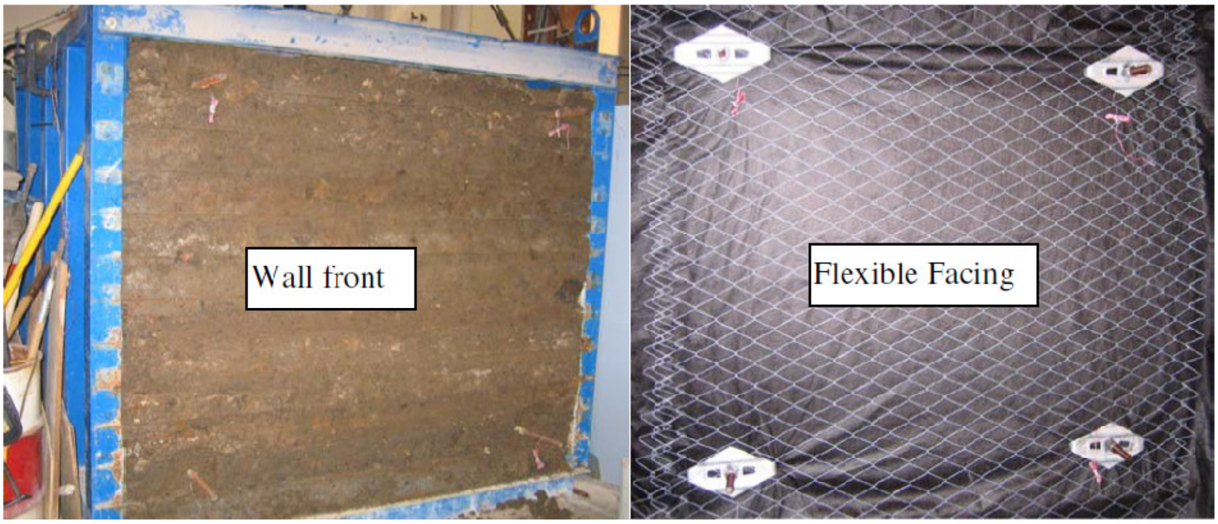

Fig. 2.24: Complete soil - nailed wall front with flexible facing used (Modified after Pokharel et al. [51])

With the failure of connection links, top row of nails were found to move out by 31 cm and top surface of wall suffered a settlement of 16 cm (Fig. 2.25). Though, vertical and horizontal deformation of walls was significant, flexible facing was still found to perform well. The authors accounted downward and outward movement of walls for breakage of connection links. At failure, pullout of 15 cm was recorded for top row of nails. Moreover, larger strains are also found to generate on top row of nails due to downward face movement (Fig. 2.26). The authors attributed this behaviour to development of bending stress rather than tension stresses which have originated due to vertical wall settlement and face slumping. The authors concluded that failure of soil – nailed wall with flexible facing primarily occurs due to vertical wall deformation and recommends flexible facing to be used for short walls with tolerance to significant deformation.

Fig. 2.25: Horizontal and vertical deformation of soil – nailed wall (after Pokharel et al. [51])

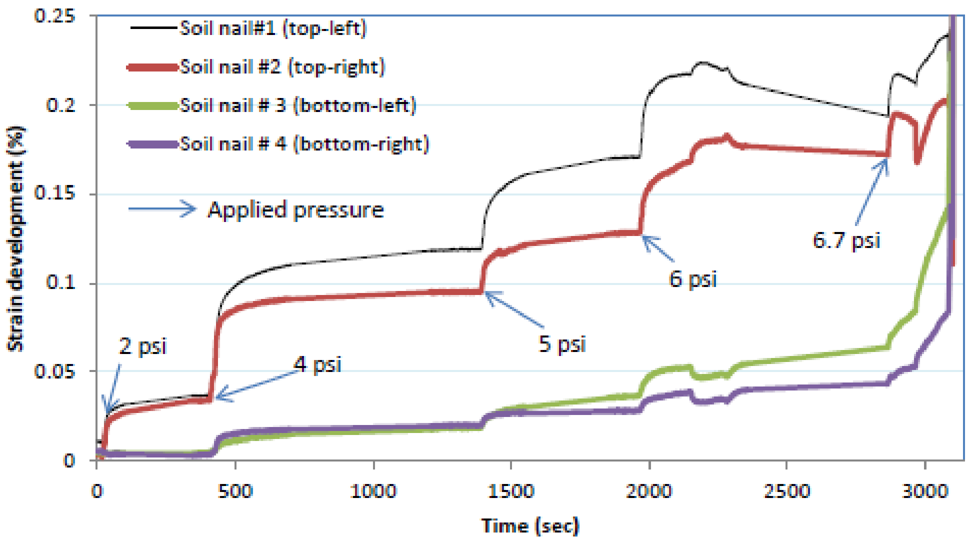

Fig. 2.26: Development of strains in nails with gradual increasing surcharge (after Pokharel et al. [51])

Jewell [52] carried out studies to study the effect of reinforcement on mechanical behaviour of soils. From his research work it was concluded that reinforcement changes the state of stress and strain in soil and thus influences the shear strength of soil. The soil stress - strains are further altered with variation in inclination of reinforcement, which can increase or decrease the soil shear strength. When reinforcement is used with soil, the principle axis of strain increment is reoriented. The presence of reinforcement close to soil strain helps achieving reduced strains due to inhibition of failure. When the reinforcement is aligned parallel to soil tensile strains, tension stresses are generated in reinforcement during failure. However, if reinforcement is far away from tensile strains and close to compressive soil strains, stresses developed in reinforcement are compressive in nature. Thus an important finding of his work revealed that shear strength of soil is increase with an optimum inclination of reinforcement. The optimum inclination is attained when soil tension strains are close to reinforcement.

Since then, many researchers have made an attempt to further enhance the understanding regarding mechanism of reinforcement inclination through laboratory investigations [45, 46]. However, for determining the optimum nail inclination very few researchers have carried out static model testing of soil – nailed slopes. Centrifuge model testing of reinforced slopes at different slope angles with investigation of effect of nail inclinations on reinforced slope failure mechanism has been conducted in past by Tei et al. [53], Zhang et al. [54], Hong et al. [55], Huang et al. [56], Deepa and Viswanadham [57], Rotte and Viswanadham [58, 59].

Rawat et al. [60] conducted static model testing and numerical study using slope angles of 30°, 45° and 60° with three different nail inclinations of 0°, 15° and 30° with horizontal to determine the failure mechanism, optimum nail inclination and nail forces. The model test box size of 750 mm x 300 mm x 400 mm was filled with Yamuna sand composed of quartz and mica flakes. The properties of sand were given as poorly graded sand with G = 2.72, γ_{max} = 15.68 kN/m^3, γ_{min} = 13.23 kN/m^3, ϕ = 37° and negligible cohesion (c). The fabrication of model tank was carried out using 10 mm thick Perspex sheet.

The soil nails were made using hollow aluminium pipes with length of 80% of slope height. One end of nail was tapered to facilitate installation while the other end was threaded to accommodated nail head. The nail head consisted of 20 mm x 20 mm square shaped 10 mm thick Perspex sheet attached at the threaded end of nail. For uniform distribution of load at slope crest a 25 mm thick Perspex sheet of dimensions 290 mm x 160 mm was used. The complete soil – nailed slope (Fig. 2.27) is placed in Hounsfield S series Compression Machine (load frame capacity of 50 kN) to apply gradually increasing surcharge load at rate of 10 N/s. Each nail is provided with three foil type strain gauges (Gauge Factor = 2.1) for measurements of strains developed during slope deformation. By addition of 3% of water, model sand slopes are prepared having 25 mm of base layer and a total height of 400 mm achieved through layer by layer construction of slope. At each layer, care was taken to ensure that 70% relative density is maintained. The physical inspection of failure surface is done through observation of deformed colored soil bands used between different layers of slope.

The results of model testing revealed that nail inclination of 0° offered the maximum load carrying capacity for all slope angles of 30°, 45° and 60°. The failure load was found to decrease with increase in nail inclination from 0° to 15° and then to 30° with horizontal. The failure surfaces observed through Perspex sheets during failure showed that circular slip surface was found to originate primarily from toe of slopes with local cracking throughout the slope body. The top of slope suffered horizontal cracks with 60°reinforced slopes depicting vertical cracks between nails.

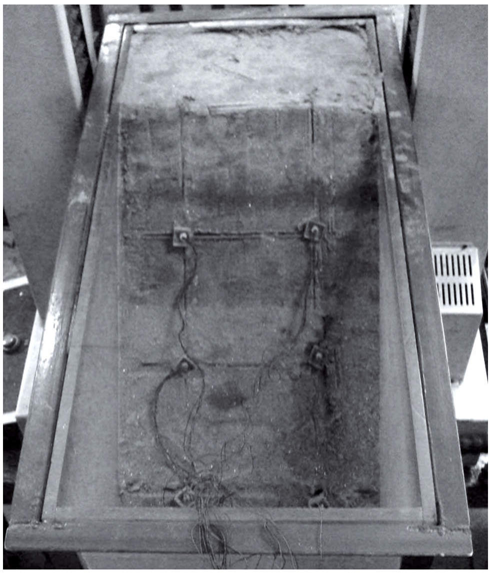

Fig. 2.27: Model tank with soil – nailed sand slope (After Rawat et al. [60])

Other features of slope failure was slope face bulging which was uniform for nail inclination of 0° for all slope angles. The bulging of slope face was also observed to have occurred at nail inclinations of 15° and 30° being small at slope top and increased near the toe of slope. The settlement of slope crest was common to all slope angles and nail inclinations. The forces generated in nails were calculated from measured strains. The top of row of nails depicted maximum strain development as compared to middle and bottom row of nails. Thus, maximum nail forces are found to develop at top row of nails in all slope angles with 0° nail inclination. Moreover, it was also investigated by the authors that different strains were observed to have occurred along the nail length of a single nail. The strain gauges fixed at the rear end of nail for top row depicted maximum strain whereas this pattern was found to shift to centre strain gauge for middle row of nails. For bottom row maximum strains were recorded by the centre or top strain gauge fixed near the nail head. These measurements also revealed that locus of highly strained points along different nails constitute the failure slip surface.

Using Adige river medium – fine sand with properties as determined by Gottardi and Simonini [61] as G = 2.71, $\gamma_{d(max)}$ = 16.5 kN/m^3, $\gamma_{d(min)}$ = 13.6 kN/m^3, $\phi_{(peak)}$ = 42 - 43°, $\phi_{(critical)}$ = 35°, C_u = 2.0 and D_{50} = 0.42 mm, Sanvitale et al. [62] modelled a slope with dip angel of 80°, face width = 39.5 cm and height = 40 cm (Fig. 2.28). During the construction of slope, 85% of relative density is maintained by using pluvial deposition method. The slope is prepared into a caisson which is inclined at 20° from slope rear for homogeneous deposition of sand. With the construction of sand layers, soil nails of external diameter 6 mm, length 32.5 cm are installed in 3 (rows) x 4 (columns) at spacing as S_v = 10.2 cm and S_h = 13.2 cm respectively. Eight strain gauges were glued pair by pair on nails situated at (x = 15.3 cm, y = 25.4 cm) from the slope top at spacing of 2.3 cm, 10.4 cm, 18.5 cm and 26.7 cm from the slope face. The distribution of axial strain and corresponding axial stress along nail length were measured using strain gauges. The slope settlement was recorded using three vertical displacement transducers and lateral images during failure were captured using a digital camera. To study the development of displacement with increase in loading was recorded using Particle Image Velocimetry (PIV) technique [63].

The slope face is attached with four different types of facing (i) Polymethyl methacrylate (PMMA), thickness = 4 mm (ii) Brass (BRASS) facing, thickness = 0.25 mm (iii) 1 mm wires used as steel mesh and welded at 6 mm spacing orthogonally (MESH) (iv) a woven steel net (NET) formed by 0.24 mm diameter wires. The axial stiffness of all the facings was constant with variation of one order from (i) to (iii) in terms of flexural stiffness. The facing formed by NET was deformable having minimum axial and flexural stiffness. Two other different types of PMMA facings were used which were made discontinuous by cutting them into tiles. These discontinuous facing were classified as PMMA95 and PMMA25, where 25, 95 corresponds to covering area protected by the facing (Table 2.3). In order to prevent leakage of dry sand from facing mesh holes, a low – resistant geosynthetics was place behind each facing. The rear of slope was also installed with similar geosynthetics material so as to build up homogeneous test conditions. The slopes with different facings were driven to failure by application of a 24 kN/m^2 surcharge load and simultaneously, removing wooden blocks from the front of facings to simulate excavation procedure.

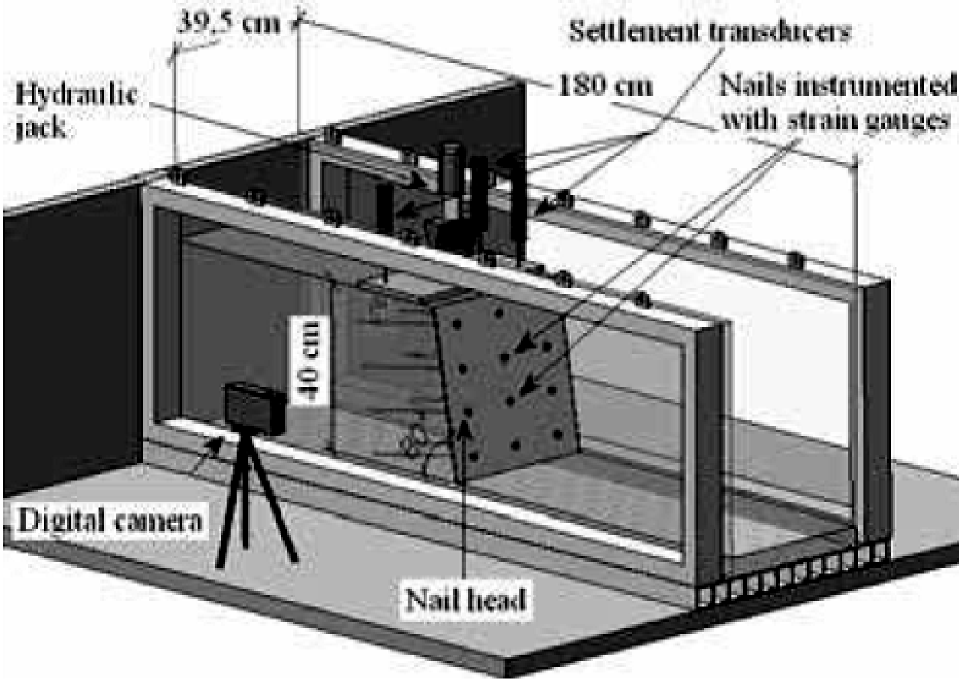

Fig. 2.28: Perspective view of modelled soil - nailed slope (After Sanvitale et al. [62])

During the model testing it was observed that slopes with continuous facing of PMMA and MESH depicted vertical settlement of 0.13% of slope height. The vertical settlement for facing with PMMA25 and NET was observed to be 0.5% of slope height. However, for discontinuous facing (PMMA95) having sufficient flexural stiffness showed settlement of 0.27% of slope height. This was attributed to stiffness provided against lateral deformation by the rigid PMMA95 facing.

Table 2.3: Properties of facing adopted for model tests (Sanvitale et al. [62])

Model	Facing	Covering ratio (%)	Wire dia. (mm)	Wire spacing (mm)	Young's modulus E (GPa)	Axial stiffness EA/m (N/mm)	Flexional Stiffness EJ/m (nmm^2/mm)
a	PMMA	100	4	-	3.2	12800	17066.67
b	MESH	100	1	6	210	26180	3318.06
c	BRASS	100	0.25	-	126	31500	236.25
d	NET	100	0.24	1.02	70	3105	22.66
e	PMMA95	95	4	-	3.2	-	-
f	PMMA25	25	4	-	3.2	-	-

The tension forces developed in nails were observed at near nail head (N_{head}) and at a distance from facing (X_{max}) where tension force was maximum (N_{max}). It was observed that facing with significant stiffness (PMMA and PMMA95) depicted highest tension values which decreased with reducing facing stiffness. The minimum tension forces are observed for NET and PMMA25. It was also found that value of N_{head} - N_{max} was gradually increased with decreasing deformability of facing and was maximum for NET and PMMA25 facing.

The load – settlement curves obtained from model testing revealed that as flexural rigidity of facing is increased, failure of model slopes is attained at higher load (Fig. 2.29). The lateral deformation of slopes suggested that deformable facing undergo larger horizontal displacement. From the findings, authors concluded that discontinuous facing with high flexural rigidity helps in attain restricted lateral deformation of slopes but limited shear stress mobilization along nails. On the other hand, if deformable facings with low axial deformability are used, horizontal deformation can also be regulated. Overall, in both the cases, safety is achieved against global stability of soil – nailed slopes.

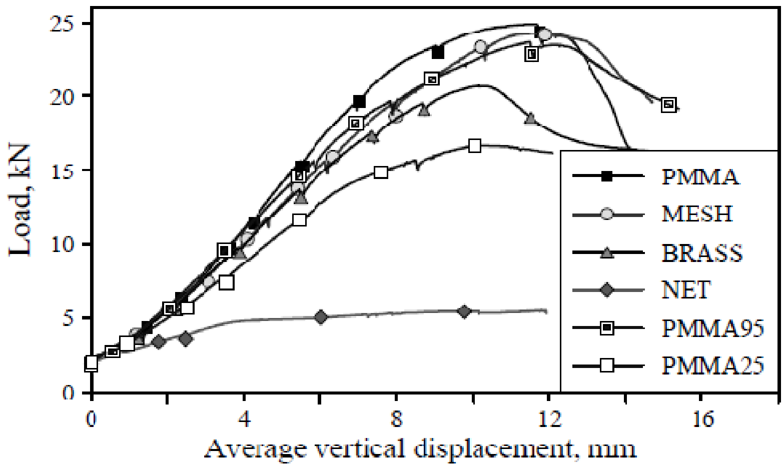

Fig. 2.29: Load versus displacement variation for different facings (After Sanvitale et al. [62])

Model testing of 1.2:1 and 5:1 slopes under various loadings was carried out by Zhang et al. [64]. The model slope was constructed in an aluminium tank of size length = 50 cm, width = 20 cm and height = 35 cm. The slopes included a 5 cm base layer with a total height of 28 cm. The slopes were composed of cohesive soil with properties G = 2.7, D_{50} = 0.01 mm, $\gamma_{(max)}$ = 1.8 g/cc, $\gamma_{d(max)}$ = 1.51 g/cc, OMC = 17%, w_L = 33.5%, w_P = 15.5%, S = 75%, ϕ' = 24° and c' = 26 kPa. The effective shear strength parameters are determined from consolidated – drained (CD) shear test. The soil nails used for model testing have diameter of 1 mm with tensile strength of 200MPa and modulus of elasticity of 210GPa.

Three different nail lengths varying between 4 cm to 8 cm were used for model testing. The nails are inserted at right angles to slope face with uniform spacing of 2 cm in both horizontal and vertical direction. The complete set – up of soil nailed model slopes (Fig. 2.30) was placed in a 50g – ton centrifuge testing arrangement.

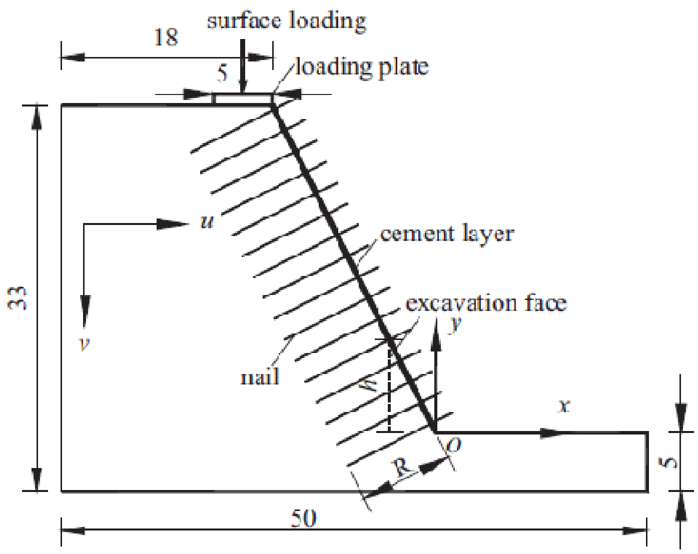

Fig. 2.30: Schematic view of testing model under different loading conditions (After Zhang et al. [64])

The facing of slope was done using a special made Portland cement which was smeared on slope face having 2 mm of thickness at 1g. The cement paste was left for two hours in which it attained the desired compressive strength of 15 MPa. Within two hours, cement layer was soft enough to facilitate the insertion of nails to desired positions. During the setting time of cement facing layer the centrifuge was maintained at centrifugal acceleration of 50g. The loading of slopes was simulated using a load transducer installed on the loading plate during the vertical loading tests. A laser displacement transducer is employed to measure settlement of loading plate. Using an image – recording and displacement measurement system, images from lateral side of slope were recorded during slope deformation. Through manual inspection and construction by hand, slip surface of the slope were determined according to the captured images.

Based on the observations for model testing with three different loading conditions of self – weight, vertical loading and loading with excavation, the authors concluded that stability of slopes can be significantly increased by soil nailing. The slip surface can be shifted to deep failure surface by using longer length of nails. The soil nailing technique also helps in arresting the tension cracks. The cement facing layer also exhibited fracture along with slippage of soil mass within slope body before the actual slide of slope was obtained. This observation leads to the conclusion that a coupled effect is observable with progressive slope failure under loading.

The deformation of slope is initially local occurring within slope body which propagates and constitutes the slip surface. The use of soil nails reduces deformation localization and hence the occurrence of slip surface is delayed. Due to loading on slope crest, deformation is observed which is different at different points corresponding to various loading conditions. The soil nails are found to deform under conditions of pullout and bending. Slopes loaded under self – weight showed slip surface generation from toe and travelling up to the surface. The slip surfaces corresponding to vertical and excavation with loading condition depicted a shallow slip surface. The authors finally remarked that degree of saturation can significantly change formation of slip surface and hence the conclusion derived should be applied with care to actual soil – nailed wall design.

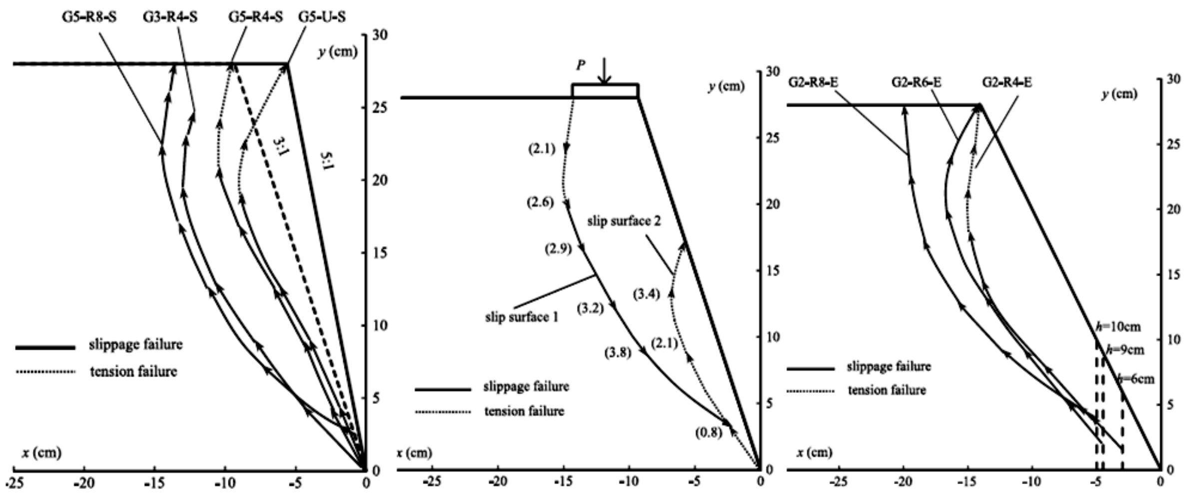

(a) (b) (c)

Fig. 2.31: Failure surfaces under different loading tests (a) self – weight test (b) vertical loading test (c) excavation test (After Zhang et al. [64])

The use of conventional soil nail has always been associated with difficulty in installation due to required drilling and grouting. The installation produced significant spoils and careful monitoring during installation. To overcome the installation problems, a new type of nail was employed for slope stability by Chan and Raman [65]. The model soil slopes are constructed from a mixture of sand, kaolin and water (8:2:1) named as SKW. The undrained shear strength parameters of SKW soil was determined by small shear box (60 mm x 60 mm x 120 mm) testing under vertical stresses of 10, 20 and 300 N/cm^2. The shear box testing revealed that SKW soil had negligible cohesion (c) with ϕ = 38.5°.

The prototype nail 190 mm (length) with 165 mm threaded by 4 mm deep groves was used to reinforce SKW soil slope having slope angle of 78.5°. The threads on nail were inclined at 10° to horizontal so as to render it helical spiral shape and facilitate screw – in mechanism during installation. With the requirement of producing minimum soil disturbances, threaded nail surface ensured that greater contact surface is available for better pullout resistance and soil – nail interaction. The hollow stem of soil nail had an inner diameter of 24 mm and wall thickness of 4 mm. The hollow stem provided accommodation of 9000m^3 of soil. The nail head was fabricated using a 60 mm diameter and 10 mm thick circular nail head with a 5 mm deep grove for insertion of straight head manual driving tool (Fig. 2.32). The SKW soil was placed and lightly compacted in Perspex sheet sided model box measuring 400mm x 300mm x 300mm. To ensure uniform load distribution a platform of 20mm width was placed at slope crest. A constant vertical stress of 700kN/m^2 was applied through ENERPAC hydraulic jack system, where a piston touching the platform transferred the load onto the slope.

The soil – nailed slope was assumed to have failed at vertical deformation of 56 mm or at slope settlement of 20% of slope height. For carrying out a comparative study and to understand the soil nailing mechanism, five types of tests were undertaken (i) Unreinforced slope testing (ii) slope with single soil nail having smooth surface (iii) slope with triple soil nail having smooth surface (iv) slope with single soil nail of screw – in type (v) slope with triple soil nail of screw – in type.

The findings of research work included determination angular distortion ratio and volumetric deformation index for different model tests configuration. It was reported by the authors that a reduction of 37% is achieved in angular distortion ratio for soil – nailed slope using triple screw – in type soil nails as compared to soil – nailed slope using smooth surface soil nails. Similarly, volumetric deformation index reflected an improvement of 33% in resisting slope deformation by screw – in type soil nails as compared to conventional smooth surface soil nails.

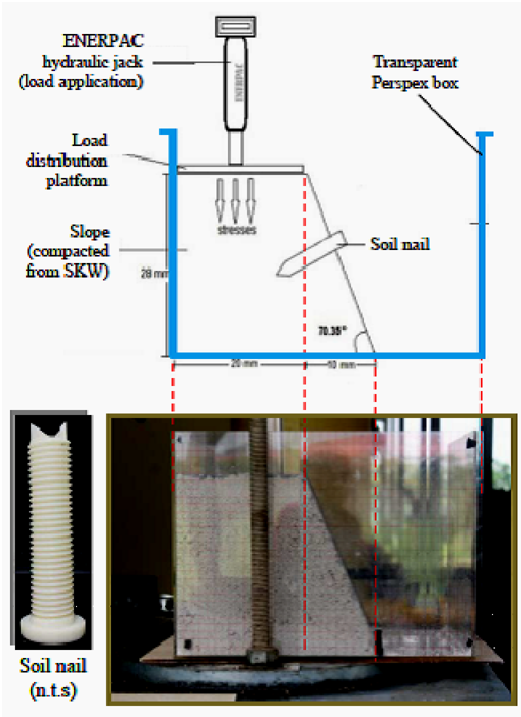

Fig. 2.32: SKW soil slope with screw – in type soil nail model set up (Chan and Raman [65])

2.3 Large – Scale Testing of Soil – Nailed Structures

Based on the observation of soil – nail mechanism from small - scale model tests, a large number of soil nailing projects has been executed since the last 40 years. The basis of soil – nail interaction, nail inclination, failure mechanism and wall deformation characteristics were well understood through laboratory testing. With these concepts, soil nailing has been used for new constructions and remedial measures for unstable structures [66]. For simplification, the field testing of soil nailed structures are covered under different types of soil nails as given in Table 2.4 to 2.6. For grouted soil nails other than circular, nail diameter (D_{nail}) and grout hole diameter (D_{grout}) for square, strip or angular cross - sectional nails are calculated as equivalent circular steel sections given by equation 2.4 and 2.5.

$$D_{nail} = \sqrt{\frac{4 \times Cross\ sectional\ area\ of\ nails}{\pi}} \quad (2.4)$$

$$D_{grout} = \frac{Perimeter\ of\ nail\ section}{\pi} \quad (2.5)$$

The ratio of maximum horizontal deflection of wall to total height of wall is defined as deflection ratio $\left(\frac{\delta_{max}}{H} \times 100\right)$.

For driven nails having cross – section other than circular, perimeter ‘p’ has been defined for square or angular sections.

Table 2.4: Summary of large – scale soil nailing application with grouted nails

Project	Construction and soil type	Ground conditions			$\beta°$	$i°$	H (m)	L (m)	D_{grout} (mm)	D_{nail} (mm)	S_v x S_h (m x m)	$\left(\frac{\delta_{max}}{H} \times 100\right)$ (%)	References
		γ	c	$\phi°$									
Foundation excavation for the Samaritan Hospital, Portland, Oregon, USA	New Construction; medium to dense silty fine lacustrine sand	-	20	36	90	15	13.7	-	100	12.7	-	0.30 to 0.32	Shen et al. [67, 68]
Temporary excavation	New construction; Uniform fine sand	-	-	-	-	-	15	8	-	30	-	0.2 to 0.3	Gassler and Gudehus [4]
Underground car parking at la Clusaz, France	New construction; Moraines clay	22	0	36	80	10	14	11	-	-	2 x 3	0.01	Guilloux et al. [69]
Deep foundation for the PPG Industries HQ, Pittsburgh, USA	New construction; cohesionless granular soil	-	-	-	90	8	10	8	127	-	1.2 x 1.2	-	Nicholson and Wycliffe – Jones [70]
Reinforced earth wall, Fraus Tunnel, France	Remedial construction; granular material	13	-	-	90	-	8	5	-	28	2 x 2	-	Long et al. [71]
Retaining wall, Denholme Clough, Bradford, UK	Remedial construction; sandstone	-	-	-	80	15	3	5	115	16	1.5 x 1.5	-	Bruce and Jewel [27]

Note: (-) Data not available

γ	Unit weight of soil, kN/m^3	$i°$	Nail inclination with horizontal	D_{nail}	Nail diameter
c	Cohesion of soil, kN/m^2	H	Maximum height of structure in project	S_v	Vertical spacing of nails
$\phi°$	Angle of internal friction	L	Maximum nail length in project	S_h	Horizontal spacing of nails
$\beta°$	Wall face inclination with horizontal	D_{grout}	Diameter of grout hole for nail	δ_{max}	Maximum lateral wall displacement

Table 2.4: cont…

Project	Construction and soil type	Ground conditions			$\beta°$	$i°$	H (m)	L (m)	D_{grout} (mm)	D_{nail} (mm)	S_v x S_h (m x m)	$\left(\frac{\delta_{max}}{H} \times 100\right)$ (%)	References
		γ	c	$\phi°$									
Two Nailed retaining walls, West Germany	One new construction, one remedial construction; Weathered debris of Keuper marl and Layer of loam	20	0	35	70	20	7	3.4	-	-	1.1 x 1.1	0.21	Schwing and Gudehus [42]
Distressed timber wall, South Carolina	Remedial construction; Stiff sand silt to dense silty sand	17.3	0	25	90	20	5.2	9.1	100	25	1.2 x 1.5	-	Harmston and Rhodes [72]
Vertical cut Rover's Long bridge work, UK	New construction; Highly weathered Keuper marl overlaid highly weathered Keuper sandstone	20	0	35	90	15	10	8	100	25	1.5 x 1.5	-	Baker [73]
Rio Piedras, Puerto Rico	Remedial construction; Uncontrolled fill, residual soils and weathered rock	18.4	14.4	30	90	15	16.5	12.2	305	25	1.5 x 1.5	0.17	Cheng et al. [74]
Stabilization of cutting slope along high speed railway line	Remedial construction; Keuper marl	21	10	-	60	15	23	20	135	28	2.0 x 2.5	-	Gassler [11]
Learai Beach Niteroi R J	New construction; Gneiss sprolites	-	-	-	75	-	35	9	90	25	1.5 x 1.5	-	Ortigao and Palmeira [19]

Table 2.4: cont…

Project	Construction and soil type	Ground conditions			β°	i°	H (m)	L (m)	D_{grout} (mm)	D_{nail} (mm)	S_v x S_h (m x m)	$\left(\frac{\delta_{max}}{H} \times 100\right)$ (%)	References
		γ	c	ϕ°									
Rail bridge Abutment	New construction; Phyllites with bedding planes in direction of slopes	-	-	-	75	-	-	10 to 25	75	25	2 x 2.5	-	Unterreiner et al. [75]
Stabilization of Mine waste slopes	Remedial construction; Dry mixture of sandstone, shale	-	-	30	75	-	6.3	3 6	200	23.3	1.5 x 1.8 1.8 x 1.8	-	Drumm et al.[76]
PIE expressway cutting, Singapore	Remedial construction; Residual clayey silt	17.5	15	27	83	15	9	7	100	25	1 x 1	0.28%	Raju [28]
New cutting realignment of Lletty Turner Bends	New construction; Glacial till deposits overlying sandstone argillaceours strata	-	-	-	45	-	20	14	140	25	1.5 x 1.5	-	Barkley et al. [77]
Experimental soil nail wall	New construction; Dense sand	16.1	3	38	90	-	5	8	63	-	1.5 x 1.5	0.06%	Benhamida et al. [78]
Hong Kong slope stabilization	Remedial construction; Decomposed Grade V volcanic rock	-	4	34	55	45	22	12	100	-	2.3 x 2.3	-	Forth [79]

Table 2.4: cont…

Project	Construction and soil type	Ground conditions			β°	i°	H (m)	L (m)	D_{grout} (mm)	D_{nail} (mm)	S_v x S_h (m x m)	$\left(\frac{\delta_{max}}{H} \times 100\right)$ (%)	References
		γ	c	ϕ°									
Diversion of French Highway road No. 94	New construction; Gravel and talus material with significant sand	20	3.5	33	90	0	10	9.8	130	40	0.5 x 0.5	-	Knochenmus [80]
			2.5	37									
Underground railway line beneath Monaco complex	New construction	20	0	45	90	0	18	10 to 16	130	40	3 x 1.7	-	Knochenmus [80]
Broughton Heath near Chester	New construction; Poorly compacted fill	20	0	21	62	30	11.5	14	120	32	5.5 x 1.86	-	Martin [81]
Under bridge 314 in gate shead	New construction;	-	-	-	85	20	10.5	8	100	25	1 x 1	0.3 to 0.4	Martin [81]
Natural cliff stabilization at Bouley Bay Jersey	Remedial construction; Fine silt sand and coarse gravel	-	-	35	55	20	21	10	100	25	1.5 x 2.0	-	Warner and barley [20]
											1.25 x 1.5		

Table 2.4: cont…

Project	Construction and soil type	Ground conditions			β°	i°	H (m)	L (m)	D_{grout} (mm)	D_{nail} (mm)	S_v x S_h (m x m)	$\left(\frac{\delta_{max}}{H} \times 100\right)$ (%)	References
		γ	c	ϕ°									
Swift delta soil nailed wall under piled bridge abutment	New construction; Mixture of gravel silt with concrete and asphalt fragment	18.5	4.8	32	63	15	5.3	6.4	127	-	0.9 x 1.37	-	Briaud and Lim[82]; Hanna et al. [83]
Temporary excavation support at the sandy spring subway station	New construction; Very dense residual soil	19.22	19.2	28	90	-	20	17	200	-	2 x 2	-	Khalil et al. [84]
	Partially weathered rock	20.82	7.2	40									
Model test soil nail wall	New construction; medium dense fine to coarse sand traces of silt and gravel	-	-	-	-	15	6	6.7	114	25	1.5 x 1.2	0.06	Soliman and Ro [85]
NGES site at University of Massachusettes	New construction; Soft clay, silt and varved clay	-	-	-	90	20	9.1	5.5	100	19	1.5 x 1.5	0.15	Oral and Sheahan [86]
Landslide stabilization Elbow site	Remedial construction; Clayey gravels and sand	-	3	27	32	15	7.6	12.2	176	32	1.2 x 1.8	-	Turner and Jensen [87]
	Medium stiff to stiff sandy clay		4	31							1.7 x 2.1		

Table 2.4: cont…

Project	Construction and soil type	Ground conditions			$\beta°$	$i°$	H (m)	L (m)	D_{grout} (mm)	D_{nail} (mm)	S_v x S_h (m x m)	$\left(\frac{\delta_{max}}{H} \times 100\right)$ (%)	References
		γ	c	$\phi°$									
Busway for public transport from Brisbane's Central Business District to Logan City	New Construction; Loose fill .	18	0	30	-	10	20	12 to 15	150	12 to 16	1.5 x 1.0	0.1	His and Taylor [88]
	Compacted fill	20	5	35									
	Residual fill	18	24	15									
	Extremely weathered rock	20	5	32									
	Highly weathered rock	22	10	35									
	Moderately weathered rock	22	50	40									
	Slightly weathered rock	24	150	45									
Bukit Batok soil – nailed slope, Singapore	New construction; soft clayey silt with sand coarse gravel, stiff clayey silt and weathered Bukit Timah granite	19 - 24	20	30	30 - 75	-	18	11.6 -24	150	40-50	-	0.04	Ann et al. [89]
8-storey high-rise building at Waterfront, Niteroi, Rio de Janeiro State, Brazil.	New construction; residual soil from gneissic rock	-	0-19	32 to 33	-	10	40	15 to 24	75	25	-	-	Sayao et al. [90]

Table 2.4: cont…

Project	Construction and soil type	Ground conditions			β°	i°	H (m)	L (m)	D_{grout} (mm)	D_{nail} (mm)	S_v x S_h (m x m)	$\left(\frac{\delta_{max}}{H} \times 100\right)$ (%)	References
		γ	c	ϕ°									
U.S. Highway 26-89 through Snake River Canyon in northwest Wyoming	Remedial construction; Layer 1: fill of clayey gravel and clayey sand	-	3	27	-	15	1.8 to 3m	10	176	25	1.7 x 2.1	0.01 to 0.02	Turner and Jensen [91]
	Layer 2: colluvial or residual soil, Layer 3: stff to hard dark gray shale	-	14-148	22 to 36			4 to 7.6	12.2		35	1.8 x 1.2		
Rehabilitation of two failed slopes, Malaysia	Remedial construction; Site A: weathered Shale facies, with the existence of mudstone and siltstone.	-	30	33	14 to 45	-	30 to 42	12	-	-	1.5 x 1.5	-	Liew and Liong [92]
	Site B: weathered metamorphic rock with massive granitic intrusion.		0		14		45	6 to 12					
BJK Fulya Complex, Fulya, Istanbul	fractured silicified sandstone	-	-	-	85	10	32.5	10.2	-	105	2.1 x 2.1	0.15	Durgunoglu et al. [93]
Istinye Park Complex, Istinye, Istanbul	extensively fractured siltstone, claystone				80	10	22.0	10.1	-		3.0 x 3.0	0.44	
Kanyon Complex, Levent, Istanbul	extensively fractured sandstone, siltstone, claystone				85	10	28.3	11.6	-		2.3 x 2.3	0.34	

Table 2.4: cont…

Project	Construction and soil type	Ground conditions			β°	i°	H (m)	L (m)	D_{grout} (mm)	D_{nail} (mm)	S_v x S_h (m x m)	$\left(\frac{\delta_{max}}{H} \times 100\right)$ (%)	References
		γ	c	ϕ°									
Mashattan Residence, Maslak, Istanbul	extensively fractured siltstone, claystone	-	-	-	85	10	18.3	6.7	-	-	2.4 x 2.4	0.32	Durgunoglu et al. [93]
Tepe Shopping Mall, Maltepe, Istanbul	extensively fractured sandstone, siltstone, claystone				85	15	10	12	-		2.3 x 2.3	0.24	
Glacial tills, Ireland	New construction; Boulder clay with limestone bedrock	20	0	36-38	70-80	-	12	8 to 10	-	20 to 25	1.2 x 1.5	0.67	Menkiti and Long [94]; Long and Menkiti [95]; Skipper et al. [96]
Retaining wall at Yas project site, Tehran, Iran	New construction; dense to very dense gravel and sand with clay and silt.	17 - 19	5 - 20	20-36	90	15	29.3	6 to 14	101	32	1 x 2.5	0.16 to 0.23	Zolqadr et al. [97]

Table 2.5: Summary of large – scale soil nailing application with driven nails

Project	Construction and soil type	Ground conditions			β°	i°	H (m)	L (m)	D_{nail} (mm)	S_v x S_h (m x m)	$\left(\frac{\delta_{max}}{H} \times 100\right)$ (%)	References
		γ	c	ϕ°								
Railway wall for French railways at Versailles – Chantiers, France	New construction	20	10	33	-	20	5.6	5.5	50 x 50 x 5 (28 mm)	0.7 x 0.7	0.11	Rabejac and Toudic [98]
Motorway trench, Paris	New construction; Silty fine sand	20	10	33	90	20	11.6	7	50 x 50 x 5 (28 mm) 60 x 60 x 6 (32 mm)	0.7 x 0.7	0.12	Cartier and Gigan [99]
Experimental wall	Silty fine sand	-	-	-	90	20	5.5	5.5	50 x 50 x 5 (28 mm)	-	0.10	Cartier and Gigan [99]
Replacement of modular block slope	New construction; Over consolidated clay with chalk	-	10 5	23 25	56	-	6.3	5 3.2	36	1.26 x 1 0.8 x 1	-	Ingold [100]; Ingold and Miles [101]

Table 2.5: cont…

Project	Construction and soil type	Ground conditions			$\beta°$	$i°$	H (m)	L (m)	D_{nail} (mm)	S_v x S_h (m x m)	$\left(\frac{\delta_{max}}{H} \times 100\right)$ (%)	References
		γ	c	$\phi°$								
Alfred Mealpine football stadium, Huddersfield	Weathered mudstone and thin layer of coal	-	0	33	79-77	-	3.5	6	38	1 x 1	-	Hall [102]
			20	33			2.5	4.5				
Subway under a national highway, Bangalore, India	New construction; residual soil weathered to moderate	18	10 -20	25	90	-	5	3.5	20	0.5 x 0.5	0.1 – 0.4	Murthy et al. [103]
										0.4 x 0.4		
Vertical cut at M/s Hero cycles limited, Ludhiana, India	New construction; Poorly graded sand	15.5	0	27.5	90	0	3	2.1	25	0.3 x 0.3	0.0	Gosavi [104]

Table 2.6: Summary of large – scale soil nailing application with different innovative nails

Project	Nail type	Construction and soil type	Ground conditions			β°	i°	H (m)	L (m)	D_{nail} (mm)	S_v x S_h (m x m)	$\left(\frac{\delta_{max}}{H} \times 100\right)$ (%)	References
			γ	c	ϕ°								
Alberta Transportation (AT), New Sarepta	Launched nails	Remedial Construction; clay with moderate to low plasticity	-	-	-	26.5	-	6	6	40	1.4 x 1.4	-	Smith et al. [105]
Widening of 68th Street under the Route 169 overpass, City of Raytown, Missouri	Helical soil nails	New construction; very stiff lean clay to soft shale	-	-	-	-	0 10	3.7	3.5 4.6	38 mm (shaft) with 203 mm (helical flights)	1.2 x 1.8	0.29 – 0.52	Deardorff et al. [106]
Vertical excavation in well categorized engineered landfill	Spiral nails	New construction;	19.6	4.8	36	33.7	10	6	4.6	64	1.8 x 1.2	0.22	Upsall [107]; Upsall et al. [108]; Stephens et al. [109]
Field pullout programme, Hong Kong	Glass fiber reinforced polymer (GFRP)	New construction; completely decomposed granite	17.75	6.2	36.1	45-55	30	36	6	9.36	-	-	Cheng et al. [110]; Cheng and Wei [111]; Cheng et al. [112]
		localized colluvial deposits	17.16	3.4	35.5								

Table 2.6: cont…

Project	Nail type	Construction and soil type	Ground conditions			β°	i°	H (m)	L (m)	D_{nail} (mm)	S_v x S_h (m x m)	$\left(\frac{\delta_{max}}{H}\times 100\right)$ (%)	References
			γ	c	ϕ°								
Bervie Braes, Stonehaven	Self-drilled hollow bar	Remedial construction; weak silts and silty sand with discrete soft cohesive layers,	-	-	-	25-35	-	40	7-24	-	-	-	Lindsay et al. [113]; DYWI [114]
Failed steel – pipe wall in Fujian, China	Moso – bamboo	Remedial construction; fill layer, silty clay layer and sludge (soft soil) layer	-	10-17	10-14.8	45	10	5.4	4-12	100-110	0.2 x 0.2	-	Dai et al. [115]

From the review of literature carried out on large - scale model testing of soil – nailed slopes as given from Table 2.4 to 2.6 and Figs. 2.33 to 2.36, it can be observed that design parameters such as wall face inclination with horizontal (β°), ratio of nail length to wall height (L/H), inclination of nails with horizontal (i°) and nail influence area (S_v x S_h) play a significant role in the performance of soil – nailed structure. From Fig. 2.33, it can be seen that soil nailing has been widely used for retaining of vertical cuts (β° = 90°). It can also be observed that for construction and remediation of steep slopes of 70° - 80° has also been achieved by designing a soil – nailed system.

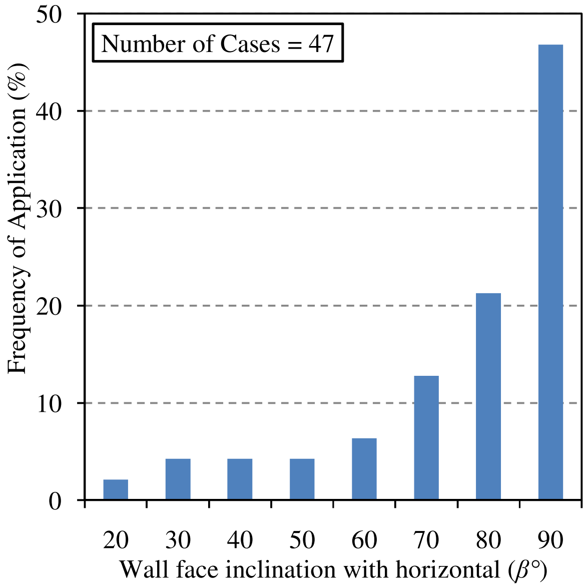

Fig. 2.33: Frequency distribution of wall face inclination

Fig. 2.34 clearly shows that commonly used length of soil nail vary between 0.5 to 0.8 times wall height. Longer nail lengths (> 1H) are primarily used for remedial construction work or experimental studies. However, using longer nail length increases the cost of construction; short length of soil nails may lead to reduction in performance of soil – nailed system. Thus, variation in nail length depicts that for designing a soil – nailed structure, an optimum nail length is required. Due to drill hole and grouting, longer tendon length varying between 8 to 20 m are used as grouting nails. For driven nails, smaller nail length are used varying between 3 to 7m. Moreover, for nails installed without grouting, variation in nail length is similar to driven nails as they make use of surface roughness to develop the necessary friction. Furthermore, it can also be reported that soil – nailed structure derives its mechanism through soil – nail interaction, which depends upon in – situ soil conditions. Though soil nailing technique has been employed in various soil types, they have always been a primary choice for $c - \phi$ soils. However, satisfactory performance has also been recorded for cohesive soils and residual soils.

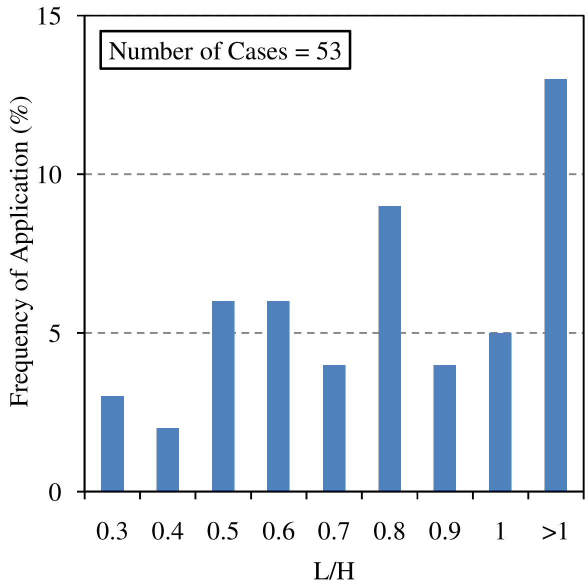

Fig. 2.34: Frequency distribution of L/H ratio

Apart from nail length, inclination of nail with horizontal has shown a variation from 5° to 20°. However, the optimum choice for nail inclination has a smaller range of variation between 10° to 15°. The frequency distribution of nail inclination (Fig. 2.35) clearly depicts that easy nail installation with best performance is attained at 15° with horizontal.

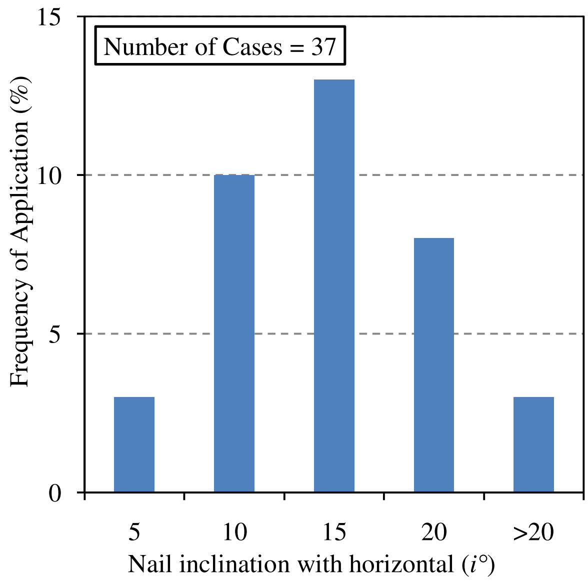

Fig. 2.35: Frequency distribution of nail inclination

The frequency distribution of nail influence area demonstrates a variation of 1 to 3 m^2 for majority of projects undertaken. It is observed that influence area for grouted nails is more (1.5 – 3 m^2) as compared to driven or nails without grouting (≤ 1m^2). The drill hole diameter for grouted nails is generally more than 100 mm which requires more horizontal and vertical spacing so as to accommodate nail without influencing the effect of adjacent nail. In case of driven nails, or nails without grouting such as helical or spiral soil nails, much smaller spacing can be achieved without disturbing the adjacent nail. It is clearly seen Fig. 2.36, horizontal and vertical spacing which renders nail influence area of about 2m^2 has been commonly implemented. Moreover, large nail spacing has yielded in higher nail influence area. The increase in influence area causes disturbances to large soil volume, which can enhance the deformation of soil – nailed structure.

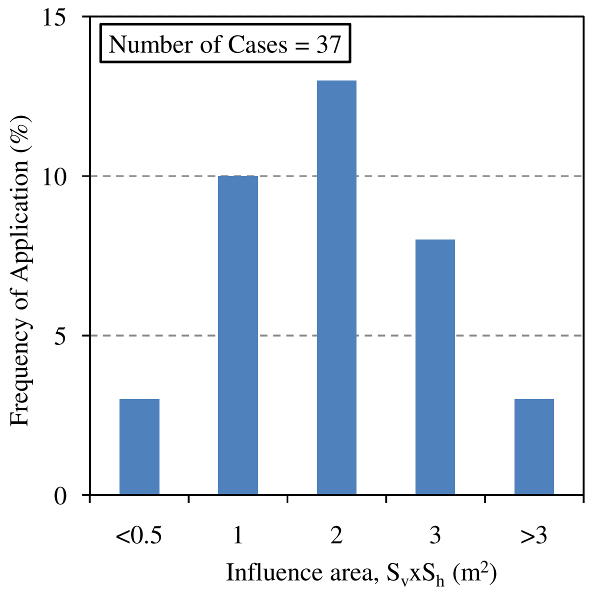

Fig. 2.36: Frequency distribution of nail influence area

The performance of a soil – nailed system is observed to be governed by the variation of design parameters. Fig. 2.37 shows that using soil nail technique as a new construction method or remedial measure has resulted in restricting the deformation of structure. Moreover, due to small deformation requirement for mobilizing the reinforcing effect of soil nails, maximum deflection obtained for various projects is within 0.4 % of wall/slope height (0.4H). This deflection becomes an important criterion in urban regions where deformation sensitive structures may be encountered adjacent to soil – nailed structures. Also, the small lateral deformation depicts the performance of soil nailing technique as a suitable stabilization method.

For majority of cases in literature, maximum horizontal displacement is found less than or equal to 0.1H.

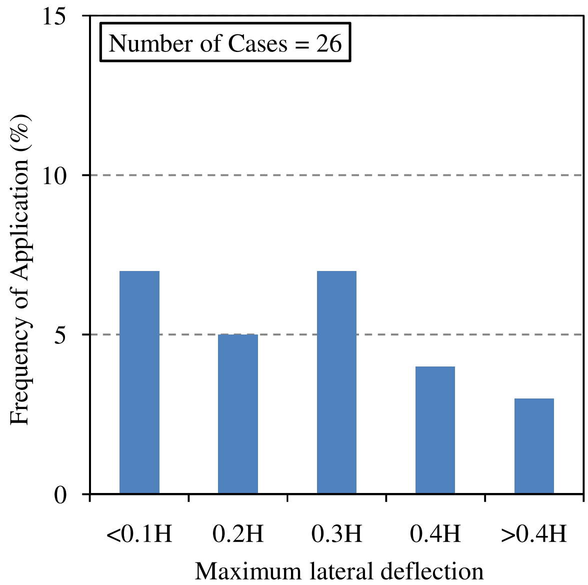

Fig. 2.37: Frequency distribution of maximum lateral deflection as % age of wall height (H)

It is also observed that soil nails can be driven or be installed without grouting. The driven nails can be well protected against corrosion which occurs in conventional nails due to the effect of grout on steel tendon. It is also found that soil – nail interaction can be derived through increased surface roughness of nails. With the advancement in technology, driving equipments are available, which facilitate ease of nail installation and produce minimal soil disturbances. Such soil nails offer less time consuming installation procedures and deliver significant results in reinforcing or stabilizing existing ground conditions as conventional grouted nails. An improved reinforcing effect is also observed by using helical soil nails and spiral groutless nails which have shown acceptable performance similar to grouted nails. To overcome corrosion of soil nails, utilization of material with higher tensile strength than steel has made glass fiber reinforced polymer be used as a replacement of conventional nails. The assessment of such innovative nails have shown that problems associated with conventional soil nails can be easily be rectified without sacrificing the performance of soil nails.

2.4 Pullout of Soil Nail

The soil nail is subjected to tensile forces during slope failure. Stresses are mobilized during shear at the intersection of slip surface with soil nails [116, 117]. However, Geoguide 7 [118] emphasis on external and internal failure modes of a soil – nail system. The internal failure modes are related to failure surface within the soil nailed ground. Along with failure at nail heads, slope facing, nail strength, and along grout-soil interface, pullout failure is also primarily an internal failure mode. The pullout of nail is defined as force mobilized along nail length in passive zone. The soil - nail interface friction governs a significant part of failure mechanism for soil – nailed structures. The interface friction helps transfer of tensile, shear and bending stresses from soil to nail. The amount of mobilized interface friction also known as apparent friction coefficient (f^*) is correspondingly determined by studying the nail pullout behavior (Eq. 2.4).

$$f^* = \frac{F_p}{p.L.\sigma_v} \tag{2.4}$$

Where, F_p = Pullout force, p = Nail perimeter, L = Nail length, $\sigma_v = \gamma.z + q$ = Normal stress, When the nail length in passive zone is insufficient, it renders a poor pullout resistance per unit length of soil nail. This leads to an occurrence of failure at the grout – soil interface. The pullout of soil nails have been investigated using laboratory tests as well as field testing. The effect of various parameters such as overburden pressure, nail surface roughness, degree of saturation and soil types has been well understood from these tests.

2.4.1 Direct Shear Tests

To understand the soil – nail interface mechanism, small and large shear direct tests was adopted by researchers like Jewell [52], Ingold [119] and Pedley [120]. Based on the direct shear box used by Jewel [52], soil nail pullout study was done by Tei [121]. A medium sized apparatus with plan dimensions of 254 mm x 153 mm was used. The height of sample box was 150 mm. Tei [121] reported the use of having a symmetrical direct shear testing because it closely reflects the actual soil shear deformation. In order to attain that lower and upper boundary were desired to be symmetrical. Moreover, with symmetrical boundary conditions, rotation of apparatus during shearing was also eliminated. This was achieved by fixing the top platen with upper portion of shear box.

The soil used for testing comprised of standard yellow Leighton Buzzard sands, 50/100 medium sand, 50/100 dense sand and 14/25 dense sand. The properties for 50/ 100 medium dense sand were given as G = 2.65, e_{max} = 0.89, e_{min} = 0.57, D_{50} = 0.18, particle size = 0.15 – 0.2,

$\gamma_{d(max)}$ = 16.65 kN/m^3, ϕ_{ds} = 39° (dense), ϕ_{ds} = 39° (medium), ψ = 15° (dense) and ψ = 10° (medium). Similarly, properties of 14/25 dense sand was reported as G = 2.65, e_{max} = 0.79, e_{min} = 0.49, D_{50} = 0.8, particle size = 0.6 – 1.18, $\gamma_{d(max)}$ = 17.5 kN/m^3, ϕ_{ds} = 48° and ψ = 26°. Each type of sand was tested with five different diameters of mild steel soil nails having a circular cross – section with length of 127 mm. The diameters used for 50/100 medium sand included 1.3mm, 2.5mm, 4.5mm, 6.4mm and 9.1mm whereas 1mm, 1.9mm 3mm, 6.4 and 9.6 mm diameter was used for 14/25 dense sand. To ensure proper interaction between soil and nail, a layer of sand was glued to nail surface. At each pullout testing, one sample of soil nail was placed symmetrical both in plan and elevation. As observed from Jewel [52], the initial orientation of nail was fixed at 25° with the vertical with the help of thin threads.

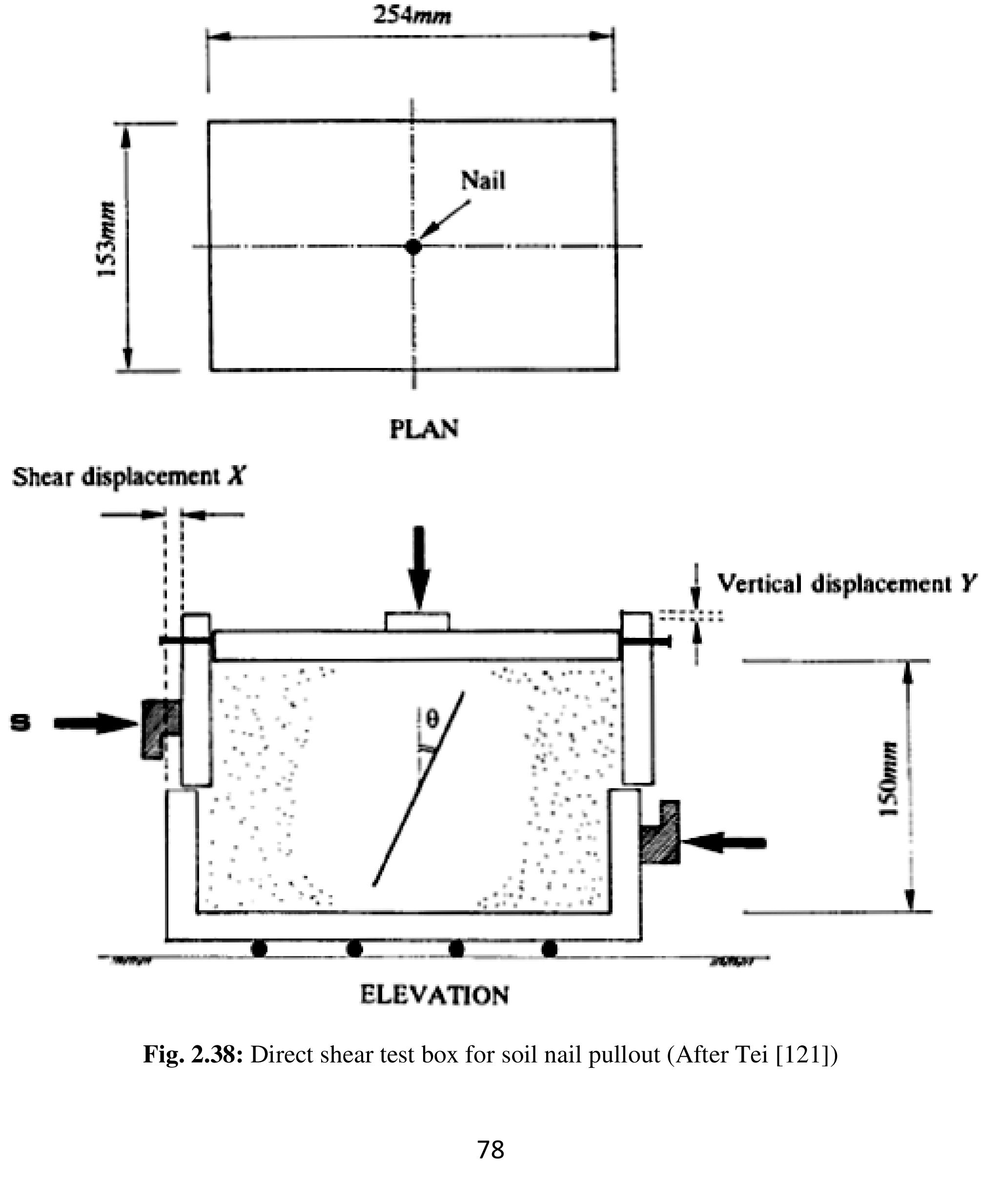

Fig. 2.38: Direct shear test box for soil nail pullout (After Tei [121])

The set up of medium direct shear box test (Fig. 2.38) included placing of nail in empty shear box and filling the box with sand using a hopper placed at 80 cm above the apparatus. The upper and lower halves of apparatus were maintained at a constant gap of 2mm by inserting aluminium sheets between them. Once the entire nail was embedded, a vertical load of 20.3 kN/m^2 was applied though the top platen. The maximum vertical load that can be applied to the system was 60kN/m^2. The shearing was achieved by a ram pushing the lower box at a speed of 0.008 mm/min. The top half was fixed with a dial gauge to read off the resistance it offered to moving lower half. Other measurements taken during testing included the shear displacement and volume increase due to sample dilation. The findings of the work carried out by Tei [121] included a successful prediction of angle of bond friction (δ_b) of nail, which can be related to mobilize interface friction (f*) as given by equation 2.4:

$$f^* = \tan \delta_b \tag{2.4}$$

$$= \frac{P_R}{\sigma_{m\theta} A_r} \tag{2.5}$$

$$= \frac{A_s}{A_r(\cos\theta \tan \emptyset_{ps} + \sin\theta)} \frac{\tau_{EXT}}{\sigma_v} \frac{\cos^2 \emptyset_{ps}}{0.87 + 0.5 \sin \emptyset_{ps} \sin(\emptyset_{ps} + 2\theta)} \tag{2.6}$$

Where P_R = limiting nail force, A_s = plan area of sand, A_r = total surface area of nail, σ_v = surcharge load, θ = angle of nail from vertical, ϕ_{ps} = plain strain friction angle of sand, τ_{EXT} = extra shearing resistance due to nail and $\theta_{m\theta} = (\sigma_1 + \sigma_2 + \sigma_3)/3$ average normal stress on nail at an angle θ. The authors concluded that nail with large diameter corresponds to a smaller interface friction value (f*). The interface friction predicted by a medium direct shear test is an intermediate value between those predicted from pullout test (maximum) and interface tests (minimum). Based on experimental observations, the authors concluded that quantitative assessment of dilation of sand on soil nail pullout could not be well estimated through direct shear testing. A similar study was also reported later by Milligan and Tei [122].

To understand the mechanism of shear strength of interface between soil and grout for a conventional grouted soil nail, Chu and Yin [123] conducted direct shear tests using a large sized apparatus 305 mm x 305 mm size upper box and 406 mm x 305 mm size lower box. For a comparative study, direct shear test were carried out on a soil – soil and soil – grout interface. The rigid boundary conditions were simulated using steel side and base walls. The loading plate consisted of a stiff plastic plate placed on top of the upper box. Above the plastic plate a flexible rubber diaphragm filled with de – aired water was placed. The reason for this rubber diaphragm was to apply a uniformly distributed load and to measure the volume change in sample during shearing. As the sample volume changes during testing, amount of water entering or leaving the diaphragm was also found to vary.

The physical modeling of grouted nail surface was carried out by creating a rough surface as that of between drill hole and soil. The grouted surface was made by using a 19.6 kN/m^3 density cement mortar on the surface of completely decomposed granite (CDG) soil. The CDG soil composition consisted of gravel (28.22%), sand (37.19%), silt (19.59%) and clay (15%). Other properties of CDG soil as reported by the authors were G = 2.64, $\gamma_{d(max)}$ = 16.67 kN/m^3, Recompacted $\gamma_{d(max)}$ = 15.84 kN/m^3, OMC = 19%, c = 45.77 kN/m^2, ϕ = 30.43°, w_L = 62.25%, w_P = 37.08% and k_{20} = 4.54 x 10^{-5} m/s. To study the effect of surface roughness of the interface at drill and surrounding soil, four different interface roughness surfaces were created. The surfaces had a zig – zag (teeth) shape at angles of 0, 10, 20, and 30° with 12.5 mm of width. After curing for 28 days, the cement grouted soil sample was placed in lower shear box for testing.

The shear displacement of lower box was recorded by LVDTs with shear resistance measured done by a 45 ± 0.05kN load cell attached at front of the apparatus. The shearing was done at a constant rate of 0.3 mm/min. Volume transducers were used to measure volume changes and all the data recorded was fed to a digital readout connected to a computer. The observations made during testing are listed below:

(i) Direct shear testing of grouted nail showed a smaller peak strength and higher post peak strength. The observed behaviour was accounted for the high confinement imposed by direct shear apparatus on soil particles during shearing. Moreover, higher vertical displacement was also observed under same surcharge load as compared to pullout test. The reason for this was attributed to the fact that surface area of nails subjected to shearing was 100% in direct shear test as compared to pullout test where it was between 44 – 57% depending on nail length. Larger shear displacements are recorded for soil – grout interface testing to reach peak shear strength.

(ii) The shear strength parameters as obtained from direct shear testing depicted that for soil – soil interface c = 45.77 kN/m^2 with ϕ = 30.43°. Soil – grout interface with 0° of roughness angle showed similar results with c = 30.53 kN/m^2 and ϕ = 28.89°. With the increase in roughness angle from 10° to 30°, 'c' was found to decrease from 54.11 to 43.09kN/m^2 respectively. However, almost similar 'ϕ' value between 32.06° to 32.68° was observed. A similar variation of 'c' and 'ϕ' was also observed with direct shear interface testing at 70 mm shear displacement. The effect of normal stress ($\Delta\sigma'_n$) on interface shear strength (τ_s) of soil – grout was related using an apparent friction coefficient (μ^*) as given by equation 2.7:

$$\mu^* = \frac{\tau_s}{\sigma'_n} \tag{2.7}$$

(iii) It was reported that with increase in normal stress, interface shear strength was found to decrease due to reduction in dilatancy of soil achieved from high confinement as in direct shear test box. The variation of shear strength against normal stress was also validated by published results from Schlosser and Guilloux [124] on ribbed strips (Fig. 2.40).

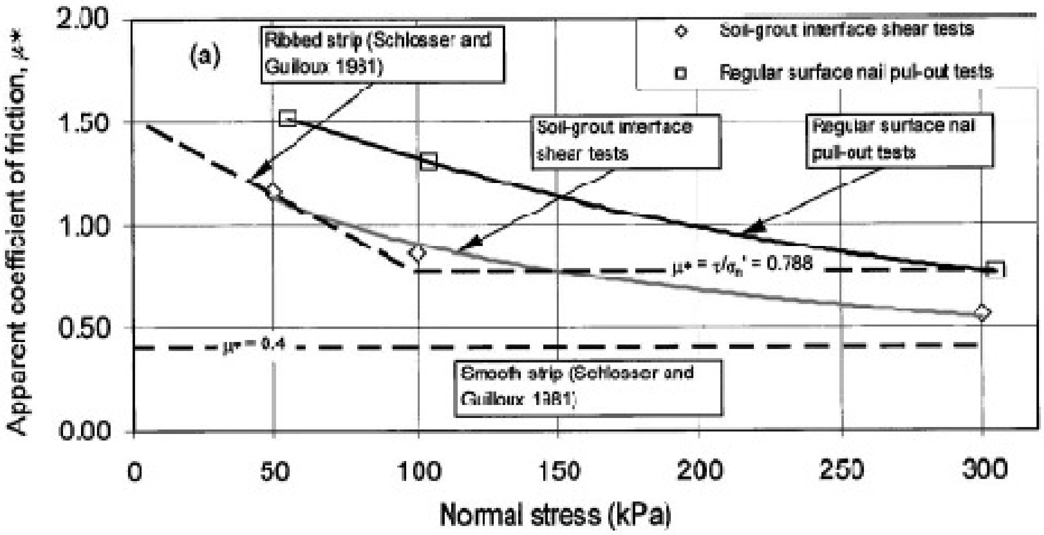

Fig. 2.39: Apparent coefficient of friction for soil – grout interface with regular and irregular nail surface (After Chu and Yin [123])

(iv) Another finding of this work was related to surface roughness of nails. The authors observed that interface shear strength increases with surface roughness (Fig. 2.41). Moreover, it was also found that failure surface for rough nails with 30° roughness angle lies above all the other roughness angles. The interface shear strength of soil – soil interface was smaller than soil – grout interface with 0° roughness angle with maximum interface shear strength being obtained for soil – grout interface with roughness angle of 30°.

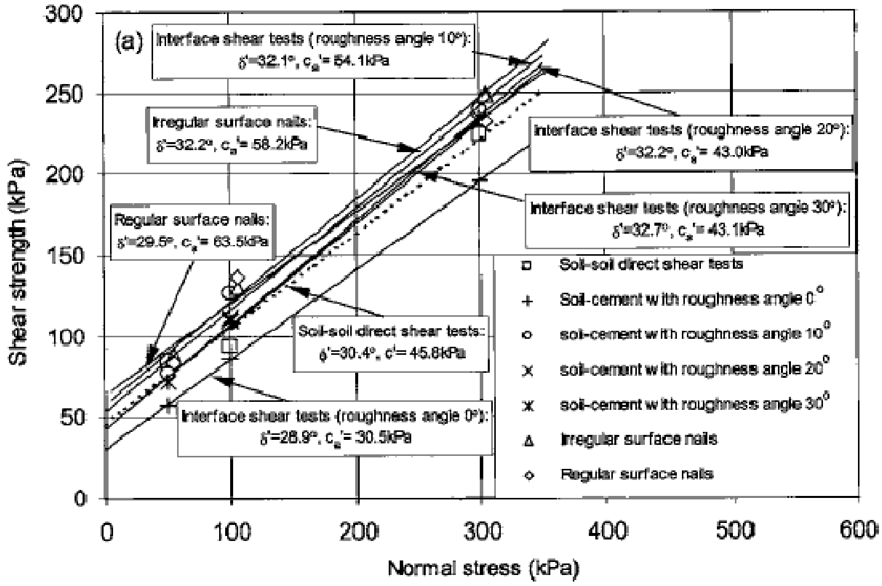

Fig. 2.40: Interface shear strength variation with normal stress (After Chu and Yin [123])

2.4.2 Interface Shear Tests

Morris [125] carried out a seven interface tests under different strain rates and vertical loading to study the interaction mechanism between clay and grout nails. The interface test was conducted in a typical shear box apparatus of standard dimension 60 mm x 60 mm. The interface sample was prepared in another mould having dimensions of 59.9 mm x 59.9 mm (Fig. 2.41). The smaller size facilitates placement of prepared sample into standard direct shear mould without disturbances.

The sample preparation of interface involved a grout layer composed of 120 g of Portland cement and 72 g of water. The water content of grout was 40%. The sealed mould was capable of handling liquid grout which was placed on a layer of clay. The entire arrangement was left for 1 day for grout to mature. The entire clay layer with grout was pressed out of preparation mould and placed in direct shear apparatus with 1 mm spacer between the two halves. To simulate symmetrical boundary conditions, top load platen was fixed with upper half of shear box. The spacer was removed and complete set up was inserted into a water bath with a specified vertical load so as to fully consolidate the sample. During this procedure, vertical consolidation deformation was recorded through dial gauges. Once the readings attained a constant value, the sample ready for testing was sheared up to a shear displacement of 5 mm. Different strain rates used for testing varied as 0.3 mm/min for base test, 1.2 mm/min for fast test and 0.01 mm/min for slow test, all under a constant surcharge of 50kPa. Two tests at 0.3 mm/min were conducted under 100kPa and 200kPa. These constituted the medium surcharge test and high surcharge test.

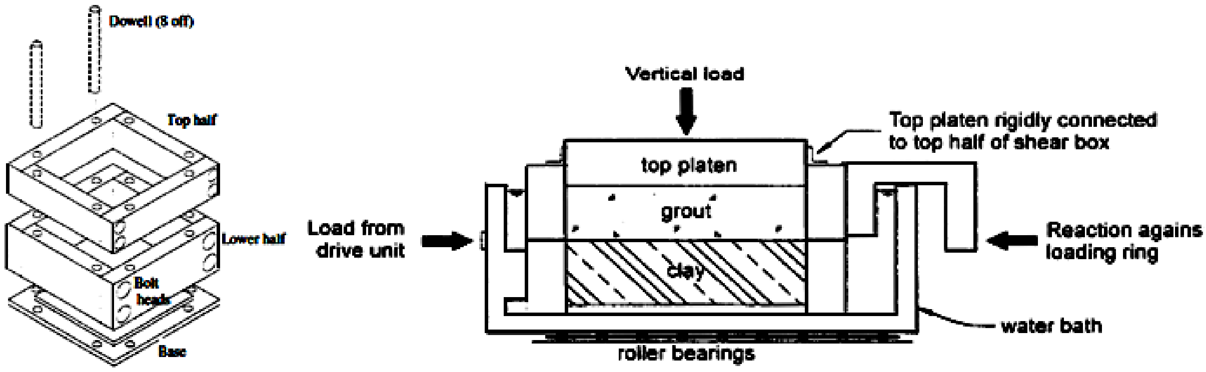

Fig. 2.41: Interface shear test set up along with preparation mould (After Morris [125])

The observations from interface testing were reported to have increased water content (10%) at soil – grout interface as compared to bulk of clay sample. The reason for this increased water content was formation of thin shear zone which is created adjacent to soil – grout interface during shearing. The large plastic strain generation in shear zone causes the soil to dilate, which in turns leads to development of capillary suction. This makes the water move from bulk of clay to the shear zone and thus raises the water content. The vertical settlement of top platen of shear box was also recorded. It was observed that a constant settlement of 0.05 mm was reported for all the tests except for test with high surcharge where this value reached a maximum value of 0.28 mm (Fig. 2.42). The small vertical displacement is an indication of small dilation angle of clay. The effective stress in shear zone increases due to clay dilation which generates pore water suction. The low permeability of soil does not provide sufficient time for suction to dissipate. However, as the soil ceases to dilate reaching critical state, dissipation of suction water occurs, which reduces effective stress and shear stress.

With the observation of shear stress (τ) and vertical stress (σ_v), a ratio τ/σ_v was plotted as shown in Fig. 2. 43. It was found from τ/σ_v curves that peak values are obtained for fast tests because non – dissipation of water suction in small time period. However, for slow tests values of τ/σ_v curved were found to decrease. As the surcharge is increased from 50kPa to 100kPa and 200kPa, τ/σ_v cuves depict reduction in peak value. This was accounted for the fact that soil dilation is reduced with increase in vertical stress. Moreover, all tests resulted in high shear resistance with increase in loading rate and vertical stress.

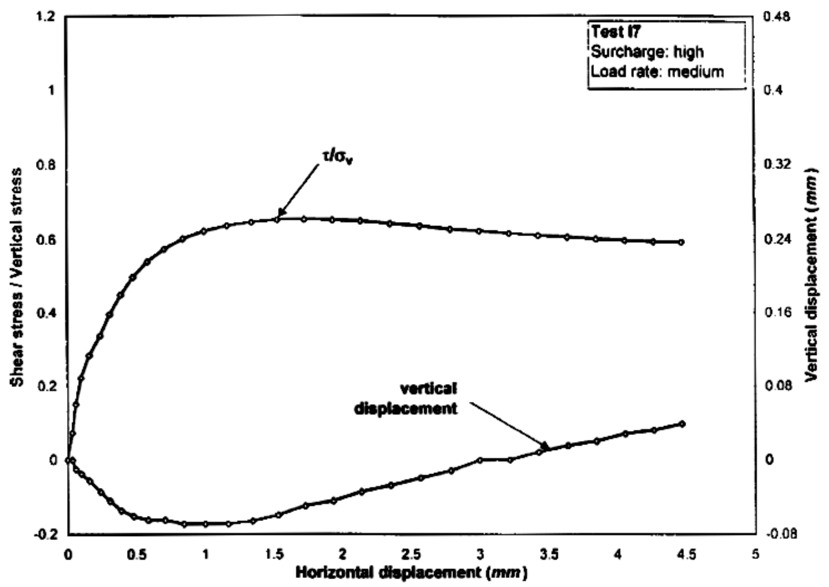

Fig. 2.42: Vertical displacement for high surcharge test (After Morris [125])

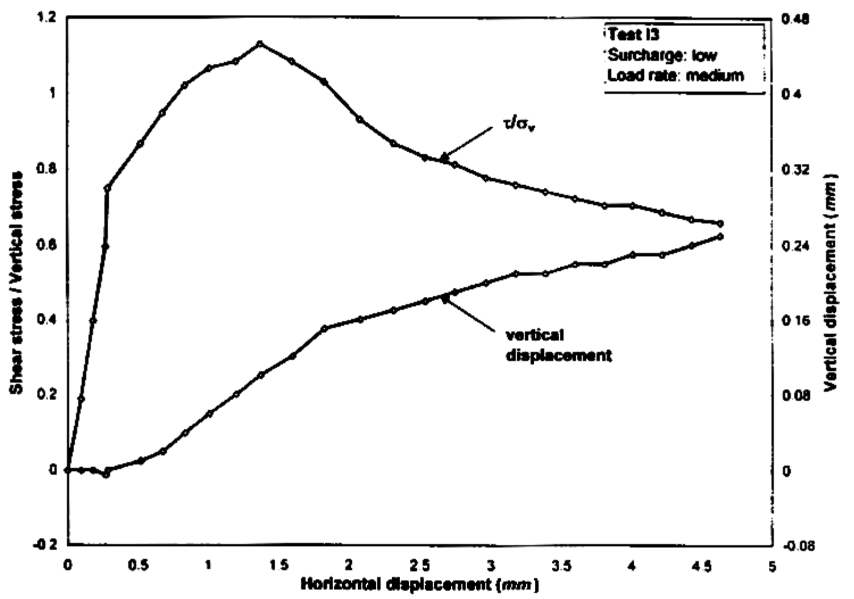

Fig. 2.43: τ/σ_v against horizontal displacement for low surcharge (After Morris [125])

2.4.3 Pullout Box Tests

Variation of apparent friction coefficient with wall depth was reported by Cartier and Gigan [99]. Pullout tests of 5.5 m long steel section (50 mm x 50 mm x 5 mm) and 7.0 m long angle sections (60 mm x 60 mm x 6 mm) was carried out in a vertical nailed excavation 5.5 m (width) and 11.6 m (height). The authors observed that apparent coefficient of friction was mobilized by a wall deformation of 2 – 3 mm. The mobilized friction was more than unity for nails within 4 m depth from wall top due to soil dilatancy. For nails at depth greater than 7 m, mobilized friction was equal to $0.5tan\phi$, where ϕ was angle of internal friction of soil. It was also investigated during pullout tests that soil nails in upper part depicted higher tensile stresses as compared to nails in lower half of excavation. Also the peak tensile stresses in lower half were found close to wall face.

The effect of nail installation on apparent friction coefficient was reported by Juran and Jewel [30]. It was observed that pre – buried nails in granular soils depicted higher apparent friction as compared to driven nails. This variation of apparent friction was attributed to imposed restrained dilatancy during driving process. Since shear displacement and volumetric expansion had already taken place during driving which restricts soil movement and correspondingly mobilization of smaller apparent friction coefficient.

Chang and Milligan [126] conducted pullout test on a single 2 mm diameter nail (E_a = 206 x 10^6 kN/m^2) using a set up of dimensions 254 mm x 153 mm x 202 mm. Variable length of soil nail was used so as to maintain a constant bond length. Under two different relative densities of 78% and 94%, pullout was done using yellow Leighton Buzzard sand (D_{50} = 0.18mm). The vertical loading of 3.4kN and 6.4kN with a low confining stress less than 10kN/m^2 was applied. The main objective of the study was to investigate the effect of 'transition zone' on apparent friction coefficient. The transition zone as reported by the authors constitutes a zone between lines inclined at $\phi°$ and (45 + ϕ/2) with horizontal. The line at ϕ represent self stable zone for soil whereas (45 + ϕ/2) line is for active zone (Fig. 2.44).

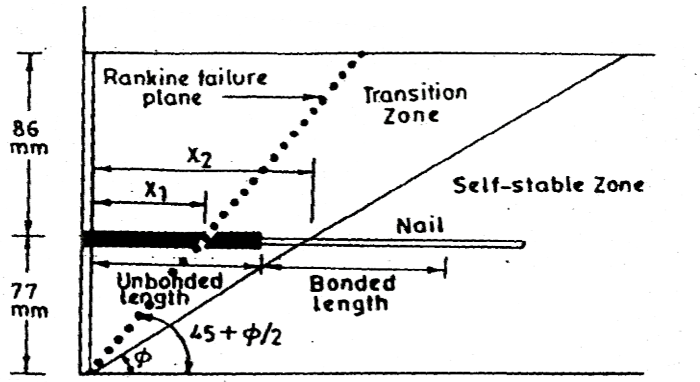

Fig. 2.44: Transition zone (After Chang and Milligan [126])

The observations during pullout testing depicted that as unbonded length reached 70 – 80 mm, peak bond stress (37kN/m^2) is reached. This specific point of peak bond stress at a particular displacement is referred to as 'saturation point'. The curves at R_D = 94% were found to result in higher bond stresses as compared to sand with R_D = 78%. Moreover, for R_D = 78%, peak bond stress ($28kN/m^2$) was achieved at a larger unbonded length of 80 – 90 mm (Fig. 2.45). Beyond the saturation point, shear stress and unbonded length resulted in almost similar curves for two different front wall conditions defined as (i) with movement (ii) without movement. The similar nature of curves depicted that pullout condition existed in the stable zone of soil. The curves in the middle portion revealed a liner increase in shear stress up to saturation point which can be accounted for local bond stresses of stable zone and mixing effect of stable and active zone.

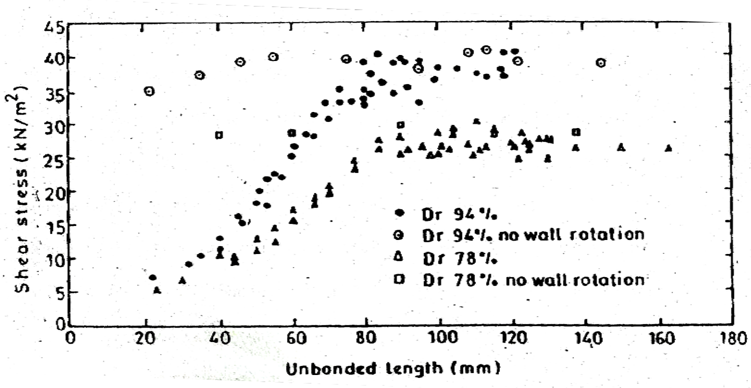

Fig. 2.45: Shear stress variation for with and without wall rotation

(After Chang and Milligan [126])

At this curve region, certain portion of nail length is still in transition zone. In the stable zone high apparent friction coefficient values $f^* = 6.3$ for $R_D = 94\%$ and $f^* = 4.4$ for $R_D = 78\%$ were observed due to increased normal stress which was the result of restrained soil dilation. Based on this observation, it was also reported that increased dilation occurs at low stress levels. Moreover, smaller apparent friction coefficient was recorded for transition zone varying between $f^* = 0.66 – 1.02$ for $R_D = 94\%$ and $f^* = 0.86 – 1.07$ for $R_D = 78\%$. From this observation it was concluded by the authors that no restrained dilation effect occurs at transition zone. The general pullout of soil nails were conducted with complete formation of active and transition zone. This would result in an improper estimation of soil nail pullout because the peak bond stress value correspond to shear stress developed in stable zone only. If soil nails are designed with such pullout values, then at ultimate failure design consideration will be unsafe.

The pullout of driven and pre – buried nails was investigated by Raju [28] using a pullout apparatus as shown in Fig. 2.46. The pullout box was filled with medium sand and two different installation techniques were used to place the 0.8 m long hollow aluminium square nails. Moreover, two different types of nail were created (i) sand glued nails (ii) plain nails without glued sand. The nails were installed at a depth of 0.7 m. The pullout mechanism involved a pulley system on which weights were placed to execute pullout of nails in horizontal direction. The pullout test depicted that buried nails exhibit larger pullout as compared to driven nails.

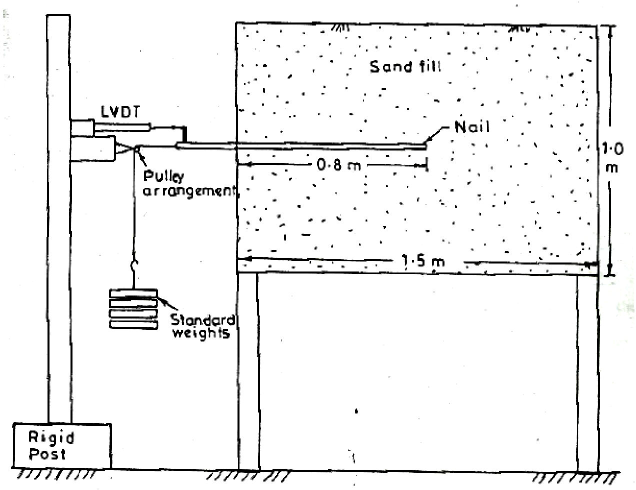

Fig. 2.46: Pullout model test box (After Raju [28])

Similarly, a series of ten pullout tests at varying depth was also carried out by Raju [28] in a concrete trench of size 3.0 m (length) x 3.0 (width) x 2.4 m (depth). The trench was filled with sand having a water content of 2.5% and traces of shell fragments. The nail length used for pullout was 1.6 m. The facing of trench was firmly fixed with the help of a metal frame. The pullout force was exerted using a hydraulic jack and 9kN capacity load cell with LVDTs used for measuring horizontal nail displacement. The pullout was applied at a rate of 25 mm/min. For strain measurements along nail during pullout, some nails were fixed with strain gauges. The depths used for pullout of driven and pre – buried nails were 0.2 m, 0.7 m, 1.2 m, 1.7 m and 2.2 m. The observations through trench pullout tests depicted a similar result of high pullout resistance for pre – buried nails in comparison to driven nails. As shown in Fig. 2.47, maximum pullout force for driven nails was also found to occur at a smaller displacement (8mm) as compared to pre – buried nail head displacement (12 – 16mm).

Raju [28] also estimated pullout force (F_p) for driven and pre – buried nails theoretically from the relationship as given by equation 2.8:

$$F_p = \left(\frac{1 + K_0}{2}\right)\gamma.z.\tan\delta.p.L \tag{2.8}$$

Where, $K_0 = 1 - sin\phi$, γ = Unit weight of fill, z = Depth of nail from ground surface, p = Nail perimeter, L = Nail length, δ = 30° (soil – nail interface friction angle). The comparison of experimental and analytical pullout forces as obtained by Raju [28] is summarized in Table 2.7.

Table 2.7: Summary of pullout trench test and estimated results (Raju [28])

Depth, H (m)	Pullout forces from experiment (kN)		Estimated pullout forces (kN)
	Driven nails	Pre – buried nails	
0.2	1.03	1.17	0.37
0.7	1.83	2.07	1.32
1.2	2.65	3.03	2.26
1.7	3.24	3.87	3.20
2.2	4.26	4.72	4.14

Based on the observations, it was reported that pullout forces estimated was lower than experimental values. However, the trend of higher pullout for pre – buried nails than driven nails was similar to pullout model box test. It was also observed that pullout forces were found to increase with trench depth.

The authors also investigated the effect of depth on friction coefficient (f^*). From the study, it was found that as depth was increased, f^* was found to decrease. However, the decrease in f^* value was close to estimated value of $f^* = tan\delta$ for depth beyond 1.7 m (Fig. 2.48). The authors also theoretically calculated average bond stress of 7.05kPa from strain gauge readings and found it to be in good agreement with experimental average bond stress value of 6.6 kPa as obtained from trench pullout test.

The pullout behavior of grouted nails at in – situ conditions was investigated by using tendon of diameter 25 mm centrally placed in a bore hole of diameter 100 mm. The testing was carried out in a 9.0 m high wall with face slope of 1 in 8. The nail length of 7 m was installed at an inclination of 15° and grouted with cement of strength 30 N/mm^2. The in – situ ground conditions consisted of clayey silt with traces of sand. The pullout was arranged at 1.5 m below ground level using a jack which applied 25% of designed load for 5mins. The monitoring of axial tensile force was done by attaching three vibrating wire strain gauges at every 2.0 m along nail length. With this in – situ pullout set up, Raju [28] also studied the load transfer mechanism between nail and soil with estimation of developed bond stress between in – situ soil – nail interface.

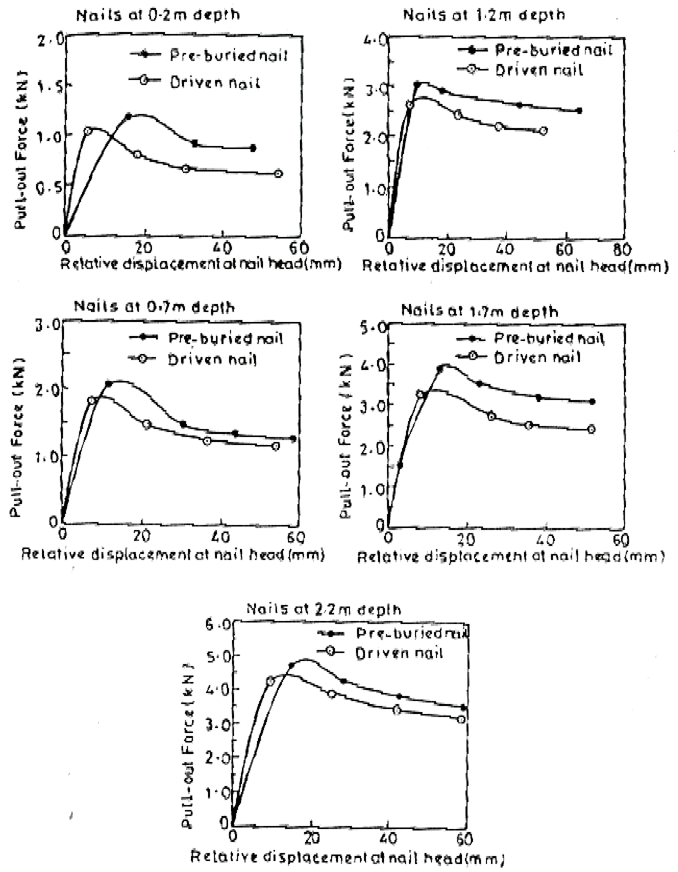

Fig. 2.47: Results from trench pullout tests at different depths for driven and pre – buried nails (After Raju [28])

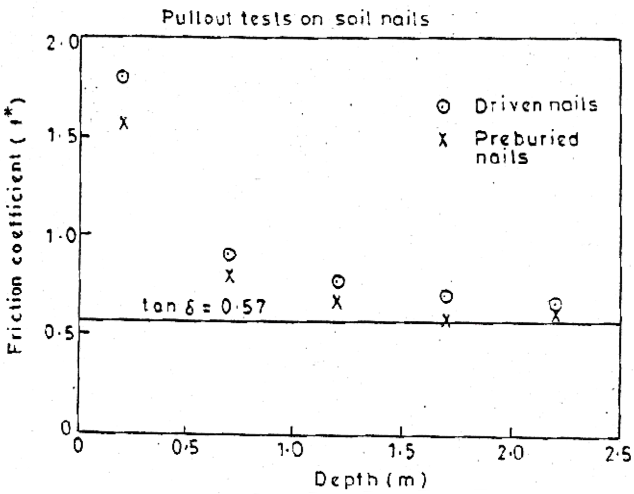

Fig. 2.48: Variation of friction coefficient with depth (After Raju [28])

The in – situ pullout testing on grouted nails revealed that bond stress developed at soil – grout interface is lower than bond stress at tendon – grout interface. Based on this observation, Raju [28] concluded that in residual soils, critical interface for bond failure is governed by tendon – grout interface instead of soil – grout. Moreover, failure bond stress of 35.5 kPa was measured as compared to 70.3 kPa of peak bond stress mobilized at the nail end. The pullout failure load was recorded as 78kN which was 40% of designed nail capacity. The pullout failure was found to occur at soil – grout interface and bond stress was completely mobilized at 8.0 mm of nail head displacement.

Investigation of radial stresses and shear stresses around a grouted soil nail for prediction of bond mechanism was done by Milligan et al. [127].Using a 100 mm diameter single nail in a pullout box of plan area 0.6 m x 0.6 m and depth 0.6 m, pullout test was conducted in fine Leighton Buzzard sand. The instrumentation of nail included measurement of normal and shear stress at top, bottom and side of nail by Cambridge type transducers. The authors reported that higher stresses were generated at top and bottom with low stress generation at the sides of nail. For a displacement of 8 – 9mm, shear stresses are found to increase rapidly. With high initial stresses at top (110 kPa) and bottom (75 kPa), shear stresses reach peak value (175kPa) at displacement of 20 mm for top with bottom of nail measuring 250kPa at 250 mm displacement.

With further displacement, a decrease in shear stress is observed. During low pressure grouting, radial stresses are found to increase, but as curing of grout occurs, stresses increase at decreasing rate. After 36 hours, radial stresses attain a value between 33kPa to 55kPa. The shear stress at sides of grouted nail depicts an increase throughout the pullout test with maximum values of 150 – 160 kPa. A smaller pullout resistance is recorded in comparison to calculated in – situ value which can be a result of low pressure grouting applied. At small displacement of 4mm, frictional angle was found to have mobilized signifying that full pullout resistance requires only a small displacement for grouted nails. Similar plots for shear and normal stress was also recorded by the authors. A study of pullout of four different types of driven nails in dry, homogeneous poorly graded sand was conducted by Franzén [128]. The four types of driven nails used were angle bar (40 mm x 40 mm x 4 mm), ribbed bar (36 mm), expansion bolt (54 mm) and round steel bar (36 mm). A total of six tests were conducted with two primary objectives (i) study of driving and jacking technique of nail installation on pullout capacity through two tests (ii) four tests for investigating the effect of relative density and nail type on soil nail pullout. Each test was carried out using three driven nails subjected to three different stresses of 25kPa, 75kPa and 125kPa. All pullout tests were performed in a model test box of size 4m x 2m x 1.5m.

The results of pullout tests (Fig. 2.49) depicted that driven nails showed peak value which was 50% greater than peak value obtained from smooth pullout curve for nails installed by jacking. However, for both nails installed by driving and jacking respectively, showed no dependency on installation method for residual pullout capacity. The pullout capacity recorded for ribbed bars was higher than smooth bars. The increase in pullout capacity of ribbed bars was accounted for increased surface area and angle of friction obtained for ribbed bars. This increase led to the shifting of failure surface from soil – steel interface to a region above bar ribs. The pullout capacity was reported to have increased with increase in relative density and overburden pressure.

The authors reported that pullout capacity of nails is influenced by displaced soil volume during installation. The observations of horizontal displacement reflected that normal stress generated on nails after installation are governed by displaced soil volume during installation. The increase or decrease of normal stress in comparison to in – situ stress depends on stress compensation which is provided by nail volume to the reduced stress condition created around nail due to soil displacement as installation of nail is performed. Thus, soil volume was classified as an important parameter by the authors to be considered while predicting nail pullout capacity.

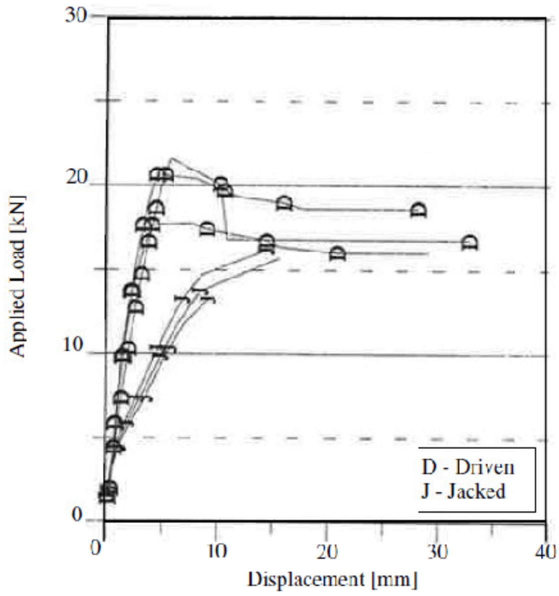

Fig. 2.49: Influence of method of installation (After Franzén [128])

The coefficient of friction from pullout test (*f**) was related to direct shear coefficient of friction (*f*) by Wang and Richwien [129]. A simple mechanical model was developed with assumptions of that reinforcement bar is stiff, volume of soil is constant during pullout and stress condition around nail is given as shown in Fig. 2.50. Based on the assumptions along with dilatancy of sand and reinforcement roughness, the following expression was developed (Eq. 2.9)

$$f^* = \frac{f}{1 - [2(1+\upsilon)/(1-2\upsilon)(1+2K_0)]f\tan\psi} \tag{2.9}$$

Where, υ = Poisson's ratio, K_0 = coefficient of earth pressure at rest and ψ = Dilatancy angle of sand. The assumption of stiff reinforcement reflected on the condition that stiffness of soil is smaller than stiffness of surrounding soil. During pullout it was observed by the authors that for soil having $\psi = 0$, f^* was equal to f. For soils with large value of ψ or reinforcement with very rough surface, denominator of equation (2.9) becomes greater than or equal to unity which makes the overall equation yield indefinite or negative value of f^*. Thus, assumption of constant volume with high dilatancy failed for the purposed model. At high soil dilatancy, tensile failure of reinforcement occurred prior to pullout failure. However, for most sands, dilatancy angle (ψ) was not likely to be greater than 15°. Hence equation (2.9) was applicable to a large number of soil – reinforcement interfaces and rendered a value of less than 0.7 i. e. interface friction angle δ = 35°. The authors predicted relationship between f^* and f as non – linear.

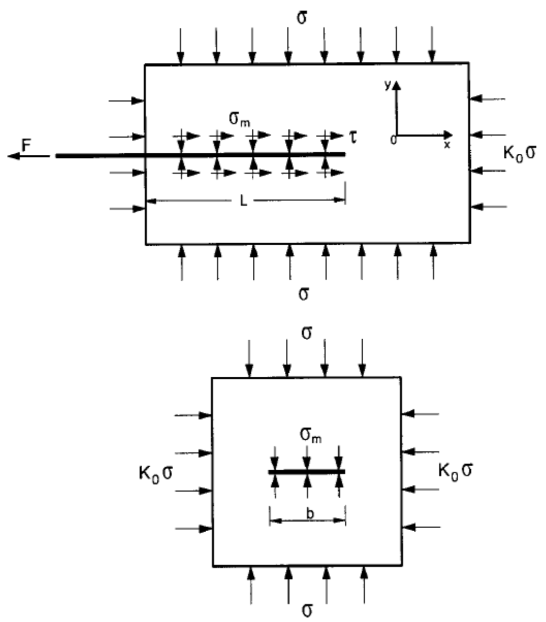

Fig. 2.50: Pullout test of nail (After Wang and Richwien [129])

Validation of model developed by Wang and Richwien [129] was performed by Milligan and Tei [122] by carrying out pullout test of steel interface with Leighton Buzzard sand. The interface properties were given as ϕ_{ds} = 39°, υ = 0.33, δ = 30° and ψ = 15°. The pullout tests revealed f^* as 2.01 – 3.00 whereas f^* = 1.91 was predicted by equation (2.9). Hence the observed results showed a close agreement in measure and predicted values.

A pullout model test to understand the effect of nail surface roughness, ratio of nail length to nail diameter, overburden pressure, distance between two nails and nail group efficiency was performed by Hong et al. [130]. A model test box of 1 cm thick steel plates of dimensions 60 cm (length) x 80 cm (width) x 40 cm (height) was fabricated with the front wall having a row with 21 holes and diameter of 11 mm at distance of 20 cm from the tank bottom. The row of holes facilitates the variation of spacing between nails and also for testing with double nails. The boundary effect on nail pullout was carefully handled by making the shortest boundary at a distance of 20d (d = nail diameter) (Hong and Chen [131]). Application surcharge pressure (196 kPa) is done by a flexible bag attached at top of the apparatus. The soil used in pullout test consisted of uniform quartz sand with properties of Gs = 2.64, $\gamma_{d(max)}$ = 16.3kN/m^3, $\gamma_{d(min)}$ = 13.8kN/m^3, D_{50} = 0.31 mm, C_u = 1.68, ϕ calculated for different R_D = 40%, 60% and 80% using a relationship given by equation (2.10):

$$\phi = 30.81 + 13.38D_r - 4.15D_r \log\frac{\sigma_3}{P_a} \tag{2.10}$$

Where, D_r = Relative density of soil, σ_3 = Confining pressure and P_a = Reference atmospheric pressure. The sand was filled in the model tank using pluviation technique so as to maintain a relative density of 70% at each of 16 layers used for pullout set up. The sides, bottom and front plates are also attached with pre – buried load cells for measuring soil pressure during pullout testing. The alluminium alloy tubes are used as nails with external diameter (D_0) = 9mm and internal diameter (D_{in}) = 4.8 mm based on the aspect ratio used in filed applications (25 - 50). The modulus of elasticity of nails is 60GPa. The nails are threaded with varying thread depths of 0.42 mm, 0.65 mm and 0.87 mm to render the surface rough. The surface roughness of nails is defined by a non - dimensionless factor (R) calculated using the equation (2.11):

$$R = \left(\frac{T_d}{D_{in}}\right)\left(\frac{1}{S_p}\right)\left(\frac{T_d}{D_{50}}\right) \tag{2.11}$$

Where, T_d = Thread depth, $D_{in} = D_0 - 2T_d$ and S_p = Screw pitch of the nail. In equation 2.11, the ratio $1/S_p$ represents asperity number per unit length, T_d/D_{in} represents relative roughness of single asperity and T_d/D_{50} = Relative roughness of nail surface with respect to particle size of soil. The nails are pre – buried at soil mid height and in horizontal orientation. Similar to field pullout rate (0.1 mm/min), pullout test was carried out at a speed of 0.02 – 0.11

mm/min. The pullout model apparatus along with used threaded nail geometry is shown in Fig. 2.51. The testing program is performed in two stages. Stage 1 involved pullout of single nail with different lengths and surface roughness. Stage 2 comprised of pullout of two nails placed at various distances in a row.

The findings of pullout test by Hong et al. [130] showed that pullout resistance increases with increase in surface roughness. For smooth nails (R = 0), maximum pullout is attained at relatively small displacement of less than 0.2mm with pullout and displacement curve reflecting an elastic – plastic behaviour. However, for rough nails ($R \neq 0$) peak pullout resistance occurred at 1.2 – 1.5 mm with unsmooth zig – zag curves due to shear stress softening as defined by Raju [28] also (Fig. 2.52).

For both smooth and rough nails, pullout resistance is also found to vary linearly with aspect ratio. With smooth nail under average normal stress calculated from equation (2.12), apparent coefficient friction (f) when calculated from equation (2.13) depicts that f lies in a range between 17° - 18° which is similar to angle of internal friction (18°) of sand from direct shear test.

$$\sigma_m = \frac{\sigma_v + \sigma_h}{2} = \frac{\sigma_v}{2}(1 + K_0) = \frac{\sigma_v}{2}(2 - \sin\phi) \tag{2.12}$$

$$f = \frac{\tau_{max}}{\sigma_m} \tag{2.13}$$

Where, σ_v = Vertical stress on the nail, σ_h = Horizontal stress on the nail, $K_0 = (1 - \sin\phi)$ = Coefficient of earth pressure at rest, σ_m = Mean normal stress and τ_{max} = Maximum shear stress. The pullout curves under different surcharge pressure also depicted that pullout was found to increase with increase in surcharge with zig – zag pattern of curves becoming more profound at higher surcharge. However, the apparent coefficient friction was not found to vary with L/D ratio and surcharge variation. The group efficiency was observed to have a linear relationship with L/D ratio of nails. The efficiency was found to increase with L/D ratio till 100% efficiency was attained. The efficiency was also dependent on surface roughness and increased linear it. Moreover, the minimum distance for 100% group efficiency of nails was found to vary with surface roughness also.

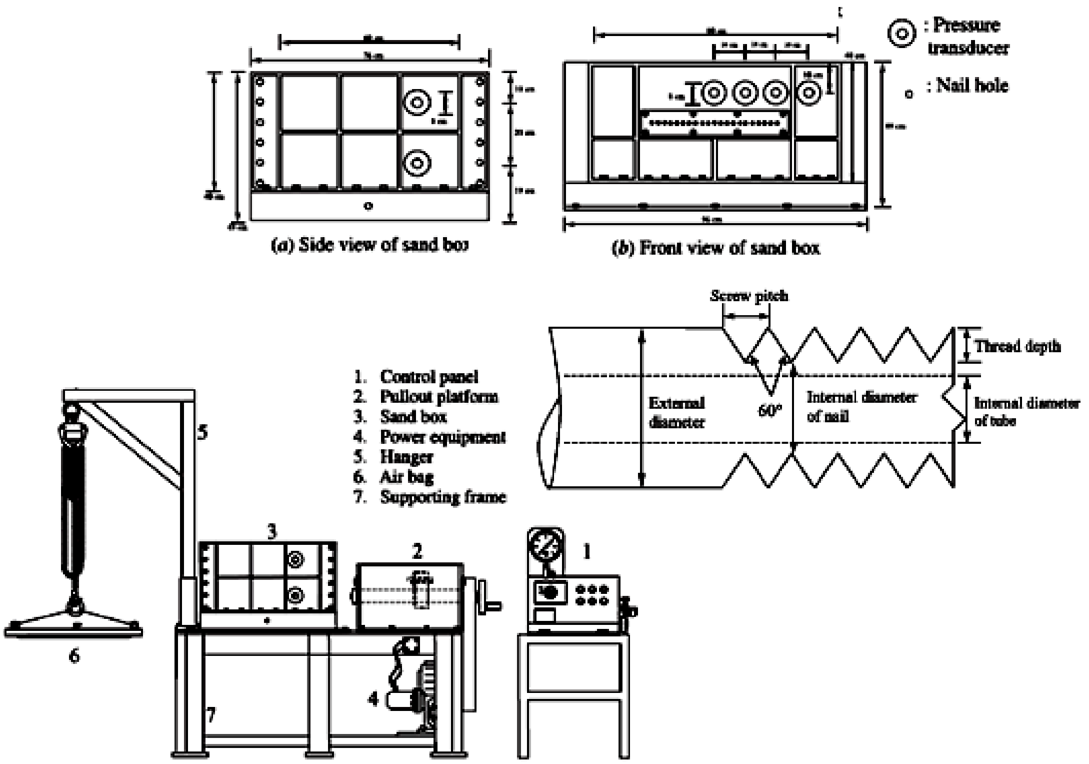

Fig. 2.51: Pullout test arrangement with nail geometry used (After Hong et al. [130])

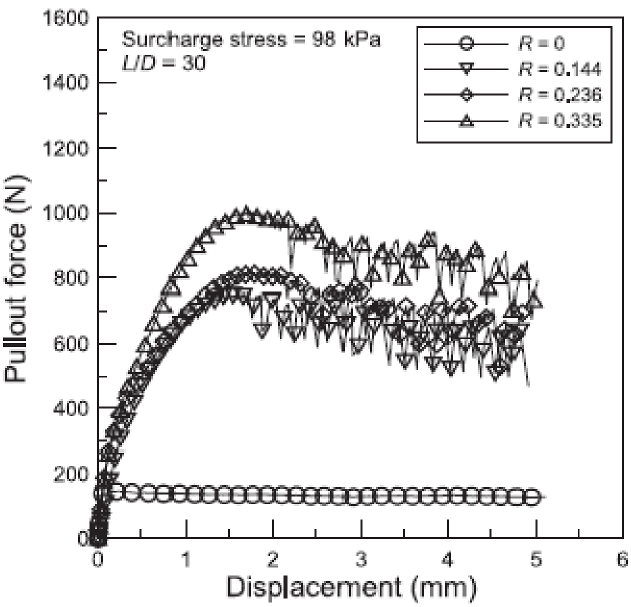

Fig. 2.52: Pullout versus displacement for different roughness factor (After Hong et al. [130])

A large – scale pullout test using an apparatus of size 2m x 1.6 m x 1.4 m (length x width x height) was carried out by Junaideen et al. [132]. Five holes were made at the front face of pullout box made up of rigid steel. The soil used for testing was CDG soil with properties of *c* =

3.8 kPa and ϕ = 38°. Three types of nails mainly smooth round bars (dia. = 25 mm), ribbed bars (internal dia. = 25 mm) and knurled roughened bars (internal dia. = 21 mm) of 2 m length are used. The vertical loading is carried out by using 25 mm thick steel plate connected with five LVDTs (four at corners and one at middle) for measurement of vertical settlement. The maximum load that could be applied was 150kPa which was equivalent to pressure from 6m to 7m of fill (Fig. 2.53). As suggested by Hsu and Liao [133], to avoid boundary effect the minimum distance of 2 – 5 times nail diameter was recommended. The minimum distance between side boundaries and nail adopted for testing was 10 times the nail diameter. The pullout of nail was carried out in a displacement controlled manner at rate of 0.025 – 1.300 mm/min.

The authors reported that pullout resistance of smooth and knurled nails increased with increase in surcharge pressure. The pullout of ribbed bar was different from smooth and knurled bars for same increase in surcharge. The peak pullout values occurred at 1.0 mm for round bars, 3.8 mm for knurled bars and 6.3 mm for ribbed bars. The pullout against displacement plots for different types of nails showed a clear peak value and decreasing pullout resistance with large displacement. The post – peak decrease in pullout resistance was attributed to change in normal stress acting around soil nail due to dilatancy and arching effect. If soil around the nail expands during pullout, it is resisted by the surrounding soil resulting in an increase in normal stress. Correspondingly, soil collapse during pullout causes stresses release which tends to decrease the normal stress. The authors also reported that conventional pullout estimations under estimate the pullout. The conventional method predicts lower value of apparent coefficient of friction and higher soil- nail adhesion. Hence, the authors developed a new formulation incorporating two main parameters as given in equation (2.14):

$$P_p = \pi D a^* + 2D\sigma'_{vo} \tan \delta^* \qquad (2.14)$$

Where, $a*$ and $\delta*$ are apparent interface parameters for interface adhesion and interface friction angle, σ'_v = Initial vertical stress on nail, D = Nail diameter. A similar interpretation on pullout of soil nails in unsaturated sandy clay was also reported by Chai and Hayashi [134]. It was observed that pullout study conducted through field and laboratory pullout tests depicted that pullout capacity of nails depend upon the water content of soil. For dry condition, bond stress increase and a large normal stress is mobilized. For wet condition, dilatancy thrust decreases with increase in water content.

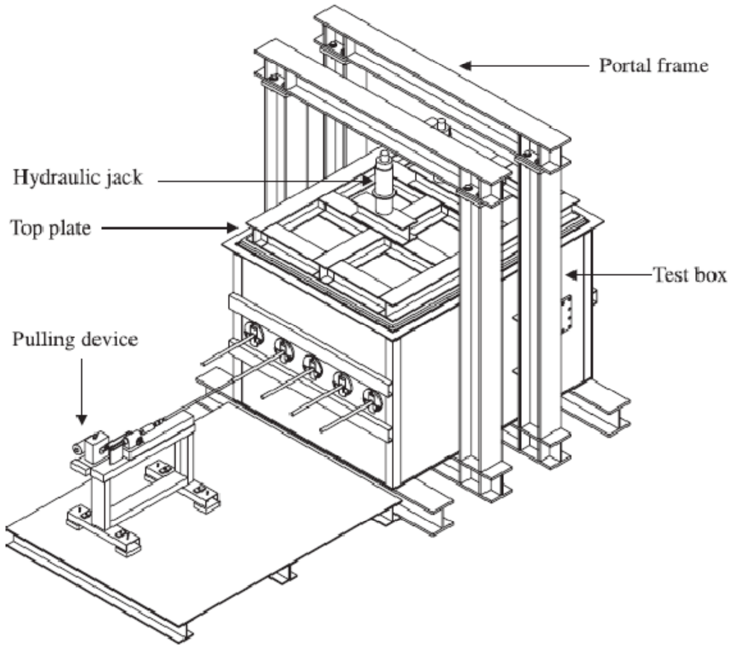

Fig. 2.53: Pullout test apparatus (After Junaideen et al. [132])

A comparative study of pullout prediction by direct shear test and pullout test was conducted by Chu and Yin [125]. From the study it was observed that apparent friction (f_δ) and interface adhesion (f_a) determined from both the tests can be related as given by equations (2.15 and (2.16):

$$f_\delta = \frac{\delta'}{\emptyset'} \tag{2.15}$$

$$f_a = \frac{c'_a}{c'} \tag{2.16}$$

Where, δ' = interface friction, ϕ' = soil friction, c'_a = soil adhesion and c' = soil cohesion. It was that smaller displacements are required for mobilization of peak pullout force form pullout test as compared to direct shear tests. For smooth surfaces or regular surface nails, f_δ can have value less than 1.0 whereas for nail rough angles of 10°, f_δ is greater than 1. Thus, it was concluded that as interface surface roughness increases, f_δ increases. However, f_a was found to increase up to a roughness angle of 10° and decreases beyond it with increase in surface roughness. The trends though as observed from direct shear and pullout tests for f_a are found to be similar. Moreover, it was also reported by the authors that shear failure envelopes from direct shear and pullout tests are close to angle of internal friction of soil and hence failure envelopes for soil – grout interface can be correctly determined by direct shear tests.

Soil – nail pullout interaction in loose fill material using a sand tank of size 2 m in length x 1.6 m in width x 1.4 m in height was conducted by Pradhan et al. [135]. With the set up of pullout similar to Junaideen et al. [132], nails were installed using conventional drilling and grouting technique. A hand augur 100 mm diameter was used for drilling holes at inclination of 10° to horizontal and grouting is done without pressure with a water/cement ratio of 0.45. The soil nails consist of 25 mm ribbed bars with elastic modulus of 200GPa. The soil used for pullout test is CDG soil with properties as given by Junaideen et al. [132]. With a pullout rate of 1 mm/min, testing is done in a displacement – rate controlled manner. The results of pullout of soil nails in loose fill material showed that pullout increases with increase in overburden pressure, degree of saturation and degree of compaction. The theoretical prediction of pullout resistance (q_s) can be made from equation (2.17) with interface friction (f) being in range of 0.9 to 1.0.

$$q_s = \frac{K_0 + 1}{2} \sigma_v' f \tan \emptyset' \tag{2.17}$$

The authors interpreted the increase in pullout as a result of constrained dilatancy. As the nail is pulled out, soil around the nail dilates. This soil expansion is restricted by adjacent soil which brings an increase in normal stress acting on the nail. The increased normal stress increases the shear stress and a subsequent increase in apparent coefficient friction. With this increased interface friction, the resistance provided to pullout force increases. The interface friction as estimated by the study was 39.6° which was close to the internal friction of soil (39°). The results obtained from the study were also found in good agreement with many published literature such as Heymann et al. [136], Feijo and Erhlich [137] and Li [138].

Tan and Ooi [139] and Tan et al. [140] conducted a rapid pullout test to study the behaviour of soil nail embedded in poorly graded clean dry sand with D_{50} = 0.7 mm. With a relative density, the sand under study showed a friction angle of 39°. The direct shear friction angle for soil was found to be 31°. The nail used for testing was rigid hollow circular stainless steel bars with diameter of 22 mm and length of 0.75 m. Two types of nails one with smooth and other one with rough surface were studied. To apply a rapid pullout force an impulse hammer (Fig. 2.54) was used and comparative study with quasi – static pullout was made. The results of rapid pullout revealed that for rough nails under impulse tensile load, the pre – peak pullout behaviour is governed by a damping coefficient which in turns dependent on the displacement parameter. The behaviour of damping coefficient in the post – peak pullout curve decreases with increase in pullout displacement. However, no damping effect was showed by pullout of smooth nails. As compared to quasi – static pullout, rapid pullout depicted a stiffer curve for pre – peak behaviour and post – peak behaviour observed a more drastic softening of pullout force.

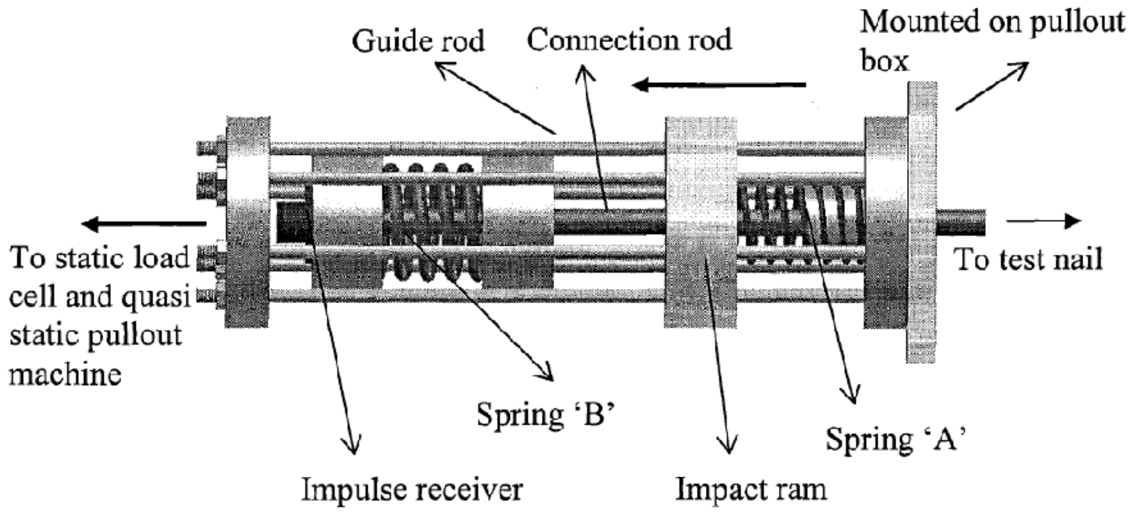

Fig. 2.54: Impulse hammer for rapid pullout (After Tan and Ooi [139])

The reason for decreasing damping coefficient was attributed to the progressive weakening of sheared zone between the nail and soil. As the nail is pulled out, discontinuities develop between soil and nail. The nail is unable to transfer load to the surrounding soil and thus a reduction in dissipation of energy occurs. This leads to a reduced damping effect with pullout displacement.

The damping coefficient (C^*) was given by the equation (2.18):

$$C^* = \frac{F_r - F_s}{vL} \tag{2.18}$$

Where, F_r = 'net' rapid soil response, F_s = Quasi – static pullout load, v = pullout velocity and L = effective nail length.

To overcome the limitations of previous pullout tests, Yin and Su [141] developed an innovative pullout box with arrangements for pressure grouting, application of back pressure for soil saturation, an extension for maintaining constant nail length during pullout and comprehensive installation of transducers for better instrumentation (Fig. 2.55). The results from pullout tests depicted that pullout increases with increase in overburden pressure, initial degree of saturation and cement grout pressure. The peak pullout is found to occur at a displacement of 5 mm which is smaller than the displacement for peak earth pressure. The peak earth pressure is 60kPa which is much smaller than the maximum overburden applied of 600kPa. The authors suggested restrained dilatancy as the probable reason for this variation. Moreover, the earth pressure measuring cells showed different values near the sides of tank before drilling reflecting that side friction plays an important part in generation of initial earth pressure. After drilling, a decrease in earth pressure was observed.

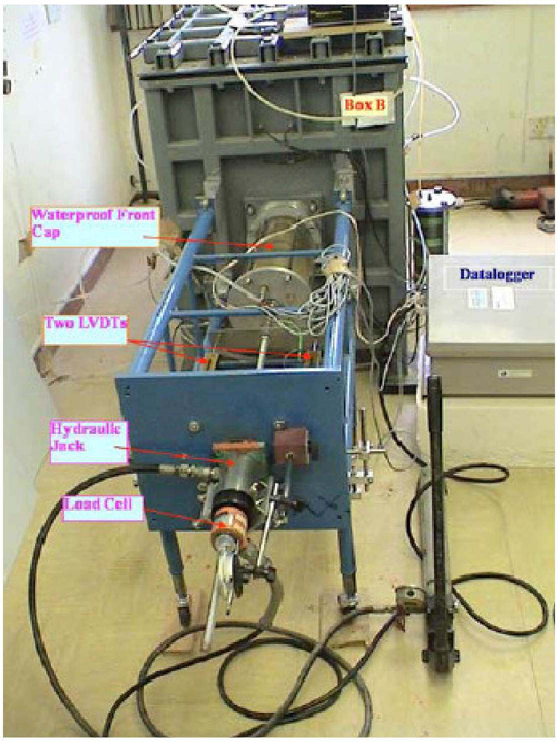

Fig. 2.55: Set - up of box with full instrumentation (After Yin and Su [141])

Later, Su et al. [142] extended the same work and carried out studies to investigate the effect of dilatancy on soil nail pullout. Pullout under different dilation angles of ψ = 0°, 4°, 8°, 10°, 14°, 18°, 26° and 29° with a constant overburden of 120kPa revealed that shear stress increases with increase in dilation angle. Moreover, the average shear stress was found to increase linearly with pullout displacement. After reaching a peak value, shear stress was observed to decrease. The response of shear stress was attributed to constrained dilatancy of soil – nail interface.

The interface friction between soil and nail was also evaluated by Gosavi et al. [143] by using a wooden tank of dimension 3.25 (Length) x 0.4 m (width) x 1.0 m (height). Various nail lengths of 3 m, 2.5 m, 2 m, 1.5 m and 1 m were used. To accommodate the changing soil nail lengths, box length was varied from 3.25 m to 1.25 m. The nails were inserted through a 50 mm circular hole at front face situated at 200 mm from tank bottom. The nails were composed of MS hollow pipe with diameter of 88 mm (external) and 80 mm (internal). The pullout box was filled with dry sand. The surcharge application was simulated by wooden sleepers and ISMC 150 channel section placed at top of pullout box. The pullout was applied by using a two pulley system (Fig. 2.56).

The results obtained by the authors reflected that pullout of nails decreases with increase in overburden pressure. However, this behavior was significant at low overburden up to 15kPa. Beyond 15kPa, the pullout was almost constant. The increasing diameter and nail length both showed an increase in pullout at low overburden pressure. It was also observed that method of installation affected the nail pullout and was found greater for pre – buried nails as compared to driven nails. The apparent coefficient of friction between nail and soil was determined using equation (2.19):

$$f^* = \frac{Pullout\ Load}{\{\pi.d.L(\gamma.z+q)\}} \tag{2.19}$$

Where, d = Nail diameter (m), L = nail length (m), γ = Unit weight of soil (kN/m^3), z = sand fill above the nail (m) and q = Surcharge intensity (kN/m^2).

Using the apparatus developed by Yin and Su [141], pullout test study on CDG soil was also conducted by Zhou [144]. The soil properties were adopted from Su [145] and Su et al. [146]. The pullout of soil nail involved test preparation by soil compaction, application of overburden with drilling of hole, preparation of soil nail with grouting, application of back pressure for saturation, observation of pullout of nail and examination of post pullout mechanism.

Fig. 2.56: Pullout model test box (After Gosavi et al. [143])

The findings of pullout test revealed that load cells measure differential pressure which becomes stable with time indicating establishment of equilibrium stress condition. As drilling and grouting is carried out change in stress is observed. The application of back pressure for saturation showed an initial suction due to use of vacuum air pump. The effective stress around soil nail is found to increase which was calculated by subtracting average pore water pressure from measured total earth pressure. The vertical effective stress was also noted to be more than effective overburden pressure. The authors conclude that saturation helps achieve relaxation of arching effect due to soil movement with flow of water through the voids.

The observations made during pullout showed that as pullout displacement was increased, an initial linear increase in pullout resistance is observed. This increase however, becomes non – linear as the peak pullout value is reached due to stress softening behaviour. The earth pressure near the soil nail showed response similar to pullout whereas load cells away from soil nail did not respond to pullout. This was interpreted as localization of stresses around soil nail is dominant during pullout. Moreover, the strains near nail head were found to larger than strains at nail end. The pullout behaviour was found to increase by gradual increasing pullout force and beyond peak pullout value, a decrease was observed. The observations after post pullout suggested that nail pullout occurs in a submerged condition which was denoted by an increase in water content around soil nail. The failure surface during pullout further indicated that failure occurs in a thin zone around the nail. Due to soil saturation, soil adheres to nail surface and consequently increases the nail diameter. However, the increase in nail diameter is not uniform due to different amount of soil adherence at different locations of nail length.

The study of effect of grouting pressure and overburden pressure was further extended by Yin and Zhou [147]. Through the investigation, they concluded that grouting and overburden pressure increase are inter – related. For high grouting pressure, pullout of nail increase with increase in overburden pressure. However, for low grouting pressure, pullout was independent of overburden pressure. Moreover, dilatancy effect of soil is insignificant in saturated soil and effect soil nail pullout under unsaturated soil conditions. The authors also developed an empirical relationship (Eq. 2.20) for predicting soil – nail interface shear resistance ($\bar{\tau}$) given as:

$$\bar{\tau} = c'_G(p_G)\sigma'_{vi}\mu'_G(p_G) \tag{2.20}$$

Where, c'_G= interception value of the initial vertical stress (overburden) σ'_{vi} = 0, μ'_G = slope of fiiting line of Eq. (2.20) and p_G = Grouting pressure.

A vertical pullout of soil nails to understand the group effect was carried out by Akis [148]. The nails were positioned at radial distance of 2ϕ, 6ϕ, 8ϕ, 10ϕ and 12ϕ from a nail placed centrally in a model test box of dimension 500 mm (length) x 300 mm (width) x 300 mm (height). The nails used were 16 mm diameter steel ribbed bars. It was observed from the experimentation that group effect did not occur beyond nail spacing of 6ϕ. Hence only two nail spacing of 2ϕ and 6ϕ were tested. The nail was pre – buried in Ankara clay and pullout was conducted at rate of 0.6 mm/min with a 100kPa overburden applied in horizontal direction. The findings of vertical pullout test revealed that centrally placed nail depicted the maximum pullout load with best group efficiency being obtained for nail spacing of 2ϕ as compared to 6ϕ. However, the authors also suggested that commonly used nail spacing at field is 6ϕ. Moreover, for nails to make ground behave as a coherent reinforced block, Phear et al. [149] recommended nail spacing should not exceed one nail per 2 – 4 m^2.

The effect of pressure grouting on soil nail pullout was performed by a series of pilot – scale chamber tests by Seo et al. [150]. The pilot – scale chamber consists of cylindrical chambers with eight side holes, pressuremeter, LVDTs and an arrangement of movable bottom for application of confining pressure. The diameter of chamber was 0.6 m with height of 0.18 (Fig. 2.57). The testing is carried out on four different residual soils namely (1)Yongsan, (2) Apgujeong (3) Mixed (Yongsan + Apgujeong) and (4) Busan soil.

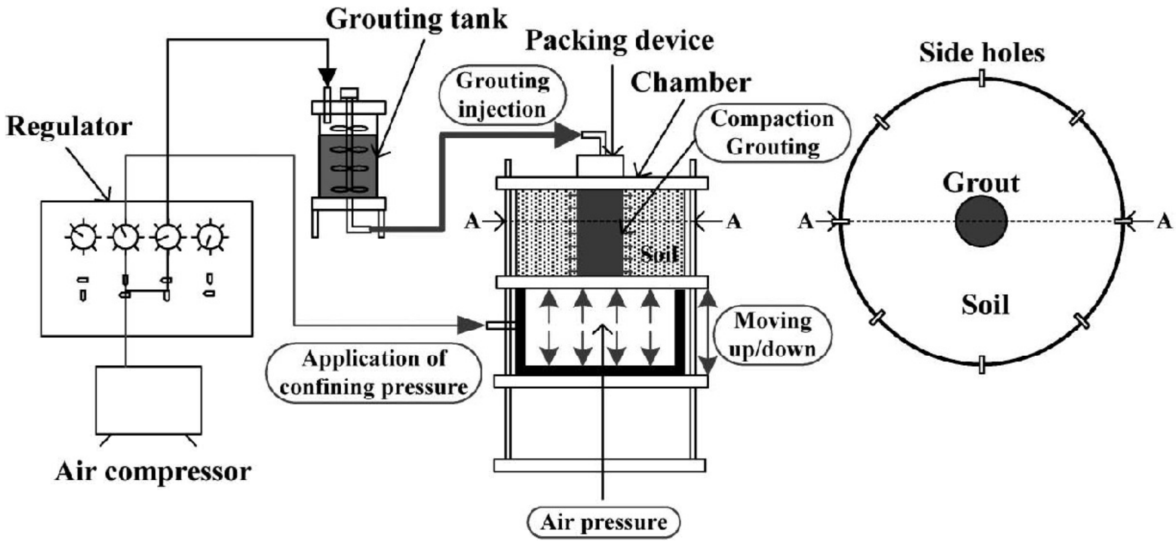

Fig. 2.57: Configuration of pilot- scale chamber test (After Seo et al. [150])

The observations of pilot tests showed that pullout of nails under pressure grouting is higher than under gravitational grouting. As the pressure grouting is undertaken, pressure along the perimeter of cavity is also found to increase. However, the pressure reaches its peak value and decreases beyond it with time. Based on this observation, it was concluded that an optimum time of injection should be maintained so as to attain peak pressure from pressure grouting. The authors suggested that initially the cavity retains the grout which leads to an increase in pressure. With increase in time, water from the grout distributes in adjacent soil resulting in pressure reduction. The results also depicted that an increase of 20% between in – situ stress and injecting pressure is observed. The increase in pullout with pressure grouting was attributed to increase compaction of surrounding soil due to cavity expansion, higher residual stress and greater dilatancy angle.

The effect of overburden and grouting pressure were further studied by making use of field studies by Hong et al. [151]. It was concluded by the field testing that pullout of soil nail decreases with increase in overburden pressure. However, under constant overburden pressure, pullout of grouted soil nails was found to increase with grouting pressure. Moreover, soil – nail interface governed the pullout failure of nails with failure zone shifting more deeper (16 mm) into surrounding soil instead of occurring at soil – nail interface. The water content at soil – nail interface after pullout was found to less than soil from drill holes.

2.5 Numerical Modeling of Soil – Nailed System

The various parameters governing the soil – nail system design were well comprehended and mathematically inter – related by various researchers by theoretical analysis. The theoretical analysis primarily involved the use of limit equilibrium method (LEM) for determination of failure mechanism of reinforced slope. The factor of safety calculation, pseudo static analysis, prediction of interface friction and analysis of soil - nail pullout, all have been theoretically analyzed in the past by Bonaparte and Schmertmann [152], Wright and Duncan [153], Huang and Tatsuoka [154], Liang et al. [155], Bang and Chung [156], Luo et al. [157], Bennis and De Buhan [158], Patra and Basudhar [159], Gosavi et al. [160], Yin et al. [161], Hong et al. [162], Gurpersaud and Vanapalli [163] and Zhang et al. [164].

With the evolution of analytical tools, software packages were developed which could handle large data and provide more accurate results. These analytical codes were mainly based on finite element method (FEM) for plastic deformation analysis of soil - nailed system whereas conventional LEM based codes were also generated for stability analysis. With results obtained from both FEM and LEM were in good agreement, FEM was highly preferred in cases where slip surface prediction by LEM was a difficulty [165, 166, 167]. The most important parameter for numerical modeling of reinforced structures was the simulation of interface between soil – reinforcement. Since during failure, slip between soil – nail interface occurs, an element reflecting the exact slippage and corresponding shear stress mobilization was necessary. Moreover, discretization of soil – nailed structure using appropriate number of nodes and elements established the accuracy of numerical modeling.

As more and more computer oriented analysis came into play, numerical modeling was extended to three – dimensional (3D) from two – dimensional (2D) analysis. It was also observed that 3D analysis was more accurate in modeling the actual soil – nail interaction as compared to 2D. However, with less computational time 2D analysis has always been the first choice of researchers.

The effect of axial rigidity of nail (E_nA_n) where, E_n is the modulus of elasticity of nail (kN/m^2) and A_n is the cross – sectional area of nail on stabilizing tunnel face was studied through FEM modeling using ABAQUS by Ng and Lee [168]. The soil nails were modeled using a 2 – noded beam element with 4 – noded shell element used for modeling the concrete lining of tunnel. The soil continuum was modeled using 8 – noded brick element with mesh discretization consisting of 4400 elements and 4000 nodes (Fig. 2.58).

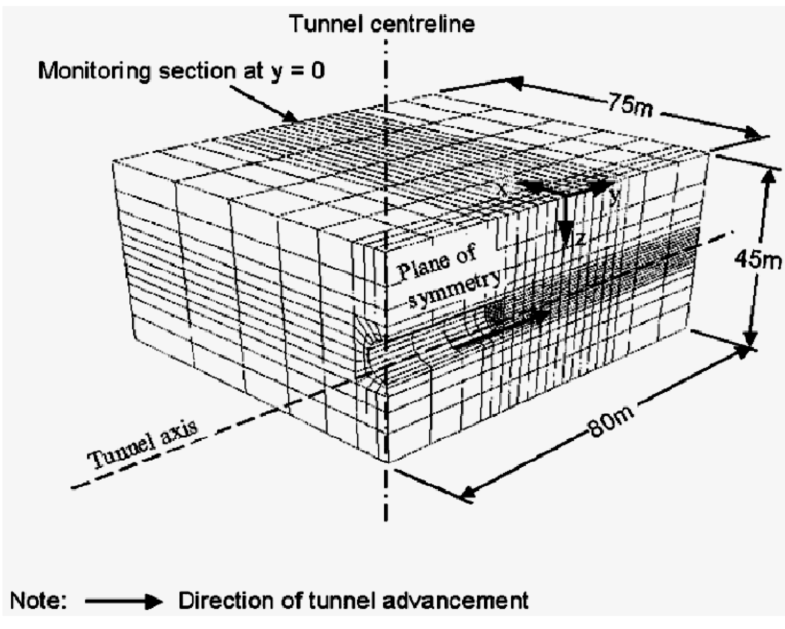

Fig. 2.58: Three – dimensional finite element mesh (After Ng and Lee [168])

Since the beam element was simulated for mobilization of tensile forces only, beam element was used. The use of shell element provided the opportunity of simulating axial force and bending moments induced in tunnel lining. With no slippage condition, the soil – nail interface was idealized to be in full contact and governed primarily by maximum angle of internal friction of soil. The constitutive model used for soil idealization was Drucker – Prager which is associated with plastic flow and non – circular yield criterion. The findings of finite element analysis (FEA) yielded that stabilization of tunnel face increases with increase in axial rigidity which was depicted by a reduced tunnel face displacement. It was also concluded by the authors that deformation of tunnel face changes from elliptical geometry to become constant with depth as E_nA_n of nail increases.

Using a 3D interface element named as 'anchor – interface element' and implementation of 16 – noded thick shell element for modeling diaphragm wall, sheet – pile wall and timber lagging tunnel, Xue [169] carried out numerical modeling of anchor – soil interaction for pullout of anchor in residual soil and granite. The interface element used was a modified form of linker element which was initially used to model soil nails. The interface element represented a wrapping interface element around solid inclusion modeled using a beam as available in CRISP software package. The results of numerical modeling revealed that load – displacement behavior of anchored system depicted the hysteresis loop which was observed during field testing. Moreover, the proposed model also results in defining the response of bonded as well as unbonded length of inclusion.

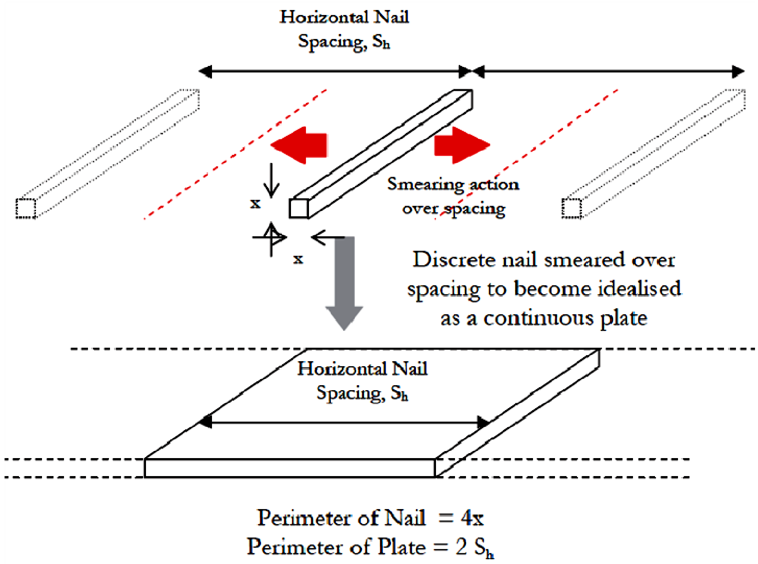

Fig. 2.59: Smearing of a discrete soil nail into a continuous plate (After Eng [170])

A comparative study between 2D and 3D idealization of soil nails was carried out by Eng [170]. To further evaluate the performance of modeling using 2D and 3D condition, pullout of soil nail was simulated with variable nail spacing and design charts were developed. From the study it was observed that soil nails are smeared as plate elements in 2D idealization for modeling plain – strain condition (Fig. 2.59). However, this smearing reduces the continuity of soil continuum above and below the plate element, thereby failing to model the side friction.

The smearing of interfacial properties mainly governed by slip behavior developed during staged construction of soil – nailed structure is modeled as fully elastic or fully plastic property. The interface friction developed between soil and nail is a function of normal stress and surface area. The normal stress developed in 2D and 3D idealization is similar but surface area of plate far exceeds that of a 3D nail. Hence, surface area has to be smeared into interfacial properties. Moreover, for accurate modeling of normal pressure, its variation along nail length and non – uniformity of stress around soil nail during shearing, interaction factors I_0 and I_1 has to be taken into account. These factors were defined by equation (2.21) and equation (2.22):

$$I_0 = \frac{\mu . A_{nail} . \sigma_{av}}{P_{3D}} \tag{2.21}$$

$$I_1 = \frac{M_{3D}}{M_{2D}} \tag{2.22}$$

Where, μ = Coefficient of interface friction in 3D, A_{nail} = Cross -sectional area of nail in 3D, σ_{av} = Average overburden pressure at nail height, P_{3D} = Pullout capacity of soil – nail interface under uniform normal pressure, M_{3D} = Mobilization factor of 3D nail forces at soil – nail interface corresponding to pullout capacity, M_{2D} = Mobilization factor of 2D plate for nail forces at soil – nail interface corresponding to pullout capacity. Using the interaction factors, interfacial properties are smeared and reduced coefficient of friction (μ_R) is determined by equation (2.23):

$$\mu_R = I_0 . I_1 . A_f . \mu \tag{2.23}$$

Where, A_f = Contact surface area factor = A_{nail}/A_{plate}. The findings of the work reported suggested that without using interaction factors, pullout is under predicted (30 – 60%) in 2D due to smaller horizontal stresses and larger interface friction. The authors recommended I_0 = 0.5 to 0.6 for all practical soil nailing applications. Moreover, it was also reported that in 2D analysis, due to improper mobilization of pullout resistance, high restrainment is observed leading to decrease in nail forces with increase in axial resistance. This behavior was dominant in stiffer soils with smaller facing deformations. A similar response was also observable for large nail spacing. Similar effect was noticeable in 3D for nail spacing less than 0.5 m. However, soil – nail models were found to be independent of restrainment with full mobilization of pullout resistance in soft soils for both 2D and 3D.

Shaw – Shong [171] studied three cut slopes, two filled slopes and one natural slope through field monitoring and numerical modeling. The results of numerical modeling done by using LEM and FEM were back – analyzed for validation of field results. With c-ϕ strength reduction method, FEM was used to predict the factor of safety. Moreover, FEM was also used to interpret the slip surface generated by non – uniform shear stress developing at slip surface. The limit equilibrium analysis (LEA) was carried out by a computer program developed by Harald [172] called PC – STABL6 and Plaxis was used for FEA. The findings of the study revealed that both LEM and FEM can be utilized for predicting the failure surface. However, by back - analysis it was found that slip surface with mobilized shear strength through numerical modeling did not coincide with identical field slip surface. Hence it was concluded by the authors that slip surface generation occurs in a weak soil band beyond which shear strength of soil is significant.

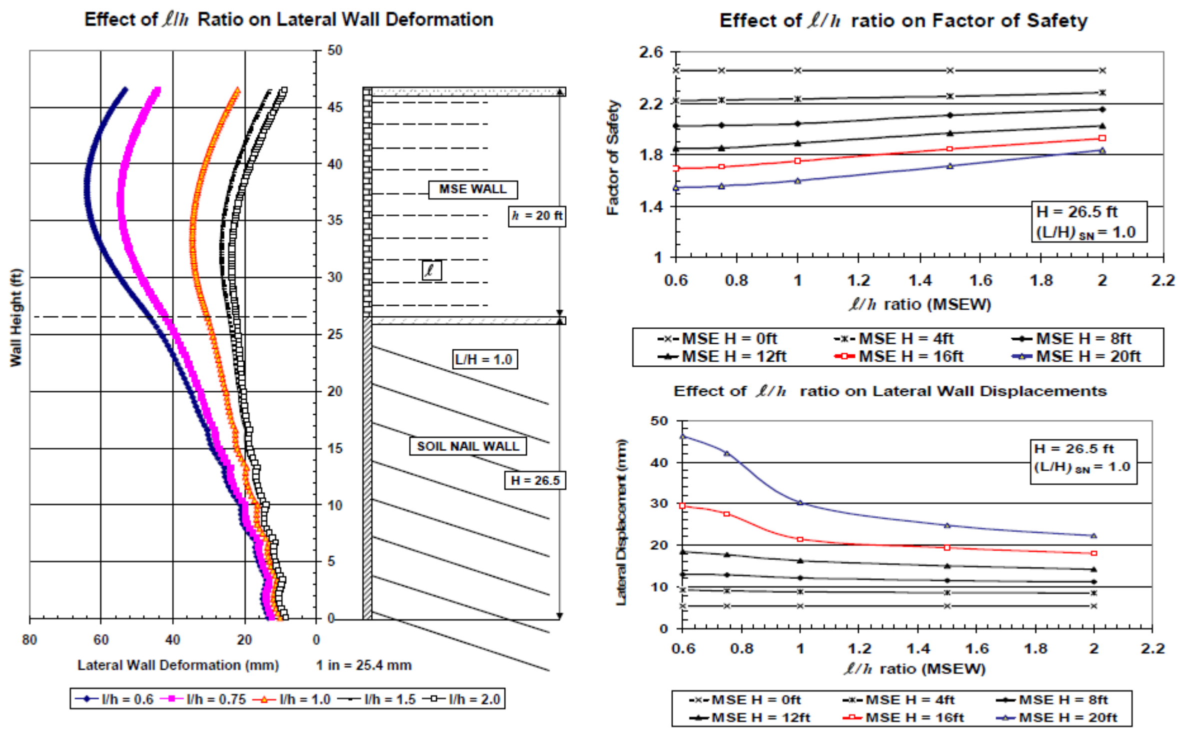

Fig. 2.60: Effect of *L*/*H* on factor of safety and wall deformation (After Alhabshi [173])

A finite element based design of MSE/ Soil nail hybrid wall was developed by Alhabshi [173]. The FEA was carried out using PLAXIS routine. The soil nails were modeled using beam element with interface element allowing slippage between soil and nail consisted of 5 – noded element with virtual thickness factor of 0.1. The MSE reinforcement was modeled using geogrid elements as available in the software package. The results from FEA revealed that reasonable quantitative agreement is achieved between the results from measured and FEM predicted values. However, for nail forces FEM predicted larger values for lower nails which were not satisfied by the measured results. Moreover, the design procedure showed that stability of MSE/soil – nail hybrid wall depends upon the selection of optimum nail and geogrid length. For soil nail and MSE wall, optimum reinforcement length resulting in optimum factor of safety and minimum wall deflection as given by the author was L/H = 0.8 to 1.0.

A simplified numerical method for analyzing effect of soil nails in loose fill slope was given by Zhou et al. [174]. The FEA was done using ABAQUS package with use of embedded element for modeling of soil nails. With introduction of embedded elements, the need of soil – nail interface element was not required. The measured and numerical results showed that nail forces in upper nails of loose slope are found to increase with increase in overburden pressure. The results also depicted the strengthening of loose fill slope by incorporating soil nails.

Wei [175] also conducted three – dimensional slope stability analysis and failure mechanism study using strength reduction method (SRM) and LEM. The LEA is carried out by the software package Slope 2000 and SRM was done using FLAC3D. The findings of the study suggested that slip surfaces and factor of safety as predicted by LEM and SRM are similar. However, with overburden pressure application, variation is observed. For steep slopes, the stability of soil – nailed slope is governed by elastic modulus of nail. In contrast to the recommended layout, the author recommended longer nails to be placed at bottom and shorter nail lengths to be used at slope top.

It was also reported that as nail inclination is increased, only small bending moment is mobilized. Hence design recommended by conventional methods was found satisfactory. The authors also concluded that points of maximum tension may not necessarily lie on critical slip surface but is dependent on state of soil slope (service or limit state) and failure modes (external or internal). For internal tension failure condition maximum tension points are found at the critical slip surface. The loading of slope also controls the mobilization of nail forces. If a slope is locally loaded, nail forces are mobilized at top row of nails in contrast to non – loaded slope where bottom rows are found to develop nail forces. Wei et al. [176] extended the study to 3D SRM and LEM analysis of slopes.

The determination of optimum layout of nails employing numerical study by FEM was done by Fan and Luo [177]. Using PLAXIS code, different slopes angles of 70°, 60°, 50° and 40° with nail inclination to the horizontal as 0°, 8°, 16°, 23°, 30° and 40° were modeled (Fig.

2.61). The optimum layout of slopes was determined by finding the factor of safety and developing stability charts. It was concluded by the author that nail inclination is found to decrease with increase in slope angle and decrease in back slope angle. The nails at the bottom 1/3 of soil - nailed wall generally regulate its overall stability. The authors also inferred that if number and horizontal spacing of nails is unchanged, vertical spacing is insignificant for wall stability.

A similar study proposing design charts for soil nailing was also carried out by Mohamed [178] by prediction of global factor of safety and wall defection using FEM based software package PLAXIS. The study also included understanding influence of effect of nail length –to - wall height ratio, nail spacing, wall inclination, nail inclination and soil properties on global factor of safety.

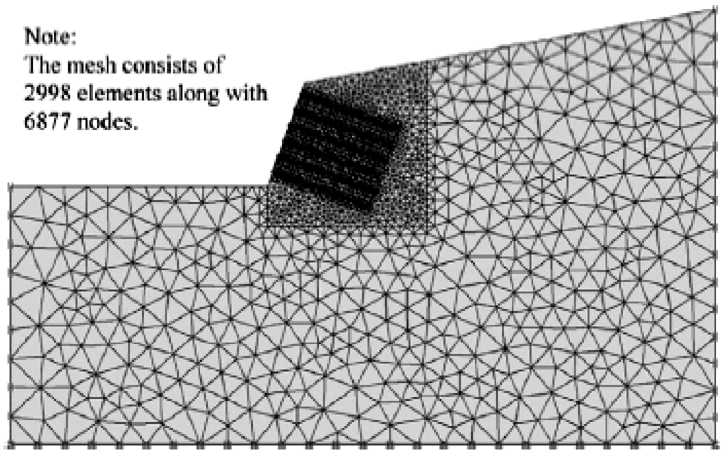

Fig. 2.61: Finite element mesh of soil – nailed slope with slope angle of 60° and backslope angle of 10° (After Fan and Luo [177])

A new soil – nail interface model known as 'embedded bond – slip model' was given by Zhou et al. [179]. The new technique incorporated the concept of modeling soil nail as a discrete element with nodal displacements being calculated by embedded approach. Moreover, the interface element was defined by a pair of interface elements with allowable slippage. Unlike conventional approach, the new proposed approach did not require consideration of pore water diffusion between separate nail element regions. The new model also facilitated ease of meshing irrespective of nail location. The authors introduced this concept as a combination of embedded element technique and conventional interface element method (Fig. 2.62).

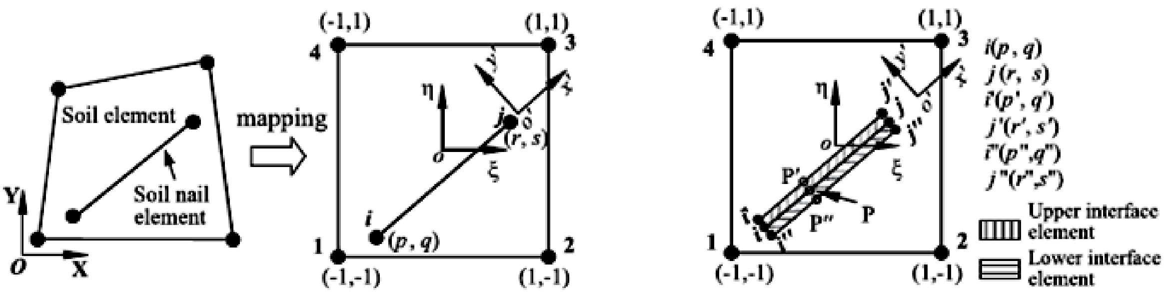

(a) Embedded element method (b) Embedded bon – slip model

Fig. 2.62: Modeling of soil nail (After Zhou et al. [179])

The validation of new proposed model was carried out by implementing it in a slope model and comparing with conventional soil nail modeling technique. The results as reported by the authors depicted that embedded bond – slip model gives a better prediction of nail forces at higher groundwater levels. Both techniques however, show under prediction of for low groundwater levels. The nail forces along nail length for bottom row of nails are under predicted at nail head by both methods with close prediction to measured values depicted by soil nail modeled with embedded bond – slip technique. Eventually, it was concluded by the authors that for large loads, embedded bond – slip method gives a better prediction due to accurate simulation of slippage location for soil – nail interface. The use of the suggested new soil nail model was also tested by Zhou et al. [180, 181] by modeling a soil nailed slope in loose fill under surcharge loading. The numerical modeling was done in FE package ABAQUS with results used for back analyzing the measured field testing data. The behavior of soil nails under application of surcharge with pore water diffusion and water content redistribution in soil was modeled. The results showed a good quantitative agreement between results of new embedded bond – slip soil nail model and field testing results.

Numerical modeling using FEM was conducted on 4,700 car underground parking garage located at the Microsoft Block C site in Redmond, Washington [182]. The base walls 335.3 m and 121.9 m were stabilized using top – down soil nailing technique. The static and seismic performance was evaluated using PLAXIS software. The evaluation consisted of estimating soil pressure and wall deflection. The authors concluded that permanent soil nails can be used for reducing soil loads acting on basement walls. Moreover, realistic estimation of soil loads can be obtained from numerical analysis. Similarly, seismic performance of a soil – nailed wall was also assessed by Babu and Singh [183]. Moreover, numerical modeling using PLAXIS of other case history included excavation retained by soil nail wall in soft deposit of Shanghai, China as given by Ma et al. [184].

Numerical modeling of soil nail pullout has been carried out Zhou et al. [185] using ABAQUS explicit code. The experimental study of pullout of soil nail done by Zhou [144] and Yin and Zhou [147] was modeled in 3D FEM condition. The effect of grouting and overburden on soil nail pullout was evaluated and numerical modeling results were validated from experimental results. The CDG soil used in testing was modeled using a constitutive soil model called Drucker – Prager/Cap model with 2 – noded beam element used to simulate the soil nail of circular cross – section. The interface element between soil and nail was modeled by using a quadrilateral element represented by a cylindrical surface around the beam which was constrained using 'tie' connection as available in the software package (Fig. 2.63).

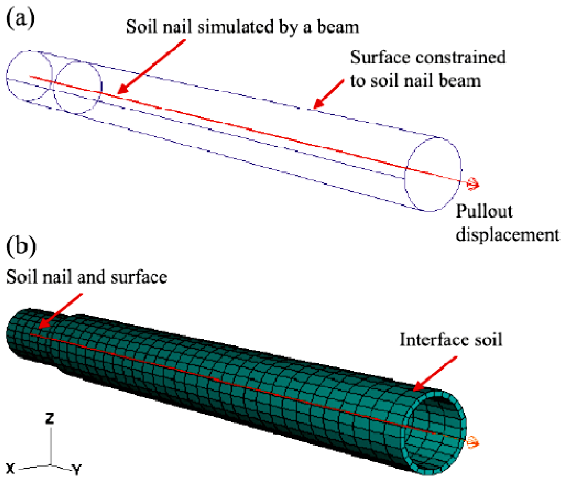

Fig. 2.63: Modeled soil nail (After Zhou et al. [185])

Mohr – Coulomb friction model was used to describe the interface between soil – nail in the cylindrical surface. The drill hole and surrounding soil interaction was attained by defining an interaction called 'contact pairs'. The modeling of soil nail pullout was performed in five steps as (1) drill hole (2) initial stress development after drilling (3) pressure grouting (4) soil saturation (5) pullout.

The numerical modeling results depicted that pullout of nails increased with increase in overburden and grouting pressure. Under a constant overburden pressure, peak pullout is achieved for higher grouting pressure. The basic trend of pullout resistance with pullout displacement shows a linear increase up to a peak value beyond which it levels off with increasing displacement (Fig. 2.64). The back analysis of numerical modeling results were verified with experimental results.

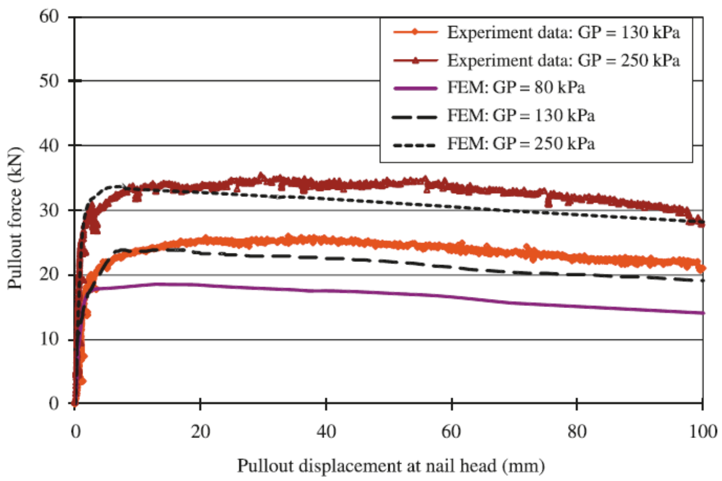

Fig. 2.64: Numerical and experimental results (After Zhou et al. [185])

Another technique of modeling soil nail using fast lagrangian analysis of continua three dimensions (FLAC3D) was given by Chen and Zeng [186] for numerical analysis of effect of soil nailing on stress and deformation behavior of foundation pit. The soil nail was modeled using double – spring nail element (Fig. 2.65).

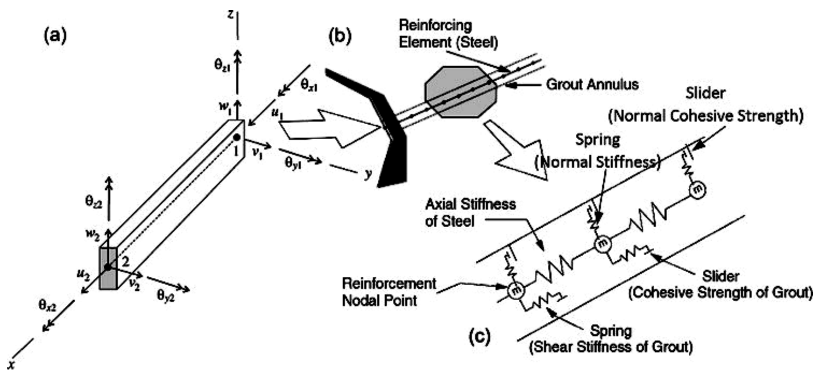

Fig. 2.65: Nail element used by Chen and Zeng [186]

The staged construction was simulated from top – down, which resulted in fourteenth row of nail depicting the largest nail forces which corresponded to the fourth stage of excavation. The study of unbalanced forces to indicate stability condition showed that with each excavation step, unbalanced forces are generated. These forces eventually fade off to zero as stability is reached. The maximum unbalanced forces were recorded for fourth and fifth excavation stages indicating the need of reinforcement for local stability. The site wall deformation of pit revealed maximum displacement at top and middle with small deflection noticed for wall bottom. Without soil nails, calculated factor of safety accounted for fourth and fifth excavation was less than 1 which increased to greater than 5, with use of soil nails.

With the conclusion of pullout as the primary factor governing slope stability over shear resistance of soil nails, Kim et al. [187] conducted a series of numerical modeling slope stability analysis using pressure – grouted soil nail. Slopes comprised of weathered soil were reinforced using soil nails which are grouted under pressure were analyzed under two – dimensional axisymmetric finite element model. The investigation focused on employing SRM method through ABAQUS for determining factor of safety. It was observed that stiffness of soil slope is increased due to pressure – grouting which consequently increases the factor of safety of soil – nailed slopes by 50%. Similarly, stability analysis using SRM was also conducted by Lin et al. [188]. Numerical analysis was also involved for calibration of load factors for pullout resistance of soil nails by Devries [189]. The measured results for predicted factors from field pullout testing were validated by PLAXIS software. A close agreement was observed for 25 field tests out of 47. The failed test load factor prediction was done statistically incorporating survival analysis. Finally, SNAILZ routine was used for comparison of required nail length from predicted load factors and conventional design method for a soil nail wall.

The commonly used Goodman model for soil nailing was encountered with numerical errors due to large stiffness value. To overcome this error, Xue et al. [190] added two rotational degrees of freedom and proposed a modified Goodman model for soil nail. The comparison of finite element program developed using modified soil nail model showed a comparable and feasible relation with the measured field values. Slope stability of soil - nailed slopes in residual soil using LEM based code GEOSLOPE was performed by Asoudeh and Oh [191]. From the study, the authors concluded that residual soils with cohesion less than 10kPa are sensitive to failure and hence should be assessed for stability after reinforcing with soil nails. A similar numerical study of grouted soil nails using PLAXIS (FEM) was done to study the performance of a vertical cut with soil nails [192].

2.6 Previous Studies on Helical Anchors

The concept of screw nails has been developed from the traditional helical foundation anchors and dates back to 1836, when a blind Irish brick maker and civil engineer named Alexander Mitchell [194], used helical pile which was patented as screw pile. With its initial application in ship moorings and light house foundations screw piles became extensively used in pier and bridge construction by late 1800s. Das [193] and Perko [194] provided a detailed historical and theoretical development of helical foundation anchors. With its increase in use as foundation anchors, screw piles has been studied theoretically and experimentally in detail by many authors such as Mitsch and Clemence [195], Kulhawy [196], Das [193] and Ghaly et al. [197].

The development of screw nails from screw piles however, brought forward fundamental difference in design and performance such as anchors are prestressed during installation whereas soil nails are not prestressed. Installation of helical anchors is governed by average torque whereas design length regulates soil nail installation. Anchors are primarily designed for tension and compression forces whereas shearing, tension and bending resistances constitute soil nail design procedure. The stress condition developed around an anchor is different from that developed around a soil nail, hence both have different failure mechanisms and influencing parameters. The pullout of anchors is predicted by 'cylindrical shear method' or 'individual plate bearing method' or 'empirical installation torque' whereas average shearing resistance is used for pullout prediction of soil nail.

The effect of helical pitch spacing to corresponding soil disturbances and density change was studied by Kenny et al. [198]. The authors conducted studies using different augurs with varying pitch to diameter ratio facilitating different penetration rates. The experimental study was performed in a loose to medium dense sand. The variation in sand density, surface heave, settlement and volume of transported sand were measured for different penetration rates. The results suggested by author that better densification of soil is attained for steeper flight and large shaft diameter. However, installation of such augurs was found to be difficult due to large torque required and limited capability of rigs. Based on the observations, authors recommended use of small pitch ratios for foundation anchors for minimal soil disturbance during installation.

Kulhawy [196] studied classified anchors as spread, helical and grouted anchors based on various geometries and construction methodology taken under consideration. It was concluded by the author that minimal soil disturbances are possibly with anchor installation and hence full utilization of in – situ shear strength properties of soil can be achieved. However, practically this was seldom possible which lead to a cylindrical shear failure for anchors. The pullout behaviour as studied by the author depicted that anchor weight, side and tip resistance generally contribute for uplift capacity of anchors. The failure mechanism of anchors based on shear surface can be 'cone or wedge break out', 'cylinder' and 'punching or bearing' failure.

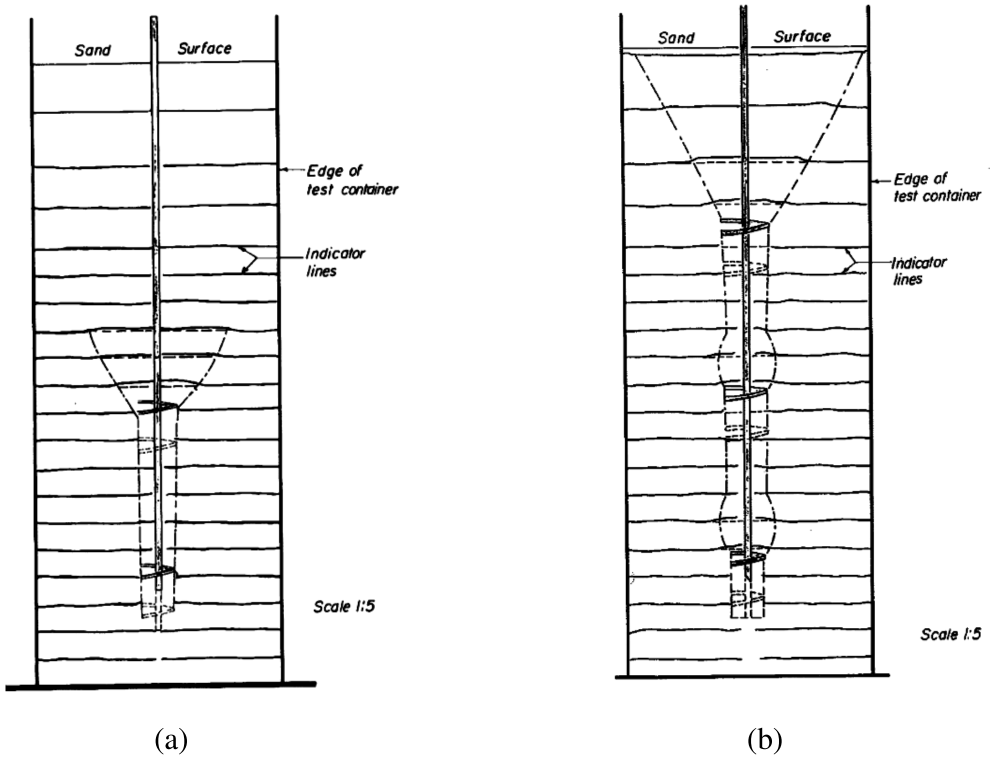

Fig. 2.66: Failure surfaces (a) Deep anchors (b) Shallow anchors (After Mitsch and Clemence [195])

The review of literature revealed that limited work has been carried out for study of multi – helix anchors. Based on experimental work, semi – empirical relationship for uplift capacity of multi – helix anchors was derived by Mitsch and Clemence [195] and Mooney et al. [199]. The relationship considered failure mechanism due to bearing and cylindrical failure as shown in Fig. 2.66. With dissimilar failure pattern to Mitsch and Clemence [195], Ghaly [197] also derive a similar relation for prediction of uplift capacity of anchors from experimental work carried out single helix anchors buried in sand compacted to different densities (Fig. 2.67).

Lateral capacity of helical piles in clay through experiment testing was done by Prasad and Rao [200]. The authors reported that lateral capacity of helical pile is 1.2 – 1.5 times greater than for a straight pile. The authors also developed a theoretical model by incorporating parameters of shaft friction, bearing resistance of bottom helical plates, uplift resistance of top helical plate and surface friction of helical plate as given in Fig. 2.68. With the uplift of helical anchors as primary parameter of study for majority research work, lateral pullout of helical anchors was also studied by Ghaly [201]. The study included assessment of horizontally loaded vertical plate through experimental and theoretical analysis as given in literature. Based on the evaluation, the authors made an attempt to develop four generalized equations for accurate prediction of pullout resistance of anchors. The results primarily involved observation of load – displacement of anchor plates.

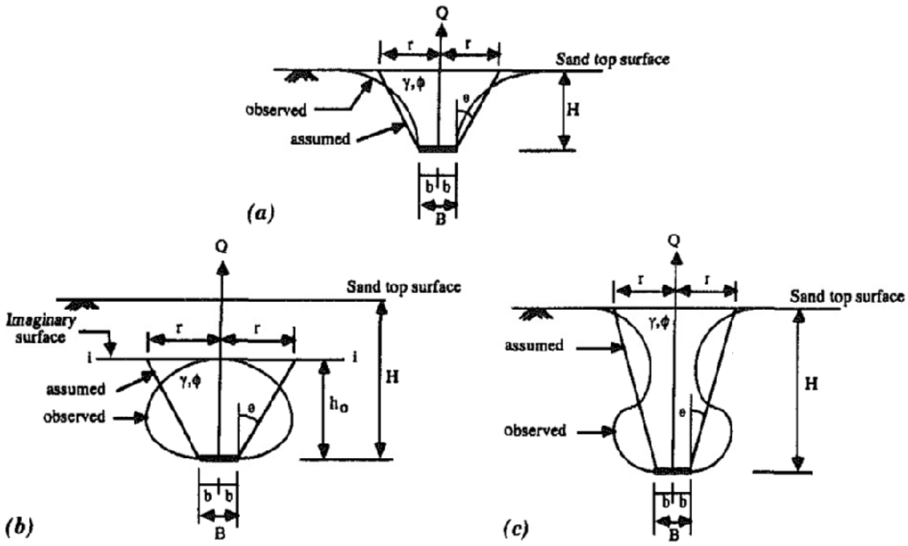

Fig. 2.67: Failure surfaces (a) shallow (b) transit (c) deep anchors (After Ghaly [197])

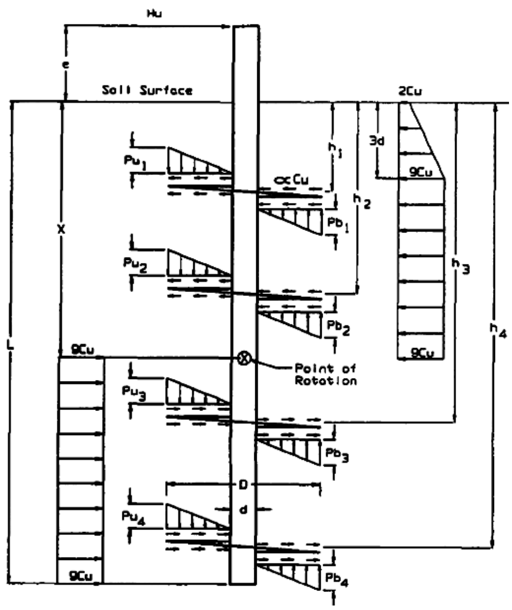

Fig. 2.68: Helical pile at ultimate lateral load (After Prasad and Rao [200])

Apart from various experimental studies on pullout of anchors, Merifield and Sloan [202] performed numerical analysis on anchor pullout using upper bound finite element and lower bound limit analysis. The results of numerical study revealed that as anchor plate is pulled out horizontally the soil above the plate extends upward and outwards from the plate edge. For vertical uplift of plate, due to restrained dilatancy, soil above the plate gets locked up. For $H/B > 2$, where H = depth of helical plate below ground and B = width of helical plate, active soil pressure immediately behind the anchor plate is insignificant but increases the pullout by 18% for plates with $H/B \leq 2$ and $\phi' \leq 20°$. The anchor roughness was found to affect the pullout capacity of vertical anchors in dense soils ($\phi' \geq 40°$). The anchor roughness was also observed to decrease with increase in embedment ratio. Transition in anchor roughness between rough to smooth caused a decrease of 67% in the pullout capacity of vertical anchor plate. Pullout capacity of vertical anchors was also found to increase by 50% in dilatant soil as compared to a soil without dilatancy. Merifield [203] also investigated the effect of anchor spacing ratio (*s/D*) and anchor embedment ratio (*H/D*) on failure mechanism and consequently on uplift capacity of helical anchors in clay. The spacing (*s*) of anchor plate was also found to influence deep failure mechanism. The depth of anchor plate from ground (H) and helical plate diameter were parameters which significantly brought transition in failure from deep to shallow failure mechanism.

The axial capacity of helical pile with square shaft was investigated by Livneh and Naggar [204] using FEM. The axial capacity was tested both for compression and tension loading. The study included examination of ultimate load capacity and load transfer mechanism of 19 full scale tests and its FEM analysis. The helical pile used for the study consisted of three circular welded helical plates along slender square shaft (Fig. 2.69).

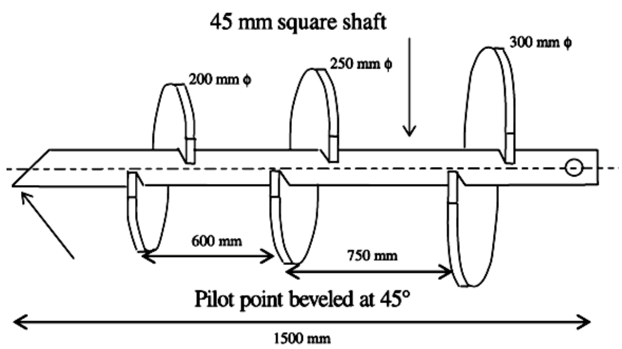

Fig. 2.69: Schematic of pile section (After Livneh and Naggar [204])

The authors proposed prediction of load capacity as load corresponding to pile head displacement of 8% of maximum diameter helical plate plus pile elastic deflection. Two torque correlation factors were also derived for compression (K_T = 33 m^{-1}) and tension (K_T = 24 m^{-1})

respectively for relating pile load capacity with installation torque. The load transfer mechanism as reported by the authors followed a cylindrical shear mechanism with top helical plate offer bearing in direction of load application and tapered inter helical soil profile. A similar study was also carried out by Tappenden et al. [205] where the lower most helix was considered to be contributing significantly to axial capacity of helical pile in tension.

The variation of helical plate spacing to diameter ratio from 0.75 to 3 and number of helical plates from 1 to 4 with constant spacing to diameter ratio of 1.5 through full scale test was performed by Luteneggar [206]. The load capacity of helical screw anchors was noted at displacement of 20% of maximum helical plate diameter. The observation depicted that failure mechanism shifts from cylindrical failure to individual plate bearing failure at spacing of 3 with efficiency still being less than 100%. This signifies that installation effect persists and affects the load capacity of screw anchors. The load capacity of screw anchors was found to decrease with increase in number of helical plates even at small spacing. The installation effect on high capacity helical piles was also examined with full scale testing by Sakr [207]. Other experimental and numerical study on helical pile was done by Papadopoulou et al. [208], Knappett et al. [209], Demir and Ok [210], Spagnoli and Gavin [211], Bagheri and El Naggar [212].

Perko [194] depicted that failure mechanism classified as plate bearing method generally involved contribution to uplift capacity of helical anchor by soil displacement. The pressure of soil acting over each plate is uniform and with shaft friction acting between helical plates (Fig. 2.70). The uplift capacity was thus given as the summation of bearing from individual plates and friction offered from anchor shaft (Equation 2.24):

$$Q_u = \alpha . L . P + \sum_n q_u A_n \tag{2.24}$$

Where, α = Adhesion factor, L = Anchor length, P = Perimeter, q_u = Terzaghi or Meyehof bearing capacity, A_n = Area of nth helical plate. The cylindrical shear failure mechanism on the other hand considers soil between the helical plates to form a cylinder. The uplift of anchor thus depends on the shear stress acting along the cylinder which is formed by inter helical soil, soil adhesion to shaft and bearing by the top helical plate. Equation (2.25) depicts the ultimate pile capacity as:

$$Q_u = q_u A + S_u(n-1).z.\pi.D + \alpha.P.H \quad (2.25)$$

Where, $(n-1)z$ = length of soil between helix. The failure mechanism based on installation torque was originally developed by Hoyt and Clemence [213]. The concept of this empirical relationship was based on the fact that denser soil will impose more resistance during installation of anchor by rotation. Moreover, more resistance require higher torque and consequently higher will be the helical pile or helical anchor capacity. The semi – empirical relation is given by equation (2.26):

$$Q_u = K_t.T \quad (2.26)$$

Where, K_t = Installation torque coefficient with value of 32.8 m^{-1} accepted for practical purposes.

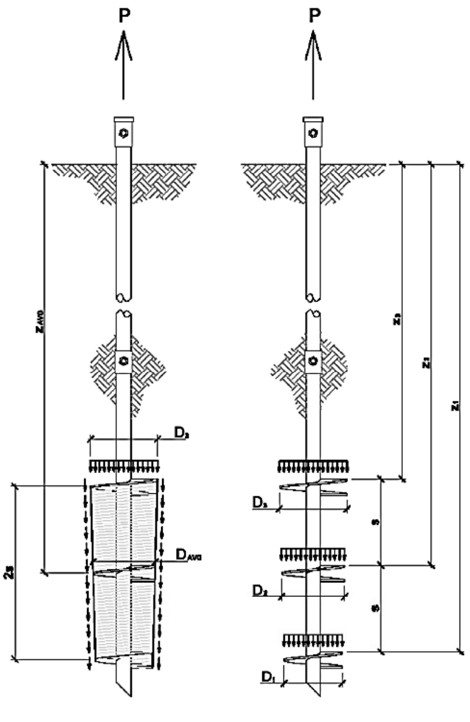

Fig. 2.70: Failure mechanism (a) Cylindrical shear (b) Individual plate bearing (After Perko [194])

Tokhi [214] conducted pullout test on a screw nail, first of its kind with the aim of rectifying the disturbances associated with installation of conventional soil nail and soil spoils produced. The screw nail consisted of three helical plates of varying diameter with smallest at nail tip for easy nail penetration. The helical geometry added to the screw in action during torque application at nail head. A fourth helical plate was welded at some distance away to increase the pullout resistance of nail (Fig. 2.71). The experimental pullout test on screw nail depicted that pullout was sufficiently increases due to helical plates with failure zone mainly forming at or around the helical plates. The FEM analysis using axisymmetric condition also depicted a similar failure mechanism with plastic strain generated mainly behind each helical plate. From the study, it was also concluded that normal stress around helical soil nail is also non – uniform and due to helical plates failure is shifted from soil- nail interface to deep surrounding soil.

Fig. 2.71: Screw soil nail (After Tokhi [214])

2.7 Summary of Literature Review

From the review of literature, it was investigated that small – scale model tests have always been used to develop first hand approximation of performance of soil - nailed structures. The analysis carried out based on model tests involved the examination of effect of soil properties, slope angles, nail inclinations, nail surface roughness, nail stiffness, nail length, nail layout and surcharge effects. Experimental analyses also lead to development of empirical relationship for predicting factor of safety against stability. Model testing of steep cuts and slopes also helped understand the development of failure surface corresponding to different geometry such as circular, block, wedge, bi – linear or log spiral. The response of different soil slope to loading condition was depicted closely to the actual field conditions. The generation of slip surface, failure mechanism undergone and stress – strain state reinforced slopes all can be inferred through model testing. Based on the usefulness of estimating stress conditions developed during failure and strains mobilized along nail length, interpretation of nail forces was also done. The tensile forces developed in nails along with their performance in shear and bending was evaluated correctly by proper instrumentation of soil – nailed prototype. Thus, it can be concluded that small – scale model testing can be employed for investigating and evaluating performance of soil nails in rendering stability and an estimate for its field application can be provided. There is always an optimum layout of soil nails corresponding to a particular soil slope at desired nail inclination which provides maximum stability against failure.

The large – scale field testing depicted that soil nails have provided satisfactory performance and serviceability for diverse structures and in – situ conditions. Not only in new construction but also as remedial measures, soil nailing has been utilized at various places and conditions around the globe. The evolution of soil nailing with transition regarding different nail types being developed reflects the adaptability of technique and its increasing demand over other earth retaining methods. The performance and monitoring of full scale soil – nailed structures showed predicted failure mechanisms, stress – strain generation and slope deformations. The reduced wall deflections, slope settlements and increased factor of safety against slope stability further defined soil nail efficiency. However, accurate evaluation of soil nails can always be attained from large – scale testing due to realistic boundary conditions and factors which may be restrained during small – scale model testing.

The soil – nail mechanism primarily involves interaction between soil and nail. The developed interface friction governs shear stress generation during failure. The studies carried out through various researchers reveals that interface friction can be understood by direct shear tests, interface shear tests and more accurately by pullout tests. Moreover, interface friction not only depends upon the surface roughness of reinforcement but also relates significantly with overburden pressure, grouting pressure, soil saturation, water content and soil dilation. Since interaction between soil and nail has been classified as complex, analytical tool like limit equilibrium method and finite element method has provided necessary solutions. The numerical analysis using LEM has revealed that external and internal stability of soil – nailed structures can be attained by determining factor of safety. However, the factor of safety is also found to vary with slope angles, nail inclination and analytical method used for assessment. The failure mechanism involving non – uniform stress – strain conditions can be well predicted by FEM. Using SRM with FEM can also be employed for determination of factor of safety of nailed system. The stress softening behaviour of soil and corresponding strain development are accurately predicted by FEM. Based on this it can be suggested that numerical modelling using LEM and FEM can evaluates behaviour of reinforced system regarding stability and performance.

It is also observed from literature review that recently researchers have developed soil nails to overcome installation difficulties associated with conventional grout soil nails. The procedure of drill hole, tendon alignment and grouting not only leads to alteration of in – situ strength but also creates large soil spoils. The innovative spiral groutless nails and screw nails have been formed from the concept of helical piles. The review of literature related to helical piles and foundation anchors depicts that increasing in load capacity of anchors is attained for optimum helical anchor geometry which is related to helical plate diameter, spacing, depth of embedment and shaft diameter. Moreover, only a limited literature is available in context of screw nails as given by Tokhi [214]. Hence, it can be summarized that development of nails with significant interaction with surrounding soil without grouting is still under explored. It also raises the question that whether failure mechanism and behaviour of helical piles and anchors can be used to predict the response of horizontally embedded soil nails.

At last, it is also reflected from review of literature that various soil nailing manual and guidelines are available for different countries. However, in India, soil nailing is still undergoing development [215] with Indian Institute of Sciences, Bangalore (IISc) and Indian Road Congress (IRC) trying to put forth guidelines for soil nailing technique in Highway Engineering [15]. Hence, the urge of conducting more studies with Indian soil conditions and its development can be fruitful contribution towards improving the application of soil nailing in India.

2.8 Objectives of the Research Work

Based on literature review and research gaps, following objectives of the research are determined:

1) To study the behaviour of soil – nailed slopes at different slope angles and nail inclinations using smooth, screw and helical soil nails by model testing.
2) To investigate the load – deformation behaviour, failure mechanism and nail forces developed along nail length in reinforced slopes during model testing.
3) To develop numerical models of different reinforced slopes with smooth, screw and helical nails using limit equilibrium analysis and finite element analysis.
4) To study and optimize the pullout behaviour of helical soil nail using two – dimesional and three – dimesional finite element analysis.
5) To carry out comparison and validation of model testing and numerical modelling results.

2.9 Scope of the Research Work

The present research works is carried out by studying the basic material prioperties of soil used and nail material. The fabrication of three different types of nails namely smooth soil nail, screw soil nail and helical soil nail is done which is used for model testing of soil slopes constrcuted at three different slope angles ($\beta°$ = 45°, 60° and 90°). For comparision, model testing of slopes at different $\beta°$ is also commenced for without nail condition (unreinforced). Each slope angle is reinforced with six nails of smooth type at different nail inclinations of $i°$ = 0°, 15°, 20° and 30°. The same procedure is repeated for all $\beta°$ using smooth nails. The testing of slopes is then carried out using screw nails and helical nails at different slope angles and different nail inclinations as smooth nails. A total of 39 small – scale model tests are conducted for investigating optimum layout of soil nails, failure mechanism, load – deformation and nail forces genrated along nail length for all unreinforced and reinfroced slopes.

The validation of model testing is performed by numerical analysis of soil – nailed slopes. The stability analysis by evaluating factor of safety for reinforced slopes is carried out by using LEM based software package Slope/W. With the use of SRM method in FEM, factor of safety are also calculated for more complex nail geometries such as screw nails and helical nails. Similar to model testing, numerical modelling of unreinforced slopes at different slope angels is carried out for comparison.

In the absence of previous studies related to pullout of helical nails, 2D and 3D FEM pullout analysis of helical soil nail to determine the most optimum geometrical configuration is done using Plaxis 2D and ABAQUS, respectively. With the knowledge of pullout from numerical modelling of helical soil nails, all reinforced slopes are analyzed using FEM based routine Plaxis 2D. The FEM based numerical analysis examined the slope – deformation characteristics, failure mechanism and nail force mobilization for different slope angles reinforced using different types of soil nails. Finally, comparison and validation of results both from experimental and numerical analysis is carried out to derive critical conclusions. Published results from literature has also been used for validation of testing and numerical modelling.

CHAPTER 3
EXPERIMENTAL PROGRAM

3.1 General

The chapter describes the experimental investigation of material used for construction of model slopes and nail fabrication. Detailed procedures of model slope construction, nail installation and instrumentation are also elaborated. The chapter also deals with complete model testing of unreinforced and reinforced slopes at different slope angles (β) of 45º, 60º and 90º with nail inclinations (i) of 0°, 15°, 20° and 30° using smooth, screw and helical soil nails.

3.2 Material Testing

3.2.1 Backfill Material

The backfill material used for slope construction is collected from Nalagarh, District Solan (Himachal Pradesh). Preliminary tests of soil identification are carried out in the laboratory to determine the backfill properties. To determine the grain size distribution of soil, sieve analysis is carried out in accordance to IS: 2720 (Part IV) [216]. The initial distinction between particle sizes are made by seiving through an arrangement of 4.75 mm IS sieve and 75µ IS sieve. With 50% of soil passing through 4.75 mm sieve and 80% retained on 75µ sieve, it was clear that soil mainly consists of coarse – grained soil with sand fraction.

The complete sieve analysis is carried out by using a series of seives arranged as 10 mm, 4.75 mm, 2 mm, 1 mm, 600 µ, 425 µ, 300 µ, 212 µ, 150 µ, 75 µ and pan. The soil as procured from the site consisted of lumps which are minimized through pulverization with care that only lumps are broken and particles are not crushed. A soil mass of 1 kg oven dried sample is fed through the sieve stack clamped in seive shaker. The automated shaking is carried out for 10 to 15 minutes and mass retained on each sieve is noted. The cumulative $N\%$ for each seive is determined with sieve size depicting the corresponding particle diameter (D in mm). Based on particle size distribution curve (Fig. 3.1), backfill material can be classified as poorly graded sand (SP) with coefficient of uniformity (C_u) = 3.08 and coefficient of curvature (C_c) = 1.25. The effective size (D_{10}) as obtained from particle size distribution is 0.18 mm.

As shown in Figs. 3.2 (a) to 3.2 (d), specific gravity (G) of 2.68 is obtained for backfill soil from pycnometer tests [217] using equation (3.1):

$$G = \frac{M_2 - M_1}{(M_2 - M_1) - (M_3 - M_4)} \tag{3.1}$$

Where, M_1 = Mass of pycnometer, M_2 = Mass of pycnometer + Soil, M_3 = Mass of pycnometer + soil + water and M_4 = Mass of pycnometer + water.

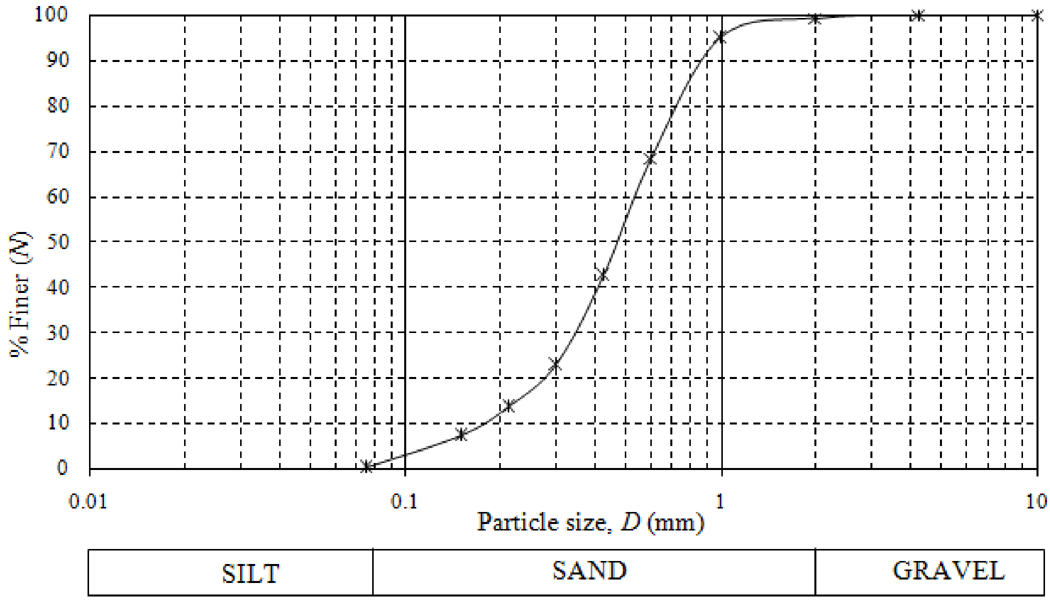

Fig. 3.1: Particle size distribution curve for backfill material

(a) M_1 **(b)** M_2 **(c)** M_3 **(d)** M_4

Fig. 3.2: Specific Gravity of backfill soil by Pycnometer test

The maximum dry density (γ_d) corresponding to optimum moisture content is determined through compaction test [218] with direct shear test under consolidated drained (CD) conditions with 18% moisture content results in shear strength parameters of cohesion (c) = 1.37 kN/m^2 and angle of internal friction (ϕ) as 30.79°. The properties of backfill soil are summarized in Table 3.1.

Table 3.1: Properties of backfill material

Properties	Values (Units)
Specific Gravity (*G*)	2.68
Soil type	Poorly Graded Sand (SP)
Optimum moisture content	18%
Cohesion (*c*)	1.37 kN/m^2
Angle of internal friction (ϕ)	30.79°
Maximum dry unit weight (γ_d)	13.98 kN/m^3
Initial void ratio (e_0)	0.88

3.2.2 Material for smooth, screw and helical nails

The smooth nails used in model testing are fabricated from hollow aluminium tubes. Tensile strength test is carried out to obtain modulus of elasticity for smooth nails as 69 GPa. Screw nails are made up of mild steel bars with threads on its surface. Similarly, shaft and helical plates of helical soil nails are also fabricated using mild steel. The modulus of elasticity as obtained from tensile testing of same mild steel bar as used for screw nails yields a value of 200GPa.

3.3 Fabrication of Model Test Tank and Soil – Nailed Slopes

A rectangular 60 cm (length) x 40 (width) cm x 60 (height) cm model tank is fabricated using Perspex sheets of thickness 12 mm. The Perspex sheets are fastened to the iron angles by bolts. The sides of the tank are braced by iron strips to restrain the lateral deformation of sheets during testing. The tank was filled with sand obtained locally for construction of slopes at desired slope angles.

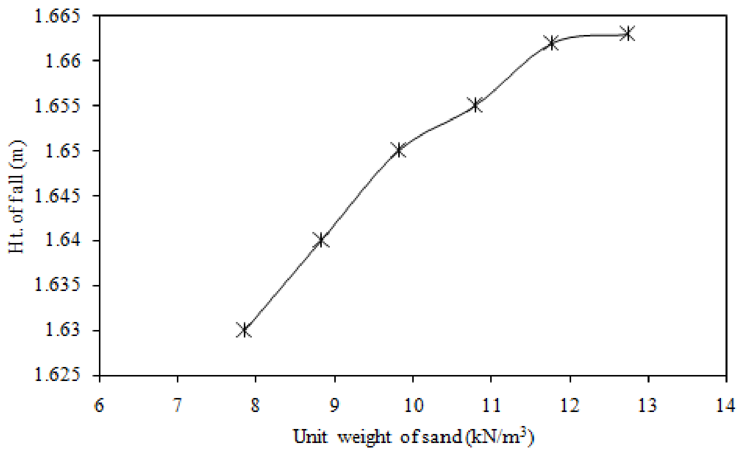

Fig. 3.3: Unit weight curve for sand used in slope construction

To achieve uniform unit weight of backfill soil, sand is placed in the model test tank using pluviation (raining) technique. The backfill soil is allowed to fall freely through a specially fabricated sieve with holes of diameter 3 mm spaced at 25.4 mm center to center. The height of fall is decided after several trials (Fig. 3.3) where known volume of sand was dropped from different heights and its unit weight is determined. The placement of backfill soil adopted in test set up is 16.5kN/m^3 which corresponds to a relative density of 70% [104]. A moisture content of 18% is added to poorly graded sand (backfill) in order to facilitate the construction of 45°, 60° and 90° slopes. The moisture content of 18% is optimum moisture content obtained from proctor test which corresponds to a maximum dry unit weight of 13.98kN/m^3. The step – wise procedure for both slope constructions of 45°, 60° and 90° is as follows: (1) A temporary plywood slope facing is fixed at the desired inclination inside the model tank. To ensure correct slope inclination, markings are made on the Perspex sheet. (2) With the plywood facing intact, the sand is filled in model tank with rainfall technique. The first layer is the base layer with a height of 10 cm. (3) At regular intervals, red colour dye tracer powder is used. It enables the observer to physically study deformation of soil layers during loading by its altered pattern. (4) Above the base layer with tracer, next soil layer is constructed as mentioned above. (5) The process is repeated till the desired height of 30 cm of slope is achieved. (6) The finished slope with model box is weighed. Since unit weight and mass is known, the volume of soil used in construction of slopes is calculated (7) Once the soil slopes are constructed nails are inserted at desired location through the perforations made at temporary facing (8) Smooth nails are driven in to place whereas screw and helical nails are inserted by cutting the soil through screw – in mechanism (Torque) applied manually at nail head (9) Inclination of nail is maintained during installation by measurements from a protractor (10) Strain gauge from each nail is connected to a multimeter. The preparation sequence of reinforced soil slopes is shown in Fig. 3.4.

3.4 Fabrication of smooth, screw and helical soil nails

The smooth nails used in model testing are fabricated from hollow aluminium tubes having diameter of 15 mm and 150 mm of length. A constant length of nails has been used throughout the model testing. The classification of smooth nails is based on surface roughness which is negligible is case of smooth surface [Fig. 3.5 (a)]. A total of six nails are used for each slope angle of 45°, 60° and 90°. Similarly for fabrication of screw nails and helical nails, mild steel bars having a diameter of 16 mm is used. The steel bar is worked upon by a thread rolling machine which renders its surface with threads of height 0.15 mm. Thus, the fabricated screw nail has major diameter (D) of 16 mm and minor diameter of 15.7

mm. The end of screw nail, about 20 mm in length is made tapered to ease the initial penetration in soil slope [Fig. 3.5 (b)].

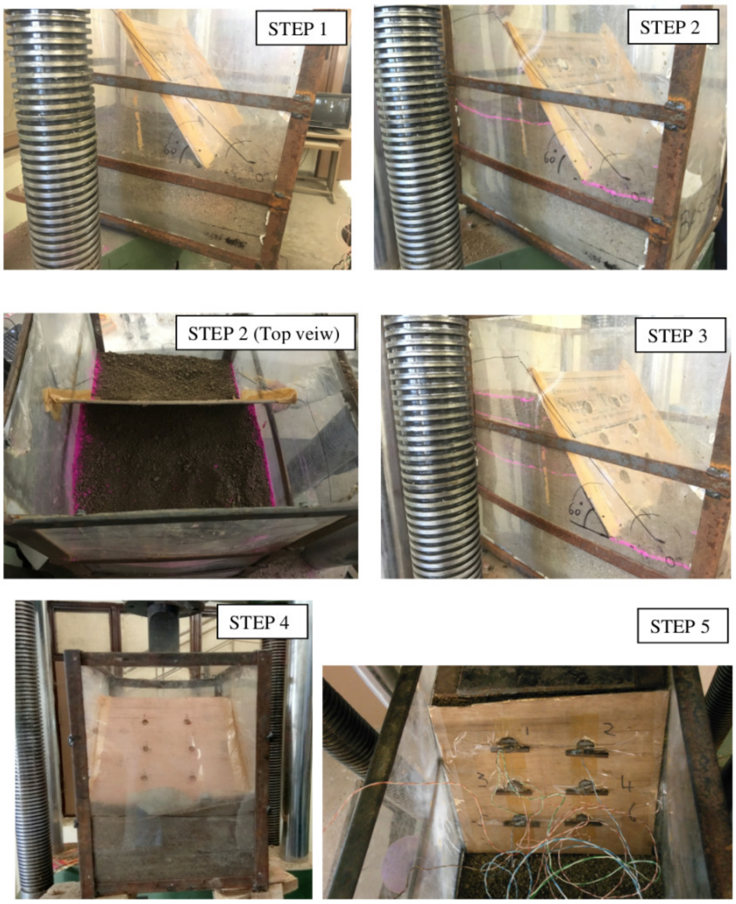

Fig. 3.4: Sequence of soil – nailed slope preparation

The helical nails are made by welding three helical plates of diameter 45 mm at 40 mm spacing. The effective screw nail and helical nail length used is 150 mm from nail head. The total nail length taken for model testing is 170 mm for slope height of 30 cm. Bruce and Jewel [27] suggested that for slopes with granular soils, the length ratio i.e. ratio of maximum nail length to excavation height for drilled and grouted soil is between 0.5 to 0.8 and 0.5 to 0.6 for driven nails. Gosavi [104] also states that the commonly used length of nail (*L*)/height of cut (*H*) ratio are in the range of 0.5 to 0.8. Using length ratio of 0.56, the nail length has been adopted as 170 mm. Moreover, smaller length ratios of 0.28, 0.21 and 0.14 have also been used by Zhang et al. [64] for model testing of reinforced slopes.

Plumelle et al. [219] and Byrne et al. [220] observed that the location of the failure surface is controlled by global limit equilibrium considerations. Strain measurements in instrumented soil nailed walls have indicated that in the upper portion of the wall, the maximum tensile force occurs approximately between 0.3 H to 0.4 H behind the wall facing, while in the lower portion of the wall, the maximum tensile force occurs approximately between 0.15 H to 0.2 H behind the wall facing. This signifies that the failure surface can be expected to intersect the nail length of 0.56 H. It has also been observed by Fan and Luo [177] that nail length on the upper 1/3 height of slope and middle 1/3 of slope height has minor influence on the factor of safety, which is governed mainly by tensile stresses mobilized in nails. However, nail length in lower 1/3 of slope height contributes significantly to stability of soil nailed slopes.

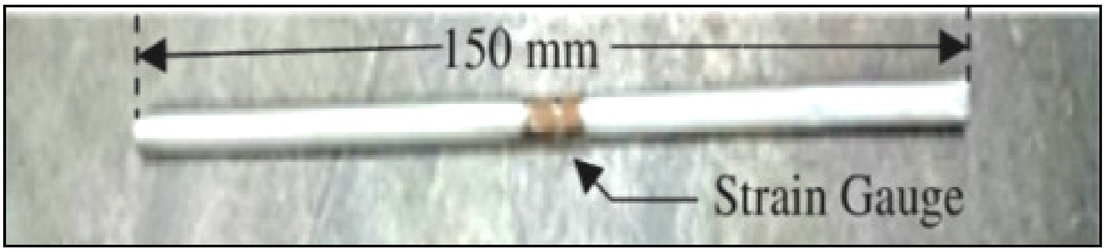

Fig. 3.5 (a): Smooth nail (Hollow aluminium rods) for model testing

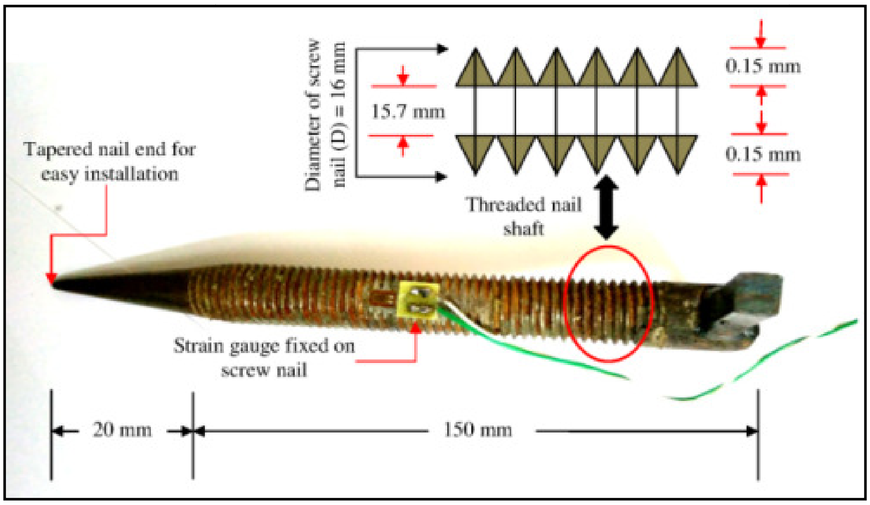

Fig. 3.5 (b): Screw nail (Mild steel rods) for model testing

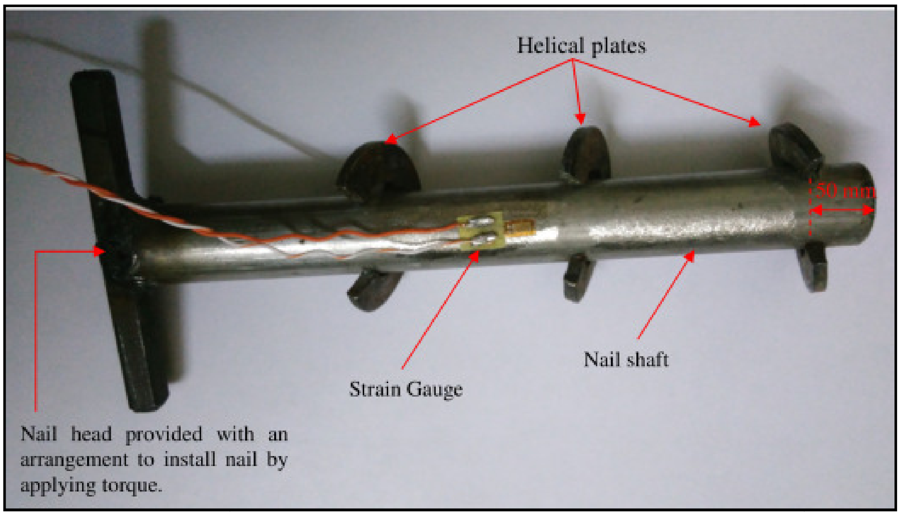

Fig. 3.5 (c): Helical nail (Mild steel rods) for model testing

This behaviour can be explained by the following reasons: (1) nails located at the lower level of slopes bear greater overburden stresses than those located at the upper part of slopes. Thus, greater pull-out resistance is expected for nails at the lower part of slopes compared to those at the upper level of slopes and (2) nails located at the lower part of slopes tend to develop more tensile forces than those located at the upper part of slopes and tensile forces in nails is more effective in mobilizing shear resistance against shear deformation in soil mass. Hence, nails located at the lower part of slopes may provide more shear resistance against shear deformation in soil mass. Based on the above reasons, it is recommended to have nail length of at least 1.0 times the height of slopes at lower 1/3 part to ensure effectiveness of nail action on the overall stability of slopes. In the present work, nail length of 1.5 times the height of slopes at lower 1/3 part has been used to stabilize the slopes. An arrangement of a small handle is provided at the nail head to facilitate the rotation of screw and helical nail during installation. This arrangement will also serve as a nail head which is fixed on the slope facing. The helical nail used in the present work is shown in Fig. 3.5 (c)

3.5 Installation of Soil Nails

The smooth nails are driven whereas screw nails and helical nails are screwed - in through the holes in slope facing. The holes are located at specified distances with equal horizontal spacing of 13.3 cm from edge of facing for slope angles of 45°, 60° and 90°. The vertical spacing of 10.5 cm between the holes for 45° is calculated from the slanting height of slope of 42.42 cm. For 60° slope, vertical spacing between the holes is maintained at 8.6 cm whereas vertical spacing of 7.5 cm is kept for 90° cut. The nails are arranged in rectangular pattern with equal horizontal spacing and different vertical spacing corresponding to slanting height of slopes. A total of six nails for each type smooth, screw and helical are installed in a pattern of three rows and two columns (Fig. 3.6). Moreover, care is taken that the influence area for each nail i.e. S_h x S_v is less than or equal to 4 m^2 as recommended by FHWA [36]. The rectangular soil nail pattern as adopted for the present study facilitates easier construction of vertical joints in shotcrete facing and continuous installation of drain pipes behind the facing in field. It is also treated as the most commonly used soil nail pattern along with square pattern [36]. The inclination of each type of nails is varied between 0°, 15°, 20° and 30° from the horizontal for all slope angles. The diameter of holes on temporary plywood facing is determined from diameter of nail to be inserted. When smooth nails are used, facing hole diameter of 15.2 mm is used for easy installation and minimum frictional effect for edges of the opening. For screw nails, hole diameter is changed to 16.2 mm so that easy rotation of screw nail is achieved during installation. However, for helical nails, helical plate diameter is for determining the facing hole diameter. The diameter used for helical nail installation is 45.2 mm. The driving and rotation of nails for installation is done with utmost care so that no damage is done to the strain gauges attached to each nail.

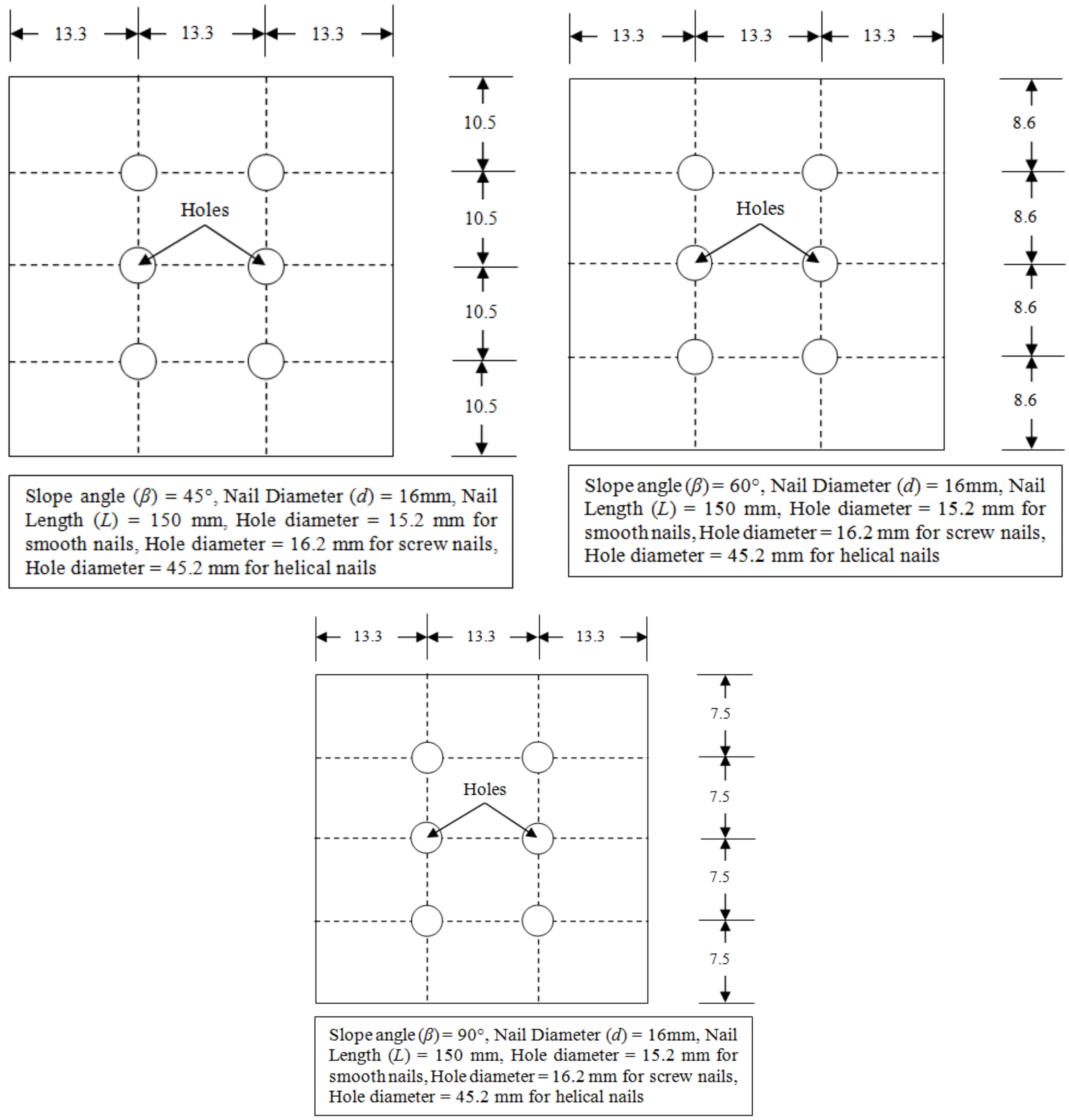

(All dimensions are in mm)

Fig. 3.6: Horizontal and Vertical spacing for model testing

3.6 Instrumentation of Soil - nailed model slopes

The Universal Testing Machine (UTM) used for application of surcharge is equipped with a digital meter which gives the load and corresponding crest settlement of the slope. The Perspex sheets are also marked with initial undeformed slope geometry so as to facilitate physical observation of deformed slope. The horizontal displacement of slope face is measured along slope height through the distance moved by slope beyond initial marking. The deformation of colored tracer from initial horizontal position after failure was also noted to study vertical deformation at different depth from surcharge load application.

The strains generated along the nails during loading are measured by strain gauges attached and read off from the multimeter connected to each nail. As shown in Fig. 3.7, strain gauges of type BKCT-3 with resistance 120 ± 0.2 Ω and gauge factor (*GF*) of 1.92 ± 2% are used. With a basal size of 6.6 x 3.2 mm made up of Phenolic – Epoxy – Acetal and wire grid size of 3.0 x 2.3 mm, the nominal tolerance of strain gauges is less than 3 Ω. The strain gauges are calibrated and mounted on each nail by soldering with copper wires.

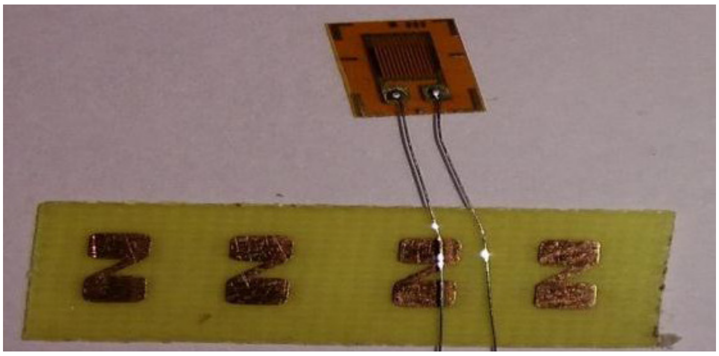

Fig. 3.7: Strain Gauges used for strain measurement of nails

The connection of each strain gauge is connected to an electrical circuit known as Wheatstone bridge [Figs. 3.8 (a) and (b)]. The wheatstone bridge is used to measure electrical resistance by balancing two legs of a bridge circuit, one leg of which includes the unknown component. The strain gauge serves as a resistor (*Rg*) for wheat stone bridge in addition to three other resistors named as *R1*, *R2* and *R3*. The initially balanced wheatstone bridge is provided with an input voltage of 5V from a direct current source. At without loading condition the initial output value is recorded and consequently resistance from connected strain gauge is calculated. Similarly, as strains are developed in nails due to loading of slopes, measurements of output voltage and respective strain gauge resistance values are calculated using equation 3.1:

$$\frac{V_{out}}{V_{in}} = \left(\frac{R3}{R3 + Rg}\right) - \left(\frac{R2}{R2 + R1}\right) \tag{3.1}$$

Where, V_{in} = Input voltage = 5V, V_{out} = Measured output voltage, *R1, R2* and *R3* = Arms of wheatstone bridge, *Rg* = Resistance from strain gauge attached on respective nail. The resistance measurement from Eq. 3.1 is used to find strain value on each nail by using equation 3.2:

$$\varepsilon = \frac{\Delta R/_{R}}{GF} \tag{3.2}$$

Where, ε = nail strain, $\Delta R = (Rg)_{final} - (Rg)_{initial}$ = Change in resistance, R = Initial resistance of foil strain gauge = 120Ω and GF = Gauge factor.

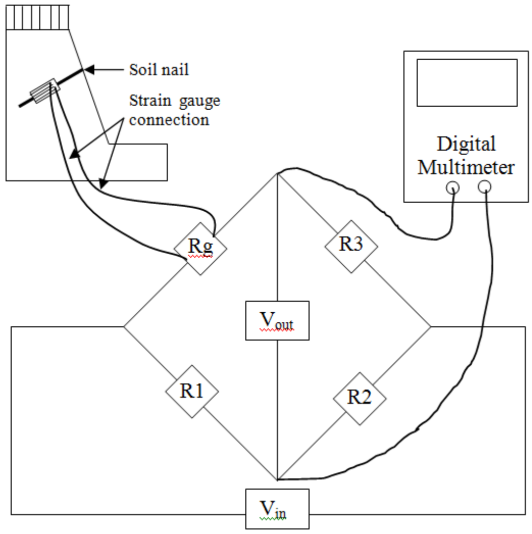

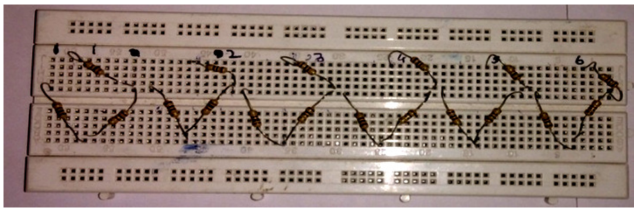

(a) **(b)**

Fig. 3.8: (a) Strain gauge connection through a wheatstone bridge **(b)** Breadboard with six separate wheatstone bridges for each nail

The V_{out} value is read – off from DT830D digital multimeters which yield output voltage in millivolts (Fig. 3.9).

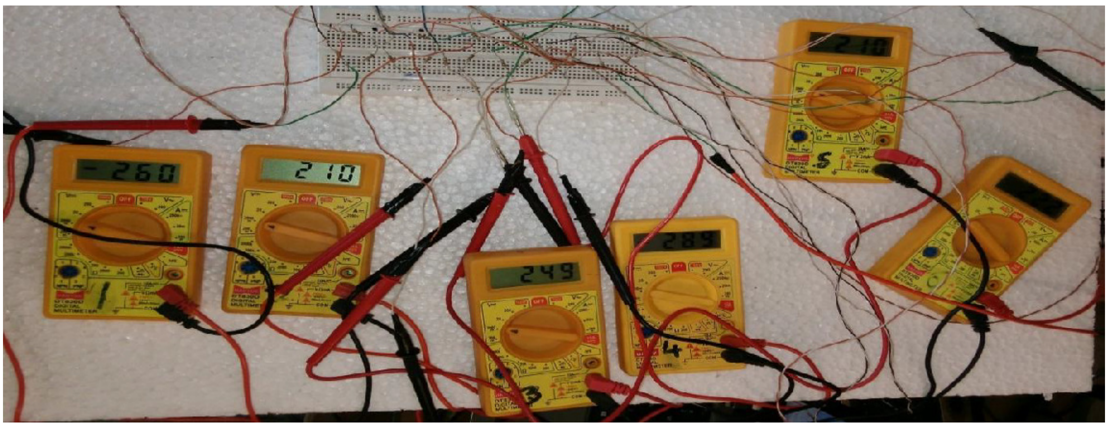

Fig. 3.9: Digital multimeter connected with each wheatstone bridge

3.7 Testing Procedure

The instrumented modeled soil - nailed soil slopes are tested for slope – deformation failure by applying an increasing surcharge load at the slope crest. To ensure uniform distribution of load on slope crest, a steel plate with a plan area of 20 cm x 40 cm and thickness 4 mm is placed on the slope crest. The thickness of iron plate for uniform distribution on slope crest is selected after repeated trials with iron plates of thickness 2 mm and 3 mm. Both iron plates of thickness 2 mm and 3 mm are found to be thin leading to bending under the point of application of load from UTM and thus leading to non – uniform pressure distribution. However, using a 4 mm thick iron plate, no such bending and plate deformation is found during load application on slope crest. Thus, uniform distribution of load on slope crest was ensured. The load is applied on 20 cm x 40 cm crest plan area. Servo hydraulic Universal Testing Machine (UTM) with a load frame capacity of 2000 kN is used to apply an increasing surcharge load on the crest of soil slopes (Fig. 3.10). The continuous application of the surcharge load is simulated by applying the load at a rate of 10 N/s. The UTM plunger is placed at centre of iron plate to apply the surcharge loading.

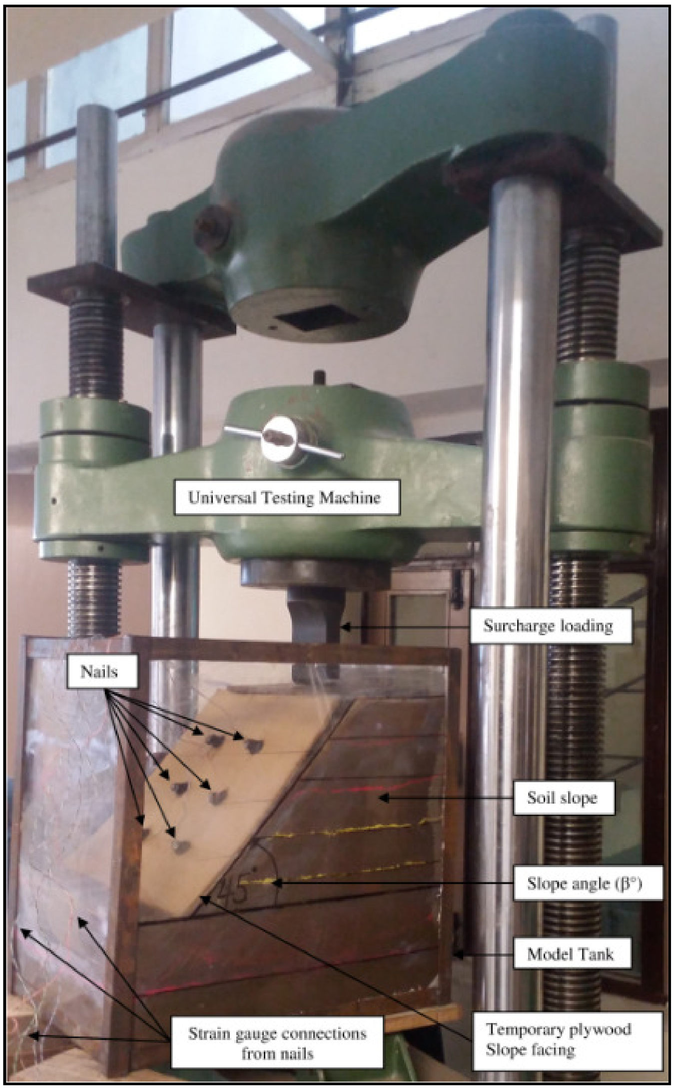

Fig. 3.10: Complete set – up of testing of soil – nailed slope

The testing is started with unreinforced slopes so that a comparison between slope without nails and slopes with nail can be drawn. The 45° slope is first tested with six smooth nails inserted in to place through the holes of facing. The first set of testing is carried out with nail inclination of 0°. Continuous monitoring of load and crest settlement is carried out through the digital meter. Simultaneously, V_{out} from multimeter for each nails are also recorded. Post failure analysis involves the observation of deformed slope captured using a photo camera with measurements from initial slope markings. The testing is found to be completed as slip surface generates due to gradual increasing surcharge load. A similar process is executed for testing of 45° slope with nail inclinations of 15°, 20° and 30°. The entire process is repeated for 60° and 90° reinforced slope with smooth nails at various nail inclinations of 0°, 15°, 20° and 30°.

The testing of slope reinforced with screw nails differ from that of smooth nails by the fact that nail installation is carried out by applying torque at nail head. The load application and corresponding measurements are similar to slope reinforced with smooth nails. The helical nails are also inserted at desired place and inclination by torque application. Using a similar procedure as for smooth and screw nails, testing of 45°, 60° and 90° slopes reinforced with helical nails is commenced. Table 3.2 summarizes the testing of various model slopes.

Table 3.2: Summary of various model slopes used for testing

Nail Type	Slope angle (β)	No. of soil nails	Nail inclination (i)
Smooth nails	45°	6	0°
		6	15°
		6	20°
		6	30°
	60°	6	0°
		6	15°
		6	20°
		6	30°
	90°	6	0°
		6	15°
		6	20°
		6	30°

Nail Type	Slope angle (*β*)	No. of soil nails	Nail inclination (*i*)
Screw nails	45°	6	0°
		6	15°
		6	20°
		6	30°
	60°	6	0°
		6	15°
		6	20°
		6	30°
	90°	6	0°
		6	15°
		6	20°
		6	30°
Helical nails	45°	6	0°
		6	15°
		6	20°
		6	30°
	60°	6	0°
		6	15°
		6	20°
		6	30°
	90°	6	0°
		6	15°
		6	20°
		6	30°

3.8 Determination of Screw nail – Soil Interface Friction

Since pullout of screw nail is required for accurate simulation of screw nail during numerical modeling, Direct shear tests (DST) are conducted with soil – soil (without nail) and soil – soil (with nail) conditions in standard Direct shear box with plan area of 6 cm x 6 cm and sample depth of 5.3 cm to study the interface friction between screw nail and soil. A screw nail sample of circular cross – section having a minor diameter of 15.7 mm with threads of height 0.15 mm along a nail length of 40 mm is placed symmetrical in both plan and elevation [121] in the direct shear box as shown in Fig. 3.11. The sample screw nail used in DST has modulus of elasticity (E_{sn}) of 200GPa and Poisson's ratio (υ_{sn}) of 0.3, which are similar to those used in model tests.

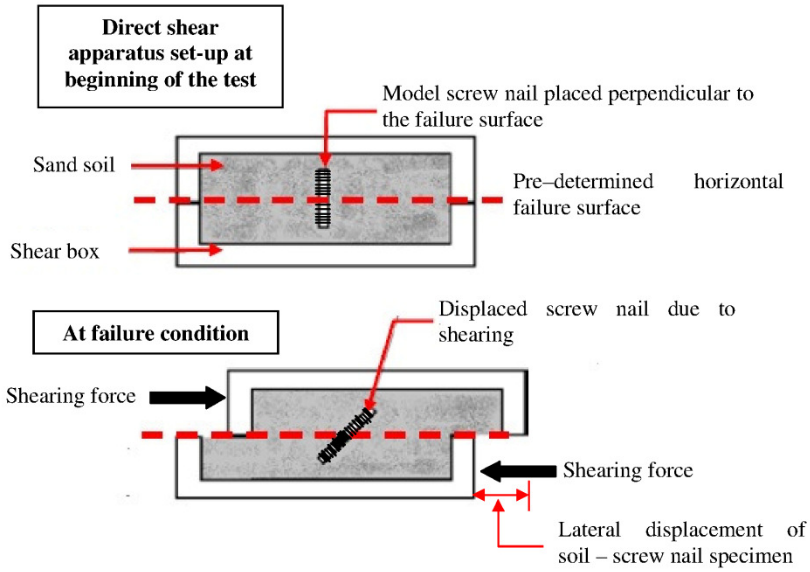

Fig. 3.11: Set – up of Direct Shear Test with screw nail

In the absence of pullout results for screw nails, the coefficient of friction for pullout test (f^*) is determined by coefficient of friction from direct shear test (f). The relation between the two coefficients is given by Wang and Richwien [129] as:

$$f^* = \frac{f}{1 - \left\{\frac{2(1-\upsilon)}{(1-2\upsilon)(1+2K_0)}\right\}(f \tan\psi)} \tag{3.3}$$

Where, υ = Poisson's ratio of soil taken as 0.33; K_0 = Earth pressure coefficient at rest which is calculated by the Jaky's formula as $(1 - \sin\phi)$; ψ = Dilation angle of soil calculated by ($\phi°$ - 30°).

CHAPTER 4

NUMERICAL MODELING

4.1 General

The chapter deals with details of numerical modeling of soil – nailed slopes using Limit Equilibrium Method (LEM) and Two – Dimensional Finite Element Method (2D - FEM). The chapter also describes complete modeling procedures involved for SLOPE/W (LEM) and PLAXIS 2D (FEM) software packages. In addition to the numerical modeling of all soil – nailed slopes used for model testing, the chapter elaborates 2D and 3D FEM analysis of pullout of helical soil nails using PLAXIS 2D and ABAQUS Explicit codes.

4.2 Limit Equilibrium Analysis of soil – nailed slopes

The response of reinforced systems is primarily governed by soil structure interaction. The interaction between soil which provides both mobilized and resisting stresses and structural members (nails) that helps in load transfer mechanism. General limit equilibrium approach ensures static equilibrium of the system, thereby providing a global factor of safety for ultimate limit state [221]. The factor of safety calculation as obtained by General Limit Equilibrium (GLE) or just Limit Equilibrium Method (LEM) incorporates the use of interslice shear - normal forces and two types of factor of safety [222].

a) Factor of safety with respect to moment equilibrium (F_m)

$$F_m = \frac{\sum(c'\beta R + (N - u\beta)R \tan\phi')}{\sum Wx - \sum Nf \pm \sum Pd} \tag{4.1}$$

b) Factor of safety with respect to force equilibrium (F_f)

$$F_f = \frac{\sum(c'\beta \cos\alpha + (N - u\beta)\tan\phi' \cos\alpha)}{\sum N \sin\alpha - \sum P \cos\omega} \tag{4.2}$$

The normal force at base of each slice (N) is the major variable in both Eqns. of factor of safety. The value of this normal force is dependent on shear forces (X_L and X_R) acting on the slices as shown in Fig. 4.1.

The base normal force is obtained by the relation:

$$N = \frac{W + (X_R - X_L) - (\frac{c'\beta \sin\alpha + u\beta \sin\alpha \tan\emptyset'}{F})}{\cos\alpha + \frac{\sin\alpha \tan\emptyset'}{F}} \tag{4.3}$$

Where, c' and ϕ' = effective cohesion and effective angle of friction, u = pore water pressure, W, P and N = slice weight, concentrated point load and slice base normal force, α = slice base inclination with horizontal and β, f, d, ω = geometric parameters.

The normal force calculated from Eq. (4.3) is used in factor of safety (FOS) calculation using Eqns. (4.1) and (4.2) for each slice for a range of λ (lambda) values. The λ value is defined as difference between specified function $f(x)$ used to relate normal - shear forces on the slice and applied function $f(x)$ used by LEM software [223]. The expression to find relationship between shear and normal forces on a slice is given by Morgenstern and Price in 1965 as Eq. 4.4:

$$X = E.f(x).\lambda \tag{4.4}$$

Where, X = inter-slice shear force, E = inter-slice normal force, $f(x)$ = inter-slice function (Half – sine function default SLOPE/W), λ = percentage of function used. The factor of safety using both conditions of moment and force is calculated until convergence is reached between FOS from both conditions. The values are found to converge, when FOS plot for moment and force intersects for a specific value of λ. This constitutes the global factor of safety as achieved by LEM analysis of slopes.

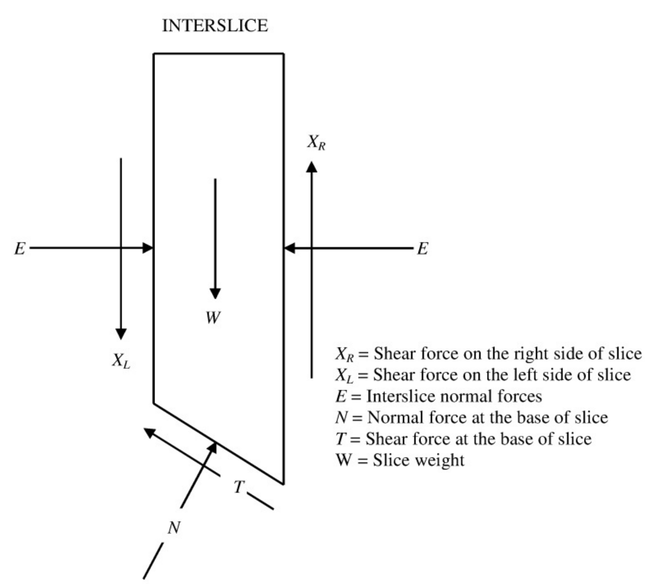

Fig. 4.1: Forces acting on an inter-slice

The stability analysis in LEM is primarily an indeterministic problem. So, in order to change the problem to statically deterministic solution, number of unknowns must be equal to number of equations. Various assumptions such as no inter-slice forces (Fellinius method), no inter-slice shear forces (Bishop's method), only horizontal force equilibrium of wedge

(Janbu's method) are accounted to achieve a factor of safety for slope failure. However, an additional complexity is introduced into the analysis with use of reinforcement to stabilize the slope. The reinforcement parameters are prescribed which do not introduce any unknowns in the analysis, but contributes additional known reinforcement forces that are included in appropriate equilibrium Eqns. [221].

The LEM method utilizes trial slip surface method, in order to locate the most optimum slip surface having lowest factor of safety. The slip surfaces considered in LEM can be circular, piece - wise linear or a combination of curved and linear shapes. The procedure to find the most critical slip surface is also affected by statigraphic boundaries of slopes. To avoid unrealistic slip surface and factor of safety, LEM package offers an option of defining regions for occurrence of slip surface on ground surface and point of axis along which moment equilibrium is to be calculated. The present study uses the software package SLOPE/W, to analyze reinforced slope by limit equilibrium method.

4.2.1 Limit Equilibrium Method analysis of slopes with smooth nails using SLOPE/W

SLOPE/W is a sub-routine of the software package GEOSLOPE. In the present study, reinforced soil slope are modelled with three different slope angles of 45°, 60° and 90°, respectively. These soil slopes are reinforced using smooth nails at four different inclinations of 0°, 15° and 20° and 30° with horizontal, respectively. SLOPE/W package enables construction of soil slopes by defining its regions. The soil slope dimensions as used for modelling are adopted from model testing of reinforced soil slopes. The slope dimensions used in model testing are changed to scale to be incorporated in SLOPE/W.

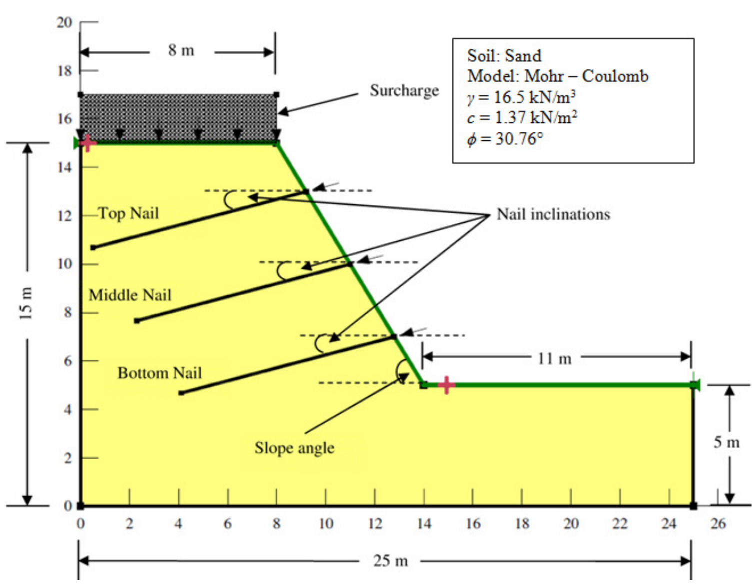

Fig. 4.2: Modeling of soil slope in SLOPE/W

The slope is modelled at different slope angles by (x, y) coordinate system available in the package. Once the slope regions have been determined, slope material is assigned to the slope geometry. The slopes are then reinforced with nails. SLOPE/W package provides the option of using reinforcement in form of anchor, geosynthetic, nail and pile. A surcharge load is applied at the top of slope, which is also scaled according to the recorded experimental values. The entry and exit of slip surfaces at ground surface, along with slip surface axis and limits are also applied to the model. The simulated model used in analysis is shown in Fig. 4.2. Amidst of all other methods available in limit equilibrium package, analysis is carried out by Morgenstern – price method which uses a relation between inter-slice shear forces and inter-slice normal forces. The inter-slice function selected in the analysis is a half – sine function with a constant factor of safety distribution calculation. The properties of smooth nails and soil used for limit equilibrium (LE) modelling are summarized in Table 4.1.

Table 4.1: Summary of material used in LE modeling

Parameters	**Values**
Soil	Poorly graded sand (SP)
Bulk unit weight of soil (γ_{bulk})	16.5 kN/m^3
Cohesion (c)	1.37 kN/m^2
Angle of friction ($\phi°$)	30.79°
Pullout resistance of nails	100 kN/m^2
Tensile capacity of nails	200 kN

The nails used for reinforcing slopes are simulated without facing by using 'no anchorage' of nails at slope face. The nail forces are treated as distributed forces over nail length and overall global factor of safety (F of S dependent) is included in the analysis. The reinforcement in SLOPE/W is treated as concentrated loads which reduces the destabilizing forces. The equilibrium Eqns. used in analysis are based on shear mobilized at base of each slice and at reinforcement. The mobilized shear (S_m) is calculated using Eq. (4.5), based on an assumption that shear resistance of soil (S_{soil}) and reinforcement ($S_{reinforcement}$) are developed at the same rate [221].

$$S_m = \frac{S_{soil}}{F\ of\ S} + \frac{S_{reinforcement}}{F\ of\ S} \tag{4.5}$$

The soil nails used in analysis are stiffer than soil. Hence reinforcement forces are limited by allowable loads in reinforcement. Instead of dividing shear resistance of reinforcements with global factor of safety, reduction factors are used to restrict the mobilized reinforcements. This option is available by not considering the F of S dependency in the analysis.

4.2.2 Limit Equilibrium Method analysis of slopes with screw nails using SLOPE/W

The Slope/W sub-routine employs LEM to calculate the factor of safety for the most critical slip surface. The input parameters required for modelling soil are unit weight of soil, soil cohesion and the angle of internal friction. All these values are taken from Table 4.1. The dimensions of soil slope are same as that used in model testing converted to scale. The most important feature of this modelling technique is simulation of screw nails. Slope/W does not provide the option of modelling the interface element between nail surface and soil. The soil nail reduces the activating driving forces and increases the shearing resistance. This leads to an increase in stability of slopes. As mentioned in section 4.2.1, in SLOPE/W soil nails are treated as concentrated loads which reduce the destabilizing forces in soil slopes.

Screw soil nails are simulated in terms of pullout load which is calculated theoretically by using coefficient of friction for pullout test (f^*). In the absence of pullout test for screw nails as used in present study, coefficient of friction for pullout test (f^*) is determined using coefficient of interface friction (f) as obtained from direct shear test (Section 3.8). The calculated f^* value is substituted in Eq. (4.6) from Gosavi et al. [143] for soil nail pullout.

$$Pullout\ load(P) = f^* \times \pi dL(\gamma z + q) \tag{4.6}$$

Where, d = nail diameter, L = Nail length, γ = Unit weight of soil, z = Depth of nail from ground, q = Surcharge. Using Eq. (4.6) also enables to incorporate the roughness in terms of interface friction of screw nails. Using the computed pullout load, screw nail pullout resistance is determined by Eq. (4.7) given by Tokhi [214].

$$Pullout\ resistance(\tau_{max}) = \frac{P}{\pi dl} \tag{4.7}$$

Thus, screw nails with its surface roughness are modelled into SLOPE/W using pullout resistance. Some pullout resistances used for modelling of different screw nailed soil slopes is summarized in Table 4.2.

Table 4.2: Pullout resistance calculated for each screw nail for Slope/W

	Screw nail 1	**Screw nail 2**	**Screw nail 3**
45°	486.36 kN	580.26 kN	674.05 kN
90°	383.96 kN	478.75 kN	573.54 kN

In addition to this, the input parameters required to simulate nails in Slope/W are tensile capacity and shear force of nails. All these input values are factored by a reduction factor. The reduction factor is defined as reduction of ultimate tensile capacity due to physical processes such as installation damage, creep and durability. It is applied to nail strength to account for uncertainties in structure geometry, soil properties, external applied loads, potential for local overstress due to load non-uniformities and uncertainties in long-term nail strength. The value of reduction factor (RF) = 0.65 used in present work has been adopted in accordance to Soil Screw Design Manual by Hubble [26].

The tensile capacity (T_a) and shear force (V) for screw nails is calculated from Eq. (4.8) given by Hubble [26].

$$T_a = A_c(RF)f_y \tag{4.8}$$

Where, A_c = cross – sectional area of screw nails (m^2), f_y = Yield strength of screw nails taken as 250 MPa, RF = Reduction factor of 0.65

$$V = 2A_b(RF)F_v \tag{4.9}$$

Where, A_b = cross – sectional area of bolt (m^2), ultimate shear stress of steel (F_v) = $0.5E_{steel}$, E_{steel} = 200 GPa. Using Eqns.(4.8 and 4.9), screw nail are modelled for slope of 45°, 60° and 90° at various inclinations. A completed 90° screw nailed slope is shown in Fig. 4.3. The reinforced slopes are then analysed using Morgenstern – price method to find critical slip surface and factor of safety from moment equilibrium and force equilibrium.

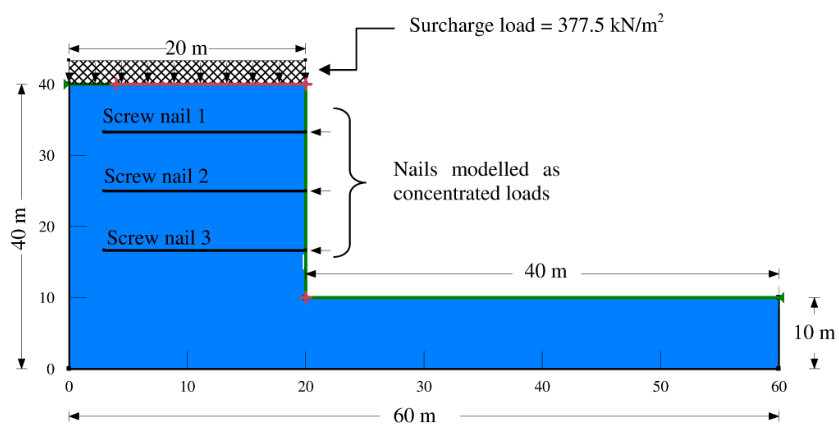

Fig. 4.3: Modeled 90° screw nailed soil slope in Slope/W

4.2.3 Limit Equilibrium Method analysis of slopes with Helical nails using SLOPE/W

The modeling of slopes reinforced using helical nails is similar to screw nails. The soil slopes are modeled without difficulty using Mohr – Coulomb soil model with required parameters of γ, c and ϕ adopted from Table 4.1. As seen for screw nail simulation, helical nails can only be incorporated by utilizing the pullout resistance of helical nails used in present study. The thorough literature review revealed that no pullout studies on helical soil nails have been reported till date. Recently, Tokhi [214] conducted pullout of helical soil nail but due to different geometry of nail used it cannot be adopted for present analysis. In order to develop helical soil nail with an optimized geometry and investigation of pullout behavior of helical soil nail, 2D and 3D FE numerical modeling has been carried out as explained in the following section. The results of pullout value obtained from 2D and 3D FE analysis are used to model reinforced slopes in SLOPE/W.

4.3 Finite Element Analysis of soil – nailed slopes

With the advantage of no assumption for location of failure surface and inter-slice forces, Finite element method (FEM) has been widely accepted for the analysis of slope stability [224]. The increased use of complex geometries and material data has made analysis non – linear and iterative in nature. In such cases the inputs (soil and geometry) are themselves function of the solutions. Since this procedure requires a large amount of calculation data and time, it is recommended to use available FE packages. One such FE software package has been used in the current study named as PLAXIS 2D v8.1. In this software, FE analysis divides the continuum into distinct elements, with each element further divided into nodes. The unknowns in the problem with a defined set of boundary conditions correspond to degree of freedom with discrete values for each node [225]. In the present work, degrees of freedom of nodes are related to displacement components. Each line element is divided into 3 nodes which are assigned displacement values. These 3 nodes contribute to 6 - noded triangles, whereas if the line element has 5 nodes, it builds up a 15 – noded triangle. The 15- noded triangles are found to yield more accurate results as compared to 6 noded, in cases involving nails, anchors or geogrids [225].

The material in FE analysis is also controlled by infinitesimal incremental stress and strain relationship. The FEM package incorporates use of Mohr – Coulomb and Hardening-soil constitutive model. The Mohr – Coulomb constitutive model simulates a perfectly plastic material condition with development of irreversible strains. A set of yield functions which constitute a yield surface are generated to check occurrence of plastic points in the continuum. These yields functions are themselves a function of prevailing stress and strain conditions. The FEM routine also enables to simulate an elastic perfectly plastic behavior of the material. Hooke's law is used to relate stress and strains. The strains and strain rates are decomposed into their elastic and plastic fraction during calculations. Smith and Griffith [226] stated that the Mohr - coulomb model consists of six yield functions which consist of plastic parameters like 'c' and 'ϕ' of soil. Using these concepts for material transition, a material stiffness matrix is developed by FE analysis to calculate stiffness of each element and ultimately of the entire volume of soil.

From the literature review, it has also been observed that researchers [188, 227] employed strength reduction method of FE to obtain factor of safety for slopes. In strength reduction analysis, the convergence criterion is most critical factor for assessment of factor of safety. The strength reduction method also known as c-ϕ reduction method is carried out by performing load advancement number of steps. The reduction in strength parameters is carried out by using an incremental multiplier M_{sf}. The factor of safety is calculated by the expression as given by Eq. (4.10):

$$SF = \frac{Available\ strength}{strength\ at\ failure} = value\ of \sum M_{sf}\ \ at\ failure \tag{4.10}$$

The precision of factor safety is a function of type of constitutive soil model selected, type and size of element, discretized mesh, node location for displacement curve and tolerance allowed for nonlinear analysis. Depending on the choice of FE routine used, model is found to reach ultimate state if either the maximum number of iteration is reached or model has undergone a continuous failure mechanism or selected points in continuum are subjected to sudden change in displacement. In order to simulate the failure correctly, FEM packages also provides the use of arc – length control in iteration procedure. At times during a non – linear analysis, a sudden failure of some points is observed which lead to generation of an "apparent" negative stiffness matrix beyond ultimate limit state. This snap through problem in FEM has been overcome by arc – length control technique. The arc-length control technique is now incorporated in commercial finite element software PLAXIS to obtain reliable collapse loads for load controlled calculations. Hence PLAXIS 2D based on finite element method accompanied with an elastic perfectly plastic (Mohr-Coulomb) stress-strain relation is used in present study which is reliable and powerful approach for calculating factor of safety of reinforced slopes.

4.3.1 Finite element analysis of slopes with smooth nails using PLAXIS 2D

The numerical modeling of reinforced slopes has been carried out by FE routine PLAXIS 2D v8.1. PLAXIS 2D considers the soil slope in plain strain with 15 – noded triangulation procedure. The dimensions of model are similar to model testing converted to scale. The standard fixities are used to simulate the actual boundary conditions persisting during model testing of soil – nailed slopes with smooth nails. The simulated model base is restricted in $x - y$ direction with back of the slope being restricted only in x direction by using standard fixities. A Mohr - Coulomb model with poorly graded sand soil is used to simulate model in FE analysis. A drained soil condition is modeled with phreatic line positioned at bottom of the model. The parameters used in the modeling of slopes and nails are summarized in the Table 4.3.

Table 4.3: Properties of soil used in modeling

Properties		**Stiffness**		**Strength**	
Soil Model	Plain strain	E_{ref}	50000 kN/m^2	c_{ref}	1.37 kN/m^2
Elements	15 – node	υ	0.3	ϕ	30.76°
Model Type	Mohr–Coulomb			Ψ	0.76°
Material Type	Drained				
γ_{unsat}	16.5 kN/m^3				
γ_{sat}	18.58 kN/m^3				
K_0	0.49				

The PLAXIS 2D package provides option of using plate element, geogrids, node to node anchors and fixed end anchors as reinforcement systems. In a 2D plain – strain FE analyses, the nail is idealized as one unit. Plaxis 2D provides an opportunity of using 'smeared' soil nail technique that transforms the discrete nails into equivalent plates. The elastic equivalent plate element is used as nails for slope reinforcement with the consideration that bending stiffness and axial stiffness plays an important role in simulation of soil nails [228]. If the nails are modeled using a plate element of circular cross section, then an equivalent flexural rigidity and equivalent axial stiffness has to be calculated for correct simulation of soil nails. The formulation for attaining equivalent modulus of elasticity (E_{eq}) for modeled nails is given by Babu and Singh [229] as:

$$E_{eq} = E_n \frac{A_{nail}}{A} + E_g \frac{A_{grout}}{A} \tag{4.11}$$

Where, E_n = Elastic modulus of smooth nails (kN/m^2), Eg = Elastic modulus of grout (kN/m^2), A_{nail} = Cross – sectional area of nail (m^2), A = Total cross – sectional area of grouted soil nail (m^2) and A_{grout} = Area of grout (m^2) = A - A_n.

Similarly Equivalent axial stiffness (EA) is given by Eq. (4.12):

$$EA = \frac{E_n}{S_h} \frac{\Pi}{4} d_n^2 \tag{4.12}$$

Where, d_n = diameter of smooth nail used (m) and S_h = Horizontal spacing of smooth nails (m). The equivalent bending stiffness (EI) and equivalent plate diameter of the nail (d_{eq}) is calculated from Eqns. (4.13) and (4.14) given as:

$$EI = \frac{E_n}{S_h}\frac{\Pi}{64}d_n^4 \tag{4.13}$$

$$d_{eq} = \sqrt{12\left(\frac{EI}{EA}\right)} \tag{4.14}$$

Where, I = Moment of inertia of circular nails. Using Eqns. (4.11), (4.12), (4.13) and (4.14), parameters corresponding to a circular cross – section of smooth nail are modelled (Table 4.4).

Table 4.4: Properties of the simulated nails used in numerical modeling

Parameters	**Values**	**Units**	**Interface Strength**	
Nail element and Nail type	Plate and Elastic	-	R_{inter}	0.5
Axial stiffness (EA)	2.98 x 10^6	kN/m		
Flexural rigidity (EI)	113.64 x 10^3	kN - m^2/m		
Diameter of nail (d_{eq})	12	mm		
Poisson's ratio (υ)	0.35	-		

The soil – smooth nail interaction is modeled using an interface strength reduction factor (R_{inter}) with a value of 0.5 adopted from Gosavi [143]. Gosavi [143] reported interface friction of 0.5 for driven nails. The interface strength reduction factor (R_{inter}) relates soil strength to strength of interface as Eq. (4.15) and (4.16):

$$R_{inter} = \frac{\tan \emptyset_{interface}}{\tan \emptyset_{soil}} = \frac{\tan \delta}{\tan \emptyset} \tag{4.15}$$

$$R_{inter} = \frac{c_{interface}}{c_{soil}} \tag{4.16}$$

Once the soil - nail interaction is modeled, a 2D mesh is generated after initial stresses are computed by K_0 procedure based on Janbu's relation $K_0 = (1 - \sin\phi)$. A finer 2D mesh is generated at soil – nail interface for achieving accurate results. No over consolidation and pre - overburden pressure are considered in the present analysis. A surcharge load is applied at slope crest and plastic analysis is carried out for soil – nailed slopes. The simulated model is also analyzed by using the c-ϕ reduction method (SRM) for factor of safety calculations of various slopes. A complete model of soil slope reinforced using smooth nail is shown in Fig. 4.4.

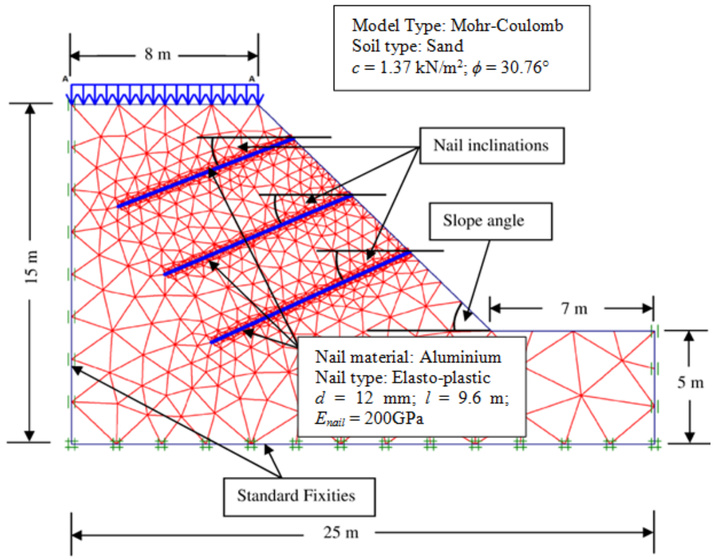

Fig. 4.4: Numerical modeling of soil slope with smooth nails in PLAXIS 2D

4.3.2 Finite element analysis of slopes with screw nails using PLAXIS 2D

With similar soil constitutive model as used for smooth nails, soil continuum for screw nails is also defined by plain – strain, Mohr – Coulomb model. The material properties of soil slope are adopted from Table 4.3. The boundary conditions, phreatic line and slope loading are all similar to previously described modeling with smooth nails. The dimensions of model simulated for FE analysis are adopted from model testing of screw-nailed slopes converted to scale so as to yield reasonable results. The primary difference between modeling of smooth-nailed slopes and screw-nailed slopes lies in simulation of soil nails. The smooth nail and screw nail are treated differently based on surface roughness which correspondingly alters soil-nail interaction. Similar to simulation of smooth nail, screw nails are also modeled using plate element. The relations for equivalent modulus of elasticity (E_{eq}), equivalent axial stiffness (EA), equivalent bending stiffness (EI) and equivalent plate diameter (d_{eq}) are modified for screw nails by substituting properties of smooth nails with screw nails.

The soil – screw nail interaction is performed by using an interface strength reduction factor (R_{inter}) as given by Eqns. (4.15) and (4.16). By substituting the value of $\tan\delta = 0.740$ and $\tan\phi = 0.596$ as determined from direct shear test (Section 3.3), R_{inter} comes out to be 1.24. However, Plaxis 2D accepts a maximum value of $R_{inter} = 1$ for rough surfaces, which is also used for the present study. Further, an interface of virtual thickness factor (t_f) equal to height of thread of 0.15 is taken on either sides of modeled screw nail to simulate nail threaded surface. During 2D mesh generation, this virtual thickness factor is multiplied by element thickness to create the desired interface. The parameters used for screw nail modeling are given in Table 4.5.

The generated 2D mesh is refined at interfaces and line of load application. The complete numerical model for 90° screw – nailed slope is shown in Fig. 4.5. The initial stresses generated in screw nailed soil slopes are considered by earth pressure at rest condition. For simulating the earth pressure, a K_0 – procedure with $K_0 = (1 - \sin\phi)$ is used. The reinforced slope models are analyzed using plastic analysis for slope deformation investigation.

Table 4.5: Screw nail modeling parameters in Plaxis 2D

Parameters	Values (Units)
Modeling Element	Plate
Modeling type	Elasto - plastic
Modulus of elasticity of screw nails (E_n)	200 GPa
Equivalent modulus of elasticity (E_{eq})	200 GPa
Equivalent axial stiffness (EA)	3.024×10^5 kN/m
Equivalent bending stiffness (EI)	4.838 kN – m^2/m
Equivalent plate diameter (d_{eq})	13.85 mm
Interface strength reduction factor (R_{inter})	1
Interface of virtual thickness factor (t_f)	0.15

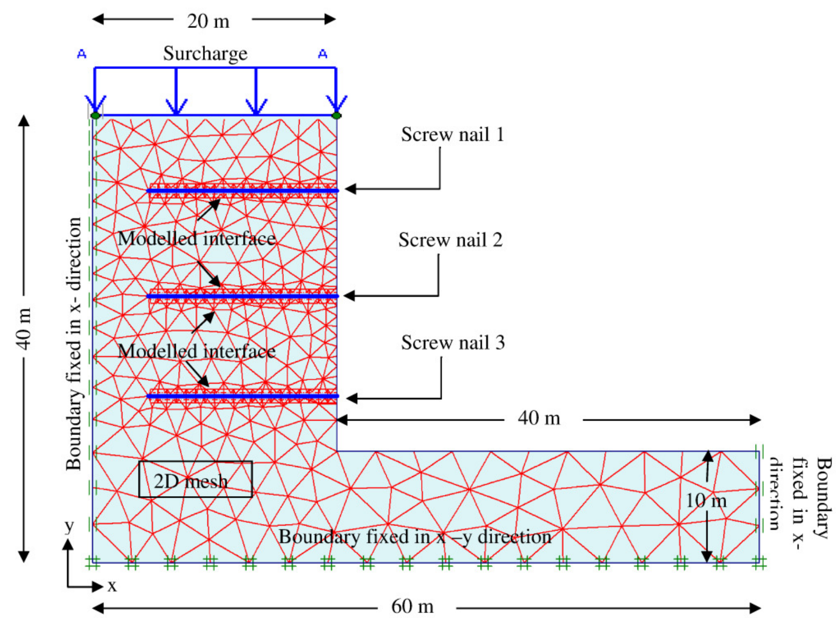

Fig. 4.5: Modeling of 90° screw nailed slope in Plaxis 2D

The factor of safety for screw – nailed slopes is obtained by analysis using SRM. The shear strength parameters c and ϕ are reduced from their original values till failure of reinforced slopes is reached. To achieve that a total multiplier $\sum M_{sf}$ is used which controls the reduction of shear strength parameters. The value of $\sum M_{sf}$ at failure is the FOS for screw nailed soil slopes under study.

4.3.3 Finite element analysis of slopes with helical nails using PLAXIS 2D

The numerical modelling of helical nailed slopes follows a similar modelling procedure as adopted for smooth nails and screw nails. The soil domain is modelled using

Mohr – Coulomb model with helical nails having similar properties to that of screw nails (Table 4.5). The most important factor that distinguishes screw nail and helical nail is the nail geometry. The nail geometry of helical nail has been adopted from helical nail used in model testing (Section 3.4). All geometries such as nail shaft and helical plates are converted to equivalent plate elements in PLAXIS 2D (Fig. 4.6).

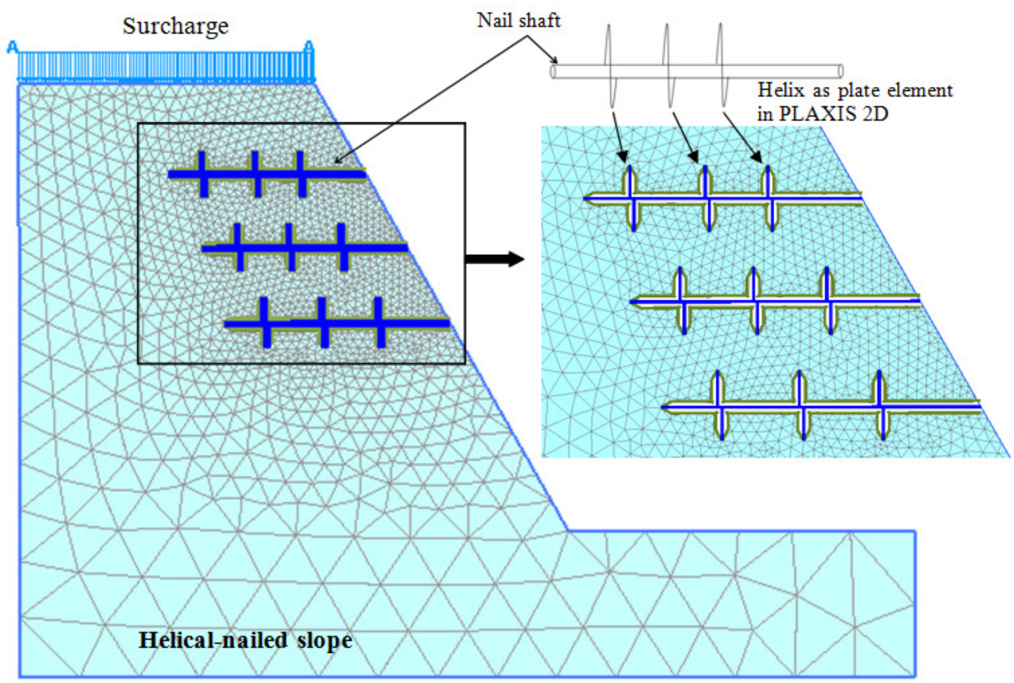

Fig. 4.6: Nail shaft and helical plates are converted to equivalent plate elements in PLAXIS 2D

The feasibility of representing helical soil nails as plate elements is verified by investigation of pullout behaviour of helical soil nail as described in the following section 4.3.4. With the simplification of geometry, helical soil nails are included in soil slopes. The analysis of helical soil nailed slopes for slope deformation under surcharge loading and factor of safety is conducted plastic analysis and SRM similar to screw nailed soil slopes.

4.3.4 2D Finite element analysis of pullout behaviour of helical nails using PLAXIS 2D

In the present study, axisymmetric finite element modelling is done for simulating pull out mechanism of helical soil nail by PLAXIS 2D. From the literature review, it is clear that insufficient information is available with regard to helical soil nail modelling. The literature provides ample data for simulation of helical piles or helical soil anchors. It is also evident from literature [230] that pullout of soil nails can be well simulated by vertical pullout in axisymmetric condition available in Plaxis 2D package. The horizontal orientation is simulated by applying a horizontal load on the absorbent boundary to account for overburden acting, when soil is pulled out horizontally. The literature review further suggests that researchers [209, 210 and 231] have modelled helical piles and helical anchors using a similar concept in Plaxis subroutine. Studies based on such modelling techniques have been used to understand the pullout or uplift capacity of screw or helical piles and anchors.

Employing the accuracy of this existing modelling technique to actual behaviour, variation in helical soil nail failure mechanism and pullout capacity with number and spacing of helical plates, varying diameter of helical plates is studied. From the literature review, it can also be concluded that the effect of overburden on helical soil nail pullout is significant. However, experimental evidence by Tokhi et al. [214] is the only available data in that context. The FE analysis of such experimental work can further enhance the understanding of helical soil nail pullout response.

In the present FEM analysis, the helical soil nail used is made up of steel with bar geometry taken as per the available dimensions given in ASTM A615 [232] for threaded nail bars [36]. The diameter of the nail shaft (D_s) is 19 mm with a nominal unit weight of 2.24 kg/m [36]. The helical plates are also considered to be made of steel with diameters varying from 26.6 mm to 83.6 mm. This variation of helical plate diameters is used in D_h/D_s ratios for numerical modelling. All nail lengths are fixed to 15 cm similar to helical nail length adopted for model testing which is converted for simulation using scale of 1cm = 0.5m. Thus, nail length of 7.5 m is used in modelling. The spacing (s) of helical plates used is varied with s/D_h, D_h is helical plate diameter, ratios to study its effect on helical nail pullout capacity. With the bottom helical plate fixed at 15 mm from the nail end, different depth of embedment of top helical plate (H) is achieved by varying the spacing of the helical plates, which is used in the analysis for embedment ratio H/D_h. A typical helical soil nail to be modelled in FE analysis is shown in Fig. 4.7.

The soil parameters used in FE analysis are taken from model testing on helical nailed reinforced soil slopes. A poorly graded, isotropic sand soil is used for constitutive modelling in PLAXIS 2D. The soil is modelled as a hardening soil which yields in plastic straining due to soil expansion. The hardening of soil is subjected to shear and compression hardening. The input E_{50}^{ref} is used to model shear hardening due to primary deviatoric loading which induces irreversible plastic strains. Irreversible plastic strains are also induced by compression obtained from oedometer loading and unloading test. This hardening of soil is simulated by E_{oed}^{ref} and E_{ur}^{ref} input values in PLAXIS 2D.

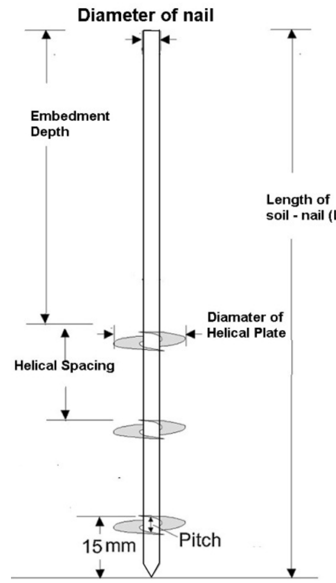

Fig. 4.7: Soil nail with helical plates to be modelled in FE analysis

The pull out test conditions are taken as drained with a low cohesion value 1.37kN/m^2 and angle of internal friction of 30.76°. A small dilatancy of 0.76° is considered with tensile failure of soil along with shear failure. This is achieved by use of tension cut - off value, which is taken as 0kN/m^2 for hardening soil model automatically by FE code. The soil parameters used for modelling are summarized in Table 4.6. The pullout response modelling is carried out in accordance to the simulation done by Ann et al. [230]**.** The horizontal soil nail is simulated by a vertical inclusion in circular soil tank employing axisymmetric condition. The axisymmetric condition uses the *x*–axis as the radius and *y*–axis as symmetrical axis of soil model.

Table 4.6: Soil parameters used in Plaxis 2D

Parameters	**Values**
Soil model type	Hardening soil
Soil model condition	Drained poorly graded sand
#E_{50}^{ref}	3 x 10^4 kN/m^2
*E_{oed}^{ref}	3 x 10^4 kN/m^2
#E_{ur}^{ref}	9 x 10^4 kN/m^2
Poisson's ratio, υ	0.3

* Value from oedometer (consolidation) tests conducted on sand used in the study.
# Values from standard consolidated drained (CD) triaxial tests on sand used in the study

Plaxis 2D [225] emphasis on the concept of using axisymmetric condition for simulation of cylindrical elements such as soil anchors, nails and piles as shown in Fig. 4.8.

The following reasons can be accounted for 2D axisymmetric pullout modelling of helical soil nail:

1. The change in stresses around a soil nail pullout is primarily due to the grouting pressure used during the installation procedure in conventional nails. Pradhan et al. [135] concluded that the installation process of soil nail induced significant vertical stress changes in soil around the soil nails and soil nail pullout shear resistance is independent of overburden pressure. Zhou et al. [185] stated "It is well acknowledged that the soil nail pullout resistance is influenced by many factors, such as the installation method, overburden stress, grouting pressure, roughness of nail surface, soil dilation, degree of saturation, and soil-nail bending." Moreover, a similar observation by Hong et al. [233] stated "It was found that the pullout resistance increased linearly with the grouting pressure, but the overburden pressure did not influence the pullout capacity." Hence the in – situ stress conditions around soil nail cannot be treated uniform. However, the installation of helical nails does not require any grouting procedure. The nails are penetrated into the soil by applying a torque at nail head. This installation procedure is believed to produce minimal disturbance to surrounding soil. A similar conclusion is also derived by Tokhi et al. [214] where it is stated "The design of new screw nail offer many advantages such as easy installation with no spoils and grouting, better nail ground interaction resulting in increased pullout capacity and it's suitability for reinforcing all ground conditions including sand and gravel." Since no spoils and grouting are expected with installation of helical nails, in – situ stresses can be assumed to be uniform around the helical nail. This assumption makes it reasonable to consider the helical nail pullout as an axisymmetric modelling problem.

2. The soil used in the present study has almost zero dilation corresponding to an angle of internal friction of 30.76°. Thus the increased angle of internal friction and induced soil reaction pressure from the surrounding soil due to soil dilation [157] does not hold good for the present pullout of helical nail situation. This further confirms that stresses around the helical nail are uniform. Moreover Lou et al. [157] states " The stress and strain near and within the rupture surface around a soil nail corresponds to a triaxial strain problem, the axial strain, ε_a, along the soil nail axial direction can be considered as constant." Since triaxial strain problem can be treated as an axisymmetric 2D

problem, a similar approach can also be made to analyse the pullout of helical nail by modelling it as 2D axisymmetric problem.

3. 2D axisymmetric pullout of soil nail analysis has also been carried out by Morris [125]. In his research work he stated "The boundary stresses in the vertical and horizontal direction are approximately equal, the stresses in the soil immediately surrounding the soil may well be very nearly axisymmetrical, since the stress field here is dominated by the effect of the circular hole driven through the medium." Similarly Tei [121] also concluded that as the relative stiffness between soil and nail increases, the axial stress distribution becomes more linear and shear stress distribution becomes more constant along the nail.

4. Tokhi [214] conducted pullout of screw nails in 3D but using an axisymmetric condition. As stated in his research work "The pullout tests were simulated by an axisymmetric, three-dimensional (3D) stress/displacement elements model." It is also found that the results of his 3D axisymmetric pullout analysis of new screw nail depicts similar patterns of failure and stresses as obtained from the present study of analysis of helical nails by 2D axisymmetric condition.
5. The Plaxis practice manual given by Ann et al. [230] also states "Due to the characteristics of the axisymmetry model, the generated normal stress with the above mentioned method is uniformly distributed on the nail's perimeter. Although this initial stress condition is different compared to the actual working nail in which the circumferential normal stress distribution is non-uniform, caused by the difference in vertical and horizontal stress, this shortcoming does not cause severe errors."

Thus keeping in view all the above stated reasons, 2D axisymmetric modelling of pullout of helical nails can be employed to study the pullout mechanism with the assumption that no variation in initial stresses are expected in circumferential direction around the nail axis. As discussed earlier, the constitutive soil modelling is carried out using a hardening soil model. The model dimensions are determined based on the effect of boundary conditions. The top and bottom boundary condition is fixed in the vertical direction. The left boundary condition is simulated with a horizontal fixity whereas the right boundary condition is set free for application of overburden.

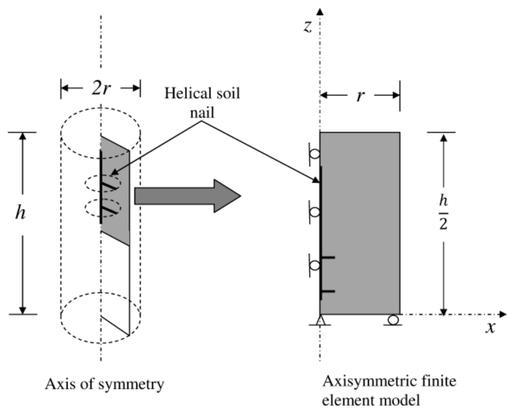

Fig. 4.8: Axisymmetric Finite element model of helical nail pullout

In order to avoid any boundary effect interference on the pullout mechanism, the right boundary is set at a distance of 60 times nail radius (60r) from axis of symmetry. To avoid confinement effects, care is taken to position the top boundary at a distance of 20 times nail radius (20r) from nail head. To model soil nail, an elastic – plastic, 15 – noded plate element is used as suggested by Babu and Singh [229]. The helical plates are modelled by the same plate element as nail shaft. However, for practical design helical plates are positioned on nail shaft at a particular angle and pitch. In this analysis, due to restriction on simulation of helical pitch, the plates are taken horizontal to the shaft with zero pitch. The axial stiffness (EA) and the bending stiffness (EI) of the helical soil nail are taken as 28355kN/m and 0.64kN-m^2/m, respectively. The Poisson's ratio for the steel helical nails is taken as 0.3 with a unit weight of 2.24 kg/m [232].

The soil – nail interaction is simulated by constructing interface between nail shaft, nail helical plates and soil. Plaxis 2D code utilizes a strength reduction factor (R_{inter}) to govern small displacements (elastic behaviour) and permanent slip (plastic behaviour) within the interface. The interface shear strength parameters are controlled by R_{inter} by the following formulation given as Eqns. (4.15) and (4.16).

The interface stiffness between soil and nail is handled by a virtual thickness '$t_{interface}$' which is taken equal to 0.1 as in case of smooth nails. The R_{inter} value used for current analysis is 0.67, which is used when no previous data is available for soil structure interaction. The numerical modelling parameters used in the analysis are given in Table 4.7. The absorbent boundary placed at right and bottom of modelled pullout is to eliminate any spurious reflected waves. $\sum -M_{weight}$= 0 is taken in the initial stress generation calculation step in order to avoid initial stresses generated by gravity (where Σ is the summation and

M_{weight} is the soil weight). The initial stress condition is created by imposing a surcharge load at right boundary in the first step of calculation.

Table 4.7: Helical soil nail parameters used in numerical modelling

Properties	Values
Nail type (shaft and helical plates)	Elasto-plastic steel nails
Modulus of Elasticity of helical nails	200GPa
υ	0.3

This creates a uniformly distributed normal stress along helical nail shaft to simulate initial stress condition for actual, horizontally, oriented nail. In this calculation step, the absorbent boundary is deleted, upper and bottom boundaries are vertically fixed, left boundary is totally fixed and right boundary is totally free to allow imposed load to be transferred on nail shaft. This is done in order to achieve actual pullout response of helical soil nail, wherein the effect of initial stress on a nail oriented horizontally is correctly simulated. All the other structural elements during initial stress generation are deactivated. The soil overburden that must be acting on a horizontally oriented helical soil nail length is simulated by activating the uniformly distributed load 7.3 kN/m^2 [140] on right boundary of soil model. The phreatic line is situated at bottom of the model to create drained condition. The complete helical nail pullout model is shown in Fig. 4.9.

A small pull out force (Q_0 = 10kN) is applied on the nail head to initialize pull out. This initial pull out load is increased to an ultimate failure load by a load incremental factor $\sum M_{load}$ generated by Plaxis [208]. Thus the characteristic load (Q_0) at failure is calculated by Eq. (4.17):

$$Q_p = \sum M_{load} . Q_0 \tag{4.17}$$

The rate of load increment can however be controlled by altering the additional step procedure available in the FE package. However, no simulation can be achieved for modelling the effects of helical nail installation by applying the initial torque. It is found from literature review, that installation torque alters the soil properties and hence the soil – nail interaction. Keeping this as a future scope of the present study, the analysis is carried out.

The helical nail configurations in FE analysis is altered by using different diameters of helical plates with a constant shaft diameter of 19 mm. The D_h/D_s ratio used are 1.4, 2.4, 3.4 and 4.4. The range for helix to shaft diameter is found to vary from 0 – 4.4 [209]. The helical plate diameter calculated from D_h/D_s ratio is 26.6, 45.6, 64.6 and 83.6 mm. All throughout the analysis, bottom helix is fixed at a distance of 15 mm from nail tip. The other helical plates are located at varying distances from bottom helix. If top and bottom helical plates are used, it is treated as a double helical soil nail (2-H) and a combination of three helical plates at bottom, middle and top will serve as a multi – helical soil nail denoted as 3-H.

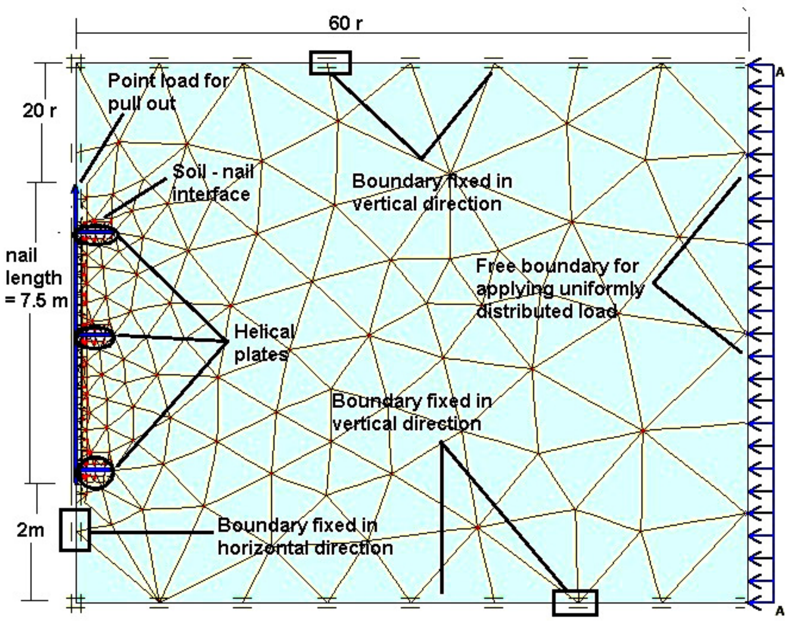

Fig. 4.9: Modelling of Helical soil nail pullout

The spacing of helical plates in 2-H and 3-H nails is calculated from s/D_h ratios. The spacing of helical plates is calculated for maximum helical plate diameter 83.6 mm corresponding to D_h/D_s ratio of 4.4. These spacing values are determined to study effect of s/D_h ratios on pullout capacity of helical nail and its failure response. With the change in spacing, embedment ratio (H/D_h) is also found to change. The behaviour of helical anchors is found to vary with embedment ratio [234] and breakout factor – embedment ratio studies reported by Mistch And Clemence [195]. The variations of helical plates carried out in FEM are summed up in Table 4.8.

Table 4.8: Different configurations of helical soil nails for PLAXIS 2D analysis

<table>
<tr><th colspan="3">Configuration of Helical Plates</th><th rowspan="2">D_s [mm]</th><th rowspan="2">D_h [mm]</th><th rowspan="2">s/D_h</th><th rowspan="2">H/D_h</th><th rowspan="2">D_h/D_s</th></tr>
<tr><th></th><th>Notation</th><th>Number of Helical plates</th></tr>
<tr><td rowspan="6">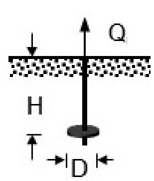</td><td rowspan="6">1-H</td><td rowspan="6">1</td><td rowspan="6">19</td><td rowspan="6">4.4 x D_s</td><td rowspan="6">-</td><td>1.0</td><td>1.4</td></tr>
<tr><td>2.0</td><td rowspan="2">2.4</td></tr>
<tr><td>3.0</td></tr>
<tr><td>4.0</td><td rowspan="2">3.4</td></tr>
<tr><td>5.0</td></tr>
<tr><td>6.0</td><td>4.4</td></tr>
</table>

<table>
<tr><td rowspan="6">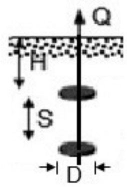</td><td rowspan="6">2-H</td><td rowspan="6">2</td><td rowspan="6">19</td><td rowspan="6">4.4 x D_s</td><td>1.0</td><td>1.0</td><td>1.4</td></tr>
<tr><td>1.5</td><td>2.0</td><td rowspan="2">2.4</td></tr>
<tr><td>2.0</td><td>3.0</td></tr>
<tr><td>2.5</td><td>4.0</td><td rowspan="2">3.4</td></tr>
<tr><td>3.0</td><td>5.0</td></tr>
<tr><td>3.5</td><td>6.0</td><td>4.4</td></tr>
<tr><td rowspan="6">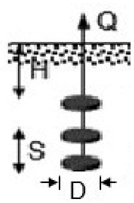</td><td rowspan="6">3-H</td><td rowspan="6">3</td><td rowspan="6">19</td><td rowspan="6">4.4 x D_s</td><td>1.0</td><td>1.0</td><td>1.4</td></tr>
<tr><td>1.5</td><td>2.0</td><td rowspan="2">2.4</td></tr>
<tr><td>2.0</td><td>3.0</td></tr>
<tr><td>2.5</td><td>4.0</td><td rowspan="2">3.4</td></tr>
<tr><td>3.0</td><td>5.0</td></tr>
<tr><td>3.5</td><td>6.0</td><td>4.4</td></tr>
</table>

Finally, helical nail is also simulated as tapered helical nail by varying the diameter of top, middle and bottom helical with different D_h/D_s ratios. Different combinations of bottom, middle and top helical plate diameters are used to constitute the tapering soil nail. A constant s/D_h ratio of 2.5 is kept constant for tapered nail. The diameters of 1-H, 2-H and 3-H are taken as 1.4 times D_s, 2.4 times D_s and 3.4 times D_s respectively, as the first trial. These values of helical plate diameter are then varied between middle, top and bottom plates to model different tapering helical soil nail combinations.

4.3.5 3D Finite element analysis of pullout behaviour of helical nails using ABAQUS

With the advancement in soil nailing technique researchers like Tokhi [214] developed a screw type soil nail to overcome the installation complexities of soil disturbance and spoils produced identified with conventional grout soil nails. It was observed from experimental and numerical analysis of screw nail that it holds the advantage of easy installation by providing torque with better pullout resistance as compared to traditional soil nails. Moreover, Tokhi [214] conducted axisymmetric finite element analysis of screw nail by simplifying the geometry of helical plates as circular rings attached along nail stem. It was stated by the author that such a modification simplified the FE analysis in terms of meshing problems and computational time which was still very large. Based on literature review carried out, the present work focuses on understanding pullout behaviour of helical soil nail by modifying helical plates as circular discs along nail shaft. To overcome the assumptions of 2D analysis and consider complete effect of helical plates, a three – dimensional (3D) finite element analysis (FEA) of helical soil nail is carried out by numerical modelling in Abaqus/Explicit v6.13.

The soil nails mounted with parallel circular discs can be driven into ground by pushing and rotation technique. To initiate the horizontal penetration of nail into ground, this type of nail needs to be pushed into ground which splits the soil and displaces it to the sides by a distance equal to radius of the shaft. This initial soil displacement allows the circular discs to be positioned into soil with small penetration. As the nail is pushed further accompanied by torque at its head, soil is cut and displaced to the sides. The volume of soil displaced is equal to volume of circular discs which is similar to a helical plate with small pitch [235]. The average distance required to displace the soil for circular disc insertion is approximately equal to half the thickness of the disc [235]. Since the thickness of discs in the present study is small, it can easily cut through loose soil condition and minimal soil displacements can also be expected. Consequently, soil – nail contact can be re – established in relatively less time. As the first disc cuts and displaces the soil, it paves way for the following discs to be located at desired locations. Moreover, these soil nails with circular discs can also be used by burying them in advance during reinstating a failed slope or a loose fill slope.

HKIE [236] reports that to reinstate a failed loose fill slope the top 3 m of slope should be excavated and re – compacted so as to increase its stability. In such cases soil nails with circular discs can be placed at desired levels during reconstruction of such slopes after excavation, which will not only reduce compaction efforts but also increase the stability of loose fill slope with much better efficiency than compaction. Some other real application examples of these soil nails can be in cases of newly built embankments, where these nails can be installed easily and effectively owing to weak soil conditions as staged construction of embankment progresses.

A soil nail may be positioned at different angles with horizontal inside the soil mass. In the present analysis, soil nail with circular disc is oriented at 0° with horizontal for all cases under study. The soil nail consists of a circular shaft having diameter (d_s) of 15 mm. The shaft has 'N' number of circular discs varying from 1 to 4 i.e. (N = 1, 2, 3 and 4). The circular discs have a diameter (D_c) which is considered on the basis of a relative diameter ratio (D_c/d_s). The D_c/d_s ratios used are 1, 2, 3 and 4, resulting in D_c variation of $1d_s$, $2d_s$, $3d_s$ and $4d_s$. The circular discs are evenly spaced along the nail shaft at a specified spacing (s). Different spacing of circular discs are adopted based on a relative spacing ratio (s/D_c) taken as 1, 1.5, 2, 2.5, 3, 3.5 and 4. The variation of s/D_c has been carried out for N = 2, 3 and 4. With the change in number of circular discs along soil nail shaft, variation in soil nail shaft length beyond the first disc to nail head (L) is used to define anchorage length ratio as L/D_c. The depth of embedment of soil nail from the top surface of pullout box (H) is 500 mm for all parametric variations. An overburden pressure of 20 kN/m^2 adopted from Tokhi [214] is considered to be acting at the surface of pullout box. The general layout of the problem definition to be analysed is given in Fig. 4.10.

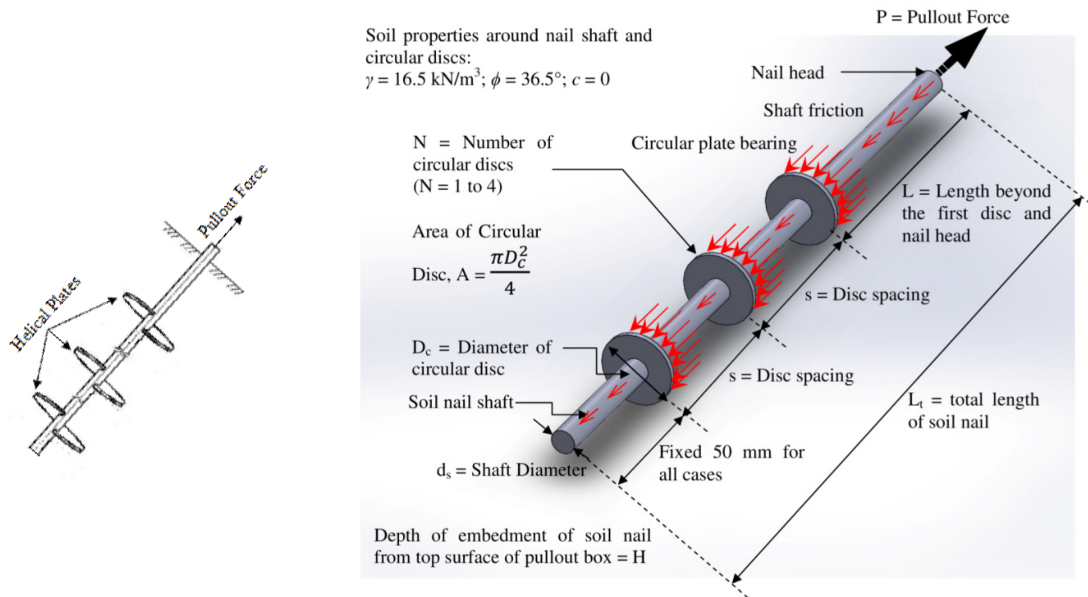

(a) Actual Helical Nail **(b)** Modified Helical nail for FE analysis

Fig. 4.10: Problem definition for pullout of helical soil nail

A conventional soil nail consists of shaft embedded in grout column so that during pullout the apparent friction at grout – soil interface is mobilized. It can be visualized that in conventional soil nail shaft friction contributes significantly in resisting the pullout force. The shear stresses are generated at nail – soil interface around the perimeter of soil nail shaft throughout its anchorage length. These shear stresses are transferred as tensile forces to soil nail. Hence it can be inferred that grout column diameter and length of soil nail behind the potential slip surface governs the pullout of conventional soil nails. Thus, pullout capacity (P) of soil nail as given FHWA [36] can be calculated from Eq. (4.18) as:

$$P = \pi . q . D_{DH} . L \tag{4.18}$$

Where, q = mobilized shear stress acting at the perimeter of nail – soil interface, D_{DH} = diameter of drill hole for grouting; L = length of soil nail. The shear stress acting along the perimeter is a function of normal stress around soil nail and interface friction. Since soil is a weaker material in comparison to nail embedded grout column, it can be said that during pullout soil will tend to fail before the grout column. This makes the soil – soil interface friction critical than soil – grout interface friction. Hence the mobilized interface friction is treated as equal to tan (ϕ), where ϕ is the angle of internal friction of soil. Thus, Eq. (4.18) can also be given as Eq. (4.19):

$$P = \pi . \sigma_v . \tan \phi . D_{DH} . L \tag{4.19}$$

Where, σ_v = normal stress around soil nail determined as (γ x Height of soil mass above nail). In the present soil nail, circular disc provides an additional resistance to pullout by increasing the surface area of nail shaft. Due to the addition of circular disc along nail shaft an extra bearing is imposed on nail displacement subjected to pullout load. The contribution of circular disk can thus be accounted for its bearing capacity due to increased area. The pullout of soil nail with circular disc will be combined action of resistance from the nail shaft and bearing by circular discs. Consequently, Eq. (4.19) can be modified to Eq. (4.20) as:

$$P = \pi . \sigma_v . \tan \phi . D_{DH} . L + \sum_{i=0}^{N} A_i \sigma_v K_0 N_{q_i} \tag{4.20}$$

Where, A_i = Area of circular disc i, K_0 = Coefficient of earth pressure at rest ($1 - \sin \phi$), N_{qi} = Bearing capacity factor at disc i.

The simulation of soil nail with circular discs in the present study deals with pullout of soil nail for a condition that soil nail has been left for a sufficient period of time after installation and soil has re – established full contact with the entire soil nail due to consolidation and creep settlement. The basis for this consideration can be accounted for the type of soil used for analysis which is dry sand. Sand can be expected to form full contact with nail within a small period of time owing to its zero sensitivity and immediate settlement. Moreover, small thickness of circular discs accounts for negligible disturbances to the surrounding soil, which further simplifies and hastens the soil – nail contact. Hence in Eq. (4.20), pullout resistance is predicted by considering the gross area of disc. The soil used for pullout simulation is dry sand with zero degree of saturation. Since the soil nail can be installed by burying it in advance without any grouting and drillhole, change in soil saturation due to grouting and pore water pressure developed during shearing in sand is also neglected.

It can also be stated that if significant circular disc thickness is considered, shear resistance provided by disc side friction will also add up against soil nail pullout and should be incorporated in Eq. (4.20). However in the present analysis, 5 mm thin circular disc are considered with negligible side friction. It can also be concluded theoretically from Eq. (4.20) that increasing the number of disc will increase the pullout resistance capacity of soil nail. Moreover, large diameter of disc will tend to provide large bearing area which should increase the pullout resistance. The effective bearing area of circular disc depends on nail shaft diameter. Similarly the contribution of shaft friction is affected by circular disc spacing. In order to understand the effect of these variations, several combinations among different parameters has been analysed. The summary of these combinations is given in Table 4.9.

Table 4.9: Different combination of parameters used in analysis

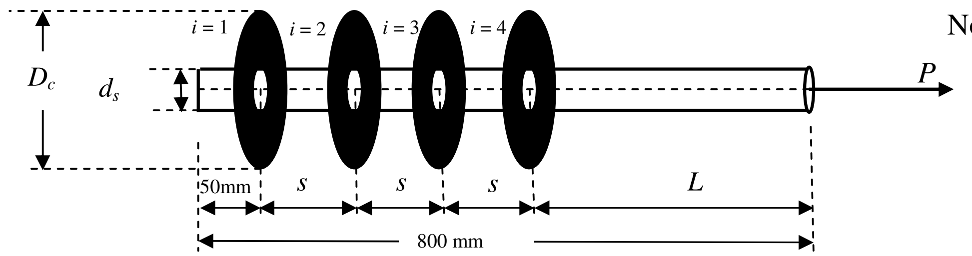

Notation: N4							
Soil nail with circular disc: $N = 4$; $d_s = 15$ mm							
s/D_c	1.0	1.5	2.0	2.5	3.0	3.5	4.0
D_c/d_s	4	4	4	4	4	4	4
L	570	480	390	300	210	120	30
L/D_c	9.5	8	6.5	5	3.5	2	0.5
D_c/d_s	3	3	3	3	3	3	3
L	615	547.5	480	412.5	345	277.5	210
L/D_c	13.67	12.16	10.67	9.16	7.67	6.16	4.67
D_c/d_s	2	2	2	2	2	2	2
L	660	615	570	525	480	435	390
L/D_c	22	20.5	19	17.5	16	14.5	13

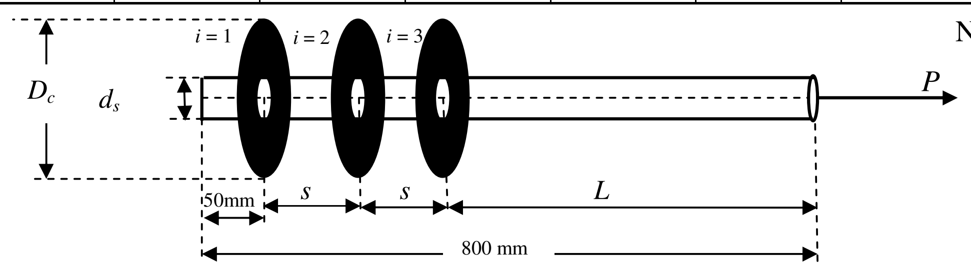

Notation: *N3*							
Soil nail with circular disc: $N = 3$; $d_s = 15$ mm							
s/D_c	1.0	1.5	2.0	2.5	3.0	3.5	4.0
D_c/d_s	4	4	4	4	4	4	4
L	630	570	510	450	390	330	270
L/D_c	10.5	9.5	8.5	7.5	6.5	5.5	4.5
D_c/d_s	3	3	3	3	3	3	3
L	660	615	570	525	480	435	390
L/D_c	14.67	13.67	12.67	11.67	10.67	9.67	8.67

D_c/d_s	2	2	2	2	2	2	2
L	690	660	630	600	570	540	510
L/D_c	23	22	21	20	19	18	17

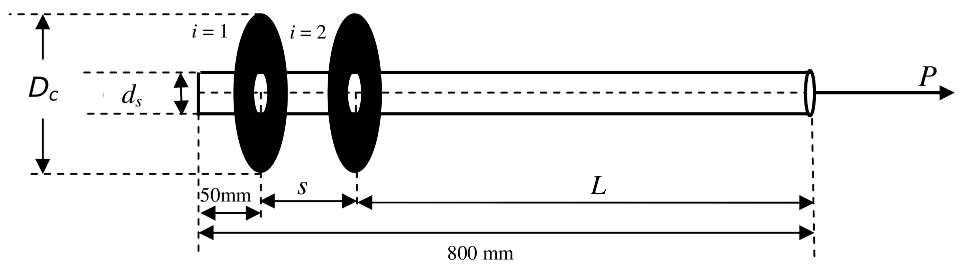

Soil nail with circular disc: $N = 2$; $d_s = 15$ mm

s/D_c	1.0	1.5	2.0	2.5	3.0	3.5	4.0
D_c/d_s	4	4	4	4	4	4	4
L	690	660	630	600	570	540	510
L/D_c	11.5	11	10.5	10	9.5	9	8.5
D_c/d_s	3	3	3	3	3	3	3
L	705	682.5	660	637.5	615	592.5	570
L/D_c	15.67	15.16	14.67	14.16	13.67	13.16	12.67
D_c/d_s	2	2	2	2	2	2	2
L	720	705	690	675	660	645	630
L/D_c	24	23.5	23	22.5	22	21.5	21

Notation: $N1$

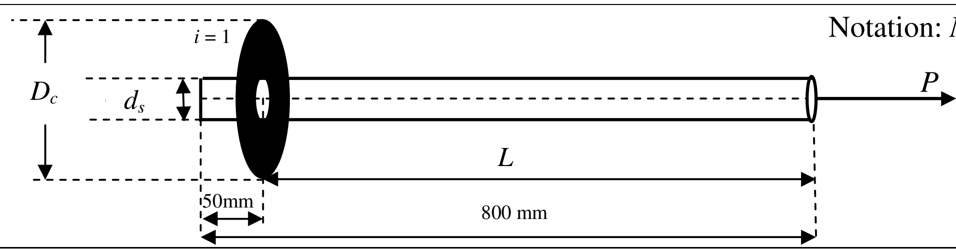

Soil nail with circular disc: $N = 1$; $d_s = 15$ mm

D_c/d_s	4
L	750
L/D_c	12.5
D_c/d_s	3
L	750
L/D_c	16.67
D_c/d_s	2
L	750
L/D_c	25

Notation: N_0

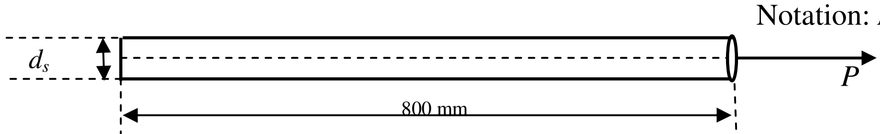

Soil nail with no circular disc: $N = 0$; $d_s = 15$ mm

D_c/d_s	1

The soil continuum is simulated by using hexahedra (bricks) continuum isoparametric elements of C3 element class in 3D. Continuum hexahedra can either be 8 - noded or 20 - noded elements. An 8 - noded linear brick element with reduced integration (C3D8R) is used to model the soil domain. Reduce integration minimizes the number of constraints introduced by an element due to internal constraints. According to Dasari and Soga [237] for problems involving contact and large distortion, the FE mesh is also highly distorted. Hence use of first - order elements with reduced integration is recommended. Soil is modeled as deformable solid with stress - strain behavior being governed by the modified Drucker - Prager/ Cap model. The modified Drucker – Prager/Cap model is mainly used for pressure – dependent yield materials. The yield surface of Drucker – Prager plasticity model is defined by a shear failure surface for perfectly plastic yield without hardening and a 'cap' for plastic compaction and soil softening due to inelastic volume increase (dilatancy). The associated flow is related to 'cap' region while shear failure region has non - associated flow rule. The non – associated flow rule is commonly adopted when the dilatancy effect is of importance [150]. The Drucker – Prager failure surface is given by Eq. (4.21) as:

$$F_s = t - p\tan\beta - d = 0 \tag{4.21}$$

Where, β = angle of friction of material, d = cohesion. The Drucker – Prager model in Abaqus is expressed in terms of stress invariants given as Eq. (4.22):

$$Equivalent\ pressure\ stress(p) = -\frac{1}{3}\ trace\ (\sigma) \tag{4.22}$$

$$Mises\ equivalent\ stress\ (q)\ = \sqrt{\frac{3}{2}S : S} \tag{4.23}$$

$$Third\ stress\ invariant\ (r) = \left[\frac{9}{2}S : S \cdot S\right]^{1/3} \tag{4.24}$$

$$Deviatoric\ stress\ at\ failure\ (t) = \frac{1}{2}q\left[1 + \frac{1}{K} - \left(1 - \frac{1}{K}\right)\left(\frac{r}{q}\right)^3\right] \tag{4.25}$$

Parameter K in Eq. (4.25) helps to control the effect of intermediate stress on yield surface. It can be stated that minimal soil disturbances will take place during the installation process of soil nail with circular discs owing to small thickness of circular plates. However, modelling in the present work has been carried out from the time when soil nail has been placed in the soil mass and surrounding soil has re – established it contact with the soil nail. In that scenario, the constitutive model for soil – nail interface zone simulation will be similar to surrounding soil domain. Hence, similar constitutive model is used to simulate the condition. Moreover, since creep is a function of state of packing of sand and is higher for loose sand [238], surrounding soil for the present study consists of drained sandy soil with a high angle of friction of 36.5° rendering it as dense, hence consolidation and creep settlement of surrounding soil is expected to occur within small time increment from the time of installation of nail. This small time interval for consolidation and creep ensures that perfect contact between nail and surrounding soil occurs soon after installation. This signifies that soil properties at and around the soil – nail interface can be treated as similar.

Soil nails are modelled as deformable solid sections consisting of two parts namely shaft and circular disc. The shaft and circular disc simulation consisted of 1200 and 216 linear hexahedral elements, respectively of type similar to soil continuum defined as C3D8R of first – order. The discs and nail shaft interaction is defined by a surface to surface 'tie' constraint, which permits the same degree of freedom as that of nail shaft. The simulated nail with circular disc is accommodated in a sandy soil domain by assigning a 'penalty – type' contact between surrounding soil and simulated nail. The parameters used for modelling soil domain and nail with circular disc are summed up in Table 4.10.

Table 4.10: Modeling parameters for soil domain and nail with circular discs

Parameters	**Soil**	**Nail shaft and Circular discs**
Type	Solid, deformable (sand)	Solid, deformable
Model	Drucker – Prager/Cap model	
Density in kg/m^3	1650	7850
Elastic Modulus (E) in MPa	50	200 x 10^3
Poisson's ratio (υ)	0.3	0.3
Drucker – Prager plasticity		
Cohesion (*d*) in KPa	0	-
Material angle of friction (β°)	36.5	-
Dilation angle (ψ°)	6.5	-
Flow stress ratio (K)*	0.778	-
Friction coefficient#	0.21	

*Value of flow stress in triaxial tension to flow stress in triaxial compression $0.778 \leq K \leq 1$ [239]

#Value of penalty – type friction coefficient adopted from Tokhi [214]

The geometry of pullout box is adopted from laboratory pullout test conducted on screw nail by Tokhi [214]. The box has a length of 1500 mm with 1000 mm of height and 1000 mm of width. The nail with circular discs is placed at a depth (*H*) of 500 mm from the top surface of model box. The total length of nail used for analysis is 800 mm. The length and location of nail has been selected such that the difference in pullout is less than 5% due to rigid outer boundaries. An optimal radial distance of 25 times the radius of inclusion is found to satisfy this condition [240] which is well within the permitted outer boundary variation for pullout in FE analysis of 20 to 50 radius of inclusion. The radius of nail used in present analysis is 7.5 mm, which calculates the minimum distance of outer boundary as 187.5 mm. However, outer boundaries for present model lie well beyond the minimum distance.

To simulate the actual boundary conditions, degree of freedom of all the sides of modeled pullout box has been restricted as x = 0, y = 0 and z = 0 at the beginning of analysis. For application of overburden of 20 kN/m^2, top surface of pullout box is allowed to displace in the vertical downward direction (y - axis) with all other degree of freedom being restricted. The pullout of soil nail is carried out in a load – control manner by applying a load 30kN at nail head. For this stage of analysis, a small circular opening near the nail head is set free in z- direction. To ensure quality of meshing, partitioning and finer meshing around shaft and circular disc is carried out. The overburden pressure and pullout load are applied in a series of steps. An initial step is set up to establish equilibrium stress conditions and contact surfaces between soil domain and inclusion. The complete analytical pullout model is shown in Fig. 4.11.

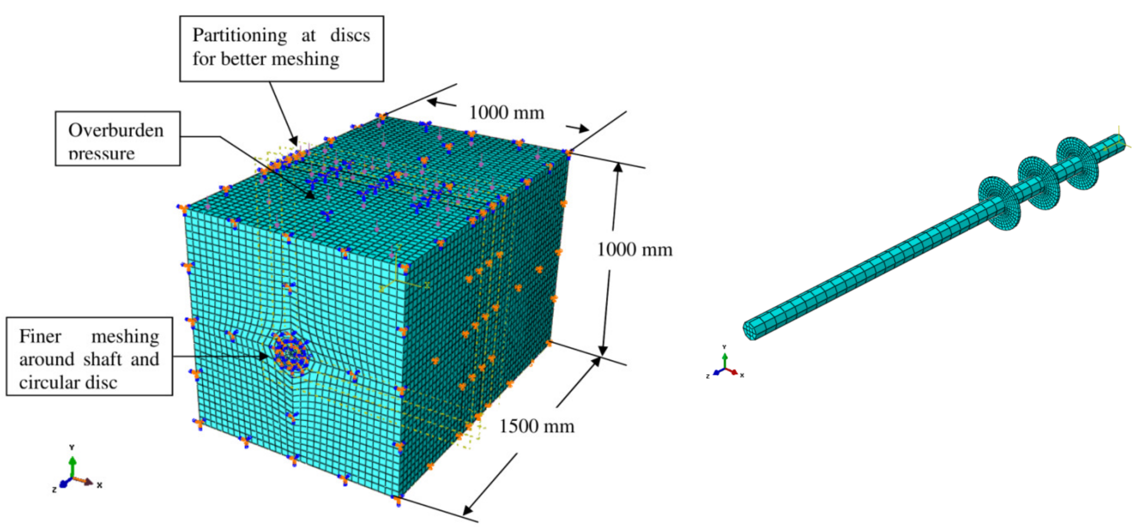

(a) (b)

Fig. 4.11: Dimensions, boundary conditions and FE meshing (a) Modeled pullout box (b) Modeled soil nail shaft with circular discs

However, installation mechanism of this type of soil nail has not been modelled in the present analysis. A soil nail with circular disc holds an added advantage over conventional nails by the virtue of its ease of installation. The installation of soil nails mounted with parallel discs in longitudinal direction can be achieved by either embedding the nails during staged construction or by push and rotate technique. These soil nails do not require a grout surface and consequently no drill hole is required. To install such nails, torque is provided at the nail head which drives the nail to desired location. This installation technique is believed to produce fewer disturbances to the surrounding soil and produces no spoils [214]. Based on the above observation, it is assumed that soil properties during nail installation are not altered significantly and hence installation process modelling prior to pullout has not been included in the present analysis.

The results from pullout behaviour of helical soil nails have been used to simulate helical soil nails in LE analysis (Section 4.2.4). Moreover, fabrication of helical soil nail has also been done according to the optimum configuration attained from numerical analysis of helical soil nail pullout response.

CHAPTER 5

RESULTS AND DISCUSSIONS

5.1 General

The chapter includes all results obtained from material testing, model testing with smooth, screw and helical nails and their corresponding limit equilibrium and finite element analysis. Comparison and discussions regarding the critical observations from results between model testing and numerical modeling are also presented here. This chapter also provides validation of model testing and numerical modeling from past literature.

5.2 Results from Model Testing and Numerical Modeling

The results of model testing and numerical modeling of soil – nailed slopes with three different types of nails namely smooth soil nails, screw soil nails and helical soil nails includes factor of safety against stability for each slope angle, load – deformation characteristics of reinforced slopes, failure mechanism and nail forces developed with loading of soil – nailed slopes. The results obtained are also used to determine optimum layout for different soil nails.

5.2.1 Results of Unreinforced slopes

The model testing of reinforced slopes at β = 45° is observed to bear load of 13.2kN as compared to 11.6kN for β = 60° and 10.2kN for β = 90°. It is clear from results of model testing that unreinforced slopes with β = 45° depicts maximum load carrying capacity without nails. The FEM analysis of unreinforced slopes further records maximum load at β = 45° having value of 15.66kN. The load carrying capacity of unreinforced slopes is found to decrease with increasing slope angle β. For β = 60°, FE analysis reveals a maximum load capacity of 12.30kN whereas smaller load carrying capacity of 11.43kN is found for β = 90°. The results of maximum load carrying capacity for unreinforced slopes of β = 45°, β = 60° and β = 90° are summarized in Table 5.1.

Table 5.1: Maximum load carrying capacity of unreinforced slopes at different slope angles

β°	Experimental	Finite Element Analysis
	Load [kN]	**Load [kN]**
45°	13.2	15.66
60°	11.6	12.30
90°	10.2	11.43

The unreinforced slopes of 45°, 60° and 90° are found to fail under the surcharge loading with settlement of crest and consequent outward movement of slope face. From Figs. 5.1 (a) to (f), it can be seen that similar failure mechanism is observed from both model testing and FE analysis.

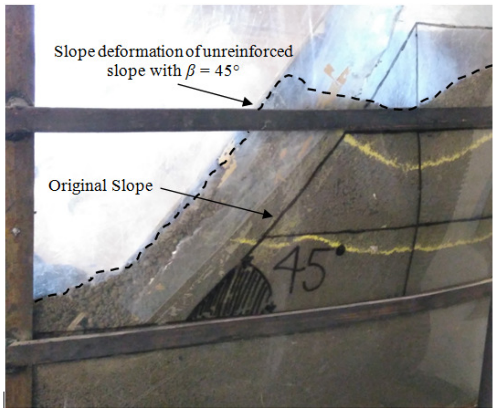

(a) Model testing of $\beta = 45°$

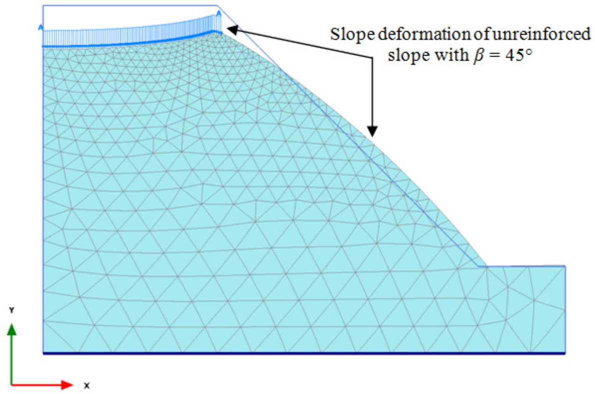

(b) FEM analysis of $\beta = 45°$

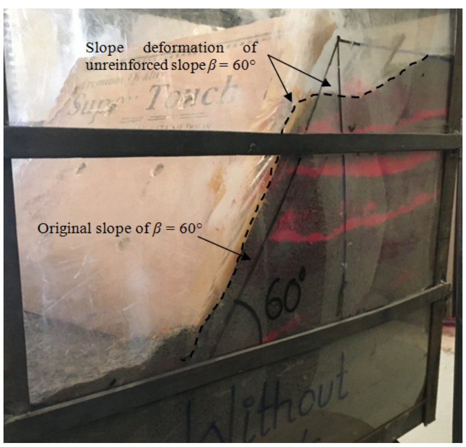

(c) Model testing of $\beta = 60°$

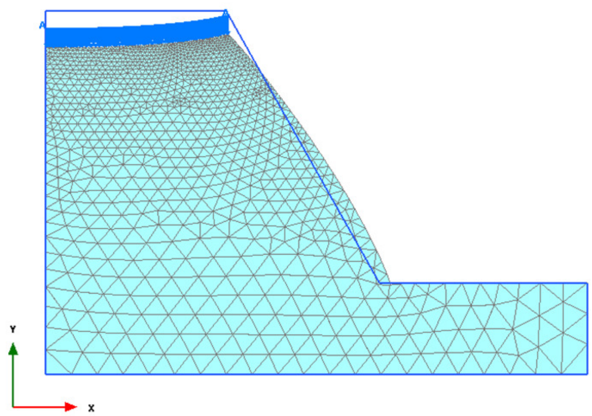

(d) FEM analysis of $\beta = 60°$

(e) Model testing of $\beta = 90°$

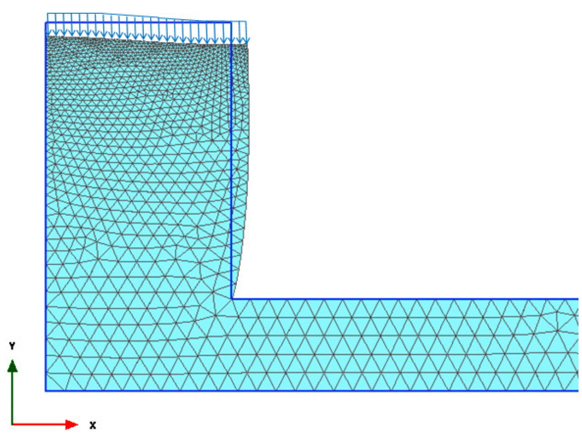

(f) FEM analysis of $\beta = 90°$

Fig. 5.1: Slope Deformation of unreinforced slopes from model testing and FEM analysis

The failure mechanism of 45° and 60° slope is similar with failure originating from slope toe and propagating towards slope crest. Simultaneously, crest settlement also occurs under gradual increasing surcharge loading. The slope is found to deform with initial slip surface acquiring a shape circular slip surface. The failure mechanism of 90° slope [Fig. 5.1 (e) and (f)], it is observed that rotation about toe occurs for vertical cut. The entire slope crest is found to collapse at slope toe under surcharge load. A similar failure mechanism is also observed from FE analysis of 90° unreinforced slope.

5.2.2 Results of Load – Settlement for Soil – nailed slopes with Smooth nails

The model testing of slopes at different slope angles (β) depicts that β = 45° is found to record maximum load similar to unreinforced slopes. However, β = 60° yields load bearing value smaller than β = 45° but larger than β = 90°. A similar trend of load carrying capacity of slopes is also found with unreinforced slopes. As slopes are reinforced using smooth nails, the load carrying capacity is also found to vary. The maximum load carried by β = 45° is found to be 20.6kN for nail inclination (i) = 0°, 21.2kN for i = 15°, 17.7kN for i = 20° and 15.8kN for i = 30°. It can be seen that as nail inclination is increasing the load carrying capacity of slopes is found to vary. However, maximum load carrying capacity is not observed for maximum nail inclination of 30° but for i = 15°. The maximum load variation for β = 60° is observed as 18.8kN for i = 0°, 20.1kN for i = 15°, 15.1kN for i = 20° and 14.7kN for i = 30°. Similarly, maximum load of 17.3kN for i = 0°, 16.4kN for i = 15°, 13.5kN for i = 20° and 10.9kN for i = 30° is found for β = 90°. For β = 60° and β = 90°, it can also be observed that maximum load is found for i = 15° instead of maximum nail inclination of 30°. The results of model testing at different slope angles and nail inclinations are given in Table 5.2.

Table 5.2: Maximum load carrying capacity for slopes with smooth nails from model testing

β°	**i° = 0°**	**i° = 15°**	**i° = 20°**	**i° = 30°**
	Load [kN]	**Load [kN]**	**Load [kN]**	**Load [kN]**
45°	20.6	21.2	17.7	15.8
60°	18.8	20.1	15.1	14.7
90°	17.3	16.4	13.5	10.9

The reason for this load variation can be accounted for the fact that slope reinforcement using smooth nails is achieved best at nail inclination which takes up maximum shear stress during loading. Moreover, if nail inclination makes the nail positioned in zones of tensile strain developed within slope during loading, it is found to yield maximum reinforcement. Another reason for increase in load capacity with 15° nail inclination can be attributed to nail length residing in passive zone of reinforced slope. Since higher bond length correspond to larger pullout capacity, slopes with i = 15° depicts maximum load capacity for all slope angles of 45° and 60°. Beyond i = 15°, load capacity of slopes is found to decrease for 45° and 60° slope because of mobilization of compressive forces rather than tensile forces along nail length.

For β = 90°, it is found that maximum load capacity is achieved for i = 0° instead of i = 15°. As the inclination increases from 0° to 30°, load capacity is found to decrease by almost 37%. The variation of load capacity with nail inclination for β = 90°can be explained by the fact that at right angles to slope face (i = 0°) nail bear the maximum normal stress due to overburden and surcharge. Now, as surcharge increases gradually which in turn increases normal stress which is beared upon by smooth soil nails and consequently maximum shear stress is mobilized. With increasing inclination, surface area of nails exposed to normal stress decreases and hence reduction in shear stress occurs. Thus, with increase in nail inclination smaller load capacity is observed for β = 90°.

Table 5.3: Maximum load carrying capacity for slopes with smooth nails from FE analysis

β°	***i*° = 0°**	***i*° = 15°**	***i*° = 20°**	***i*° = 30°**
	Load [kN]	**Load [kN]**	**Load [kN]**	**Load [kN]**
45°	24.22	26.45	22.84	20.13
60°	23.99	25.69	2.18	19.68
90°	22.76	19.70	16.99	15.09

The result of finite element modelling of slopes with smooth nails depicts that β = 45° with nail inclination of 15° is found to yield maximum load. A similar observation is made for β = 60° from FE analysis. For i = 15°, β = 45° records a maximum load of 26.45kN in comparison to 25.69kN as observed for β = 60°. For β = 90°, maximum load of 22.76kN is observed for i = 0°. The results of FE analysis are similar to experimental results in terms of maximum load obtained for corresponding nail inclination. However, it is also noted that higher load capacity is obtained from FE analysis as compared to model testing. The reason for discrepancy in load values can be accounted for installation procedure which is not modelled during FE analysis. The driving of smooth nails causes in – situ soil properties to vary which is not simulated in numerical modelling. The reduction of soil properties c and ϕ during nail installation in model testing alters the mobilized shear strength and consequently renders smaller load carrying capacity of soil – nailed slopes. The results of FE analysis are reported in Table 5.3.

A comparative study of model testing and numerical modelling of soil – nailed slope using smooth nails is given in Fig. 5.2. From Fig. 5.2, it can be examined that FE analysis predicts a higher load capacity of slopes as compared to model testing. However, maximum load attained by respective slopes occurs at a smaller horizontal displacement from FE analysis than model testing. For nail inclination of 15°, model testing depicts horizontal displacement of 11.2 mm whereas 3.8 mm horizontal displacement is observed from FE analysis.

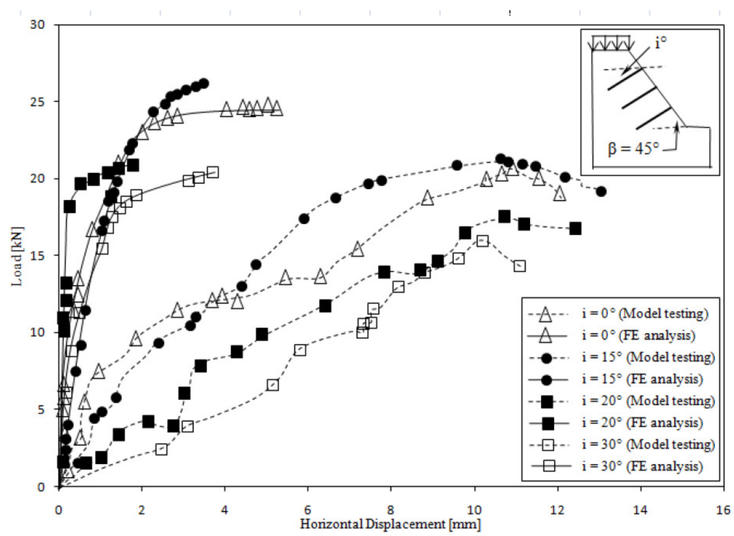

Fig. 5.2: Load – displacement of 45° with smooth nails at different nail inclinations

Similarly, for 60° slope at 15° nail inclination maximum load from model testing corresponds to 9.4 mm of slope movement with 3.4 mm as predicted by FE analysis (Fig 5.3). The load – displacement plot for 90° slope (Fig. 5.4) depicts horizontal displacement of 9.6 mm to attain maximum load capacity from model testing. However, FE analysis reveals that for β = 90°, maximum load capacity is attained at displacement of 2.8 mm for nail inclination of 0°. The variation of horizontal displacement at failure between FE analysis and model testing can be due to rigid boundaries simulated during numerical modelling. Even the minimum of deformation of sides of tank during testing can lead to variation is slope movement which is not accounted in FE modelling. Moreover, change in soil properties during nail installation are difficult to model in PLAXIS 2D subroutine which results in load variations.

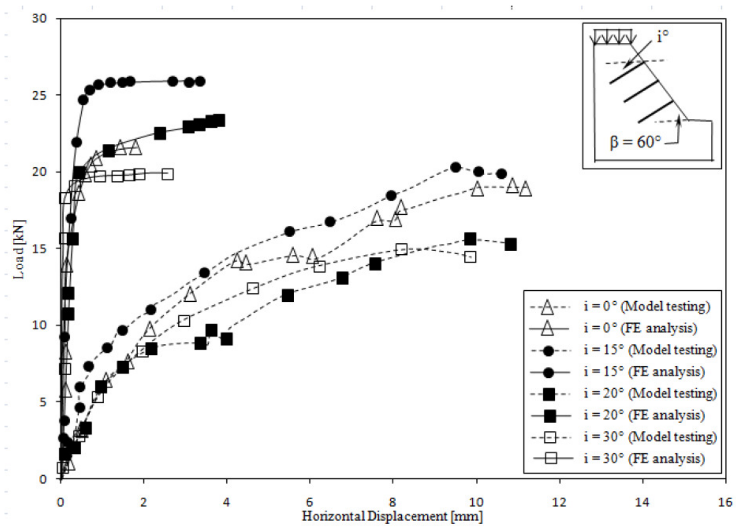

Fig. 5.3: Load – displacement of 60° with smooth nails at different nail inclinations

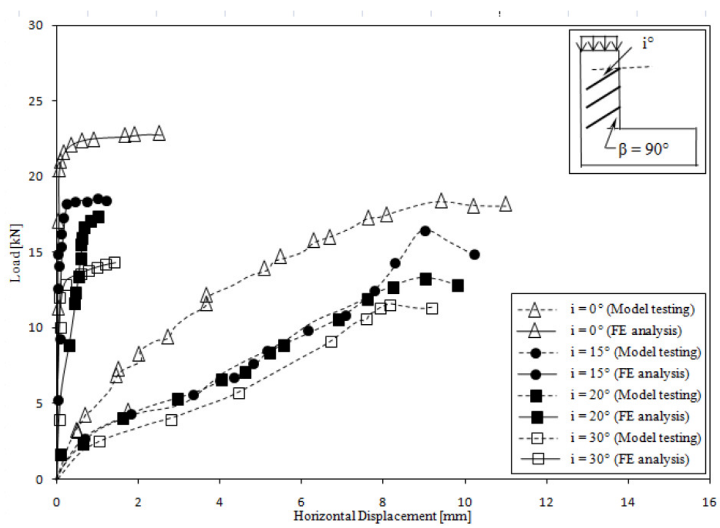

Fig. 5.4: Load – displacement of 90° with smooth nails at different nail inclinations

5.2.3 Results of Failure Mechanism for Soil – Nailed slopes with Smooth nails

During model testing of reinforced slopes with smooth nails, it is observed that failure mechanism of 45° and 60° with all nail inclinations of 0°, 15°, 20° and 30° is characterized by slope crest settlement and outward movement of slope face. As the reinforced slopes are loaded, settlement of bearing plate occurs. The settlement is non – uniform with inclination of plate towards slope crest. This signifies that edge of slope crest is critical to failure with load increase. Moreover, vertical settlement of slope is also verified by vertical displacement of tracer colour bands used as marking along slope height. The tracer marking deformations signify that movement of slope under surcharge loading. It is observed that tracer marking under larger settlement near the slope face as compared to rear of slope. The slope deformation before and after failure for β = 45° and β = 60° with i = 15° is shown in Fig. 5.5(a), Fig. 5.5 (b), Fig. 5.6 (a) and Fig. 5.6 (b), respectively. As slope approaches towards failure, cracks are found to develop around slope toe. Initially a small crack develops from slope toe which extends radially into the slope body and extends toward slope crest. Apart from this prominent crack, many local cracks are also observed for 45° and 60° reinforced slopes. As the crack grows larger, it marks the beginning of reinforced slope failure and slope is found to fail along the same crack. The slip surface generated is primarily classified as circular slip surface originating at slope toe and terminating at some distance beyond the edge of slope crest.

Fig. 5.5(a): Reinforced slope before failure

(β = 45°, i = 15°)

Fig 5.5(b): Reinforced slope after failure

(β = 45°, i = 15°)

Fig 5.6 (a): Reinforced slope before failure

(β = 60°, i = 15°)

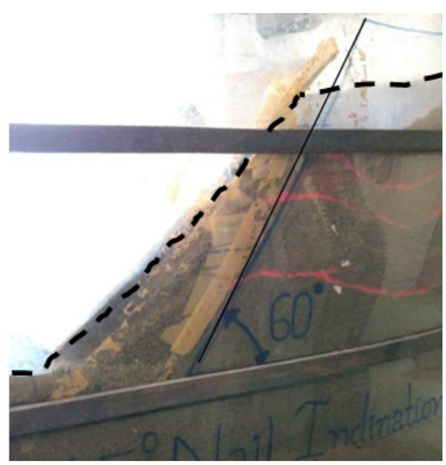

Fig. 5.6(b): Reinforced slope after failure

(β = 60°, i = 15°)

The failure mechanism for β = 90° is characterized by rotation of slope crest about its toe. The slope crest is found to fail as surcharge loading is increased. Due to highly unstable geometry of slope, at failure the soil face is found to move outwards such that horizontal deformation is maximum at slope crest and minimum at slope toe [Fig. 5.7 (a) and 5.7 (b)]. The slip surface so developed during failure of β = 90° with i = 0° is classified as log – spiral surface.

Fig 5.7 (a): Reinforced slope before failure (β = 90°, i = 0°)

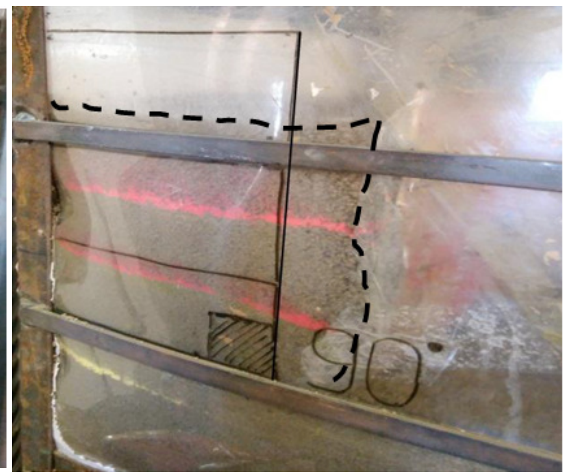

Fig. 5.7 (b): Reinforced slope after failure (β = 90°, i = 0°)

From Figs. 5.8(a), 5.8(b) and 5.8(c), it can be seen that a circular slip surface is generated for reinforced slopes of 45°. It is also observed that the slip surface is passing through the entire crest in cases with nail inclination of 0° and 15°. However, with nail inclination of 30°, a much smaller slip surface is observed. The red shaded portion of slip surface indicates the band of trial slip surfaces with same factor of safety. The most critical slip surface is shaded green among all trial slip surfaces.

From the analysis carried out in SLOPE/W, it is found that installed nail length and mobilized nail length during slip failure vary with the nail inclination and location of nails. Nails at all inclinations of 0°, 15°, 20° and 30° are initially installed with a constant length of 7 m converted to scale. The SLOPE/W analysis yields that nail inclination of 20° and 30° for 45 ° slope angle, enables less than 50% of nail length mobilization to resist slope failure. For the other two nail inclinations 0° and 15°, it is found that more than 90% of nail length has been used to resist the shearing action. It is found that if failure surface uses maximum nail length, reinforcing action of the nails is completely mobilized. The summary of the percentage mobilized nail length for i = 0°, i = 15° and i = 30° is given in Table 5.4. The LE analysis of the reinforced slope also accounts for the fact that load transfer mechanism of nails is governed by pull – out resistance or tensile capacity of nails. It is visible from Figs. 5.8 (a) and 5.8 (b), that 45° slope with 0° and 15° nail inclinations do not depict any nail breakage. This signifies that the load transfer mechanism is governed by nail pull – out resistance capacity. For 30° nail inclination on 45° slope, nails are found to break denoted by dashed line in Fig. 5.8 (c). This also stands for the fact that nail has completely utilized its pull out capacity and is now transferring load by nail tensile capacity. A similar pattern of nail load transfer mechanism is also observed in 60° reinforced slope with 30° nail inclination as shown in Fig. 5.10 (c).

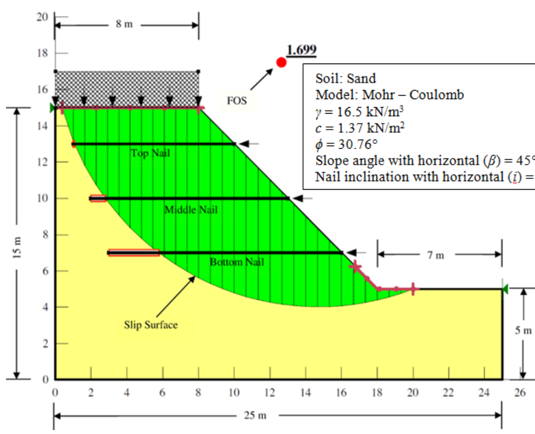

(a) Slip Surface for 45° slope with 0° nail inclination

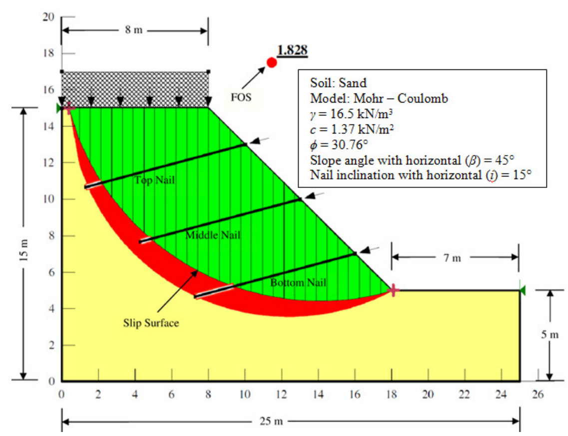

(b) Slip Surface for 45° slope with 15° nail inclination

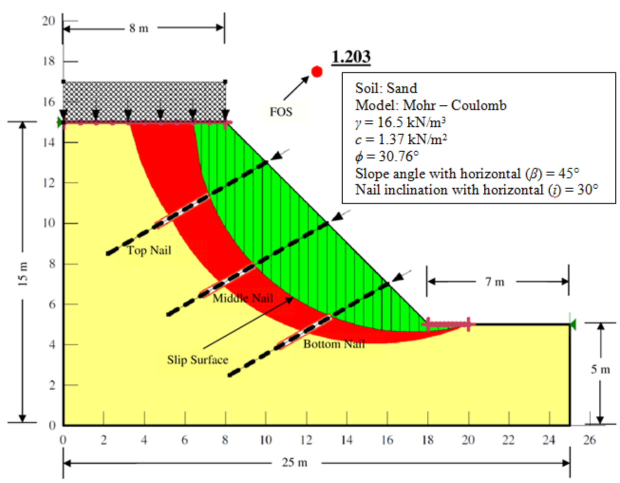

(c) Slip Surface for 45° slope for 30° nail inclination

Fig. 5.8: Slip surface of β = 45° with different nail inclinations for slopes with smooth nails from SLOE/W

Similarly, FE analysis of 45° with different nail inclinations indicate that failure slip surface passes through slope toe for all nail inclinations. Moreover, slip surface is characterized by intersection with slope crest which may take up entire slope crest [Fig. 5.9

(a)] or meets slope crest at some distance (0.3 H to 0.5H) beyond edge of slope face. The FE analysis also depicts that maximum movement is primarily concentrated with slope face as indicated by red in Figs. 5.9 (a), (b) and (c). Both LE and FE analysis brings forth another important observation that for i = 0°, slip surface is not found to intersect nails at all locations. The slip surface escapes top nail length and intersects nail in middle and bottom rows. However, for i = 15° and i = 30° clearly shows that nail length are sufficient enough to intersect slip surface. A similar failure surface is also obtained for i = 20° with nails intersecting the slip surface which passes through slope toe and slope crest.

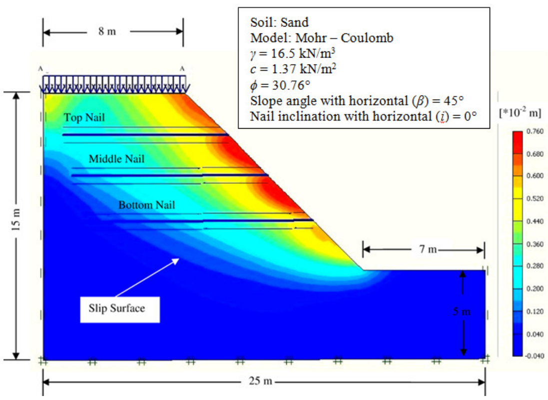

(a) Slip Surface for 45° slope with 0° nail inclination

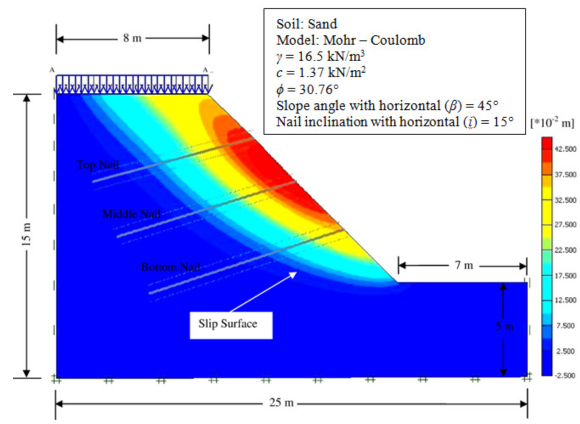

(b) Slip Surface for 45° slope with 15° nail inclination

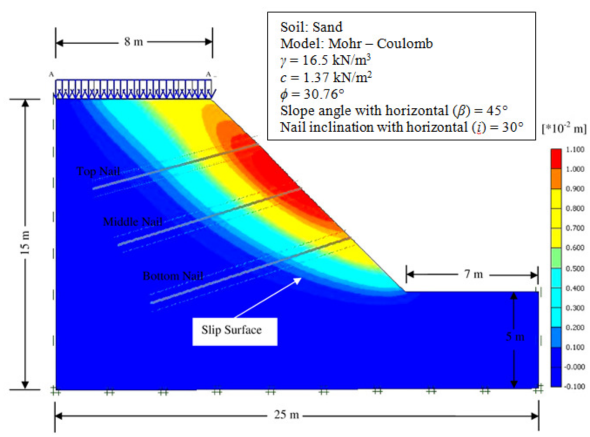

(c) Slip Surface for 45° slope for 30° nail inclination

Fig. 5.9: Slip surface of β = 45° with different nail inclinations for slopes with smooth nails from PLAXIS 2D

For 60° slope also, it can be seen from the Figs. 5.10 (a), 5.10 (b) and 5.10 (c) that slip surface is circular in shape. For slopes with nail inclination of 0° and 15°, variation in factor of safety for trial surface is small. This is indicated by thin red shaded portion of the slip surface. However, 60° slope reinforced with 30° smooth nail inclination is found to have a small slip failure and critical slip surface is found to lie close to the slope face. Unlike 45° slope nails in 60° slope are found to intersect slip surface for all nail inclinations. The critical slip surface for i = 0° and i = 15° are again observed to have occurred from slope crest with slip surface for i = 30° only covers a portion of slop crest. A similar slip surface pattern is also observed for 45° slope. Moreover, bottom row of nails for i = 0° and i = 15° are found to have completely mobilized pullout capacity which is depicted by breakage in nails. The tensile strength of nails now governs the reinforcement action of nails. For i = 30°, nails at all location top, middle and bottom are found to resist failure by virtue of their tensile strength.

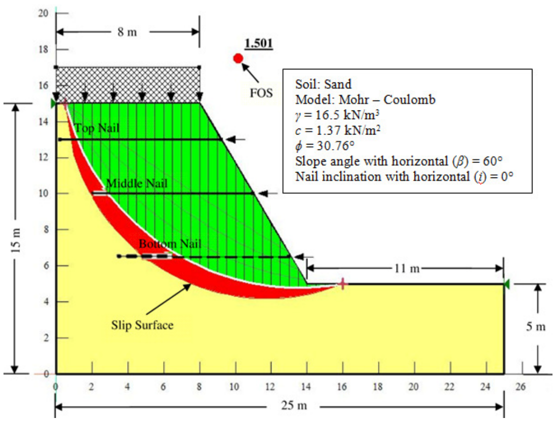

(a) Slip Surface for 60° slope with 0° nail inclination

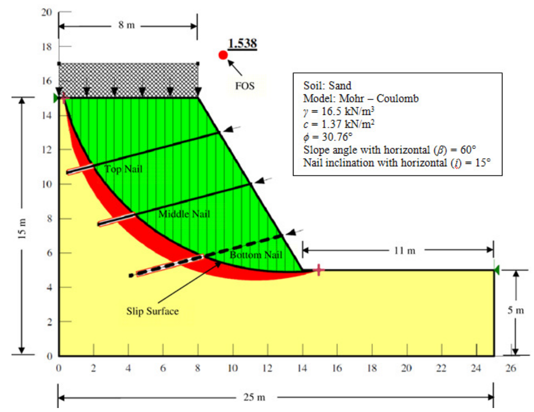

(b) Slip Surface for 60° slope with 15° nail inclination

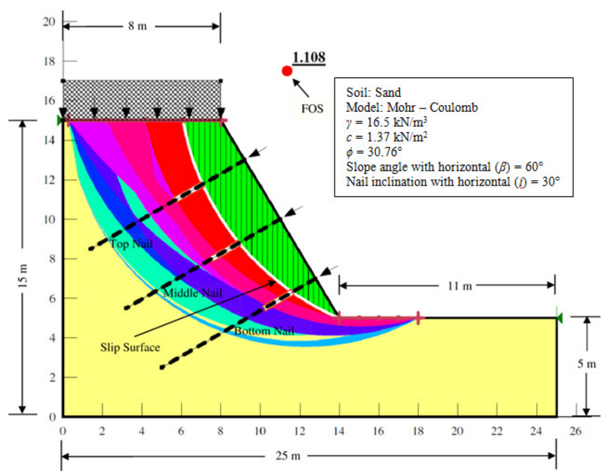

(c) Slip Surface for 60° slope for 30° nail inclination

Fig. 5.10: Slip surface of β = 60° with different nail inclinations for slopes with smooth nails from SLOPE/W

The FE analysis of smooth-nailed soil slope of 60° with different nail inclinations shows that different slip surfaces are observed as compared to LE analysis [Figs. 5.11 (a), (b) and (c)]. For i = 0° FE analysis fails to predict a circular slip surface instead a log – spiral curve combined with a block failure is found to occur. Moreover, slip surface is also found to run beyond nail length for top and middle nail rows and intersects nail length only for bottom row of nails. This signifies that failure is mainly governed by external mode of failure. On the other hand, i = 15°, much defined slip surface is observed. The slip surface is classified as circular slip surface which intersects nail at all locations. For i = 30°, a highly deformed slope is observed with slip surface similar to i = 0°. For nail inclinations it can be seen that most critical zone for failure mainly concentrates around slope face which is similar to result as given by LE analysis.

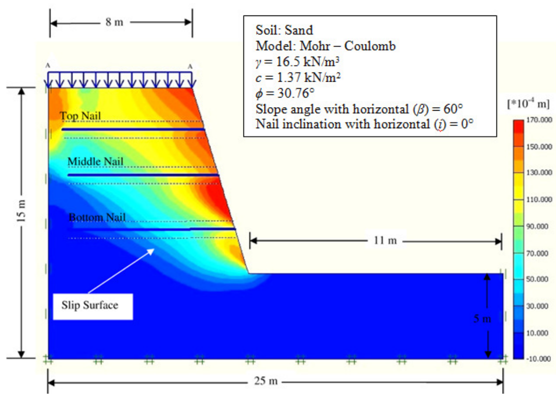

(a) Slip Surface for 60° slope with 0° nail inclination

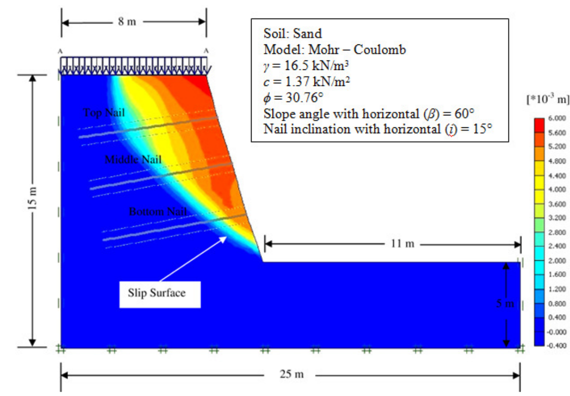

(b) Slip Surface for 60° slope with 15° nail inclination

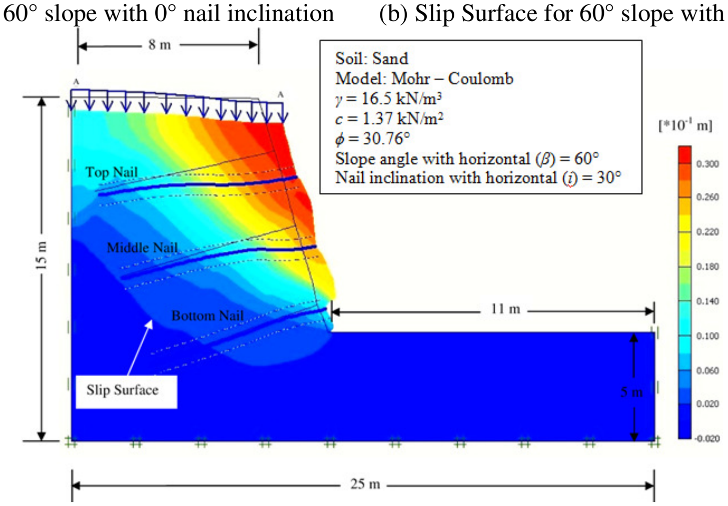

(c) Slip Surface for 60° slope for 30° nail inclination

Fig. 5.11: Slip surface of β = 60° with different nail inclinations for slopes with smooth nails from PLAXIS 2D

For β = 90° slope with nail inclination of 0° is found to be the most stable layout for smooth – nailed slopes. For all other inclinations a similar failure mechanism of rotation about slope toe with significant slope crest movement is observed. With the limitation of LE analysis for prediction of failure mechanism by assuming a slip surface within circular, bi – linear or block failure, the predicted slip surface for 90° is practically not feasible to occur at field. The slip surface and slope deformation as depicted by FE analysis is found to be more apt for a vertical cut. It clear demarcates slope crest settlement with slope face movement being pronounced at slope crest and smaller at slope toe (Fig. 5.12).

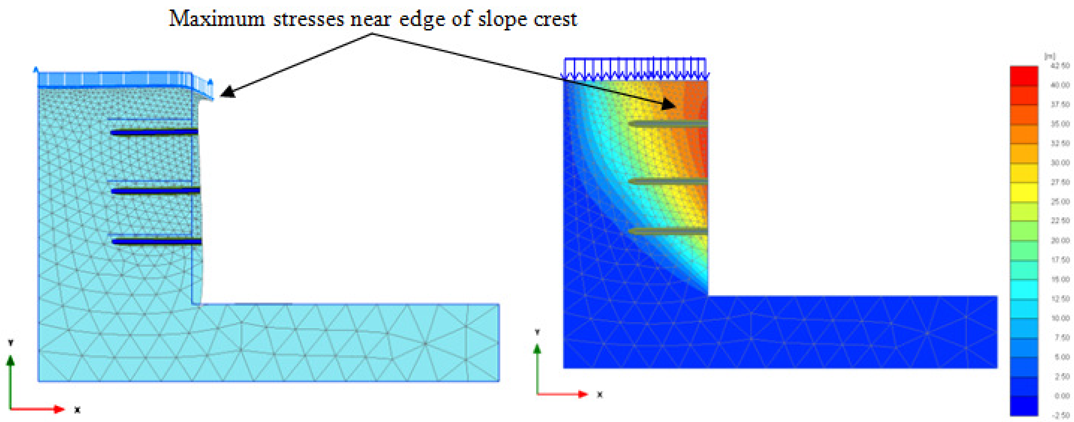

Fig. 5.12: Failure mechanism of 90° slope with i = 0°

The factor of safety of smooth nailed slopes as obtained from SLOPE/W (LEM) and PLAXIS 2D (FEM) are given in Table 5.4. It can be seen from Table 5.4 that factor of safety greater than 1 is obtained for majority of slopes reinforced with smooth nails. The highest factor of safety for β = 45° is found for i = 15° both from LE (FOS = 1.82) and FE (FOS = 1.43) analysis. A similar observation can be made for β = 60°, with FOS = 1.53 from LE analysis and FOS = 1.37 from FE analysis. For β = 90°, highest FOS = 1.33 is attained from LE analysis and FOS = 1.31 from FE analysis. However, β = 90° highest FOS corresponds to i = 0°. The obtained factor of safety values further signify that for β = 45° and β = 60°, maximum stability is achieved with smooth nails inclined at i = 15°. For β = 90°, nail inclination providing maximum stability corresponds to i = 0° both from LE and FE analysis. Moreover, it can also be noted that factor of safety for β = 45° and β = 60° factor of safety increases from 0° to 15° thereby decreasing beyond 15°. The variation is however different for β = 90° where factor of safety is found to decrease with increase in inclination being maximum for i = 0° and minimum for i = 30°.

Table 5.4: Factor of safety for different slopes reinforced with smooth nails at different nail inclinations

β°	i° = 0°		i° = 15°		i° = 20°		i° = 30°	
	LEM	**FEM**	**LEM**	**FEM**	**LEM**	**FEM**	**LEM**	**FEM**
45°	1.69	1.36	1.82	1.43	1.29	1.27	1.20	1.15
60°	1.50	1.17	1.53	1.37	1.14	1.21	1.10	1.08
90°	1.33	1.31	1.26	1.00	1.12	0.88	0.96	0.79

As observed from Table 5.4, it can be seen that limit equilibrium method calculates a higher factor of safety as compared to the finite element method. The LEM utilizes the equilibrium of forces among the slices which requires assumptions and compromises on the accuracy of the method. The FOS given by the FEM analysis is on the lower side. The FEM is based on the displacement of nodes till the occurrence of slope failure. However, FOS as obtained from both the analysis show a similar pattern with the maximum FOS for nail inclination of 15° in both 45° and 60° slope. This is followed by the FOS for 0° nail inclination. The minimum FOS of safety from LEM and LEM is obtained for slope with nail inclination of 30°. The % increase in FOS with respect to FOS from FE analysis is about 24.26% with nails inclined at 0°. For 15° nail inclination, LE analysis predicts 27.27% higher FOS as compared to FE analysis. For 30° nail inclination this increase is significantly small which comes out be 4.34%. All the above mentioned percentage changes are for 45° slope angle. In case of 60° slope angle, this percentage variation in FOS between LEM and FEM ranges from 1 – 28%. For nails inclination of 0° a significant percentage increase of 28.20% is observed, which falls to 11.68% for 15° nail inclination. An increase in FOS of just 1.85% is found with nail inclination 30° from both analyses. Similarly, a small increase of 1.5% is observed between FOS between FE and LE for 90° slope with inclination of 0°. For nail inclination of 30°, LE estimates 21.5% higher FOS as compared to FE analysis. The reasons for this higher FOS from LEM more as compared to FOS from FEM can be:

a) LE and FE analyses have fundamental difference in the basic principles. The first is based on the limit equilibrium formulations, which are dependent on static force or moment equilibrium. As in Morgenstern – Price model used in LEM a half–sine inter-slice function is used to relate the inter-slice normal – shear forces. This in turn is used to find slice base normal force which gives the factor of safety with respect to force and moment equilibrium. The variation in FOS is obvious since inter-slice weight and slice base force will depend on the shape of assumed slip surface which is circular in case of LEM. Whereas FEM is based on a stress-strain relationship, which can effectively accommodate the change in stresses. The FE analysis in PLAXIS, for example finds the slip surface, where the excessive strains are localised, and computes the FOS by a c - ϕ reduction procedure for the Mohr-Coulomb soil model.
b) The FOS is primarily related to the normal stress distribution along the slip surface. A significant difference in normal stress distribution, particularly in the toe area, can be found between FE and LE analyses for a particular slip surface [241]. This difference in normal stress distribution results from the shear stress concentrations, which are not, captured in the LE analyses. In LEM, the normal forces at the base are primarily

derived from the weight of the sliding mass and not the shear stress distribution which results in higher FOS prediction (Fig. 5.13).

c) In this study also, no similarity in the inter-slice force and critical shear surface was found between the analyses in LE and FE methods. Both analysis utilizes different shear forces and on different critical surfaces.

d) The FE analysis computes factor of safety for each element along the slip surface, whereas a single, weighted average FOS is computed in the LE analyses. This lead to over prediction of FOS in LEM. Moreover, Krahn [241] states, “FE analyses can handle variations in FOS without any difficulty of convergence, due to stress redistributions for change in loading conditions”. However the convergence of simulations in LE is found problematic for steep slip surfaces, whereas FE overcomes such difficulties. This is why the computed FOS from the FE analysis is regarded more reliable for the analysed slopes.

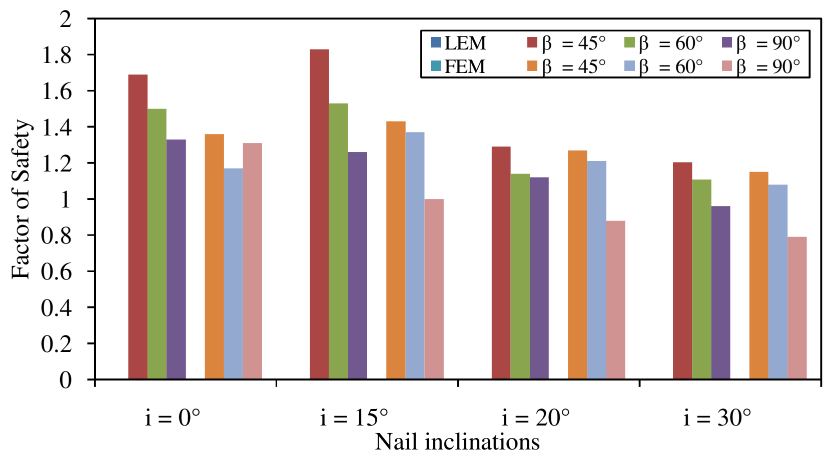

Fig. 5.13: Factor of safety variation with nail inclinations from LE and FE analysis

The variation in slip surfaces from the two approaches can be accounted for the following reasons:

a) Different inter-slice shear forces and base normal forces are predicted from LEM and FEM. LEM uses the different slip circles and predicts the slip circle with minimum factor of safety as critical. The convergence of force equilibrium and moment equilibrium governs the FOS and hence critical slip surface. Moreover, the local factor of safety is constant throughout the analysis in LEM, thus eliminating the cases of local slip failure. On the other hand, the slip surface obtained from FEM is based on stress distribution within the continuum. The stress distribution in more realistic in

FEM as local factor of safety is not constant and thus convergence of results is achieved.

b) The line of thrust is different in both the analytical methods. The point of application of interslice normal in LE and FE is different varying from the crest to the toe. The location of thrust line depends on the slip surface geometry and loading condition. Thus, a variation in FOS and consequently in slip surface is obvious.

c) The variation from deeper slip surface in LEM to shallow slip surface in FEM is due to different shear and normal stresses values generated in the respective analysis.

It can be observed that the failure surface captured from LEM analysis (SLOPE/W) and FEM analysis (PLAXIS 2D) are comparable to the failure slip surface obtained from model testing with slight variations. The slip surface found from model testing is not necessarily a circular slip surface but a non – circular slip surface or a log spiral surface. The experimental results yield a shallow slip surface which is concentrated near the slope face. The slip surface is found to originate at the slope crest near the slope face. It propagates towards the toe. For reinforced slope of 45°, the slip surface intersects the slope face above the toe which can be categorized as a slope failure. Moreover, a much visible toe failure is found to occur for 60° reinforced slope. The numerical modeling of this slope with LEM subroutine SLOPE/W shows a rather circular slip surface with failure. Also it can be seen that a deep failure surface is predicted by limit equilibrium analysis which is not the case from model testing. The slip surface by LEM is also found to pass well below the slope toe for 45° reinforced slope, whereas a slope failure is obtained from model testing. In case of 60° reinforced slope, both model testing and LEM analysis depicts toe failure with variation in slip surface depth. Similarly, for 90° slope FE analysis and model testing are found to depict similar failure surfaces and mechanism with LE analysis yielding circular slip failure which is difficult to be expected at field condition. As mentioned earlier, LEM gives a deep slip surface which originates away from slope face and close to rear of slope crest, whereas the slip surface from model testing is also circular but slightly steeper as compared to LE analysis result. It can also be observed that the experimental slip surface starts near the slope face at the crest and ends at the toe unlike LEM result.

The slip surfaces obtained from PLAXIS 2D (FEM) analysis are found to give results which are in good agreement with model testing slip surfaces. For 45° reinforced slope, non – circular slip surface originating from slope crest slightly away from slope face is observed from both FEM analysis as well as experimentally. However, PLAXIS also gives a base failure in contrast to slope failure found by testing. It can also be seen that the stresses are found to be concentrated near the slope face and decreases as distance from the slope face increases. The slip surface for 60° reinforced slope obtained from FEM is similar to the experimental slip surface. Both slip surfaces are toe slope failure with non – circular shape of slip and lie close to the slope face.

Hence it can be said that FE analysis carried out by PLAXIS 2D gives more realistic failure surfaces as compared to LE analysis by SLOPE/W. However both the analytical methods failed to predict the significant crest settlement which occurred in model testing. The variations between experimental work and analytical methods can be accounted for the following reasons:

a. LEM works on the concept of assumed failure surface (circular in this case) with lowest factor of safety in contrast to FEM where critical slip surface is generated by failure stress–strains on the displacement nodes. This makes FEM results more realistic than LEM results.
b. The boundary conditions modeled in LEM and FEM are different from model testing. SLOPE/W does not incorporate tools for boundary condition simulation whereas in PLAXIS 2D the bottom boundary is fixed in x – y direction, left and right model boundaries are fixed in x – direction for all cases of reinforced slopes, whereas no boundaries are perfectly fixed in model testing which can be accounted to the flexibility of Perspex sheets used.
c. The model testing is effected by settlement and lateral displacement in all x, y and z directions, which is not taken care of when simulated in either LE or FE analysis as both are 2D analysis codes. The slope and crest displacements observed in model testing are significantly different from LEM and FEM displacements of slope and crest, thus a variation in slip surface generation also exists.

5.2.4 Results of Nail forces for Soil – Nailed slopes with Smooth nails

The nail forces obtained from model testing with most stable nail inclination 15° for 45° and 60° slope and nail inclination of 0° for 90° slope is shown in Figs. 5.15 (a), 5.15 (b) and 5.15 (c). For all the model slopes it can be observed that nail forces are found to increase as surcharge load is increasing on slope crest. However, increase in surcharge load leads to an increase in normal stress in addition to overburden acting due to soil weight above the respective nail position. With increase in normal stress, shear stress is mobilized along nail length. The nail bearing higher normal stress consequently resists more shearing of soil during failure. For all slope angles, it is observed that top row of nails depict higher nail forces as compared to middle and lower row of nails. The nail forces are found to increase with increase in settlement which in turn reflects increase of surcharge loading. However, nail forces are found to level off beyond peak value with increase in crest settlement. The reason for decrease in nail value corresponds to decrease in nail strain as soil mass movement is restrained by nails. The notation of nails is given in Fig. 5.14.

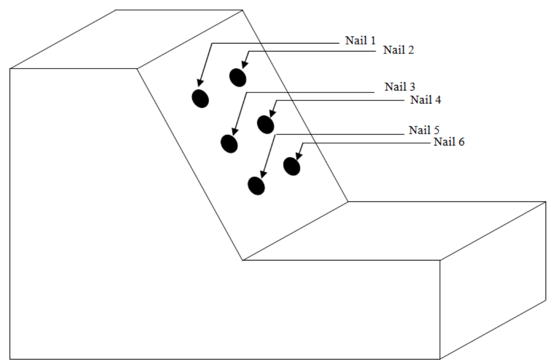

Fig. 5.14: Nail configuration and notation for all slopes

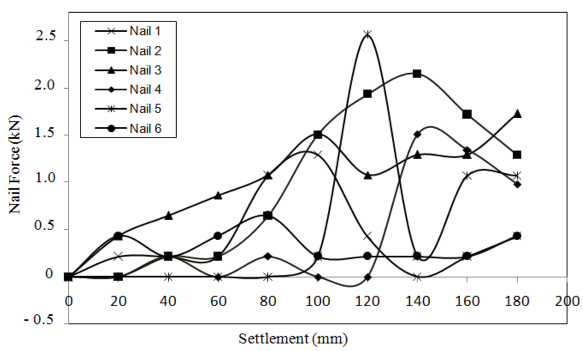

(a) Nail force for $\beta = 45$; $i = 15°$

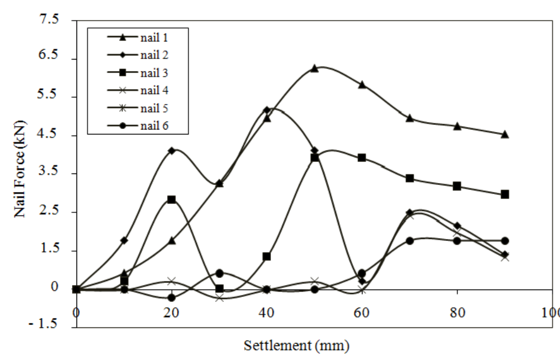

(b) Nail force for $\beta = 60$; $i = 15°$

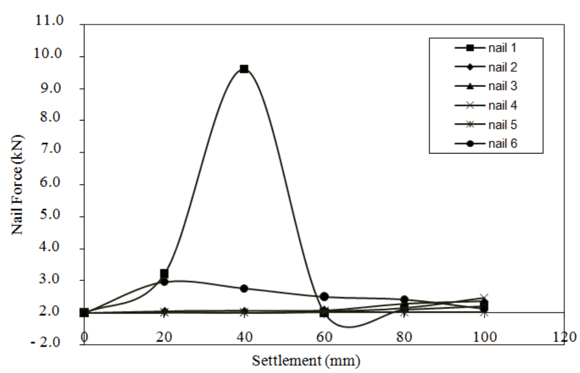

(c) Nail force for $\beta = 90$; $i = 0°$

Fig. 5.15: Nail force distribution for different slopes and nail inclinations from model testing with smooth nails

The maximum nail force for 45° slope with nail inclination of 15° of 2.53kN is found for nail 1. Similarly, for 60° slope with nail inclination of 15°, nail 1 depicts maximum nail force of 6.42kN with nail 2 recording the second largest nail force. Nail 1 in 90° slope with nail inclination of 0° also found to result in maximum nail force of 9.86kN. However, unlike 45° and 60° slope, 90° slope depict nail 6 to have second maximum nail force.

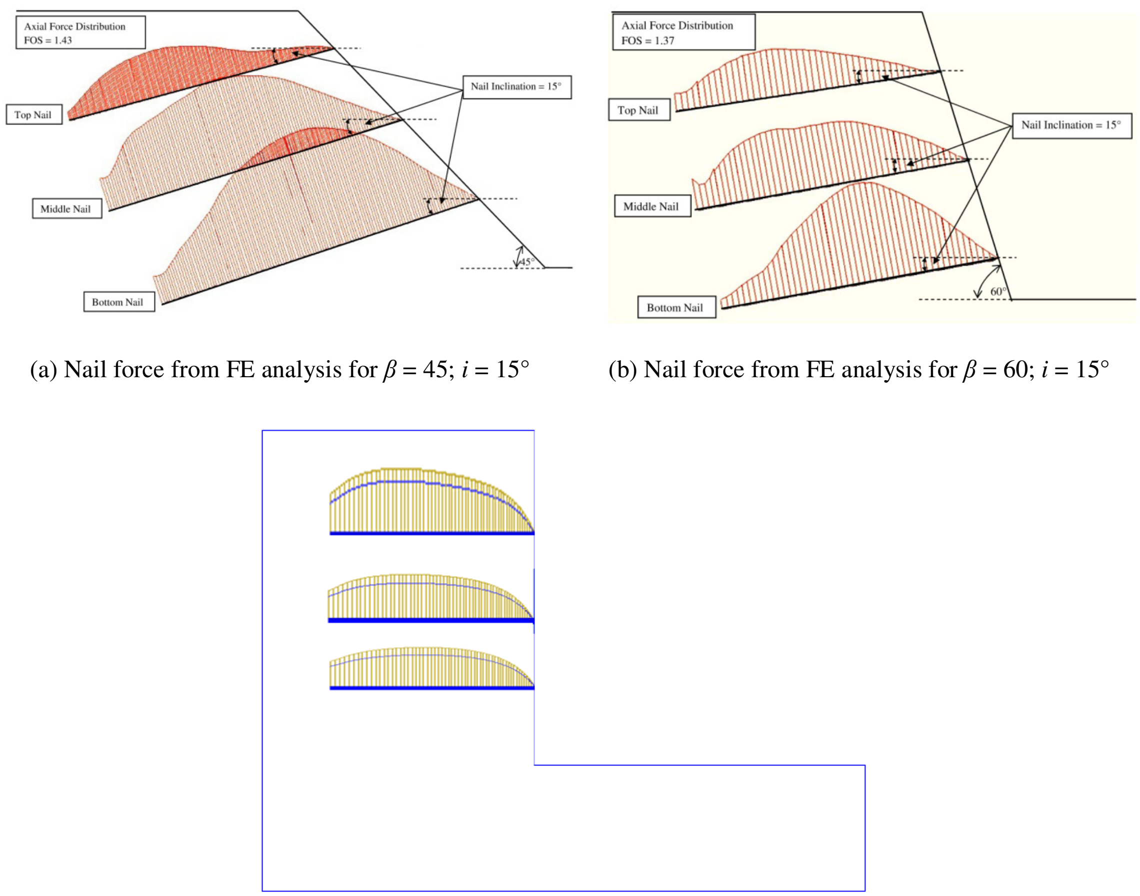

(a) Nail force from FE analysis for $\beta = 45$; $i = 15°$

(b) Nail force from FE analysis for $\beta = 60$; $i = 15°$

(c) Nail force from FE analysis for $\beta = 90$; $i = 0°$

Fig. 5.16: Nail force distribution for different slopes and nail inclinations from PLAXIS 2D

The nail forces for most stable slope of 45°, 60° and 90° from FE analysis are compared with nail forces as obtained from model testing. The maximum nail forces from FE analysis are observed for bottom row of nails for 45° and 60° slope angles and top row of nails for 90° slope angle [Fig. 5.16 (a), (b) and (c)]. In case of analysis carried out by FEM, the nail forces depend on displacement and strain developed in soil. The displacement induces shear forces which is taken up by soil – nail interface. The distribution of this induced shear force is controlled by interaction between soil and nail. Hence soil – nail friction leads to axial tension and axial compression in nails. The axial forces developed in nails are found to vary with nail inclinations. Both model testing and FE analysis method both predict the increase of nail forces with small nail inclination from 0° to 15°. The nail orientation i.e. angle between nail and normal to the shearing plane changes with change in nail inclination. As long as nail orientation is positive nails are acting in tension which increases the shear strength of soil. The transition of nail orientation from positive to negative due to change in nail inclination from small (0 - 15°) to steep (15° - 30°), alters the nail behaviour from tension to compression. This change reduces the reinforcing action of nails and soil strength decreases. Thus nail forces are found to increase from 0° to 15° and then decrease is observed between nail inclinations of 15° to 30°. These results are consistent with analysis carried out by Mittal and Biswas [242] which states "for soil nailed vertical cuts, FOS initially increases with the increase of nail inclination with horizontal (up to 15°) after which it decreases. Shiu and Chang [243] also found a similar variation in nail axial force which increased up to nail inclination of 20° and then found to become zero at inclination of 65°.

5.3 Results from Model Testing and Numerical Modeling for Screw nails

5.3.1 Results of Screw nail – Soil Interface Friction from Direct Shear Test

Direct shear tests (DST) results as observed from Fig. 5.17, it can be clearly seen that an increase in coefficient of friction and cohesion is observed as surface roughness increases between soil – soil interface due to the presence of a screw nail. Chu and Yin [123] states that "The shear failure envelope for the irregular surface of soil nails is mostly above the shear failure envelope for the regular surface of soil nails, and the slope of the failure envelope is increased as the soil–grout (i.e. grout and soil surrounding the grout) interface surface roughness increases. The peak interface friction angle can be higher than the soil friction angle for irregular surface nails." The surface roughness of screw nails can thus be accounted for producing a better sliding friction than conventional smooth surface nails.

The soil – nail interface is higher than soil friction angle because when screw nail is embedded in sand during direct shear test with nail condition, soil is displaced. This soil displacement and soil enclosed between threads of screw nail leads to further densification of soil around the screw nail which causes an increase in normal stress along nail length. This change in stresses around screw nail moves the failure surface away from the soil – nail interface. The weak planes are found to lie within the thin densified soil zone created around the screw nail. The shear failure of soil – nail interface is now governed by this interface between the newly dense soil zone. As the friction angle of soil has increased in this zone compared to the surrounding soil, higher soil – nail interface friction angle is observed. However, pullout test on screw nail can further enhance the understanding of the increase in interfacial friction and cohesion. The results of direct shear tests are summarized in Table 5.5.

Table 5.5: Shear parameters from Direct Shear Tests on soil – screw nail

Interface	**Angle of internal friction**	**Interface friction coefficient**	**Cohesion (c) (kN/m^2)**
Sand – sand	$\phi = 30.79°$	tan (ϕ°) = 0.596	10.41
Sand – screw nail	$\delta = 36.5°$	tan (δ°) = 0.740	11.48

The cohesion value obtained is attributed to moisture content added in sand to facilitate model slope preparation. This moisture content induces 'apparent cohesion' in between the soil particles which is reflected by obtaining a value of 'c' for sand. The difference between values of 'c' for sand – sand and sand – screw nail is also quite less because introduction of screw nail in sand only influences interface roughness and not the induced apparent cohesion. However, a slight increase in 'c' value between with and without nail condition can be accounted for soil densification due to displacement of soil when the nail is embedded in the soil sample.

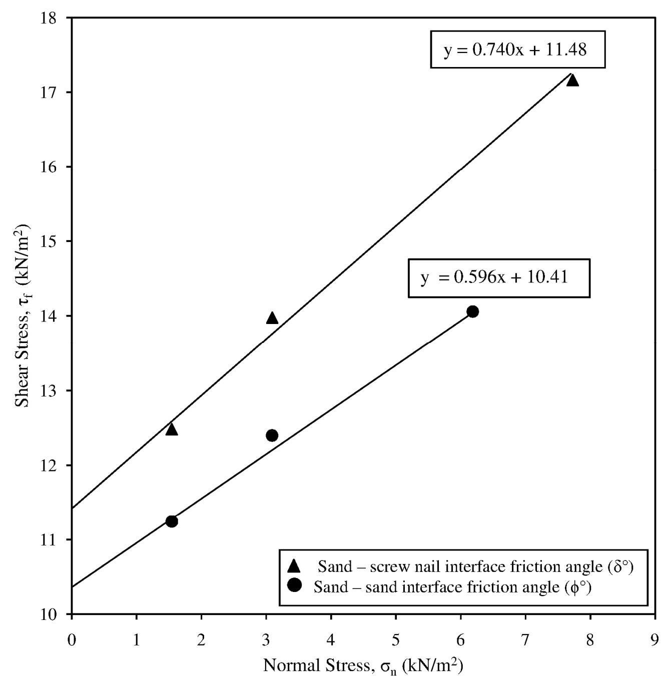

Fig. 5.17: Shear failure envelop from Direct Shear Tests

Using Eq. (3.3), the coefficient of friction from pullout for screw soil nail is calculated as f * = 0.766. It can be seen that 'f *' is slightly greater than 'f' for sand – screw nail interface, which is in agreement to the observation made by Kulhawy and Peterson [244] stated as "The interface friction angle δ' is less than the soil friction angle ϕ' for smooth interfaces, and the interface friction angle δ' is equal to or greater than the soil friction angle ϕ' for rough interfaces.

5.3.2 Results of Load – Settlement for Soil – nailed slopes with Screw nails

The model testing of soil – nailed slopes with screw nails reveals that for β = 45° and β = 60°, maximum load carrying capacity is found with screw nail inclination of 15°. The maximum failure load for 45° slope with i = 15° is found to be 48.1kN which is greater that for β = 60° with i = 15° recording maximum failure load as 41.3kN. The maximum load carrying capacity is found to vary with nail inclination. For i = 15° maximum load is observed followed by i = 0° (45.1kN), i = 20° (43.7kN) and minimum with i = 30° as 41kN. A similar variation with nail inclination is observed for β = 60°. Maximum load is attained for i = 15° with decreasing load capacity for i = 0°, i = 20° and i = 30°. However, for β = 90° is found to depict maximum load carrying capacity for i = 0° with a value of 30.2kN. The failure load is found to decrease with increase in nail inclinations from i = 15° to i = 30°. For variation in nail inclination of 15° from maximum load at 15° to minimum load at 30°, 45° slope and 60° slopes depicts a percentage decrease of 14.7% and 10.7%, respectively. For β = 90°, between optimum inclination of 0° to minimum load carrying capacity at 30° yields a percentage decrease of 39%. The variation in load carrying capacity of various slope angles with changing nail inclination is summed up in Table 5.6.

Table 5.6: Maximum load carrying capacity for slopes with screw nails from model testing

β°	***i*° = 0°**	***i*° = 15°**	***i*° = 20°**	***i*° = 30°**
	Load [kN]	**Load [kN]**	**Load [kN]**	**Load [kN]**
45°	45.1	48.1	43.7	41.0
60°	35.2	41.3	37.5	36.9
90°	30.2	25.7	21.8	18.4

The FE modeling of screw – nailed slopes depict that similar to model testing maximum load carrying capacity for 45° and 60° slopes are found for i = 15°. In case of vertical cuts, i = 0° is found to yield maximum failure load. The results of variation with nail inclination for maximum load carrying capacity of slopes is similar to as obtained from model testing. FE modeling predicts maximum load of 44.46kN for 45° slope and 37.35kN for 60° slope both at a nail inclination of 15°. For nail inclination of 0°, maximum load carrying capacity of 27.37kN is observed for β = 90°. The results from FE analysis are summarized in Table. 5.7. However, load magnitude from FE is found to at lower side as compared to model testing results. These results are in contrast to results obtained for smooth nails where model testing results were found to yield higher values as compared to FE modeling. The reason for lower prediction through FE analysis can be accounted to soil – nail interface interaction simulated in FE modeling. In actual model testing, installation of screw soil nails causes soil densification and alters in – situ soil shear strength parameters.

Table 5.7: Maximum load carrying capacity for slopes with screw nails from model testing

***β*°**	***i*° = 0°**	***i*° = 15°**	***i*° = 20°**	***i*° = 30°**
	Load [kN]	Load [kN]	Load [kN]	Load [kN]
45°	37.91	44.46	41.72	40.40
60°	35.05	37.35	34.67	34.17
90°	27.37	23.28	20.11	17.02

However, installation is not modeled during FE analysis and also threaded surface of screw nails is modeled using virtual thickness which develops a uniform rough surface around nail. The shortcoming in actual modeling of screw nail, models reduced surface roughness of screw nail and hence interface friction mobilized by FE analysis differs from actual interface friction acting during model testing. Since it can be a possibility that FE analysis has modeled screw equivalent surface roughness but fails to simulate actual threaded geometry of screw nail resulting in rough surface only in comparison to a smooth nail. Thus, modeling restriction is attributed for smaller load carrying prediction of respective slopes as compared to model testing results.

As shown in Fig. 5.18, maximum load carrying capacity of 45° slope with nail inclination of 15° is found to occur at a horizontal displacement of 121.8 mm. However, due to variation in actual modeling of boundary conditions and soil property variation with time as discussed for smooth nails, maximum load carrying capacity for 45° slope from FE analysis is found to occur at smaller slope displacement of 79.3 mm. Similarly, peak load carrying capacity for 60° is found to occur at 70.1 mm as compared to 90° where maximum load at failure is noted to be 65.8 mm. A similar variation between horizontal slope displacements is observed for 60° and 90° slopes (Fig. 5.19 and Fig. 5.20).

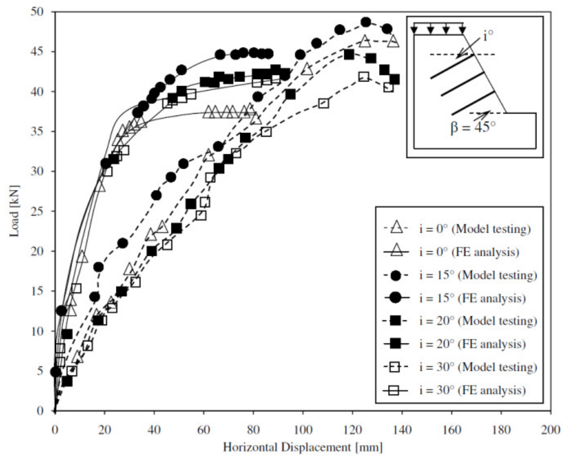

Fig. 5.18: Load – displacement of 45° with screw nails at different nail inclinations

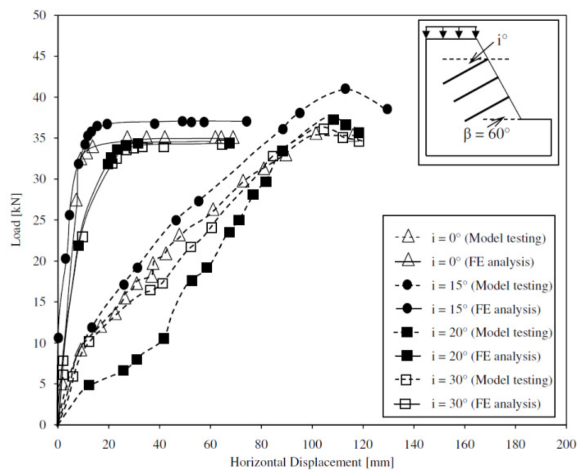

Fig. 5.19: Load – displacement of 60° with screw nails at different nail inclinations

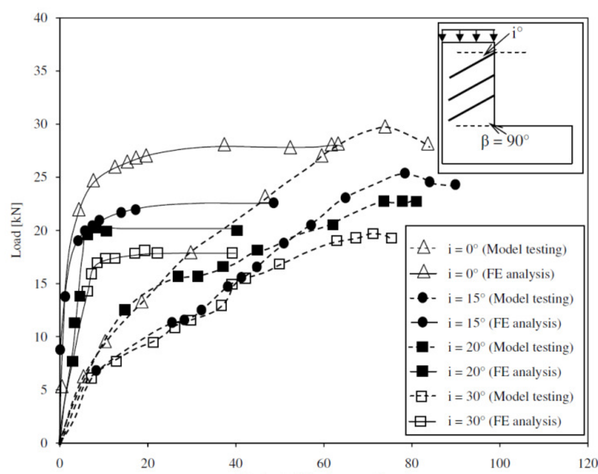

Fig. 5.20: Load – displacement of 90° with screw nails at different nail inclinations

5.3.3 Results of Failure Mechanism for Soil – Nailed Slopes with Screw nails

From Figs. 5.21(a), 5.21(b), 5.22 (a) and 5.22 (b), it can be observed that as the slope is subjected to surcharge loading, 45° and 60° reinforced slope undergoes deformation. This is evident from the settlement C_1, C_2 and C_3 and slope deformation D_1, D_2 and D_3 as marked in Fig. 5.21(b). Before the surcharge load is applied on the slope, the slope face is flush with the marked undeformed slope face. As the surcharge loading increases, the shear strength of soil is mobilized. As the mobilized shear strength reaches it limiting value, soil movement takes places which causes the deformation of slopes. Once the shear strength of reinforced soil exceeds it limiting value, a slip surface generates. The slip surface generates at slope face above the toe and propagates towards slope crest. For a 45° and 60° reinforced slope, potential slip surface starts at the slope face and terminates at slope crest. In addition to this slip surface, small local cracks are also observed during testing. These local cracks mark the other weaker zones of the slope. Fig. 5.21 (b) also suggests that surcharge also makes the slope settle along with longitudinal movement of slope. This can be visualized from final level reached by the tracer marking along the slope height. This soil movement is also important with the view that a soil nailing system is a strain compatibility problem. A certain amount of strain or soil movement is required in order to stimulate the reinforcing action of screw nails.

A similar deformation pattern is observed for reinforced soil slope model of 90°. The undeformed 90° vertical slope or cut is shown in Fig. 5.23 (a), which corresponds to the stage when no surcharge is applied to slope crest. With the increase in surcharge loading, the 90° slope with screw nails undergoes deformation marked by as C'_1, C'_2 and C'_3 along the slope height and D'_1, D'_2 and D'_3 along the slope length. The settlement of slope crest and the slope body can be observed by the change in tracer level from initial level. The slope face deformation in the horizontal direction can be investigated from the soil mass movement beyond the undeformed slope face marking as shown in Fig. 5.23 (b). The slip surface at failure is found to generate from slope crest but much near to slope face as compared to that in 45° and 60° reinforced slope. Moreover, large horizontal deformations are observed at the slope crest with respect to that at toe. During testing it is observed that as the load increases, the 90° screw nailed slope initially rotates about its toe and then moves outwards. Similar to 45° and 60° screw nailed slope, this slope also develops local cracks at other locations within the slope which signify soil failure of weaker zones. This movement of soil under loading leads to mobilization of interface shear force between screw nail and soil, which makes the nails participate in load transfer mechanism of soil – screw nail system.

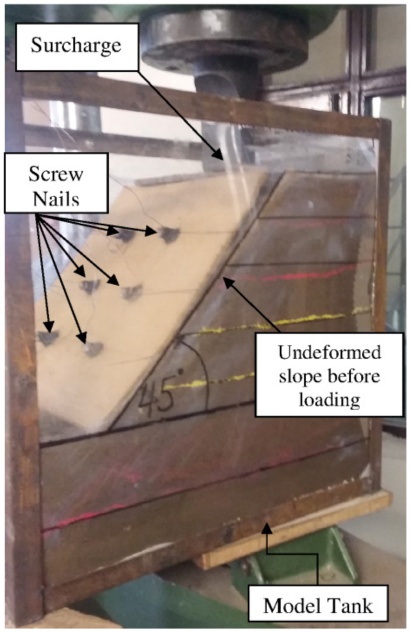

(a) Before testing

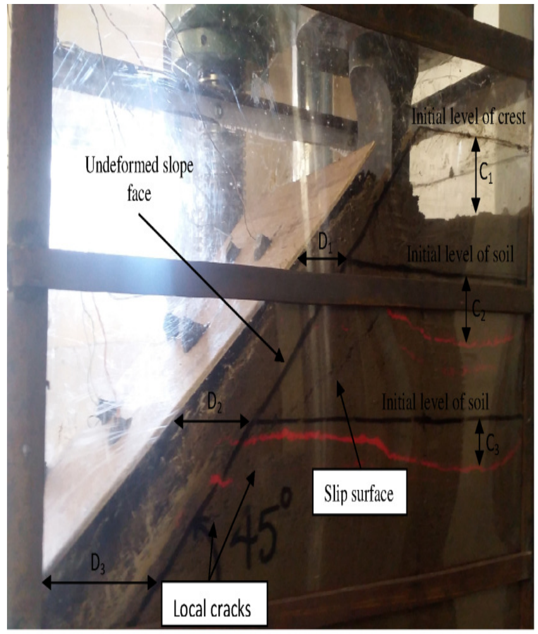

(b) After testing

Fig. 5.21: 45° screw nailed soil slope

(a) Before testing

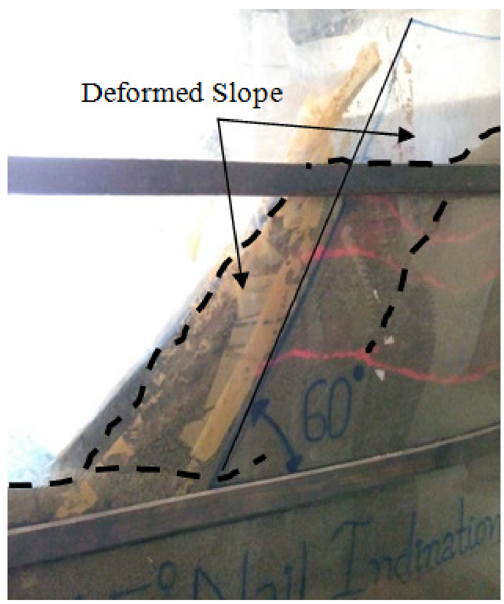

(b) After testing

Fig. 5.22: 60° screw nailed soil slope

The settlement of slope crest is due to soil compression under loading. The reinforced slope initially bears the load which causes densification of soil mass. As surcharge load increases, it is transferred to the nails along with soil overburden. As the crest starts to fail in bearing, cracks are generated at the crest. This initiates the failure surface. As the crack develops progressively, movement of slope occurs in horizontal direction along the slope length. This soil movement develops strains in reinforced soil slope. Due to these strains, the shear stresses are developed at soil – screw nail interface.

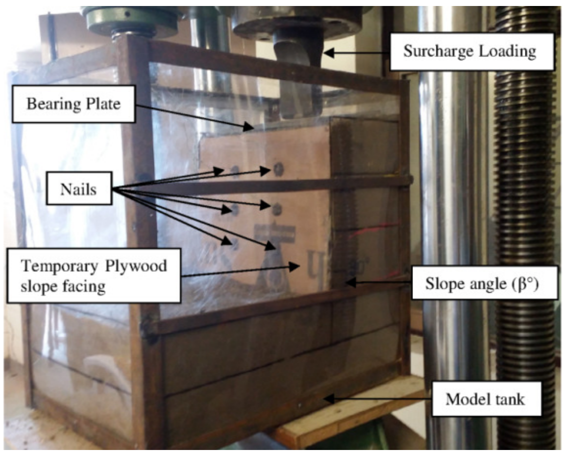

(a) Before testing

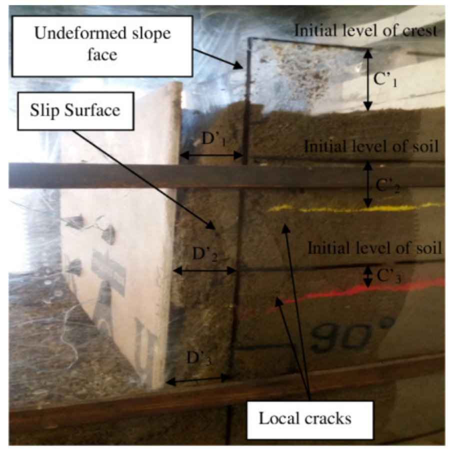

(b) After testing

Fig. 5.23: 90° screw nailed soil slope

Moreover, with increase in normal stress due to surcharge and overburden, additional stabilizing shear forces are also developed around screw nails. Since interface friction is greater than angle of internal friction of soil, the developed shear forces are also increased. This increase the bearing capacity of reinforced slopes and decreases the soil movement. Another reason for settlement of slope crest could be due to shearing of soil mass which causes an outward movement of slope.

As the loading of reinforced slopes is carried out, it is observed that 45°, 60° and 90° slopes have undergone volumetric deformation. In order to study this parameter, model boxes are marked with 5 cm grids to quantify the amount of soil that has collapsed due to slope failure. Due to similar failure observed for 45° and 60°, only one slope angle is investigated (β = 45°). From Fig. 5.24 (a), it is investigated that the amount of collapsed soil at crest and residual soil at slope face are not equal. The amount of soil collapsed is about 10000 cm^3, whereas the residual soil amounts to 4000 cm^3 only. This can be calculated by observing the number of grids corresponding to change in slope height (ΔH) and change in slope length (ΔL) through the grid pattern. This further signifies that under loading condition the reinforced slope has not only deformed from original state but has also undergone compression.

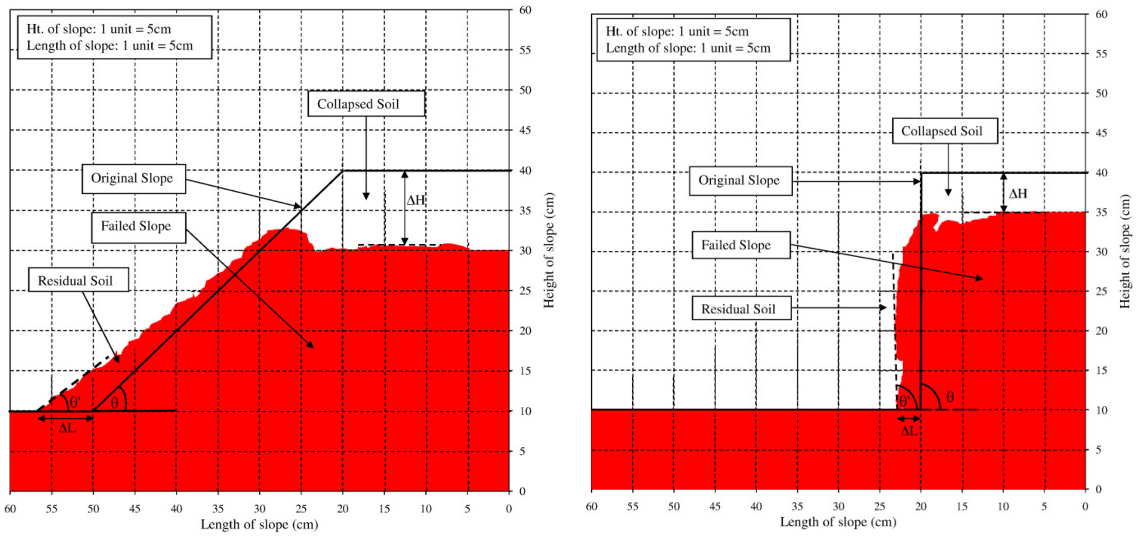

(a) 45° screw nailed soil slope

(b) 90° screw nailed soil slope

Fig. 5.24: Volumetric deformation of screw nailed soil slopes

From Fig. 5.24 (b), volumetric deformation for 90° slope can be estimated by a similar calculation using 5 cm grid pattern. The collapsed soil amounts to 4000 cm^3 in comparison to the amount of residual soil of 2500 cm^3. This unequal amount of collapsed and residual soil also signifies densification of slope soil under surcharge loading. The results of volumetric deformation as studied through grid method are summarized in Table 5.8. A dimensionless parameter, Volumetric deformation index (V_D) defined as the ratio of change in slope volume (ΔV) to original slope volume (V) has also been derived.

Table 5.8: Volumetric deformation of screw nailed slopes using 5 cm grid

Reinforced slope angle	**Original Volume (V) in cm^3**	**Width of slope (cm)**	**Area of collapsed soil (cm^2) using 5 cm grids**	**Volume change (ΔV) in cm^3**	**Volumetric deformation index ($V_D = \frac{\Delta V}{V}$)**
45°	90278.78	40	250	10000	0.110
90°	71345.45	40	100	4000	0.056

The volumetric deformation of reinforced slopes can be studied from percentage volumetric strains as obtained from Plaxis 2D analysis. Percentage volumetric strain is change in strains in x, y and z directions respectively. It also corresponds to change in reinforced slope volume to original slope volume under failure load. As shown in Figs. 5.25 (a) and 5.25 (b), volumetric strains for 45° slope is 9.12%, whereas 2.85% is observed for 90° screw nailed slope. From volumetric strain figures, it is evident that large volume changes occur in 45° slope as compared to 90° slopes. Moreover, this can be justified by the fact that 45° reinforced slope depicts a greater displacement of 79.3 mm in contrast to 90° reinforced slope where displacement of only 65.8 mm is observed. Figs. 5.25 (a) and 5.25 (b) further suggests that more volume changes occur at slope crest, screw nail ends and slope toe for 45° slope. However, for 90° screw nailed slope, the major volume changes are concentrated at the crest. This also can be a reason for greater displacements at slope crest than slope toe for 90° slope. From Fig. 5.25 (b), it can be seen that large volume change occurs between top and middle screw nails than middle and bottom screw nails. Moreover, a small volume change is observed below the bottom screw nail. The increase in displacement with wall height can be attributed to these variations in volumetric deformation.

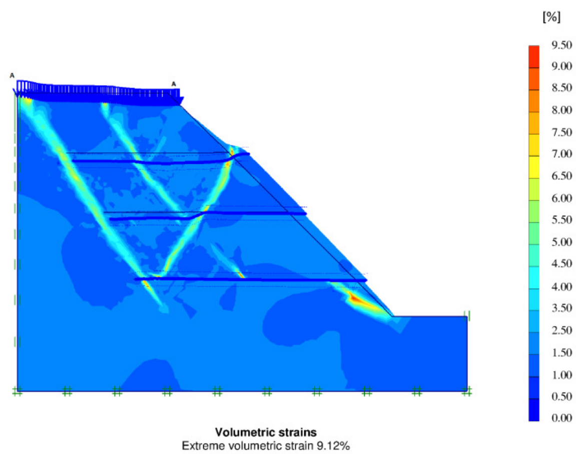

Fig. 5.25 (a): Volumetric strains developed in 45° screw nailed slope

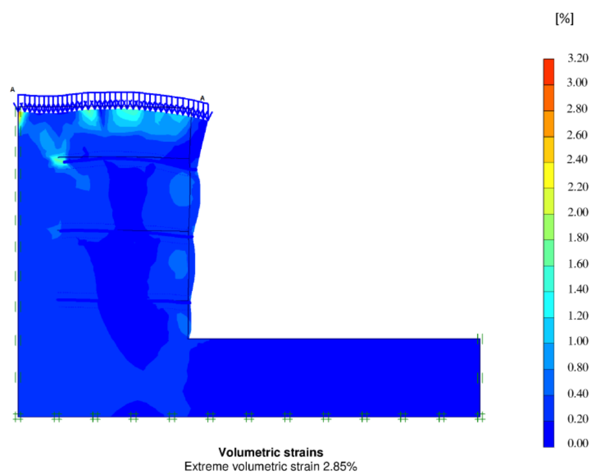

Fig. 5.25 (b): Volumetric strains developed in 45° screw nailed slope

The failure mechanism from FE analysis is evident that under surcharge load settlement of crest has taken place. This settlement of slope crest can be accounted for the fact that soil undergoes compression as surcharge is gradually increased. This effect of increasing surcharge is transferred to the top screw nail. In addition to the overburden, an additional surcharge is now being beared by the top nail. Simultaneously, the strain values are increasing due to increase in stress. This leads to the formation of plastic strain zones in reinforced slopes. If these plastic strain zones lie within the reinforced slope mass, the deformations are small and within limit. These deformation characteristics are a necessary for assessing the serviceability of screw nailed soil slope system. It can also be investigated from Fig. 5.26 (a) and 5.26 (b), that due to development of plastic strain, the slope geometry has changed at slope face.

The deformation of slope face together with displaced screw nails signify that both the axial stiffness and bending stiffness of screw nails have been mobilized. The bending of screw nail can be due to the overburden acting above each nail. The displacement of slope mobilizes the interface shearing between screw nail and soil. As more and more soil goes into plastic deformation, an increase in interface friction takes place. This increased shearing between soil and screw nails develops tensile forces in the nails. This developed tension in screw nails along with increased surface roughness regulates the slope movement to a minimum.

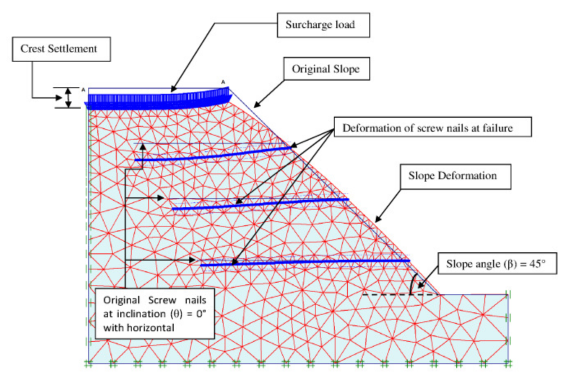

Fig. 5.26 (a): Deformation at failure load for 45° screw nailed slope

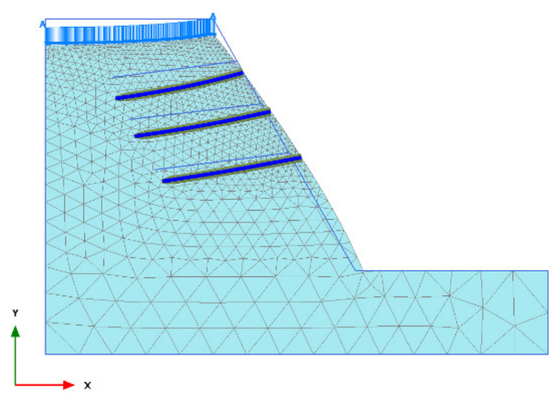

Fig. 5.26 (b): Deformation at failure load for 60° screw nailed slope

As the height of wall increases, the deformations increase towards the crest. Analogous to crest settlement in 45° reinforced slope, the crest of 90° screw nailed slope is also found to settle. This settlement can be attributed to soil compression under surcharge load. It can also be said from deformation pattern obtained for 90° that large plastic strain are developed at slope face near the crest [Fig. 5.26 (c)]. This also means that screw nails near the top of slope plays more part in slope stabilization of steep cuts as compared to bottom screw nails. This is evident from the dislocation of top and middle nails as observed from their initial level, which is greater than the displacement of bottom screw nail from its original position. Also negligible bending of nails can be observed for all three screw nail locations. This signifies that for 90° reinforced slope, axial stiffness of screw nails is mobilized than bending stiffness.

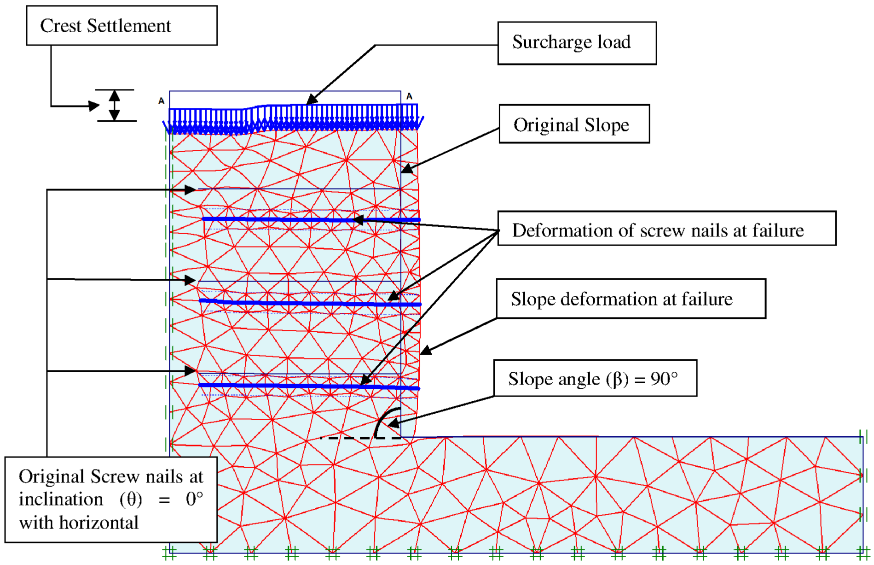

Fig. 5.26 (c): Deformation at failure load for 90° screw nailed slope

The factor of safety against stability for screw nailed slopes of 45°, 60° and 90° are analyzed by LEM and FEM and given in Table 5.9.

Table 5.9: Factor of safety for different slopes reinforced with smooth nails at different nail inclinations

***β*°**	***i*° = 0°**		***i*° = 15°**		***i*° = 20°**		***i*° = 30°**	
	LEM	**FEM**	**LEM**	**FEM**	**LEM**	**FEM**	**LEM**	**FEM**
45°	2.95	2.68	3.17	2.83	2.23	2.13	2.07	1.93
60°	2.94	2.23	3.02	2.60	2.18	1.89	1.90	1.68
90°	2.60	2.31	2.46	1.76	1.92	1.65	1.65	1.49

It can be observed that for slope angles of 45° and 60°, factor of safety greater than 2 is achieved both from LEM and FEM. The 45° screw nailed slope has a factor of safety of 3.17, while a factor of safety of 3.02 is obtained for 60° slope reinforced with screw nails at 15° with horizontal by LEM. For 90° slope with nail inclination of 0°, factor of safety of 2.60 is achieved by LEM. These values of FOS are found to be much higher than the recommended FOS = 1.4 against failure [118], FOS = 1.5 for overall stability [36], FOS = 1.3 for global stability with screw nails [26]. Similarly, FEM using SRM for 45°, 60° and 90°

screw nailed soil slopes for most optimum nail inclination predicts factor of safety > 2. The 45° screw nailed slope with i = 15° has FOS = 2.83, 60° screw nailed slope with i = 15° has FOS = 2.60 whereas for 90° screw nailed slope with i = 0°, FOS = 2.31 is obtained. A higher FOS is found for β = 45° than β = 60° and β = 90°, which is similar to FOS variation as obtained from SLOPE/W. However, FOS from SLOPE/W are found to be on higher side as compared to FOS obtained from PLAXIS 2D. The reason for this can be dependency of inter-slice weight and slice base force on assumed slip surface by SLOPE/W. Whereas FEM based PLAXIS 2D locates the potential slip surface in zones of excessive strains and calculates the FOS. This difference in slip surface determination and corresponding FOS can be accounted for higher FOS by SLOPE/W than PLAXIS 2D [Fig. 5.26 (d)].

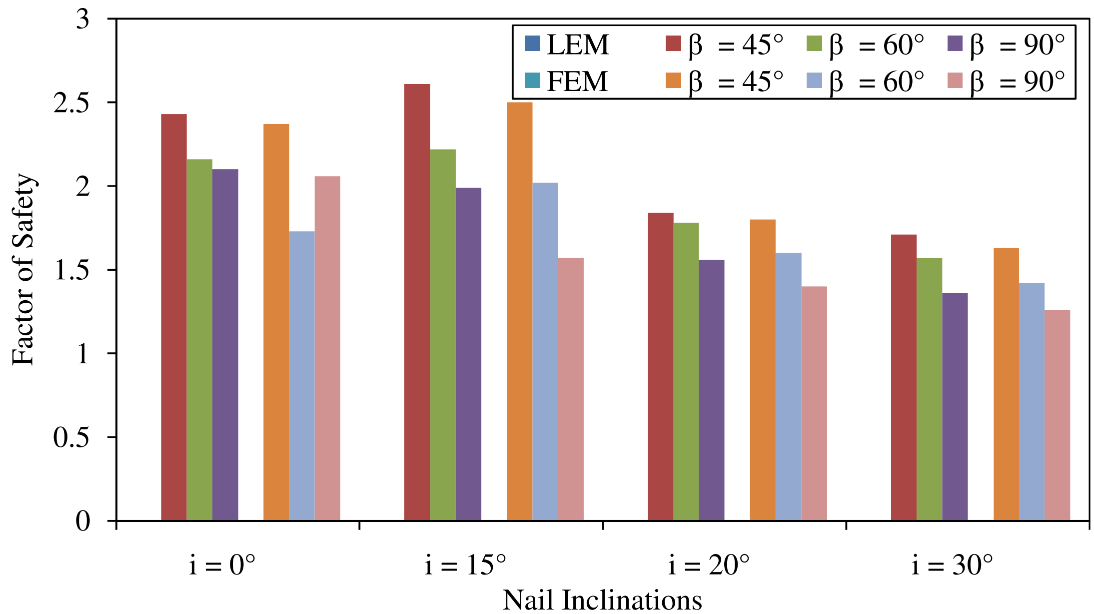

Fig. 5.26 (d): Factor of safety variation with nail inclinations from LE and FE analysis

As shown in Fig. 5.27 (a), the critical slip surface is found to pass through all screw nails. The contribution of screw nails for stability of reinforced soil mass is a function of its tensile strength and pullout resistance of screw nails beyond the failure surface. The length of screw nails behind slip surface represents the bond length or length of nail which provide the pullout resistance during slope failure. This constitutes the passive zone during slope failure. The active zone is the soil enclosed by shear failure surface. The stability of this zone leads to stability of slope. With the inclusion of screw nails in active zone, the normal force on the failure surface intersecting the screw nails is increased. This increase in normal force increases the overall resisting forces acting on failure surface. In addition to the mobilized cohesion along slip surface and soil weight normal component, an extra shear force due to horizontal component of pullout resistance is developed along slip surface. This additional resisting force induced due to screw nail introduction increases the stability of reinforced soil slope of 45°. The slip surface for 45° is found to pass through the toe of slope which is a mode of failure for global stability. The FOS of 2.95 > 1.3, suggests that screw nails in 45° soil slope provides global stability.

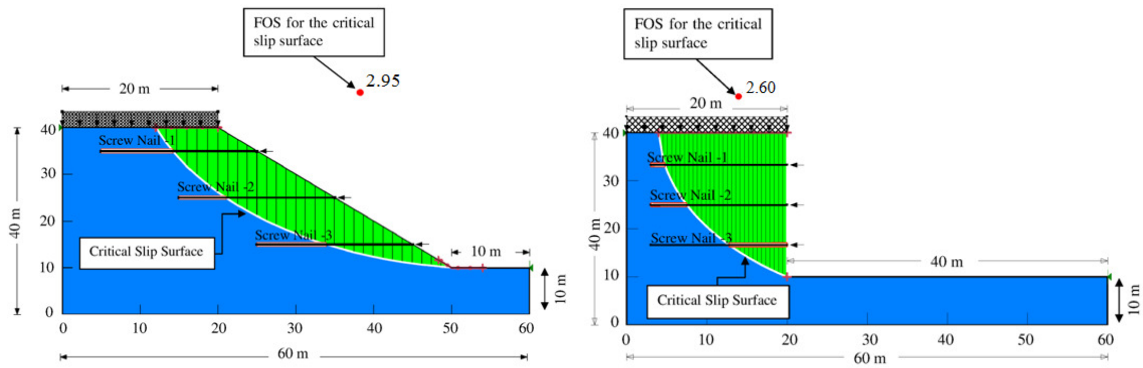

(a) 45° screw nailed slope (b) 90° screw nailed slope

Fig. 5.27: Factor of Safety corresponding to critical slip surface

The global stability for 90° is also achieved by using screw nails, since the FOS of 2.60 > 1.3 is obtained. Moreover, failure slip surface for 90° is also found to pass through the toe of slope. It can be seen from Fig. 5.27 (b), failure surface intersects all the nails as in screw nailed slope of 45°. However, for screw nail – 1 and screw nail – 2, the pullout resistance of nails governs the load transfer mechanism during failure. For screw nail – 3, the bond length required to mobilize the pullout of nails lies within the active zone of failure surface. This signifies that the load transfer mechanism is controlled by tensile strength of screw nails.

The slip surfaces as obtained from Plaxis 2D given in Figs. 5.28 (a) and 5.28 (b) clearly shows that at failure the plastic strains are developed within the reinforced slopes. The location of plastic stain points yields the potential slip surface and corresponding FOS values. As shown in Fig. 5.28 (a), 45° screw nailed slope has a slip surface intersecting nails at all locations. The slip surface can also be seen passing through the slope toe. The critical slip surface corresponding to maximum displacement clearly divides the soil mass into active and passive zones. The length of screw nails in active soil zone is sufficient enough to arrest the slip occurring between soil – soil interface. Due to rough surface of screw nails, the interface friction increases between soil and nail. This increased interface friction is mobilized as the soil mass fails under surcharge load. As the soil deformation increases, large strains are generated in the vicinity of screw nails, which enhance the reinforcing action of nails and hence the stability of reinforces slope. A similar slip surface is also obtained from Slope/W analysis.

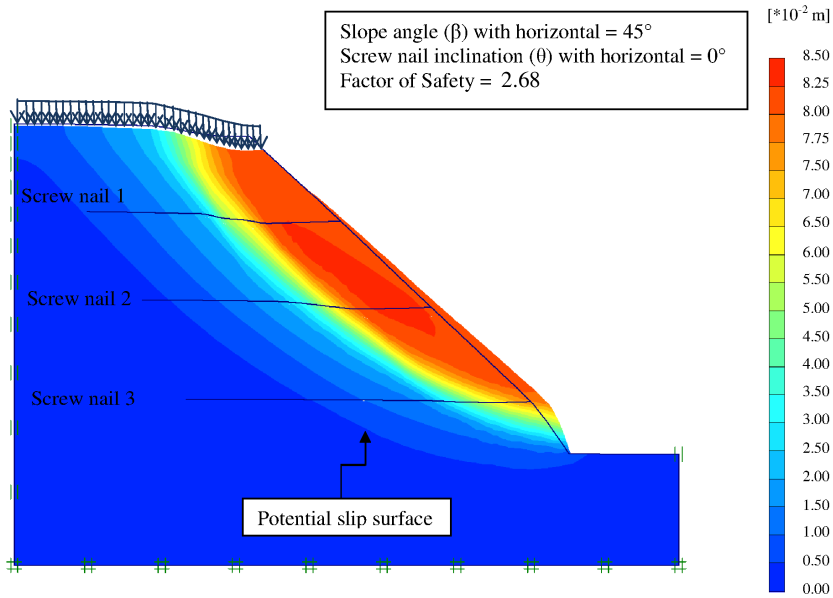

Fig. 5.28 (a): Failure slip surfaces for 45° screw nailed slope

As shown in Fig. 5.28 (b), the slip surface for 90° screw nailed slope is also found passing through the slope toe. The slip surface passes through the nail and thus utilizes its pullout resistance towards horizontal deformation. Fig. 5.28 (b) also suggests that the length of top and middle screw nail is completely utilized to mobilize the pullout resistance of screw nails. However, for bottom screw nail, a smaller length of nail is sufficient for providing the shear resistance against failure. The failure slip surface from Plaxis 2D is found in good agreement with Slope/W analysis.

As observed from Figs. 5.21 (b) and 5.23 (b), model testing of screw nailed soil slopes of 45° and 90° shows a slip surface originating from the crest and propagating towards the slope face terminating above the toe under the surcharge load. Such failure surface has also been reported by Schlosser [31] for soil nailed structures using limit equilibrium method. Gassler and Gudehus [4] has also identified bi – planar and circular slip surface in small model tests on slopes. Local cracking is also observed near the toe and around the slip surface. For 90° screw nailed slope, the slip surface is rather complex and highly irregular. The slip surface is closer to slope face which causes it to deform significantly.

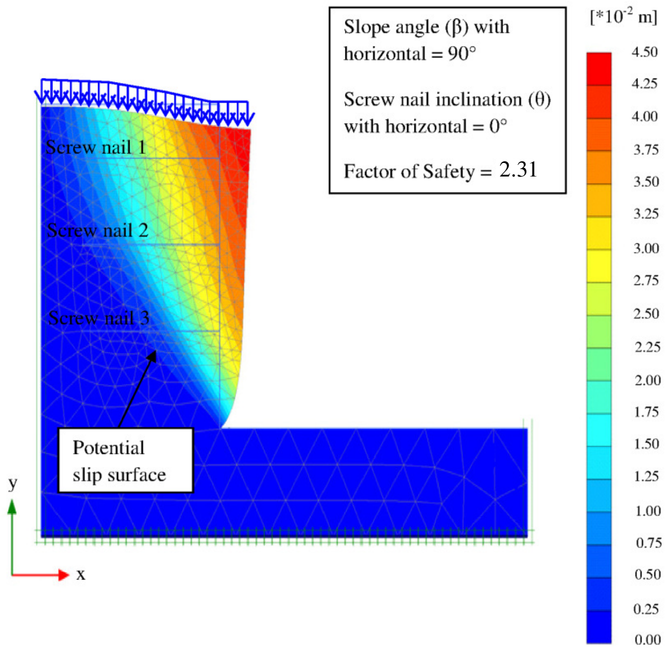

Fig: 5.28 (b): Failure slip surfaces for 45° screw nailed slope

The slip surface generated by Slope/W as shown in Fig. 5.27 (a) and 5.27 (b) depicts that for both 45° and 90°, the slip surface begins under surcharge load at slope crest and end at slope toe. The shape of slip surface can be treated as circular. However, Fig. 5.27 (b) depicts critical surface for reinforced slope of 90° with minimum factor of safety of safety of 2.60. The slip surface is very unlikely for slope of 90° as it has also been observed from model testing. The reason for this clearly brings out a limitation of limit equilibrium method in evaluating the stability of nailed slopes. The limit equilibrium method (SLOPE/W) does not incorporate the deformation of slope during failure. The critical slip surface is obtained by error and trial method such that a minimum factor of safety is obtained for which force and moment equilibrium are found to converge.

To overcome this limitation, critical slip surface and corresponding factor of safety are also validated by finite element method (PLAXIS 2D) which incorporates the load – deformation of slopes at failure. The slip surfaces obtained from Plaxis 2D [Figs. 5.28 (a) and 5.28 (b)] are similar to failure surfaces from Slope/W such that the rupture surface starts at slope crest and terminates at toe with variation in shape of slip surface. Plaxis 2D yields non – circular failure surfaces for both 45° and 90° screw nailed slope. Moreover, finite element analysis of 90° slope depicts that rupture surface passes through the toe and meets the crest at right angles. For this reason, it has been treated as a non – circular slip surface.

The origin of slip surface developing from slope crest is common for model testing and numerical modelling. However, numerical modelling of reinforced slopes suggests that failure envelop should terminate at toe of slope. On the contrary, model testing shows that failure surfaces terminate above slope toe for both slopes. This variation in slip surface location can be due to remoulding of soil around screw nails at the time of installation. The installation torque remoulds the in – situ soil and can alter its shear strength properties. Due to this variation in 'c' and 'ϕ' around screw nails with respect to rest of the soil slope brings about a change in failure surface shape. In case of numerical modelling, the installation torque is neglected both in Slope/W and Plaxis 2D, hence soil properties are homogeneous throughout the slope body. Thus, defined shear strength parameters of soil are mobilized only, which are different from shear parameters mobilized during testing. This accounts for variation in shape of failure surface obtained from model tests and numerical modelling.

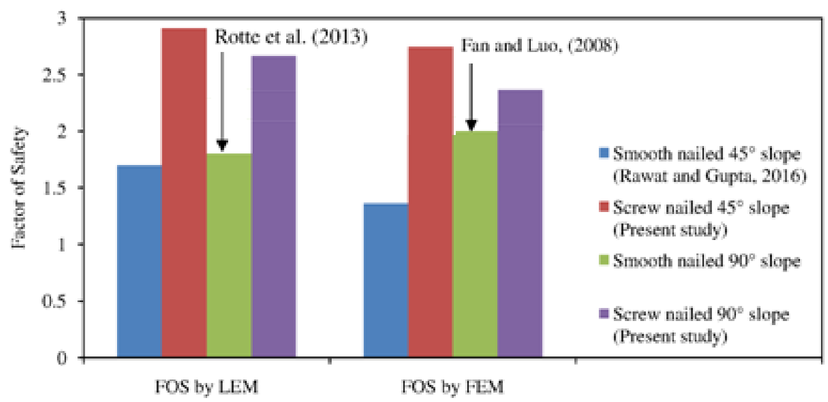

Fig. 5.28 (c): Comparison of FOS between screw-nailed slopes and smooth-nailed slopes

The factor of safety obtained from numerical analysis are compared with FOS against failure found from literature on same reinforced slope of 45° and 90° with smooth nails. As shown in Fig. 5.28 (c), it can be seen that screw nails gives a better slope stability than smooth nails for same slope angles. For numerical modelling of screw nailed slopes both by LEM and FEM, FOS > 2 is obtained, whereas FOS < 2 is reported for stability of slope using smooth nails. This increase in FOS for screw nailed slopes can be accounted for the increased interface friction provided by surface roughness of screw nails in comparison to smooth nails.

5.3.4 Results of Nail forces for Soil – Nailed slopes with Screw nails

As seen from Fig. 5.29 (a), it can be seen that movement of soil mass under surcharge loading induces strains in nails. The amount of soil movement restrained by nails corresponds to strain generations. The maximum nail force of 4.71kN is observed during model testing of 45° slope with i = 15° for nail 1. Moreover, nail 1 and nail 2 which constitute top row of nails depict mobilization of maximum nail forces. Similarly, with increase in depth on nails along slope height, it is found that nail forces are found to decrease. This signifies that top row of nails provide maximum reinforcement for soil – nailed slopes under surcharge loading.

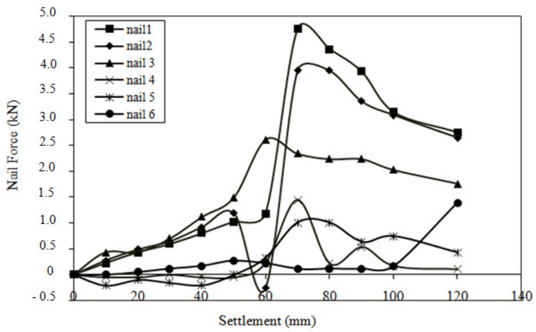

(a) Nail force for $\beta = 45$; $i = 15°$

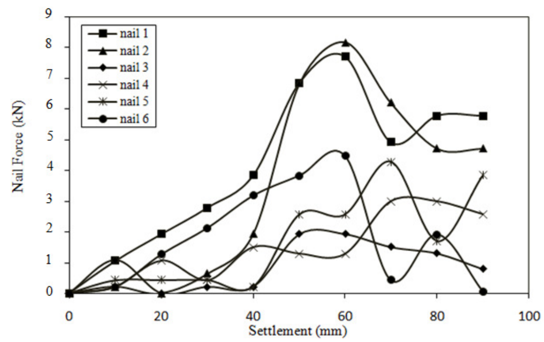

(b) Nail force for $\beta = 60$; $i = 15°$

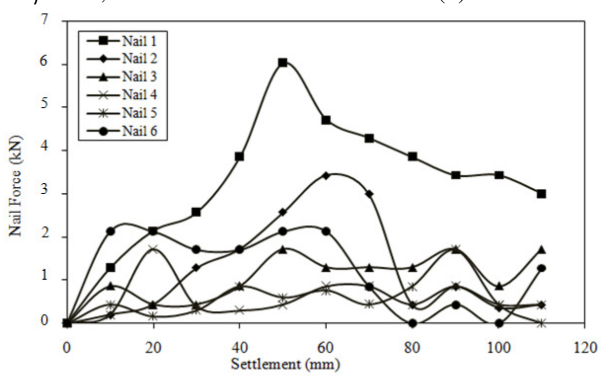

(c) Nail force for $\beta = 90$; $i = 0°$

Fig. 5.29: Nail force distribution for different slopes and nail inclinations from model testing with screw nails

It is also evident from Fig. 5.29 (b), that maximum resistance against deformation is governed by top row of nails in 60° slope with $i = 15°$. Nail 2 in top row depicts maximum nail force of 8.3kN closely followed by nail 1. Similarly, 90° slope with $i = 0°$ is also found to yield maximum nail force of 6.4kN in nail 1. Nail 2 in this case if observed to have higher nail force as compared to nail 3, 4, 5 and 6 but smaller than nail 1 [Fig. 5.29 (c)]. For all slope angles 45°, 60° and 90°, nail forces are found to increase to a peak value and then decrease as settlement of slope increases. A similar pattern of nail force increase with post peak decrease is also observed for smooth nails as well. The nail force pattern clearly indicates that increase in nail forces is associated with movement of soil mass over nail surface which consequently develops strains in nails. As more and more tensile force is mobilized in nails, interface friction increases and soil mass movement is restricted. Now, small or no soil movement occurs with increase in surcharge load, development of strains is reduced. This reduction in nail strains reflects decrease of nail forces.

The nail forces generated along nail length are depicted by FE analysis of screw – nailed soil slopes as shown in Figs. 5.30 (a), (b) and (c).

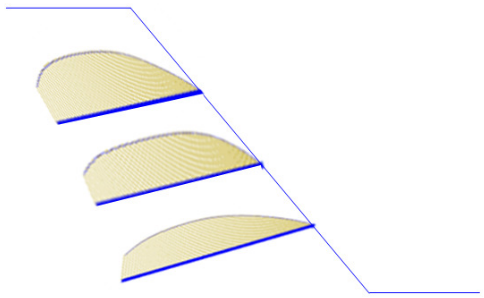

(a) Nail force from FE analysis for β = 45; i = 15°

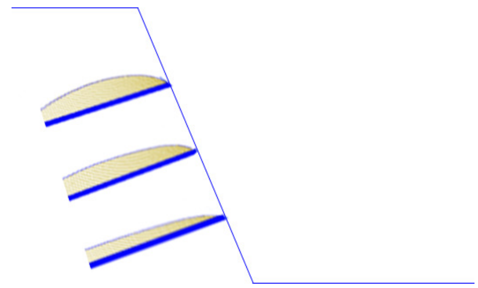

(b) Nail force from FE analysis for β = 60; i = 15°

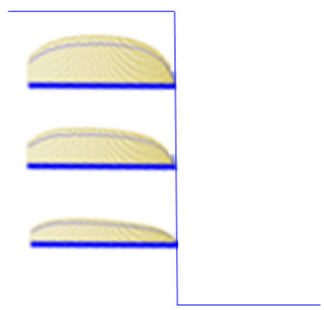

(c) Nail force from FE analysis for β = 90; i = 0°

Fig. 5.30: Nail force distribution for different slopes and nail inclinations from PLAXIS 2D

It can be seen that FE analysis depicts maximum nail force for top row of nails for all slopes of 45°, 60° and 90°. The top row of nails under surcharge load undergoes maximum strain due to high normal stress acting on nails. The increase in normal stress mobilizes large shearing strains and correspondingly high interface shear stress is generated at interface of top nail and soil. Thus, it can also be stated that in order to achieve stability of screw nailed – soil structures, top row of soil nails play a critical role. Moreover, top row of nails may or may not intersect failure surface and hence not only pullout but tensile strength of nails govern the nail force development. Due to the absence of installation procedure in numerical modelling of screw nails, in – situ shear strength is treated as same throughout the analysis. However, during model testing certain variation of shear strength parameters of soil can be expected to vary. Hence difference in magnitude of nail force from model testing and FE analysis is also recorded.

5.4 Results from Model Testing and Numerical Modeling for Helical nails

The model testing carried out using helical nails is dependent on pullout capacity of helical nails. The pullout study of helical nails is determined from numerical modeling both in 2D and 3D FE analysis. The pullout study is used to determine optimum configuration of helical plate diameter and number of helical plates required to develop helical nail. Hence results of pullout behavior of helical soil nails is covered initially with model testing results discussed later using fabricated helical soil nail.

5.4.1 Pullout behavior of helical soil nail Using 2D Finite Element Method

The results obtained from Plaxis 2D analysis for different types of helical nails namely 1-H, 2-H, and 3-H are compared with the existing literature. In the absence of direct results on helical soil nails, the comparison is done with helical soil anchors and helical piles to validate the results and trends. Fig. 5.31 shows the pullout force against displacement of nail head obtained from pullout model simulation in Plaxis 2D. From the FE plot, it can be observed that pullout resistance of helical nail increases with increase in nail head displacement from its original position. A similar pattern as shown in Fig. 5.32 for pullout with displacement is also observed from analytical and field investigation on multi helix screw anchors carried out by Lutneggar et al. [245] and FE analysis by Papadopoulou et al. [208] on helical micropiles.

The FE analysis of present study depicts the fact that pullout resistance of helical soil nail also increases with number of helical plates. It is well observed from Fig. 5.31, that as number of helical plates are increased from 1-H to 2-H and then to 3-H, a sufficient increase in helical nail pullout capacity is attained. As the helical plate is introduced along nail shaft, an increase in bearing area is achieved. The pullout resistance is governed by nail shaft – soil shearing and an increased surface area due to helical plate. As number of helical plates is increased from 1-H to 2-H, in addition to increased bearing area, soil between helical plates gets compacted. This inter helical soil densification increases the angle of internal resistance of soil. Moreover, inter helical soil now starts to behave like a compacted block of soil. The cylindrical shear failure mechanism is thus dependent on the soil block – soil shearing resistance which is greater than nail shaft – soil shearing; thereby a significant increase in pullout force is achieved. As number of helical plates are increased from 2-H to 3-H, soil densification is further increased. However, pullout is still governed by shearing between inter – helical soil block and surrounding soil i.e. cylindrical shear failure mechanism. Since only an additional shearing soil block is introduced in the mechanism, a smaller increase in pullout capacity of helical nail is observed from 2-H to 3-H as compared to 1-H to 2-H.

The increase in pullout capacity of 1-H helical screw nail with a shaft diameter of 19 mm and single helical plate of diameter 83.6 mm, 2-H helical screw nail with a shaft diameter of 19 mm and two helical plates of diameter 83.6 mm, respectively spaced at a distance of 250.8 mm apart and 3-H helical screw nail with a shaft diameter of 19 mm and three helical plates of diameter 83.6 mm, respectively spaced at a distance of 250.8 mm apart is shown in Fig. 5.33.

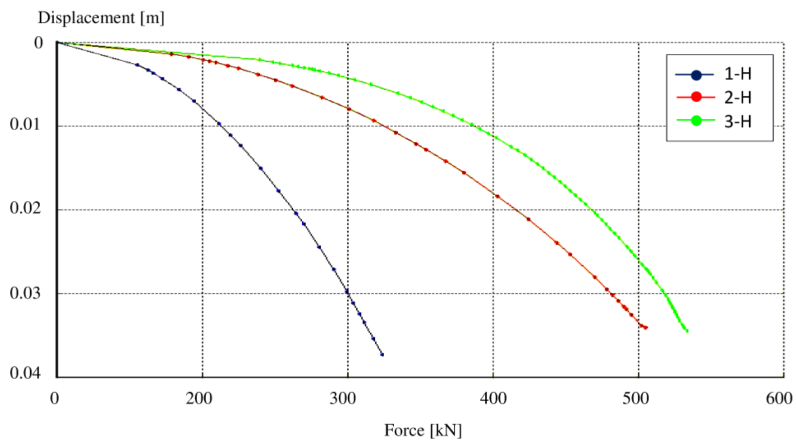

Fig. 5.31: Pullout Force with nail head displacement from Plaxis 2D

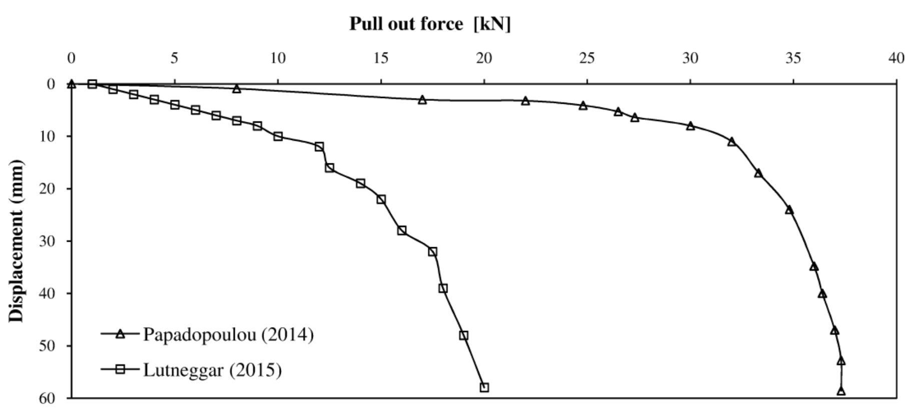

Fig. 5.32: Pullout force with displacement from literature review

It is found that pullout capacity is increased by 221.36 % with the introduction of a single helical plate. A percentage increase in pullout of 1016.20% and 1211.870% is obtained for soil nail with double helical (2-H) and multi helical (3-H) plates with diameters 4.4 times that of nail shaft (D_s) and spacing of 250.8 mm. Kurian and Shah [246] also concluded that the percentage increase in ultimate tension load is 207% between smooth slip and no-slip screw piles with 900 mm diameter helical plates. It was also observed from his studies that increasing the diameter of the screw piles by introduction of helix can increase the ultimate pile strength by a large margin of 1240%.

The increase in pullout of helical soil nail with nail head movement can be accounted for the fact that helical plates increases the bearing due to increase in overburden on helical plates. The increase in number of helical plates, increases inter helical soil densification. With this densification of soil, the angle of internal resistance of soil increases. To overcome this increased frictional resistance, a higher pullout force is required as more and more soil gets compacted with nail movement between the helical plates.

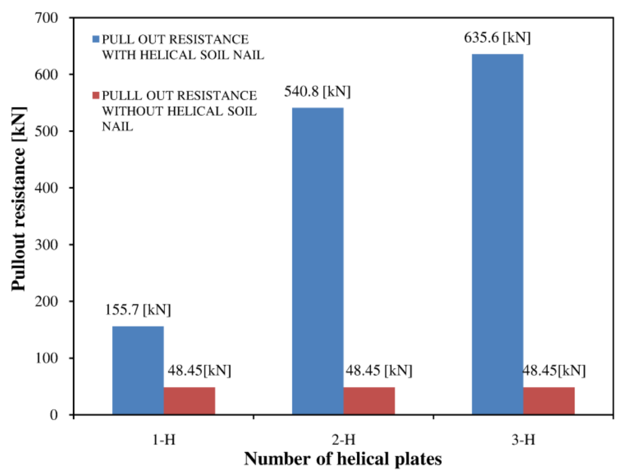

Fig. 5.33: Increase in the pullout capacity with different number of helical plates

As the nail head starts to move, pullout force varies linearly due to an elastic slip taking place between the interfaces under small displacements of 10 – 14% of nail head displacement at failure. A transition phase is achieved thereafter which causes a non - linear pullout force variation. A relatively smaller increase in pullout is observed with large displacements of nail head. The reason for this variation is the occurrence of plastic – slip between the soil and nail. Due to this permanent slip, the pullout force at failure is achieved at higher nail head displacements as shown in Fig. 5.34. Tokhi et al. [247] obtained the same shear force distribution with displacement curves from laboratory testing carried out on screws soil nail.

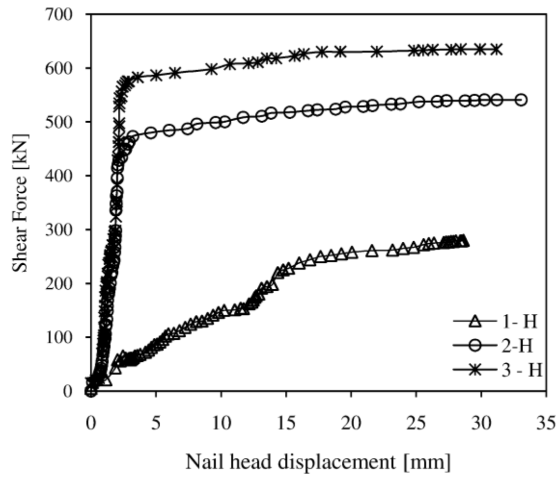

Fig. 5.34: Shear force variation with displacement of nail head

The failure mechanism of helical soil nails is found to vary with spacing of helical plates. The spacing of helical plates is determined by s/D_h ratio ranging from 1.0 to 3.5. As seen from Fig. 5.35 (a), for 1-H nails an individual plate failure mechanism is found due to deep local failure of helical nail. Figs. 5.35 (b) and 5.35 (c) shows that in 2-H nail condition failure mechanism change from deep global failure to deep local failure mechanism [210]. The Plaxis analysis demonstrates that for all $s/D_h < 3$, cylindrical soil failure is observed for helical nail. This is due to the fact that soil gets compacted and starts to behave like soil block between helical plates. In 3D, it can be imagined as a cylindrical soil mass. The failure is governed by soil – to – soil shearing resistance between this cylindrical soil and adjacent soil.

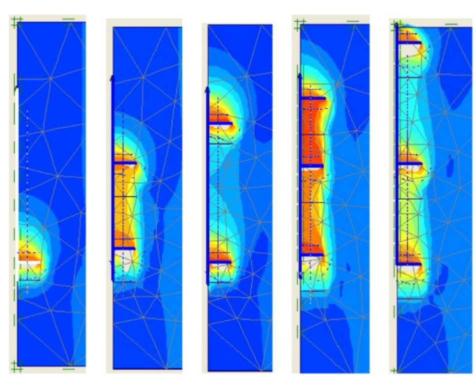

(a) (b) (c) (d) (e)

Fig. 5.35: Variation in failure mechanism with different spacing of helical plates (a) 1-H (b) 2-H at s/D_h = 1.5 (c) 2-H at s/D_h = 3.5 (d) 3-H at s/D_h = 1.5 (e) 3-H at s/D_h = 3.5

As soon as the s/D_h ratio is increased beyond 3, the failure undergoes a transition from cylindrical shearing failure to individual plate failure. In this case the bearing of each plate acts separately, without effecting inter - helical soil. In 3-H nail, the increase in number of helical plates from two to three reduces the embedment depth (*H*). This reduction in depth changes deep global failure to shallow failure as the failure is found to propagate to the ground surface. Thus it can also be stated that there also exists a critical depth (*H*) beyond which failure changes from deep to shallow. Moreover, this reduction in embedment depth with increase in helical plate spacing also leads to an individual plate failure as shown in Figs. 5.35 (d) and 5.35 (e). Merifield [203] observed similar failure patterns for different spacing of helical plates in soil anchors as shown in Fig. 5.36.

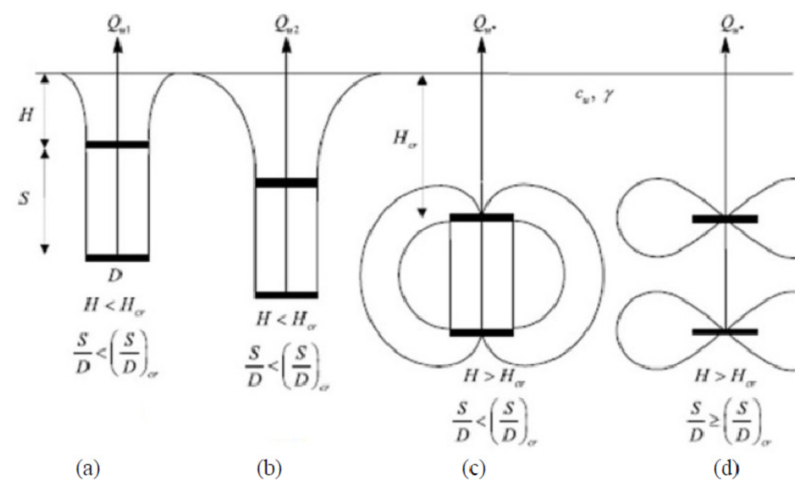

Fig. 5.36: Anchor behaviour (a), (b) Shallow failure mechanism (c) global deep failure mechanism (d) local deep failure mechanism from Merifield [203]

As seen from Table 5.10 and Table 5.11, pullout behaviour of helical nail changes with change in helical plate spacing. Such variation in uplift or tension capacity of helical piles and screw anchors has also been reported in the literature by Rao et al. [248], Merifield [202], Mittal and Mukherjee [249], Demir and Ok [210].

Table 5.10: Pullout force on 2-H nail with varying s/D_h

Nail with 2 helical plates (2 - H) and nail diameter D_s = 19 mm						
Diameter of helical plate D_h = 4.4 x D_s = 83.6 mm						
s/D_h	1.0	1.5	2.0	2.5	3.0	3.5
Pull out resistance [kN]	180.71	271.07	360.53	450.67	540.80	631.11

It is observed that pullout capacity increases with increase in spacing between the helical plates. At s/D_h < 3, helical nails have failure surface which do not reach the ground surface. This deep global failure is characterized by development of cylindrical shear failure mechanism. Individual plate failure is found to occur, if spacing is increased further such that s/D_h becomes greater than 3. The pullout capacity is found to increase by approximately 16% beyond $s/D_h > 3$, in contrast to $s/D_h < 3$ which bring about an increase of 19% in the pullout force for 2-H and 3-H nails.

Table 5.11: Pullout force on 3-H nail with varying s/D_h

Nail with 3 helical plates (3 - H) and nail diameter D_s = 19 mm						
Diameter of helical plate $D_h = 4.4 \times D_s$ = 83.6 mm						
s/D_h	1.0	1.5	2.0	2.5	3.0	3.5
Pull out resistance [kN]	212.39	318.59	423.73	529.67	635.60	741.74

The comparison of pullout capacities obtained from FE analysis by Luteneggar [245] as given in Fig. 5.37 suggests that the critical s/D_h ratio is 3. However, a linear increase in the pullout capacity is observed from literature as well as from the current study. A small increase in the pullout results beyond s/D_h critical is also reported by Lutneggar [206].

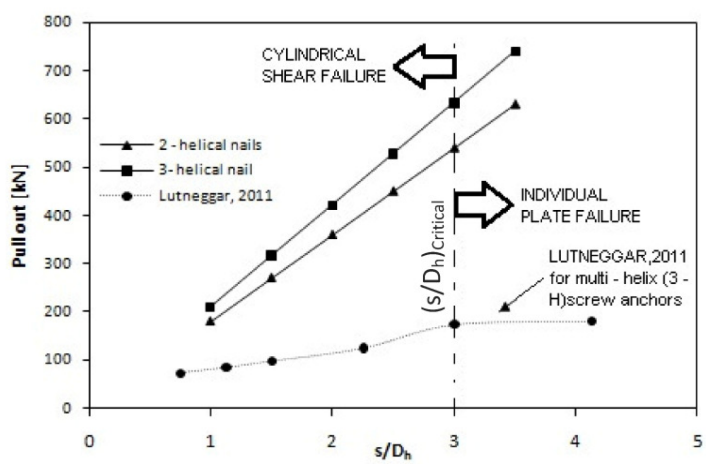

Fig. 5.37: Pullout force variation with different s/D_h ratio

With the increase in spacing between helical plates, inter-helical soil begins to experience shaft friction in addition to helical plate bearing. This development of shaft friction is attributed to movement of inter helical soil due to increased space. The soil between closely spaced helical plates does not undergo sufficient movement during pullout. Thus soil – soil interface provides the resistance against pullout along with helical plate bearing for all spacing less than the critical spacing. Beyond critical spacing, this soil- soil interface friction changes to interface frictional resistance between nail shaft – inter helical soil. This leads to an increase in pullout resistance with increased spacing.

To further enhance insight on this behaviour, researchers in the past has carried out studies in terms of a dimensionless parameter called breakout factor for helical piles and screw anchors. Mitsch and Clemence [195] and then Ghaly et al. [201], gave breakout factor charts as function of embedment depth ratio. Embedment depth ratio is defined as the ratio of depth of top anchor to the diameter of top helical plate. The results of the present study are found to be in good agreement with the results from literature as shown in Fig. 5.38. The breakout factor is calculated from the formulation given by Das [193] as:

$$Breakout\ Factor\ [F_q] = \frac{Q_p}{\gamma'.H.A} \tag{5.1}$$

From Eq. (5.1), it can be seen that breakout factor depends on embedment depth ratio up to a point which reflects the critical (*H/D*$_h$). It is observed in the present study that till *H/D*$_h$ > 3, a linear increase in the breakout factor is found. Beyond this critical embedment ratio, F_q is independent of embedment ratio. Sakr [207] states the critical embedment ratio from 4.4 to 7.8, whereas critical embedment ratio for the present analysis is 3. This under estimation of critical embedment ratio can be due to the failure of soil nail interface under 'immediate break away' condition. It can be seen from Figs. 5.35 (a) to 5.35 (e) that in each case the soil below the helical plate is found to break away from helical plate as shown by the white shading. This is due to the fact that vertical stress below the plates reduces to zero and the helical plates are no longer in contact with the soil [250].

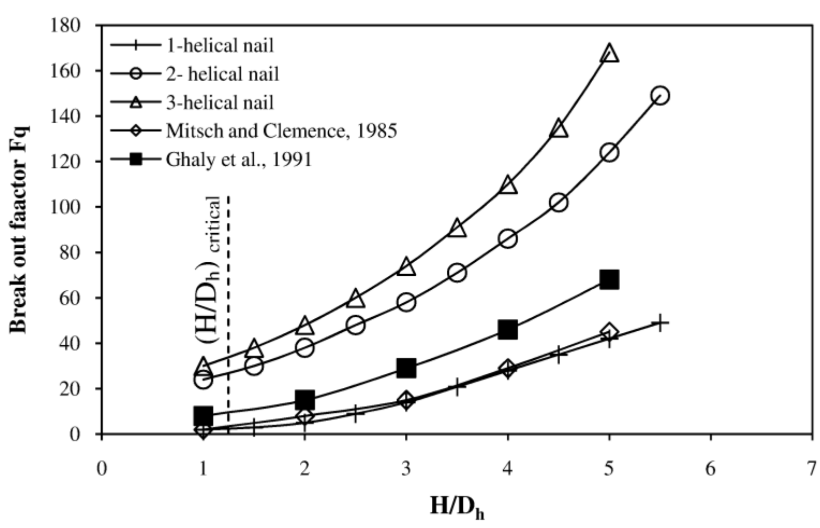

Fig. 5.38: Break out factor with different embedment ratio

From Fig. 5.38, it can be seen that breakout factors for 1-H, 2-H and 3-H are found to increase with embedment ratio. Similar trends of breakout factors are also observed by Mitsch and Clemence [195] and Ghaly et al. [205]. The breakout factors are found to increase linearly up to an embedment ratio called the critical embedment factor. Beyond the critical embedment ratio, the breakout factors follow a non- linear pattern. It is also observed from Fig. 5.38, that breakout factor increases with increase in number of helical plates. Higher breakout factors are found for 3-H nail followed by 2-H, with the lowest breakout factors are found for 1-H nail. The reason for this can be the transition of failure surface from shallow to deep global failure Merifield [203].

The increase in breakout factor with embedment ratio can also be accounted because bearing of top helical plate reduces as embedment ratio decreases. The overburden above top helical plate reduces which decreases the pullout capacity and consequently a lower breakout factor is found. This can also be stated in context of soil nails as soil ahead of helical plate near the nail head reduces due to smaller embedment depth rendering a smaller bearing and lower breakout factors.

The study conducted by Merifield [203] suggested that the ratio of shaft diameter to plate diameter < 0.5 do not have significant affect on pullout capacity of helical anchors. Under the light of this observation, ratio of nail shaft diameter to helical plate diameter selected for the present study is greater than 0.5 for all cases. It can be seen from Table 5.12, 5.13 and 5.14 that the pullout capacity of helical nail increases with increase in D_h/D_s ratios. This pattern of pullout increase is common for in 1-H, 2-H and 3-H nail configurations. Based on this observation, one can also suggest that as greater the number of helical plates, larger pullout capacities is observed with increasing shaft ratios.

Table 5.12: Pullout of 1-H nail with different D_h/D_s

Nail with 1 helical plates (1 - H) and nail diameter D_s = 19 mm				
D_h/D_s	1.4	2.4	3.4	4.4
Pull out resistance [kN]	50.05	85.60	120.69	155.70

The reason for this increase in pullout capacity with helical plate diameter is introduction of shaft friction that comes into play as the helical plate diameter is increased. The increase in plate diameter increases the bearing area of plates. At lower D_h/D_s ratios and smaller spacing between helical plates, the shaft diameter reduces the helical plate bearing area. Since the spacing between the plates is small, cylindrical shear failure mechanism is predominant. This reduces the affect of shaft friction as no soil movement can take place between helical plates. The nail derives its pullout resistance completely by soil – to –soil interface friction.

Table 5.13: Pullout of 2-H nail with different D_h/D_s

Nail with 2 helical plates (2 - H) and nail diameter D_s = 19 mm				
Helical plate spacing (s) = 3 x D_h				
Spacing (s), mm	79.8	136.8	193.8	250.8
D_h/D_s	1.4	2.4	3.4	4.4
Pull out resistance [kN]	173.87	297.32	419.22	540.80

Table 5.14: Pull out of 3-H nail with different D_h/D_s

Nail with 3 helical plates (3 - H) and nail diameter D_s = 19 mm				
Helical plate spacing (s) = 3 x D_h				
Spacing (s), mm	79.8	136.8	193.8	250.8
D_h/D_s	1.4	2.4	3.4	4.4
Pull out resistance [kN]	204.35	349.44	492.71	635.60

However, with the increase in spacing, the increase in helical plate diameter enables shaft friction to mobilize during failure. Since the failure transits from cylindrical shear failure to individual plate failure, the soil between plates is able to move and mobilize the shaft friction. Though a reduction in helical plate bearing area is observed, the overall pullout resistance is now being derived from the bearing of helical plates and the mobilized shaft friction. Thus, with increase in spacing and diameter of helical plates, pullout resistance is found to increase.

An attempt is also made to find the effect of using a tapered helical soil nail on pullout capacity. The top, middle and bottom helical plates are modelled with helical plate diameter of $2.4D_s$, $3.4D_s$ and $4.4D_s$ respectively. A similar study was also carried by Livneh and Naggar [204] on tapering tension piles. Figs. 5.39 (a) and 5.39 (b) depict a close match between the two studies. Livneh and Naggar [204] concluded that the uplift capacity of helical tension pile is not much affected by taper. However, the diameter of upper helical shaft governs the uplift capacity. It was inferred from his study that the bearing of the top helical plate and frictional resistance of inter - helical soil contributes to pile capacity. A similar pattern of failure mechanism can also be suggested for helical soil nail by FE package

Plaxis. However any other finding on tapered helical soil nails is beyond the scope of present work.

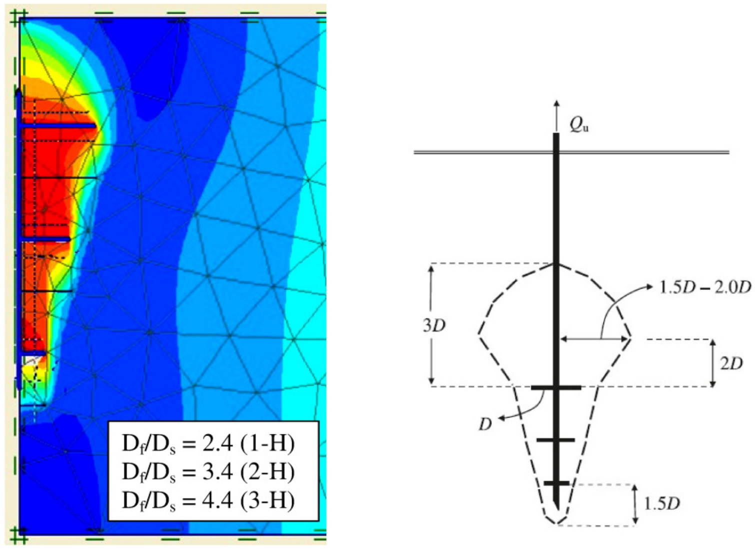

(a) (b)

Fig. 5.39: Failure mechanism (a) Helical soil nail from present study (b) Helical shaft piles from Livneh and Naggar [204]

The normalization of multi – H soil nail pullout capacity with respect to pullout capacity of nail without helical plates is done in term of a dimensionless factor known as efficiency factor (Q/Q_0). The effect of helical spacing variation shows that efficiency increases with increase in s/D_h ratio. Moreover, higher increase in efficiency is observed for helical nails with larger number of helical plates i.e. efficiency of 3-H is greater than 2-H. Fig. 5.40 (a), shows the variation in efficiency ranging from 15 for 3-H nail to 13 for 2-H nail.

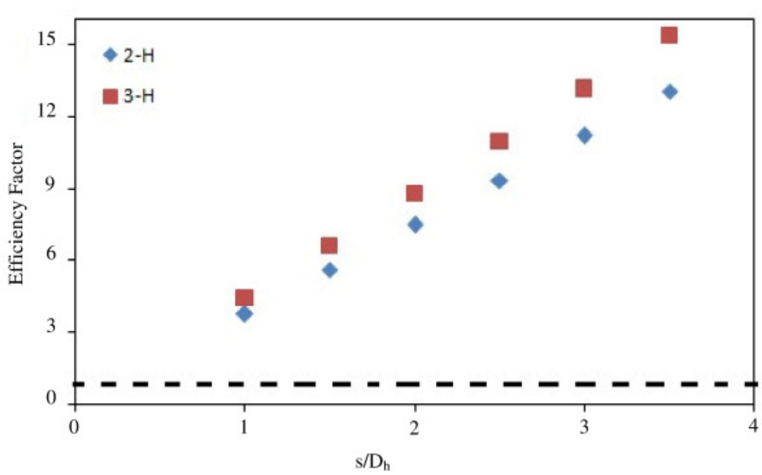

Fig. 5.40 (a): Efficiency factor as a function of s/D_h and D_h/D_s ratio

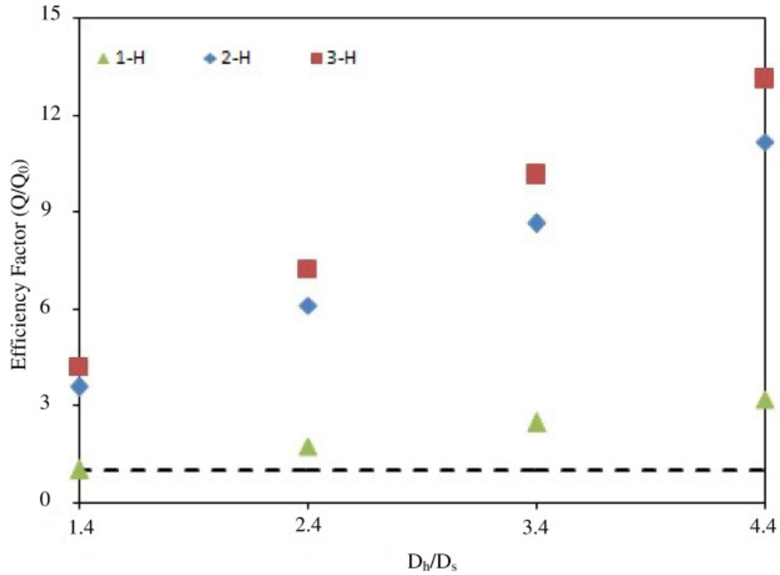

Fig. 5.40 (b): Efficiency factor as a function of s/D_h and D_h/D_s ratio

From Fig. 5.40 (b), it can be seen that efficiency of helical soil nail also increases with increase in D_h/D_s ratio. The efficiency factor of 13.12 is observed for 3-H followed by 11.16 for 2-H and a subsequently low value of 3.21 as efficiency factor for 1-H. The high values for Q/Q_0 signifies that increasing the number and diameter of helical plates has a significant effect in pullout behaviour of soil nail. Low value for single helical plate nail depicts that it has a pullout capacity that is as good as a nail with no helical plate. This low efficiency of single helical nail can be attributed to the fact that pullout capacity is derived largely by nail shaft in comparison to bearing offered by single helical plate. This signifies that bearing of helical nail is more prominent increasing pullout resistance as compared to interface friction between nail shaft and soil.

5.4.2 Pullout behavior of helical soil nail Using 3D Finite Element Method

A total of 67 simulations has been carried out to obtain the pullout load with nail displacement, stresses around the nail during pullout, developed rupture surface in soil and nail, variation in normalized pullout capacity with parametric variation by 3 – D FE analysis using Abaqus/Explicit for pullout capacity of a modified soil nail with circular disc along the shaft placed in sandy soil. The pullout load with displacement of soil nail for different circular disc diameter of 30 mm, 45 mm and 60 mm and different number of circular discs varying between N = 1 to 4 are shown in Figs. 5.41, 5.43 and 5.44. As it can be observed from Fig. 5.41, that peak pullout load is achieved for N4 nail with maximum load capacity of 20.34kN for nail displacement of 27.12 mm. The peak pullout load for N3 nail is 18.10kN and that for a N2 nail is 17.41kN for displacements of 25.40 mm and 24.96 mm, respectively. However, a maximum of 16.51kN pullout load is obtained for a N1 nail with 24.68 mm nail displacement. For N_0 nail (nail without disc) the pullout load reaches a value of 11.77kN with nail displacement of 21.88 mm. Similarly, from Fig. 5.43, it can be observed that pullout load of 19.99kN, 17.79kN, 16.80kN and 14.93kN is obtained for N4, N3, N2 and N1 nails. The corresponding nail displacements are 26.58 mm, 25.29 mm, 24.84 mm and 24.20 mm respectively. As the disc diameter decreases from 60 mm to 30 mm, a significant fall in pullout load is also observed. Nail N4 depicts a peak pullout load of 15.04kN with 25.12 mm displacement, nail N3 shows a displacement of 25.18 mm and peak load of 15.48kN. Pullout load of 14.17kN for N2 nail and 13.35kN pullout load for N1 nail can be observed from Fig. 5.44. Nail N2 and Nail N1 attains pullout load at nail displacement of 24.72 mm and 23.73 mm.

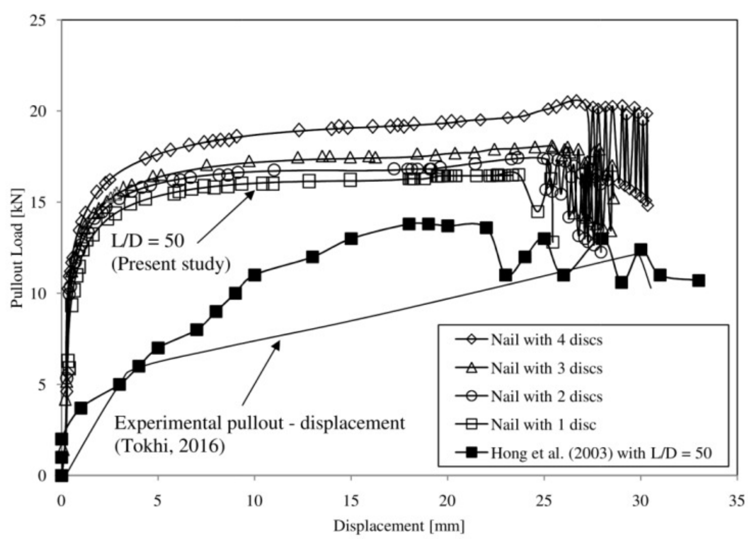

Fig. 5.41: Pullout load variation with nail displacement for $D_c/d_s = 4$

It is a common observation from Figs. 5.41, 5.43 and 5.44 that as the number of circular discs increases; it leads to an increase in pullout load. Also, as the diameter of circular disc increases, the pullout load is found to increase. The reason for this variation in pullout capacity can be given on the basis of Eq. (4.20). It can be seen from Eq. (4.20) that as the number of disc increases, contribution of circular discs in pullout resistance increases.

The physics of the increase in pullout resistance with increase in number of discs can be attributed to the densification of soil sandwiched between circular plates during pullout. As a nail with single circular disc moves out under pullout force, local soil influence around circular plate is found. With increase in the number of circular plates, the local soil influence is found to change and soil is influenced to a much greater depth from nail shaft. The soil sandwiched between two circular plates is compacted due to nail pullout and creates a cylindrical soil mass. This cylindrical soil mass behaves as a composite part of nail. The nail with circular discs now appears as a nail with an enlarged diameter equal to that of circular discs.

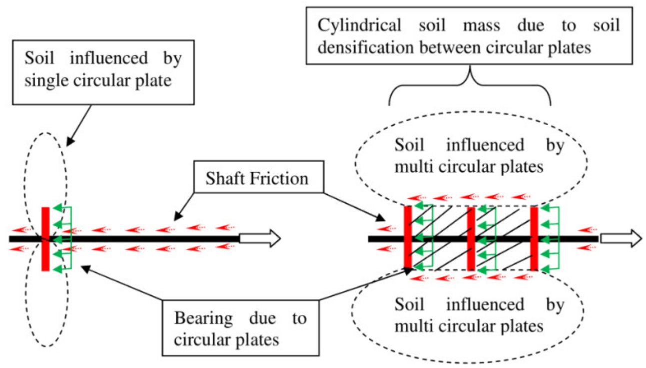

Fig. 5.42: Pullout resistance with increase in number of discs

This leads to a shift in failure interface from soil – nail for single disc nail to compacted soil – surrounding soil interface for multi circular discs. For nail with smaller number of discs shaft friction and plate bearing contributes to pullout resistance, whereas with increase in the number of circular discs, shaft friction effect diminishes and pullout is predominantly governed by bearing from the enlarged diameter due to dense cylindrical soil mass formed between circular discs as shown in Fig. 5.42.

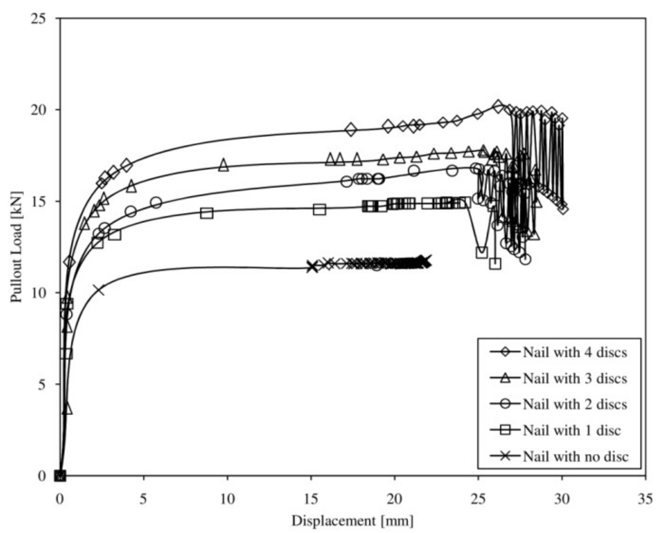

Fig. 5.43: Pullout load variation with nail displacement for $D_c/d_s = 3$

As a circular disc is introduced along the nail shaft, it displaces the soil adjacent to it. With increase in number of circular discs, more soil displacement takes place. This leads to densification of soil lying in a zone sandwiched between two circular discs. The degree of densification of displaced soil will depend upon the spacing of circular discs. Moreover, nail without circular disc (N_0) utilizes only its shaft friction to resist the pullout force, but with circular discs an additional bearing component acts along with shaft friction to restrain pullout from soil. Similarly, as the circular disc diameter is increased, the bearing area of disc increases. This increase in bearing area helps nail accommodate large quantity of soil in between circular discs. If the spacing between the discs is small, this compacted soil between two discs will act as a part of nail and move together as one composite unit. Due to this, the shear stresses which were mobilized at the nail shaft – soil interface are pushed deep into the soil. The shear stresses are now acting at the interface of this compacted soil between discs and surrounding weak soil. Also, with increase in disc diameter, the effective perimeter of nail increases which contributes significantly in increasing the pullout load.

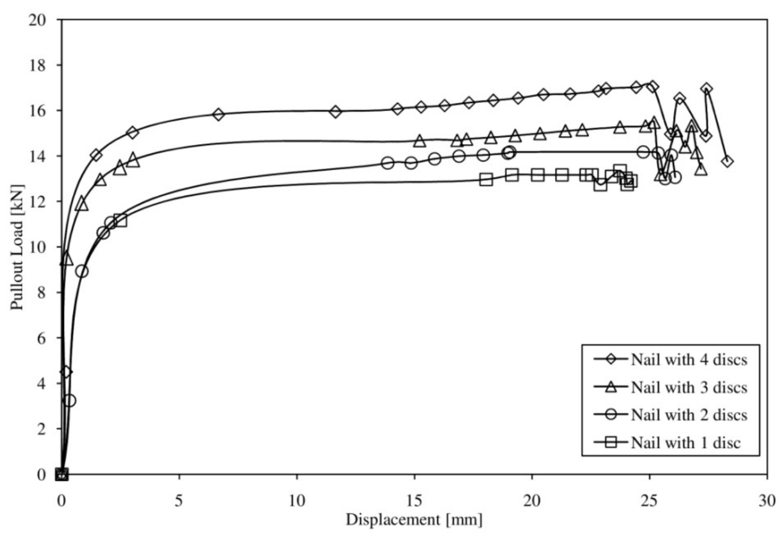

Fig. 5.44: Pullout load variation with nail displacement for $D_c/d_s = 2$

From Fig. 5.41, it can also be observed that as the peak pullout load is attained by soil nails, a sharp reduction in pullout capacity is found. As the nail displacement continues to increase a rise and fall in pullout load is observed for all nails with 4, 3, 2 and 1 disc, respectively. Hong et al. [130] concluded from his study on pullout of single and double soil nails that rough nails depict a profound unsmooth (zig - zag) phenomena load - displacement curve, whereas a smooth curve is obtained for smooth surface nails. A similar observation has also been reported by Raju [28]. As seen from Fig. 5.43, the zig - zag profile of load -

displacement curve changes to smooth as the number of disc along nail shaft decreases from 4 to 1. A relatively smoother load - displacement curve is obtained for nail without any disc. Another important observation can be made from Fig. 5.44 is that as the diameter of circular disc decreases and approaches shaft diameter, zig - zag pattern of load - displacement curve becomes more flat with small difference between the maximum and minimum pullout magnitudes. The load - displacement curve for nail N1 with $D_c/d_s = 2$ is comparable to the smooth curve obtained for N_0 nail in Fig. 5.43. Tokhi [214] reported a similar curve from laboratory pullout test on screw nails (Fig. 5.41), where helical plates of varying diameter for pullout testing in laboratory were used. However, Tokhi [214] simplified the FE analysis in terms of meshing problems and analysis time by using circular plates of varying diameter along shaft for simulation of screw nails in Abaqus. By far this is the only available material which can be closely related to the present soil nail with circular discs for validation.

However, the nail used by Tokhi [214] differs geometrically with the soil nail mounted with circular discs but for FE analysis, screw soil nail was taken as soil nail with ring plates, hence the comparison is carried out. Moreover, Tokhi [214] carried out a displacement control pullout test with maximum pullout load achieved at a displacement of 49 mm. Beyond this displacement a sudden drop in the pullout force is observed. It can thus be believed that if pullout was carried out to a larger displacement, then a zig – zag profile could have also been observed. Also, the finite element analysis was conducted by considering failure at a displacement of 20 mm and hence observed a plot which ended abruptly. In the absence of literature regarding soil nail with circular discs, comparison is carried out with nails that can be approximated with the present soil nail geometry. Moreover, Hong et al. [130] studied pullout load capacity with surface roughness for different *L/D* ratios. With insufficient literature available on this context for nail with circular discs, soil nail used in the present analysis is also treated as a rough nail and similar *L/D* ratio nail has been compared. The results of Hong et al. [130] are comparable because similar zig – zag pattern is observed to increase with increase in roughness of soil nail. An identical pattern is also observed for the present soil nail because as the number of discs increases, soil nail roughness can be believed to have increased. This can be observed by an increase in the zig – zag pattern from soil nail with 1 disc to 4 discs respectively.

However, it can be approximated that if further nail displacement would have been allowed, load - displacement curve for screw nails would have also depicted a similar unsmooth curve. The unsmooth (zig - zag) nature of these curves can be accounted for soil softening around the nail. As the nail is pulled out, soil softens under large strain. The soil around circular discs detaches itself from the soil mass and begins to move with nail disc. This softening of soil decreases the pullout load. As nail movement continues to progress under pullout load, the soil between two discs is also undergoing densification. This densified soil increases the disc bearing and hence the pullout load. Soil behind the last disc on nail shaft remains detached from the surrounding soil till the end of pullout test, hence all load - displacement curves are found to terminate at a low pullout load magnitude. The smooth curve for N_0 nail can be related to perfectly elastic - plastic behavior of soil. The reason for curves to smooth out with decrease in D_c/d_s can be explained by location of shear stresses around the nail.

A decrease in D_c leads to less soil displacement which moves the soil - nail interface closer to nail shaft from deep within soil mass. Correspondingly, shear stresses are mobilized at this lightly densified inter disc soil to nail shaft interface. As D_c/d_s approaches 2, soil nail pullout behavior is similar to that of smooth nail or a nail with larger diameter. During pullout, an increase in the volume of soil takes place around the soil nail. This soil dilation is restrained by normal stress around soil nail. As the inter disc soil is compacted, it imparts a higher overburden stress which increases the normal stress around soil nail. On the other hand, soil between small diameter discs densifies a relatively smaller soil mass and hence only small increase is normal stress is observed. The soil dilation is not significantly restrained by this normal stress and hence soil nail with smaller disc diameter can be pulled out of soil mass easily as compared to nails with large disc diameters.

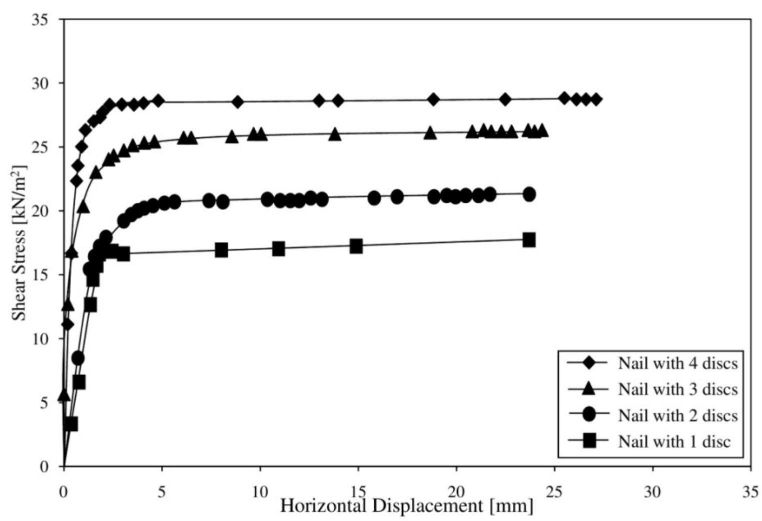

Fig. 5.45: Shear stress variation with horizontal displacement

It can be seen from Fig. 5.45, that as the number of discs increase, an increase in shear stress is observed. The increase in shear stress can be accounted for the fact that with increase in number of discs, a relatively larger soil comes into interaction with the nail. The failure occurs at a new interface corresponding to diameter of the disc mounted on nail shaft. The increase in number of discs leads to higher densification of soil mass around it, thereby increasing the interface friction between compacted soil within discs and weaker surrounding soil. However, the maximum shear stress for different number of discs occurs at a relatively smaller displacement as compared to the corresponding pullout load. This signifies that within a small displacement of nail the bearing due to discs begins to contribute in pullout resistance which leads to compaction of soil. As the pullout of nail continues, shear stress remains almost constant due to continuous yielding and re - compaction of soil which effectively shows no further increase or decrease in shear stress.

During the pullout of nail, shear stresses are induced in the soil. The shear stress mobilization governs the pullout capacity of nail. The stress contours obtained from FE analysis are given in Figs. 5.46 to 5.50. It can be seen from Fig. 5.46 that stresses are generated all along the nail shaft with high concentration of stress being near the nail end. The stress contours for N_0 nail signifies that shear stresses are mobilized at some distance away from the soil – nail interface.

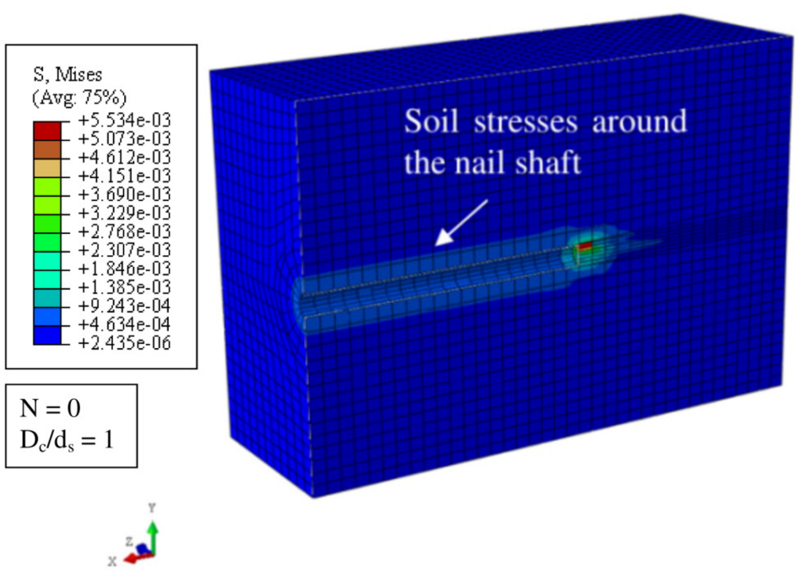

Fig. 5.46: Stress contours for nail without circular discs (N = 0)

However, from Fig. 5.47 (a), 5.47 (b) and 5.47 (c), it can be depicted that development of stresses around a N2 nail depends upon the spacing between circular discs. As the spacing is increased from $3D_c$ to $4D_c$, stress contours travel all the way along the shaft and stress the soil near the nail head. This signifies the fact that there exists critical spacing between circular discs after which stresses are transferred up to the nail head or slope face in case of field pullout of nails. This behaviour of soil nails can be compared to vertical pullout of multi plate soil anchors which are classified as shallow anchors and deep anchors based on the slip failure surface [28].

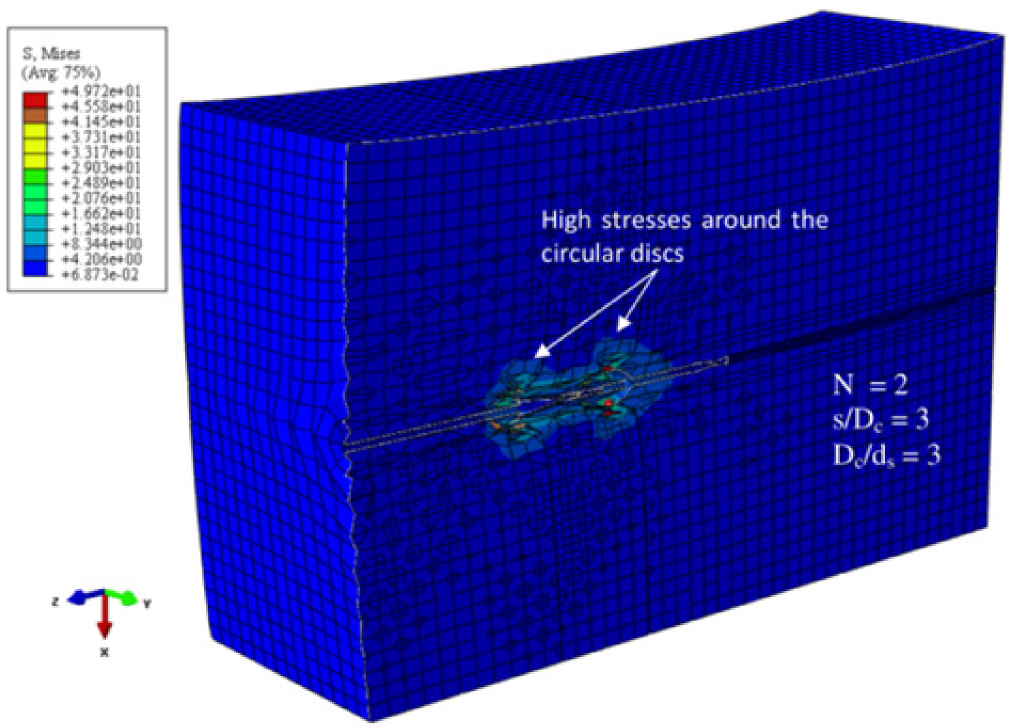

Fig. 5.47 (a): Stress contours for N2 nail with spacing of circular discs = $3D_c$

For deep anchors the failure surface is local around the anchor plates whereas if the failure surface propagates to the ground surface, the anchors are termed as shallow anchors. A similar local and global failure surface is also obtained for soil nails under pullout and hence can be categorized as deep soil nails ($s/D_c \leq 3$) and shallow soil nails ($s/D_c > 3$). From Fig. 5.47 (c), it can be seen that as N2 nail is pulled out, the soil behind the circular discs is highly stressed. The reason for generation of these high stresses can be due to active earth pressure condition that develops behind each disc. As the nail moves under pullout force, the soil in front of the discs is in a passive state of earth pressure, with active earth pressure acting from behind the discs. It can also be seen from Fig. 5.47 (c) that soil between circular discs gets densified and moves under pullout force as a part of nail.

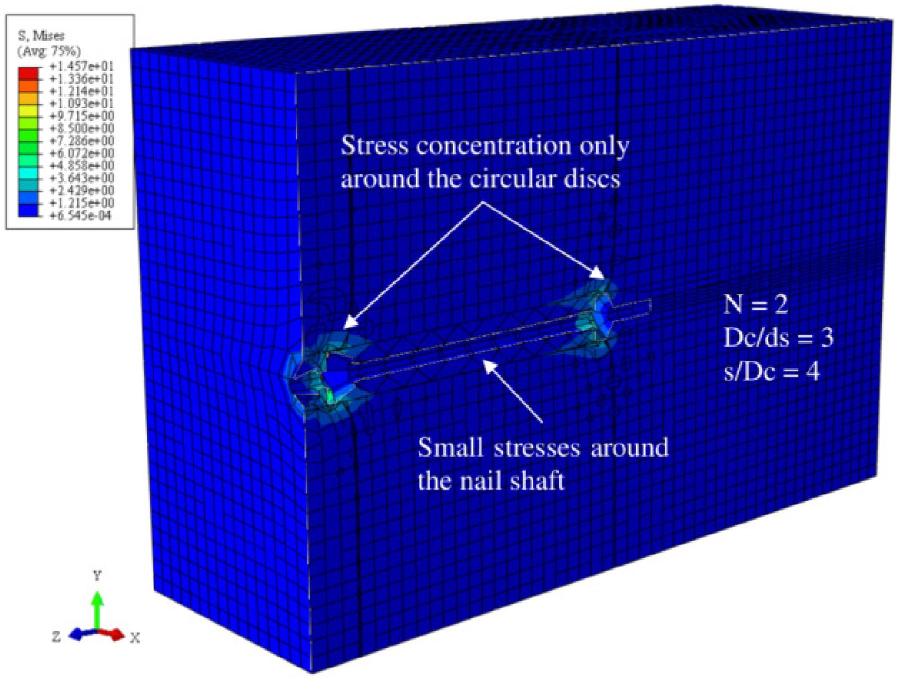

Fig. 5.47 (b): Stress contours for N2 nail with spacing of circular discs = $4D_c$

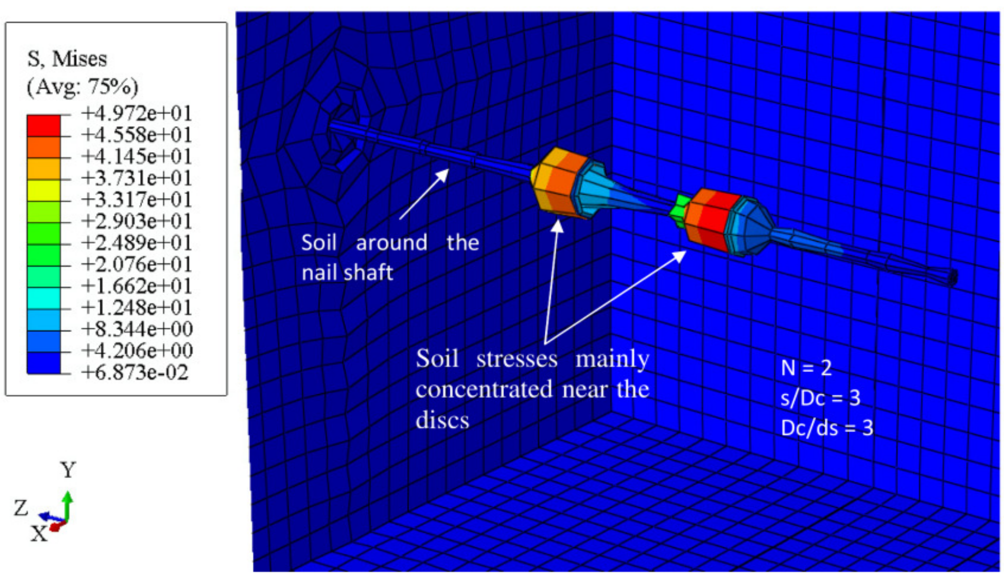

Fig. 5.47 (c): 3D stress contours for N2 nail with spacing of circular discs = $3D_c$

A similar stress contours are observed for N3 nail with s/D_c = 3 and s/D_c = 4. The soil between three discs is highly stressed with stresses propagating radially towards the nail end. The complete pullout model for N3 nail is shown in Fig. 5.48 (a). As observed from cross – section A – A, when the spacing between discs is small, the stress zone is confined around the circular discs. It is obvious to state that failure during pullout occurs at these stressed zones [Fig. 5.48 (b)]. On the other hand, for large spacing between discs, the stress zone extends up to the nail head, thereby a global failure mode can be expected for such soil nails [Fig. 5.48 (c)]. From Fig. 5.48 (d), it can be seen through cross – section B – B that soil gets compacted between the discs and form a cylindrical mass of soil which is highly stressed. During pullout the interface friction is mobilized at this interface of cylindrical soil mass and surrounding soil rather than nail shaft – soil interface.

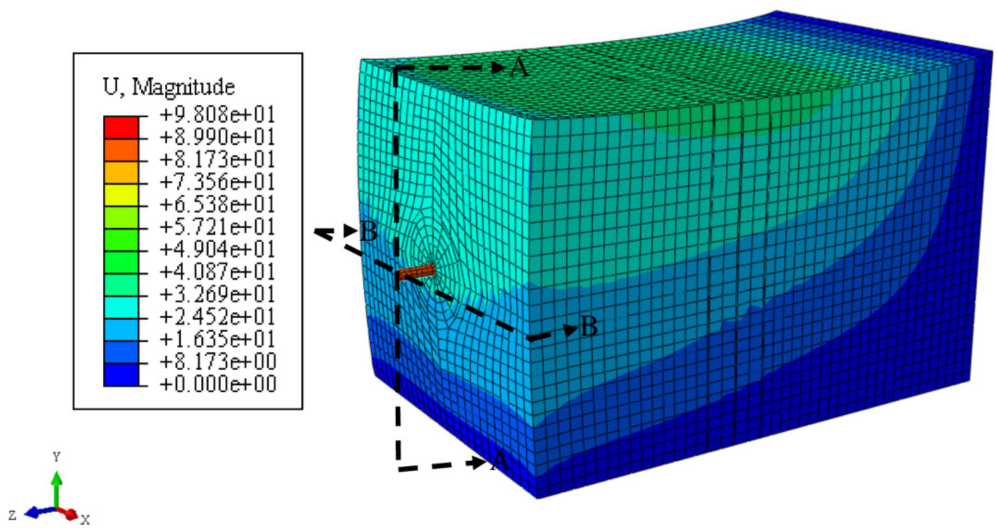

Fig. 5.48 (a): Complete pullout model for N3 nail

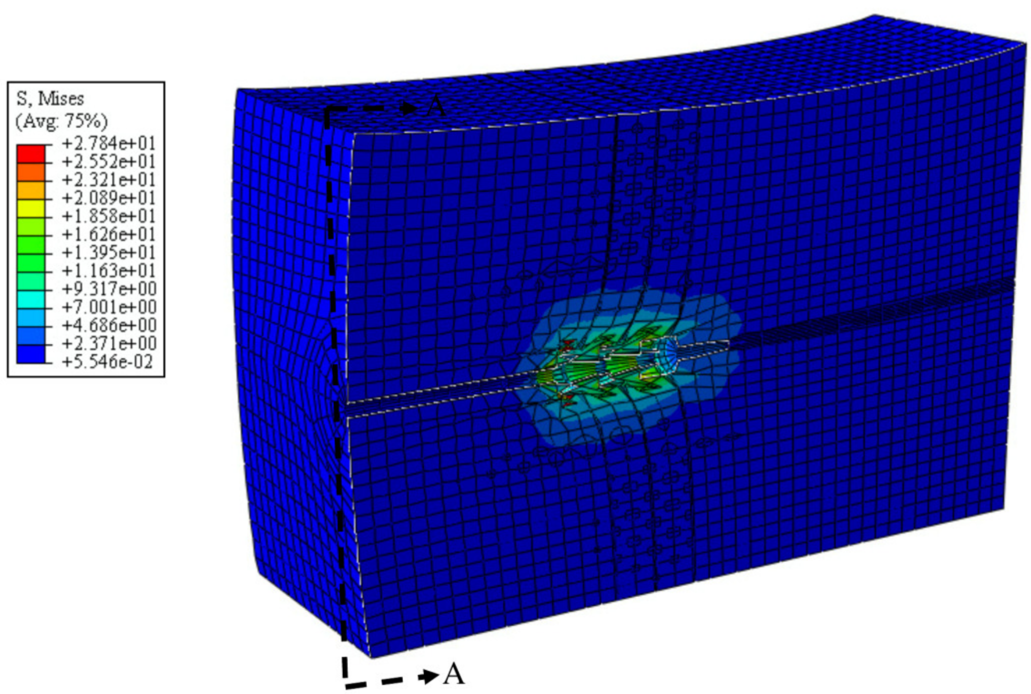

Fig. 5.48 (b): Stress contours for N3 nail with spacing of circular discs = $3D_c$

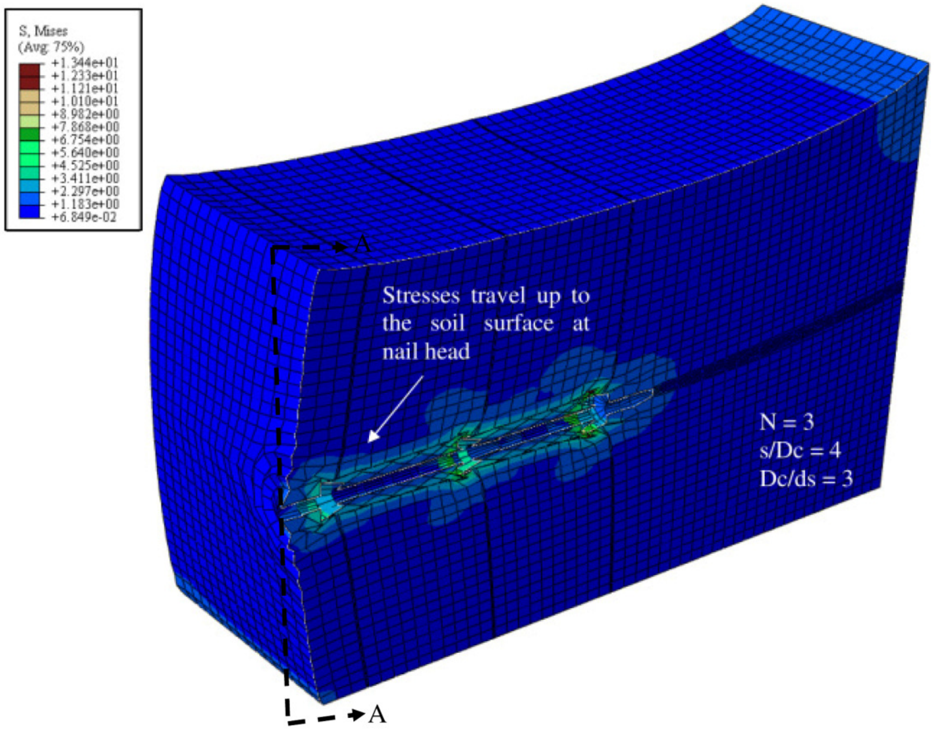

Fig. 5.48 (c): Stress contours for N3 nail with spacing of circular discs = $4D_c$

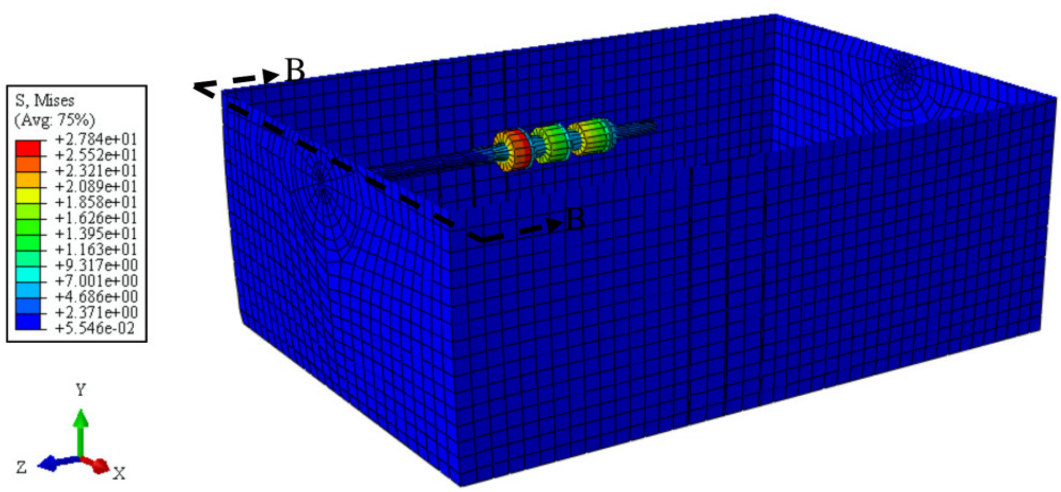

Fig. 5.48 (d): 3D stress contours for N3 nail with spacing of circular discs = $3D_c$

For N4 nails, the stress contours follow a similar pattern. The complete pullout model for pullout of soil nail with 4 circular discs is shown in Fig. 5.49 (a). The stress contours generated during soil nail pullout are studied by splitting the model through two sections namely A – A and B – B. As shown in Figs. 5.49 (b) and 5.49 (c), transition in failure mode from local deep failure to global shallow failure is observed with increase in spacing. It can also be observed from the stress contours that high stresses are mainly found between the top two circular discs. As the pullout of nail begins stresses are mainly concentrated at the nail end. With the nail displacement, the soil mass that detaches itself from the surrounding soil releases its stress and transfers it to the soil mass ahead. In this way stress progresses in direction of nail displacement. It can also be seen from Fig. 5.49 (d) that the soil around the circular discs is stressed such that it form a conical soil mass ahead of each disc. Moreover, the stresses are transmitted radially from discs during soil nail pullout.

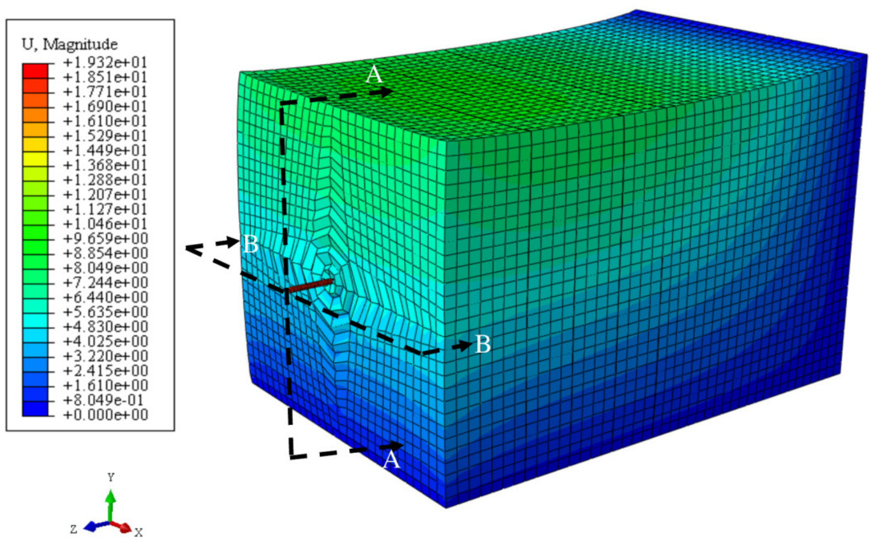

Fig. 5.49 (a): Complete pullout model for N4 nail

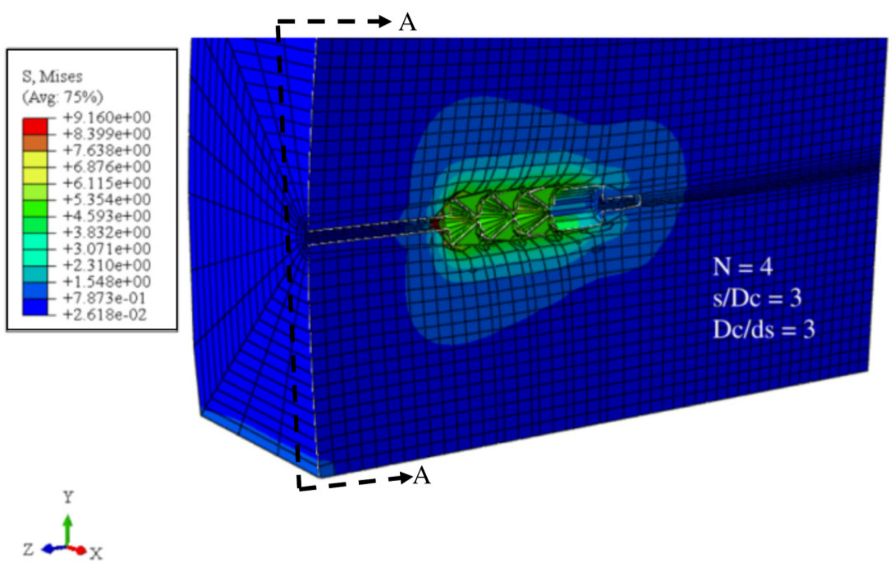

Fig. 5.49 (b): Stress contours for N4 nail with spacing of circular discs = $3D_c$

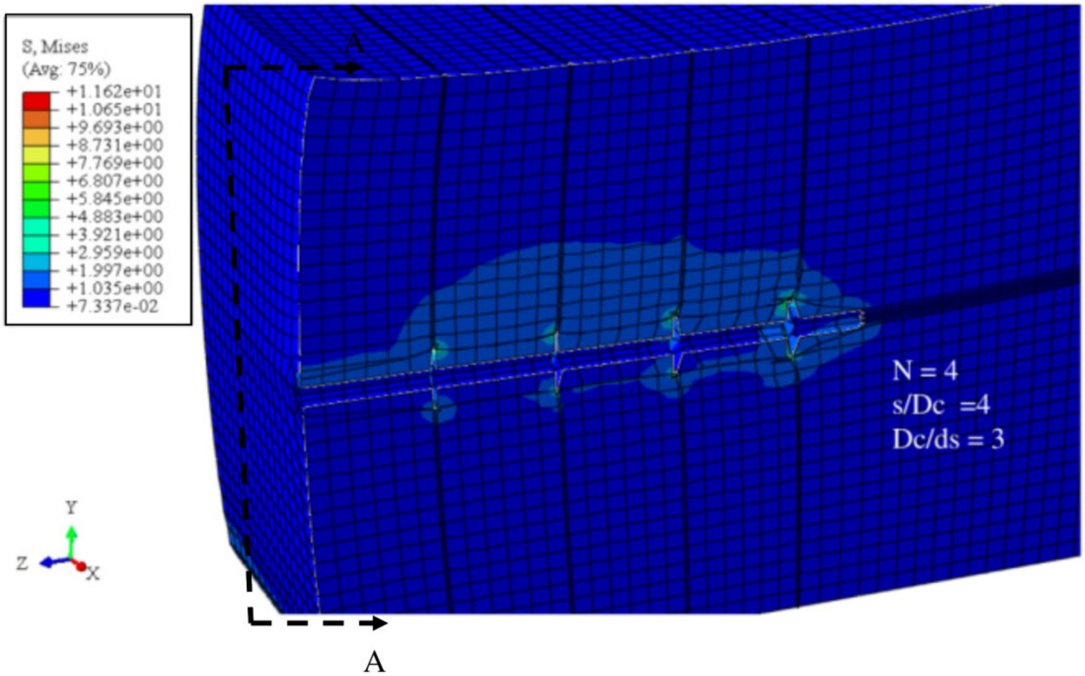

Fig. 5.49 (c): Stress contours for N4 nail with spacing of circular discs = $4D_c$

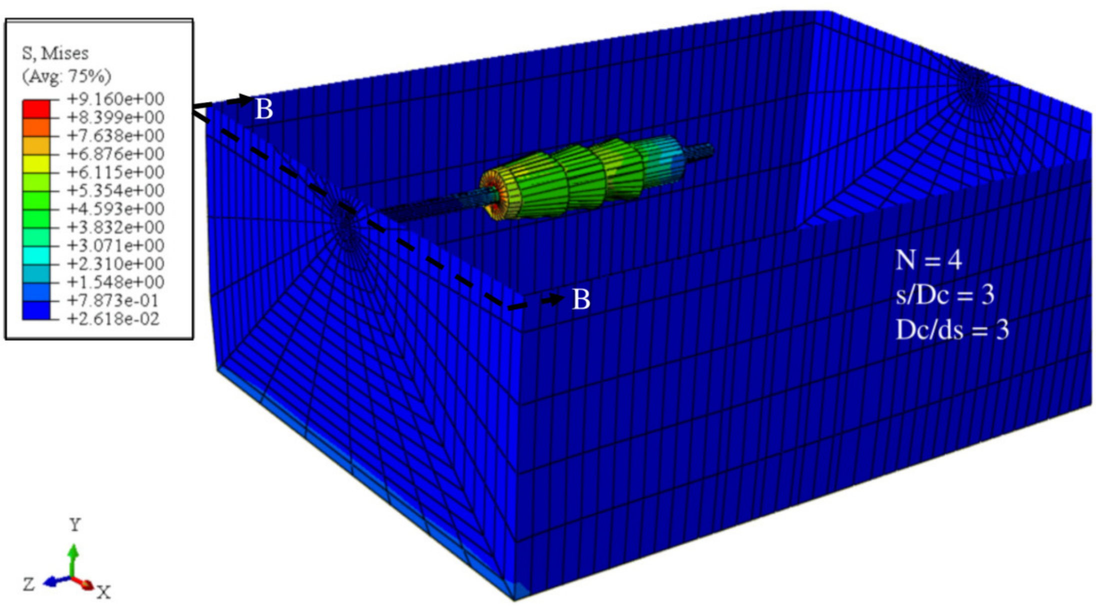

Fig. 5.49 (d): 3D stress contours for N4 nail with spacing of circular discs = $3D_c$

The variation in stresses also occurs if the diameter of circular discs is increased. However, the phenomenon of local and global failure modes still exists. It can be seen from Fig. 5.50 that by increasing the diameter of circular discs, large soil displacement occurs. This displacement of soil shifts the critical interface deep into the surrounding soil. This reduces the contribution of shaft nail towards pullout resistance but the same is compensated by an increase in the bearing area of circular discs. Hence increasing the diameter of circular disc beyond $D_c/d_s > 3$, pullout capacity of nail should increase or remain constant.

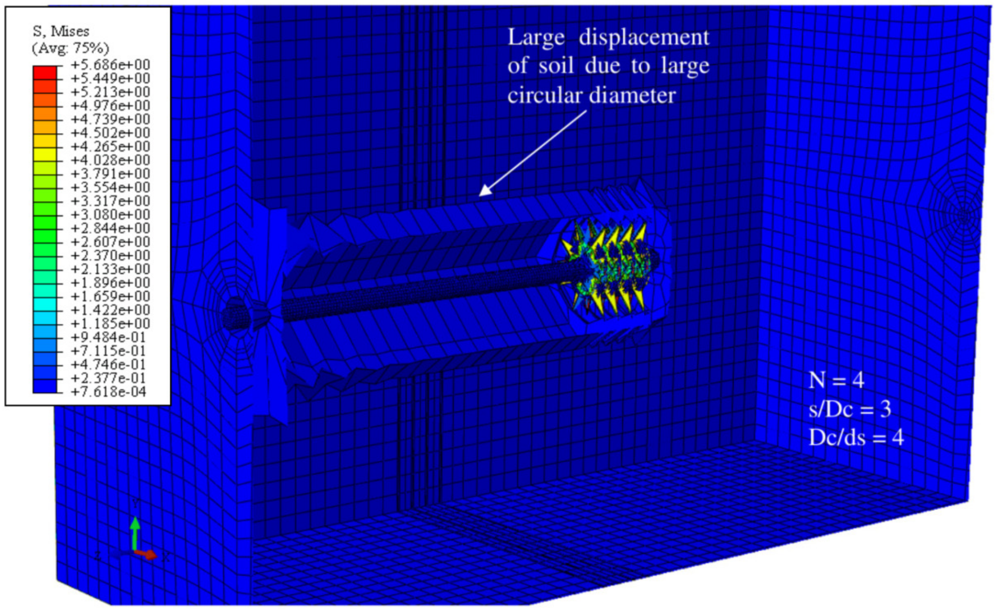

Fig. 5.50: Stress contours for soil nail with $D_c/d_s = 4$

From the stress contour plots, it can be deduced that the rupture surface during pullout of soil nail with circular disc has a defined pattern. The potential rupture surface will consists of a cylindrical soil zone between two discs with a curved conical soil zone at the front of first disc and an extended curved zone around the circular discs. To validate this, the rupture surface as predicted by Tokhi [214] for pullout of screw nail in laboratory model test can be stated as "Based on the soil deformation patterns, the area could be separated into three distinct zones: (1) the curved conical zone at the front of rear helix, (2) the extended curved zone around the helix, and (3) extended cylindrical zone approximately between the two helices."

As shown in Table 4.9, different combinations of parameters are used to study the pullout load variation. The pullout load for various combinations is converted to a dimensionless factor normalized pullout load (P/P_0) defined as the ratio of pullout load for the combination under study (P) to pullout load for N_0 nail (P_0). It can be observed from Fig. 5.51 that pullout load shows a non – linear relationship with variation in relative disc spacing ratio (s/D_c). The pullout load increases almost linearly till $s/D_c = 3$, thereby it remains almost constant with increasing s/D_c ratio. This signifies that there lies a critical s/D_c ratio beyond which pullout capacity remains unaffected. This can be well understood from the stress contours shown in Figs. 5.47, 5.48 and 5.49. For all $s/D_c \leq 3$, soil nails with circular discs act as deep anchors. The failure mode is a cylindrical soil mass local failure. The increase in pullout capacity up to $s/D_c \leq 3$ can be accounted for compacted soil mass between discs which moves as an integral part of soil nail. The nail now behaves like an enlarged diameter shaft at the disc level. Moreover soil densification increases the angle of internal friction of soil in and around the discs. The shear failure occurs at an interface in this densified zone of soil mass just outside the circular disc diameter. The increase in internal friction also leads to an increase in interface friction, which contributes in increasing the pullout capacity of nail. Beyond $s/D_c > 3$, a transition in failure mode occurs. The deep soil nails shifts to behave like shallow soil nails with failure surface reaching the soil around nail head. No compaction of soil occurs between the discs and each discs acts individually in bearing. The contribution of shaft friction in pullout resistance decreases. The pullout capacity of nail is predominantly governed by individual bearing of circular discs. It is also the reason for increase in pullout load beyond $s/D_c > 3$ with increasing N.

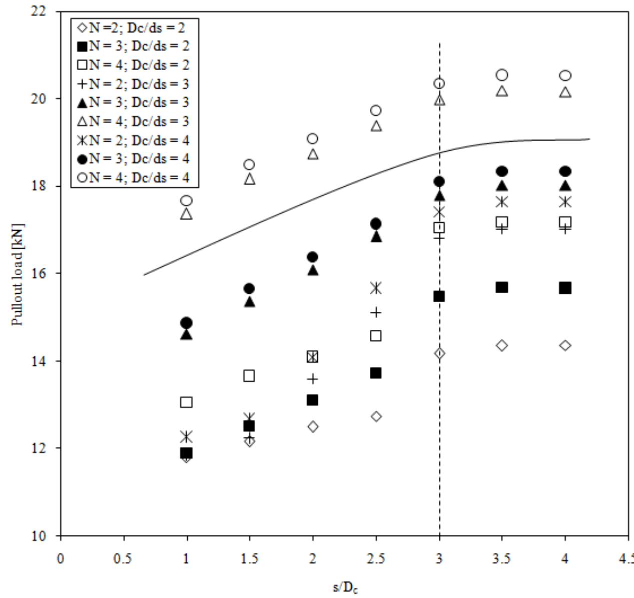

Fig. 5.51: Variation of pullout load with relative disc spacing ratio

The average shear stress of soil – nail interface also follows a similar non – linear relationship with variation in relative disc spacing ratio (s/D_c) as the pullout load. The average shear stress is found to increase up to a critical relative spacing ratio. The reason for this increase in average shear stress can be densification of inter - disc soil due to which soil nail now behaves like an enlarged shaft with diameter equal to that of discs. Moreover, soil densification increases the angle of internal friction of soil in and around the discs. The shear failure occurs in this densified zone of soil mass. The increase in internal friction also leads to an increase in interface friction, which contributes in increasing the pullout capacity of nail. Beyond critical relative disc spacing ratio (s/D_c > 3), shear stress variation will remain constant due to soil - nail shaft interface which will contribute in shaft friction during pullout resistance . The deep soil nails shifts to behave like shallow soil nails with failure surface reaching the soil around nail head. No compaction of soil occurs between the discs and each discs acts individually in bearing. The shear stress contribution will predominantly governed by shaft friction.

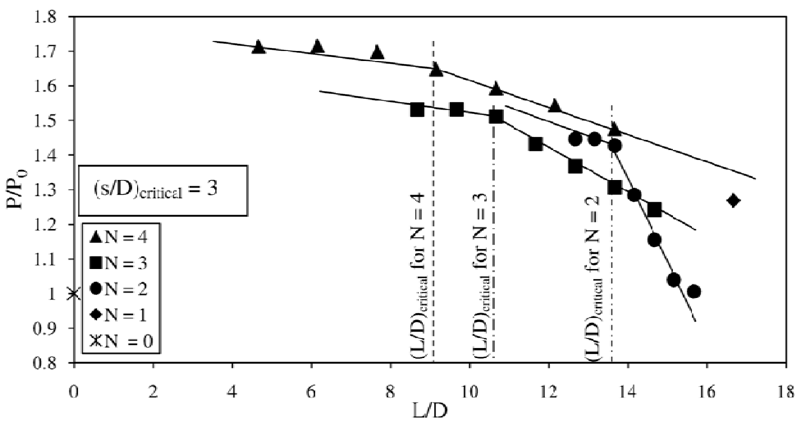

Fig. 5.52: Variation of Normalized pullout load with anchorage length ratio

Variation of normalized pullout load with anchorage length is shown in Fig. 5.52. It can be observed that as the anchorage length ratio increases the normalized pullout load decreases. However, the decrease in normalized pullout load is almost linear up to L/D_c < 9.16 for nail with 4 circular discs, L/D_c < 11.67 for nail with 3 circular discs and L/D_c < 13.67 for nail with 2 circular discs. Beyond these L/D_c ratios a sharp decrease in normalized pullout load is observed. This decrease in pullout load beyond specified L/D_c ratios can be attributed to the contribution of shaft friction in pullout resistance. In order to mobilize maximum shaft friction, significant length of shaft should extend beyond the passive soil zone. This reduction in shaft friction can only be compensated by increasing the number of circular discs, which increases the bearing capacity of nails against pullout. Hence it can be seen that if the number of circular discs are increased from 2 to 3, a decrease in required anchorage length is found from 13.67D_c to 11.67D_c. Similarly, for increase in number of discs from 3 to 4, required anchorage length decreases from 11.67D_c to 9.16D_c.

The contribution of circular disc bearing with anchorage length variation can also be understood from Fig. 5.53. A dimensionless bearing capacity factor (N_q) for circular disc bearing has been calculated from Eq. (4.20). As can be seen from Fig. 5.53, increase in number of circular discs leads to an increases bearing of soil nail. Moreover, for soil nails deriving their pullout resistance primarily from bearing, smaller anchorage lengths can be used. It is evident from the Fig. 5.53 that higher anchorage length is observed for soil nails with less number of circular discs. Hence this would lead to a decrease in the bearing component of pullout resistance.

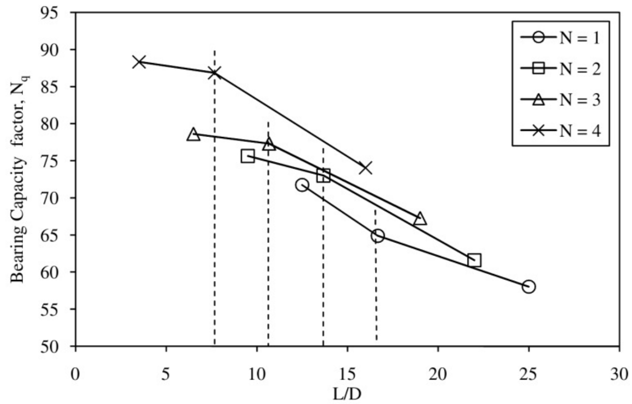

Fig. 5.53: Variation of bearing capacity factor with anchorage length ratio

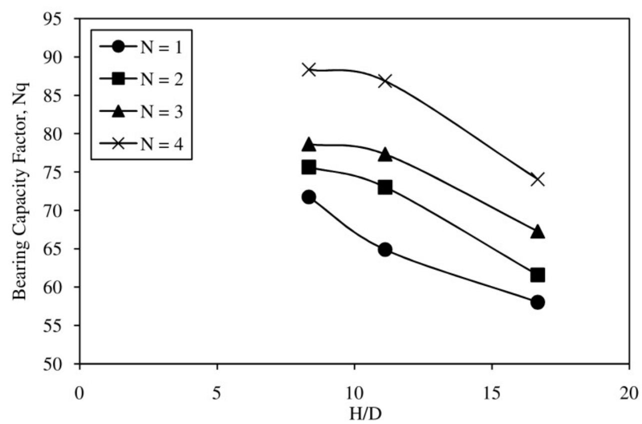

Fig. 5.54: Variation of bearing capacity factor with embedment depth ratio

The depth of soil nail below overburden is also found to affect the bearing capacity of soil nails. In the present analysis embedment ratio is calculated corresponding to change in circular disc diameter with a constant height (*H*) of overburden above the nail as 500 mm. As shown in Fig. 5.54, as the embedment ratio (H/D_c) is increased i.e. diameter of disc is reduced, bearing capacity factor is found to decrease. This signifies that at a constant depth below the overburden, if the diameter of circular discs is reduced, it will led to decrease in pullout load due to reduced bearing surface offered by circular discs. However, this reduction in bearing capacity will be smaller for nails having more number of discs. Reducing the circular disc diameter will significantly affect the pullout of nails in order of N1 nails >N2 nails > N3 nails > N4 nails.

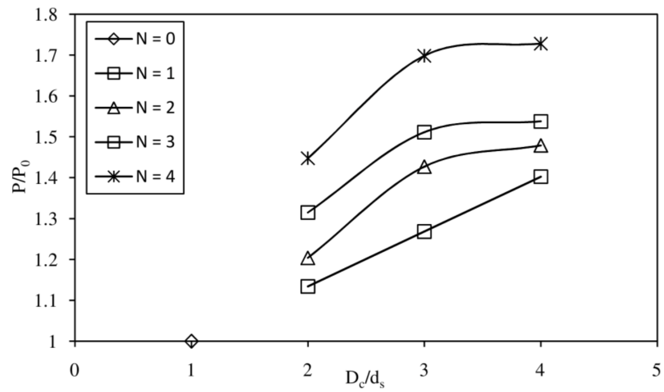

Fig. 5.55: Variation of normalized pullout load with relative diameter ratio

The affect of reduction in circular disc diameter on overall pullout capacity of soil nail can also be understood from Fig. 5.55. It is evident that as the diameter ratio increases, it brings about an increase in normalized pullout load. However, it is interesting to note that this increase in pullout is significant only up to D_s/d_s = 3. Beyond D_s/d_s > 3, the increase in pullout load is almost constant. Thus it can be stated that after a critical diameter ratio of 3, variation in D_s/d_s does not affect the nail pullout load significantly. This can be validated by screw nail design manual Hubble [26] which states that the diameter of helical plates in a screw soil nail should be equal to a minimum of three times the diameter of shaft. The reason for this variation can be summed up to large soil displacement due to large circular disc diameter. As shown in Fig. 5.50, soil nail with large diameter circular discs displaces the soil to a great extent such that no shaft resistance can be utilized by soil nails. The nail shaft moves easily under the pullout force through the dilated soil mass without offering significant resistance. The shear stresses acting at soil – nail interface are shifted away from nail shaft into a zone marked by restrained dilatancy. This zone where overburden along with normal stress restrains the soil dilation behavior forms the new interface for shear stress mobilization and is dependent on circular disc diameter.

The shear stress at soil – nail interface is mobilized with displacement of nail. However, nail displacement depends upon the anchorage nail length available for pullout. It can be seen from Fig. 5.56 that as the displacement ratio defined by displacement of nail to anchorage nail length ratio increases, normalized pullout load is found to increase. This increase in pullout load with nail displacement follows a non – linear path. After a certain nail displacement, the affect on pullout load is constant.

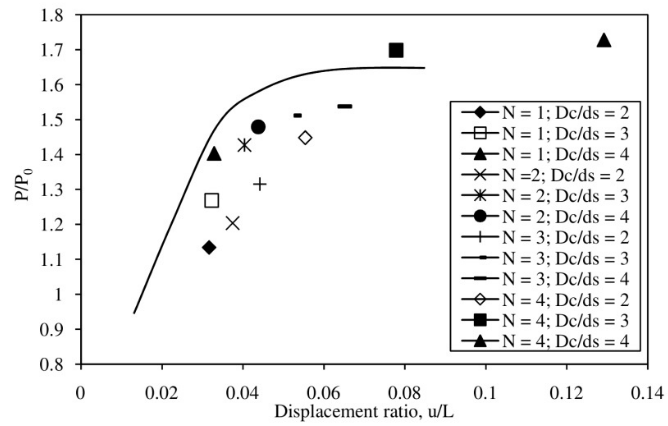

Fig. 5.56: Variation of normalized pullout load with displacement ratio

Fig. 5.56 clearly depicts the fact that displacement ratio brings about a steep increase in normalized pullout load initially but this effect dies out as displacement ratio continues to increase. The increase in the normalized pullout load initially corresponds to the fact that as displacement increases the entire embedded length develops shaft friction and the discs acts in bearing. However, as the pullout of soil nail continues, the embedded shaft length contributing to shaft friction decreases. The amount of soil in front of the top disc is also decreasing which bring reduction in the bearing capacity of discs. Due to this relative reduction in shaft friction and bearing, the pullout resistance decreases and thus a flatter normalized pullout resistance against displacement ratio are observed for high displacement ratio values. Moreover, normalized pullout load variation also depends on the number of discs on soil nail along with its displacement. A nail with greater number of discs as compared to nail with lesser number of discs for the same displacement ratio will depict a higher pullout load. This is due to the increased bearing offered to soil with increase in number of discs.

5.4.3 Results of Load – Displacement for Soil – nailed slopes with Helical nails

As given in Table 5.15, it is observed that maximum load carrying capacity of 57.3kN is found for 45° slope with nail inclination of 15°. Likewise, for 60° slope maximum load carrying capacity is observed with 15° nail inclination having a value of 49.19kN. On the other hand maximum failure load as observed for 90° slope is found to be 44.69kN for nail inclination of 0°. The results are consistent with results obtained from model testing of smooth and screw nailed slopes. However, it can be seen that an increase of 170% with respect to smooth nails and 19% with respect to screw nails is examined for load carrying capacity with helical nails for slope of 45° with 15° nail inclination.. In comparison to an unreinforced slope, helical nails provide an increase of 334% in load carrying capacity of slopes.

Table 5.15: Maximum load carrying capacity for slopes with helical nails from model testing

β°	***i° = 0°***	***i° = 15°***	***i° = 20°***	***i° = 30°***
	Load [kN]	**Load [kN]**	**Load [kN]**	**Load [kN]**
45°	53.76	57.3	52.06	48.84
60°	44.69	49.19	41.93	40.04
90°	35.97	22.86	19.57	16.57

For 60° slope with 15° nail inclination, percentage increase found for helical nailed slope as compared to smooth nailed and screw nailed slope is noted as 144% and 19%, respectively. Again in comparison to unreinforced slope of 60°, helical soil nailed slope depict an increase of 324%. For 90° slope with nail inclination of 0°, helical nailed slopes are found to provide an increase of 108% as compared to smooth nailed slopes and 19% as compared to screw nailed slopes for load carrying capacity of slopes. The percentage increase in failure load as compared to unreinforced slope of 90° comes out to be 253%. These significantly large percentage increases in load carrying capacities of slopes clearly depicts that maximum reinforcement is provided by helical nails as compared to screw nails and smooth nails.

Table 5.16: Maximum load carrying capacity for slopes with helical nails from FE analysis

β°	***i° = 0°***	***i° = 15°***	***i° = 20°***	***i° = 30°***
	Load [kN]	Load [kN]	Load [kN]	Load [kN]
45°	42.39	51.5	46.65	45.17
60°	39.19	43.26	38.77	32.79
90°	30.6	26.03	22.49	19.03

The FE analysis of for helical nailed soil slopes are found to depict similar pattern of load carrying capacity nature for slope of 45°, 60° and 90° with inclinations of 15° and 0°, respectively. However, it can be seen that FE estimates low load carrying capacity of slopes as compared to model testing due to difference in actual geometry of helical plates used in FE analysis and installation procedure not being modeled. Moreover, reasons of difference in boundary conditions and alteration of soil properties during model testing can also be accounted for variation in load carrying capacity as found from model testing and FE analysis as in case of screw nails also.

The variation of load – displacement for 45° clearly depicts that model testing and FE analysis reach peak load carrying capacity for different horizontal displacements of 78.7 mm and 54.1 mm, respectively. Similarly, for 60° slope with 15° nail inclination, failure load peak value is obtained at 60.5 mm horizontal displacement from model testing and 28.8 mm horizontal displacement from FE analysis. The reasons listed for variation of load carrying capacity between model testing and FE analysis can also be accounted for smaller horizontal displacement obtained in FE analysis.

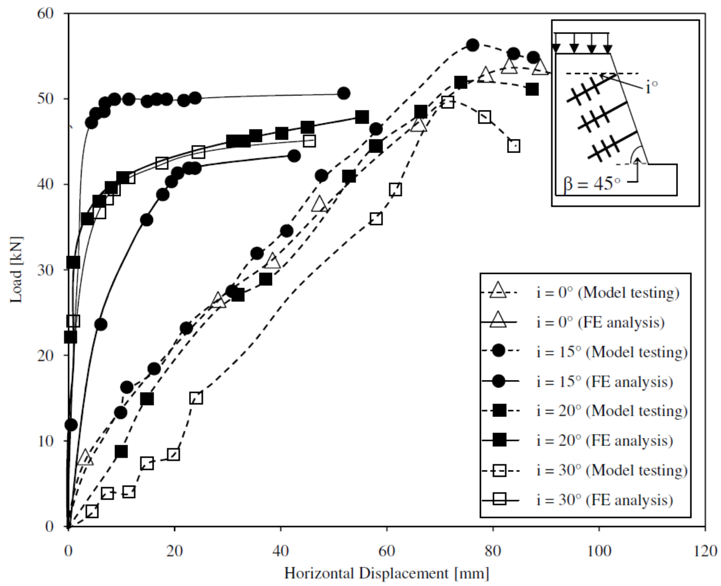

Fig. 5.57: Load – displacement of 45° with helical nails at different nail inclinations

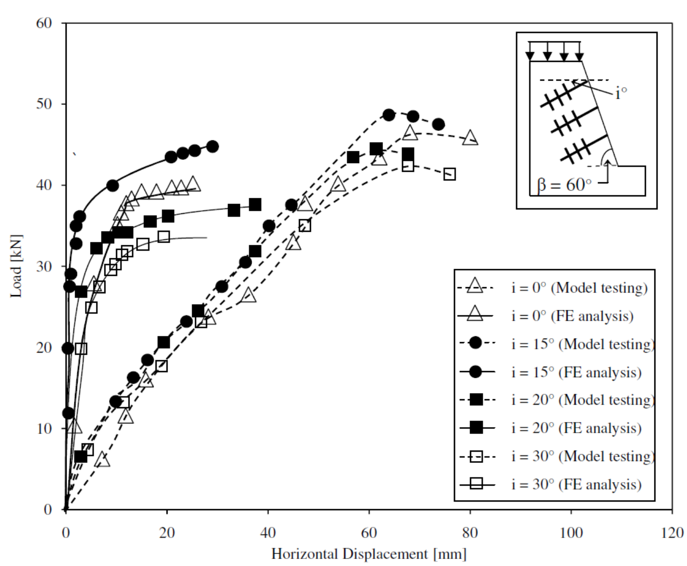

Fig. 5.58: Load – displacement of 60° with helical nails at different nail inclinations

For 90° slope with 0° nail inclination, it is found that similar to 45° and 60°, smaller horizontal displacement of slopes is found from FE analysis. The peak load from model testing is reached at a horizontal displacement of 37.2mm whereas horizontal displacement of 22.8 is estimated from FE analysis to reach peak value.

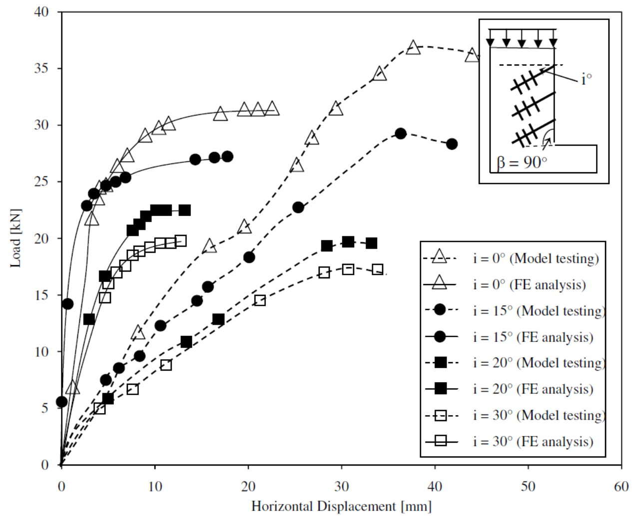

Fig. 5.59: Load – displacement of 90° with helical nails at different nail inclinations

For all load – displacement curves as obtained from model testing, it can be observed that as beyond peak load value, load carrying capacity of slopes is found to decrease with increase in horizontal displacement of slopes. The peak value constitutes failure load beyond which soil mass cannot be retrained by soil nails.

5.4.4 Results of Failure Mechanism for Soil – nailed slopes with Helical nails

The failure mechanism as obtained from model testing for slope angles of β = 45°; i = 15°, β = 60°; i = 15° and β = 90°; i = 0° depicts a similar pattern as that obtained for screw nailed slopes. The failure mechanism is characterized by crest settlement under surcharge loading with consequent slope face bulging due to slope movement. The degree of slope face movement though varied from small for 45° slope to moderate for 60° and large for 90° slope. The settlement of crest caused an increase in compression of soil which was compensated by soil displacement in horizontal direction. All lateral displacements being restricted by Perspex sheets equivalent to reaction provided by lateral earth pressure in actual field condition did not allow the slopes to deform laterally. Hence horizontal movement initiating from slope face and ultimately leading to slip surface development is observed. Figs. 5.60, 5.61 and 5.62 depicts similar pattern of slope settlement and slope face deformation for reinforced slopes of 45° and 60°. The deformation of tracer soil further signifies vertical deformation through soil slope body.

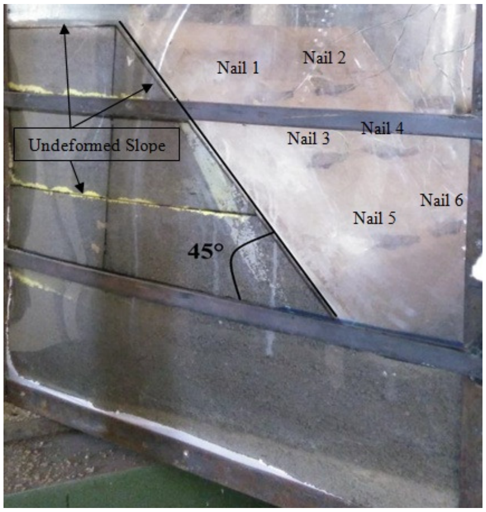

(a) Before testing

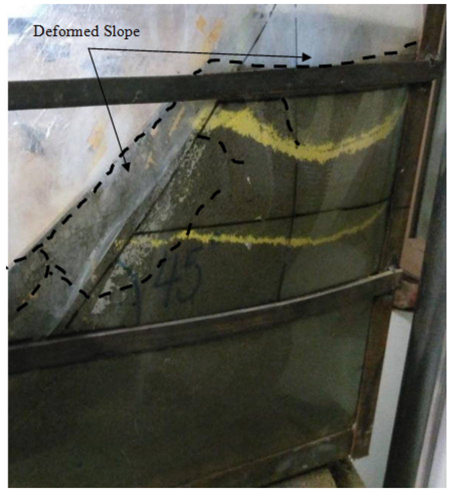

(b) After testing

Fig. 5.60: Failure mechanism of 45° Helical nailed soil slope

(a) Before testing

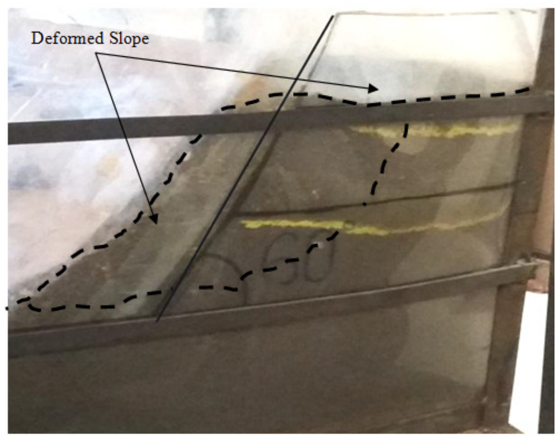

(b) After testing

Fig. 5.61: Failure mechanism of 60° Helical nailed soil slope

(a) Before testing

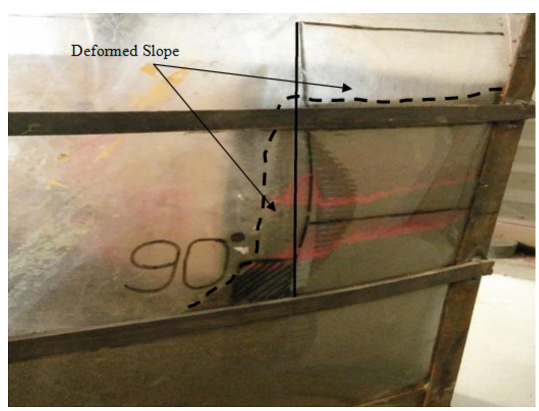

(b) After testing

Fig. 5.62: Failure mechanism of 90° Helical nailed soil slope

The validation of failure mechanism as observed from model testing can be made from slope deformation as predicted by FE analysis. It is evident from Figs. 5.63 (a), (b) and (c), that FE analysis also estimates settlement of slope crest under surcharge loading and outward slope face movement. For 90° slope however, it can be observed that failure is more prominent near slope face at start of slope crest. Moreover, similar failure is also observed from model testing [Fig. 5.62 (b)]. The slope face near slope crest moves out with increase in surcharge loading and slope face rotates about its toe before undergoing failure. The slip surface developed is not vivid but complex due to highly deformed slope body at failure. The failure mechanism of reinforced slope with helical nails also depicts that helical nails also undergo bending and certain deformation during failure. This is investigated both from model testing and FE analysis.

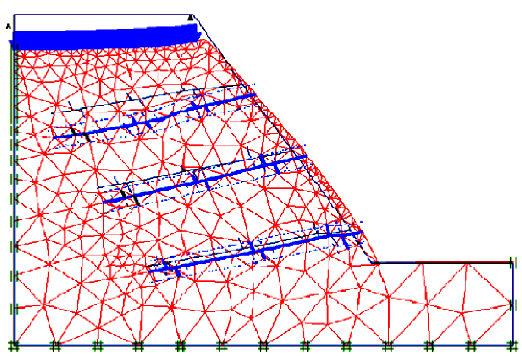

(a) Deformed 45° slope with 15° nail inclination

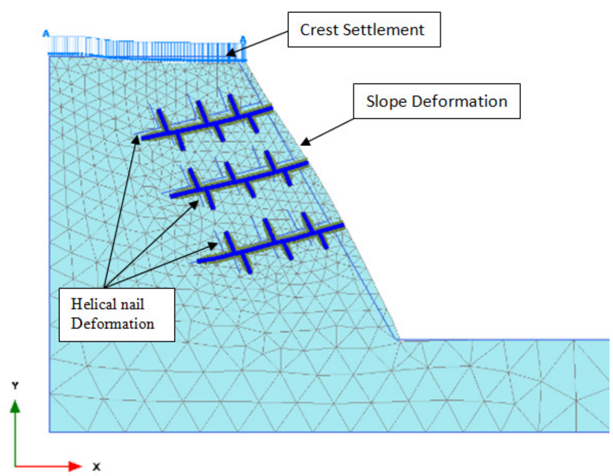

(b) Deformed 60° slope with 15° nail inclination

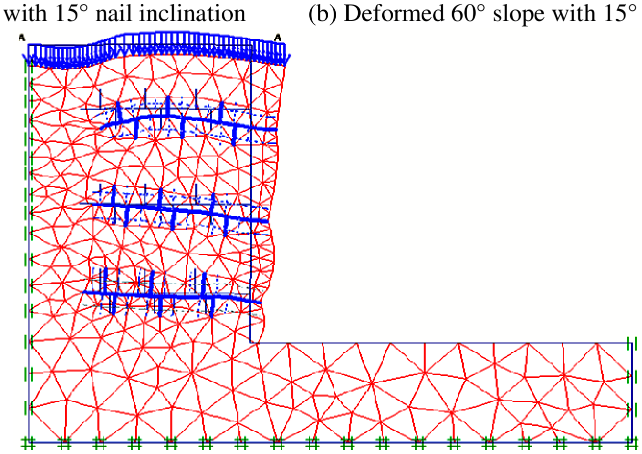

(c) Deformed 90° slope for 0° nail inclination

Fig. 5.63: Failure mechanism of Helical nailed soil slopes from FE analysis

The slip surface observed for helical nailed slopes with β = 45°; i = 15°, β = 60°; i = 15° and β = 90°; i = 0° are shown in Figs. 5.64 (a), (b) and (c). Similar to screw nailed soil slopes, slopes reinforced using helical nails also depicts slip surface intersecting lower nails for all cases. However, slip surfaces are found to originate from slope toe and terminate at slope crest at some distance beyond rear of slope crest. This signifies that failure ends below the loaded area of crest for 45° and 60°. For 90° slope, failure surface as obtained from FE analysis [Fig. 5.64 (c)] cannot be investigated in field and is against complex slip surface as obtained from model testing. However, maximum stressed zone can be seen concentrated near the slope face close to slope crest which makes 90° slope fail by rotation about slope toe.

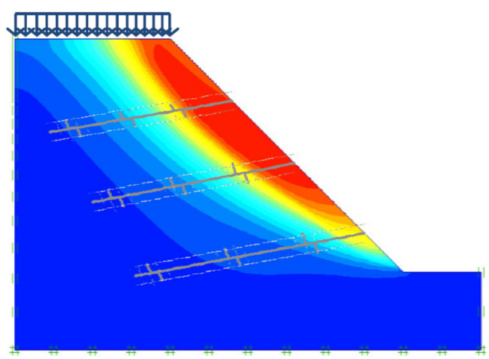

(a) Slip surface of 45° slope with 15° nail inclination

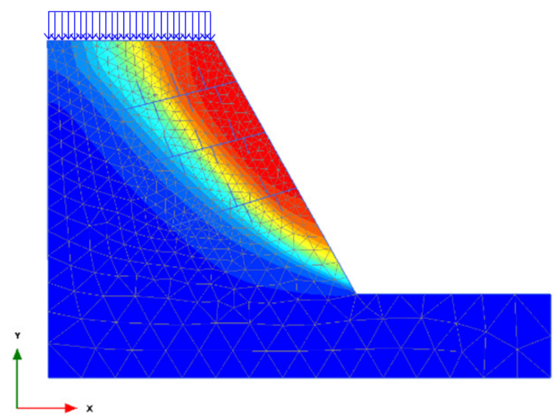

(b) Slip surface of 60° slope with 15° nail inclination

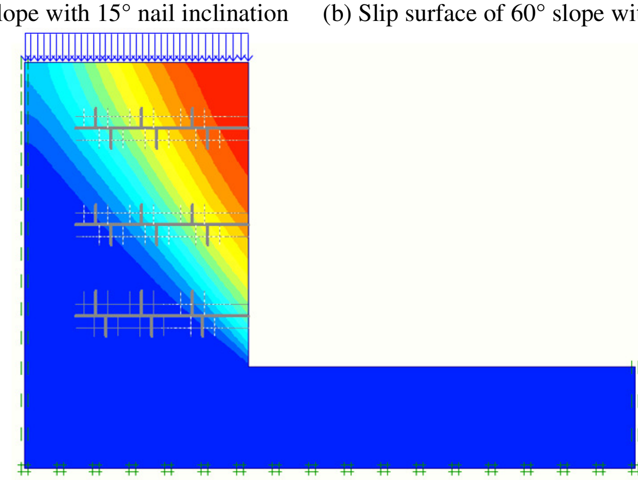

(c) Slip surface of 90° slope with 0° nail inclination

Fig. 5.64: Slip surface for helical soil nailed slopes from FE analysis

Another critical observation made during model testing is that after failure of helical soil nailed slope, it is found that soil is dislodged from surrounding soil and act in conjunction with helical plates. An observation similar to numerical modelling of pullout behaviour of helical soil nails. It can be deduced from Fig. 5.65 that helical plates act in bearing in addition to shaft friction which makes the surrounding soil attach to helical plates. Due to soil being compacted between inter helical plates; helical soil nail behaves as an enlarged diameter soil nail. The enlarged diameter shifts failure zone into deeper soil mass and failure interface friction is then not governed by soil - nail interface but densified soil – soil interface. This further contributes to enhanced reinforcing action of helical soil nails as compared to screw and smooth nails.

Fig. 5.65: Post failure state of helical soil nails

The factor of safety obtained for different slope angles with different nail inclinations is given in Table 5.17. The most optimum nail inclination of 15° for 45° and 60° is found to yield maximum FOS of 3.17 and 3.02, respectively. Similarly for 90° slope maximum FOS of 2.60 is observed for nail inclination of 0°. Similar to smooth nails and screw nails, factor of safety of helical nails are also found to vary with nail inclination. From nail inclination of 0° to 15°, FOS is found to increase for 45° and 60°. Beyond 15°, FOS is found to decrease with increase in nail inclination. However, for 90° slope variation of FOS decreases with increase in nail inclination from 0° to 30°. The variation of FOS reflects on whether helical nails are acting in tension or compression. For nail inclinations of helical nails which mobilize tensile forces, a higher FOS is attained whereas compression force development in nails leads to a decrease in FOS.

Moreover, it can also be viewed from Fig. 5.66 that LEM predicts a higher FOS as compared to FEM. Similar to screw and smooth nails this can b e accounted for accurate modelling of slip surface and non – linear stress strain conditions accurately incorporated by FEM.

Table 5.17: Factor of safety for different slopes reinforced with helical nails at different nail inclinations

β°	***i° = 0°***		***i° = 15°***		***i° = 20°***		***i° = 30°***	
	LEM	**FEM**	**LEM**	**FEM**	**LEM**	**FEM**	**LEM**	**FEM**
45°	2.95	2.68	3.17	2.83	2.23	2.13	2.07	1.93
60°	2.94	2.23	3.02	2.60	2.18	1.89	1.90	1.68
90°	2.60	2.31	2.46	1.76	1.92	1.65	1.65	1.49

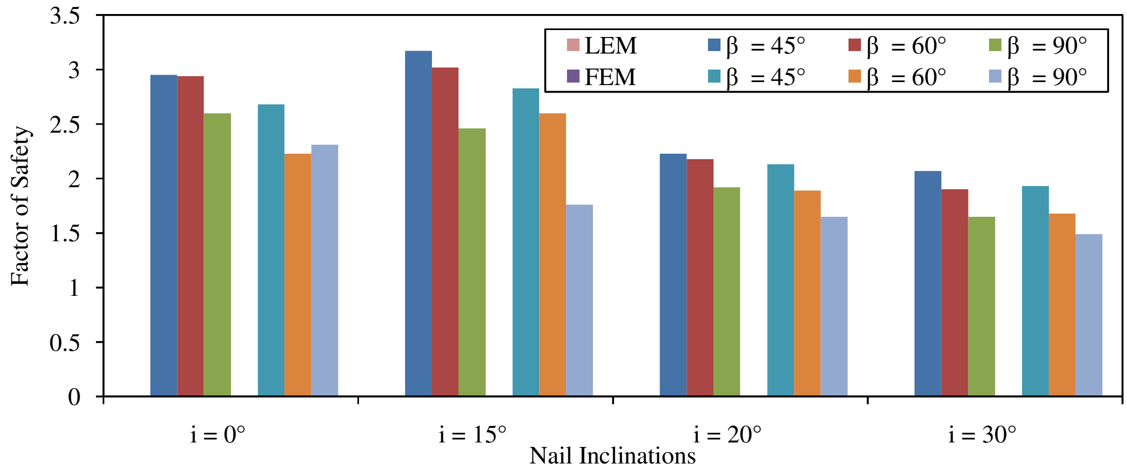

Fig. 5.66: Factor of safety variation with nail inclinations from LE and FE analysis

5.3.5 Results of Nail forces for Soil – Nailed slopes with Helical nails

The nail forces developed in helical nails during model testing are found to be similar to screw nails and smooth nails with variation in magnitude. The maximum nail forces are observed for top row of nails which is also depicted by FE analysis. The maximum nail force for 45° with 15° nail inclination is found to be 4.95kN occurring at nail 1. For 60° slope with nail inclination of 15°, nail 1 is found to have maximum nail force of 11.8kN. However, helical nails at 0° nail inclination for 90° slope depicts maximum nail force 0f 16.1kN which is greater than maximum nail forces developed at nail 1 for 45° and 60°. This result is evident for that fact that for vertical cut of 90°, slope movement is predominant at slope crest edge. Maximum strains are developed in the region around slope crest near edge of slope face which causes highly stressed soil zone as also depicted from Fig. 5.64 (c). The large stress corresponds to high normal stress on helical soil nails and consequently significantly large nail forces. The nail forces for all other locations are very small as compared to maximum nail force which is evident for reinforcing action produced by top nails.

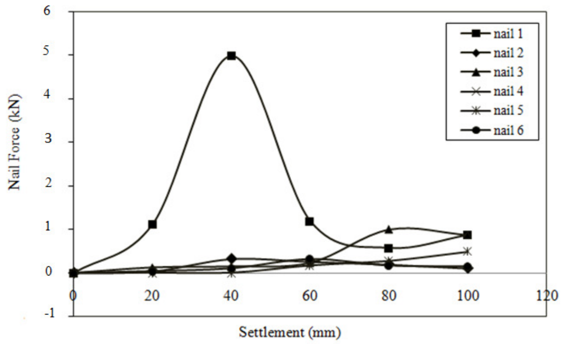

(a) 45° slope with 15° nail inclination

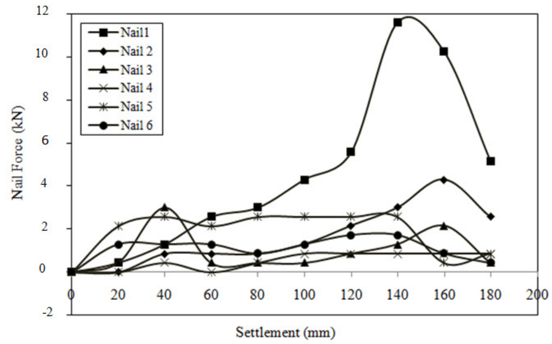

(b) 60° slope with 15° nail inclination

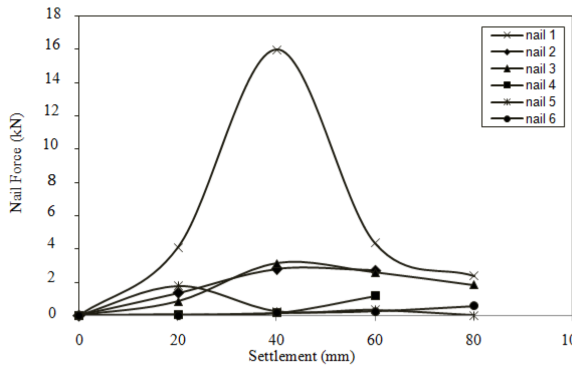

(c) 90° slope with 0° nail inclination

Fig. 5.67: Nail force distribution for different slopes and nail inclinations from model testing with helical nails

The FE analysis of helical nailed slopes also reveals similar results as that obtained from model testing. As observed from Figs. 5.68 (a), (b) and (c), it is clear that maximum nail forces along nail length are also developed for top nails.

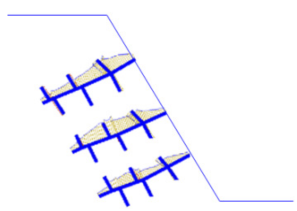

(a) Slip surface of 45° slope with 15° nail inclination

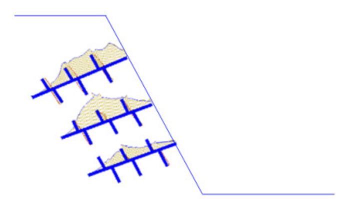

(b) Slip surface of 60° slope with 15° nail inclination

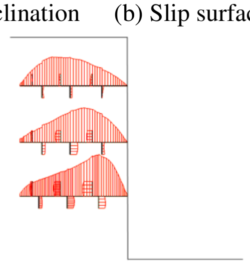

(c) Slip surface of 90° slope with 0° nail inclination

Fig. 5.68: Nail forces for helical soil nailed slopes from FE analysis

Moreover, deformation of helical plates during slope failure is also observed from FE analysis. The helical plates can also be found to contribute in nail force mobilization as observed from Figs. 5.68 (b) for top nail and Fig. 5.68 (c) for top, middle and bottom nails. The FE results on nail forces as obtained for smooth, screw and helical nails also bring forth the observation that in a soil – nailed slope maximum nail axial stresses are generated at top nails. From this observation it can also be inferred that for top row of nails longer soil nails are required which can be reduced in length with slope height. For bottom row of nails smaller nail lengths can also suffice the condition of reinforcement due to small stress development and intersection of slip surface at smaller length of soil nails.

It should also be noted that constitutive models like Mohr – Coulomb used for FE analysis perform better regarding its strength behaviour. However, for perfect plasticity, the model does not include strain hardening or softening effect of the soil. The simplification of Mohr-Coulomb model where the hexagonal shape of the failure cone is replaced by a simple cone is known as the Drucker - Prager model. Generally, it shares the same advantages and limitations with the Mohr-Coulomb model. In Drucker - Prager Model the yield is circular, from centre to the yield surface it is equidistance. The only difference between Mohr - Coulomb and Drucker - Prager models is that intermediate principal stress is not considered in case of Mohr - Coulomb model. Both models assume elasticity up to failure surface and predictions obtained are elastic-plastic in nature.

The shortcomings of constitutive models such as non-linear elastic (e.g., hyperbolic), classical plasticity (e.g., von Mises, Drucker – Prager and Mohr –Coulomb), advanced plasticity (e.g., critical and cap) and classical damage (softening) can be overcome by realistic constitutive models like Disturbed State Concept (DSC) with a Hierarchical Single-Surface (HISS) plasticity model. For instance, it is capable of accounting for elastic, plastic, and creep responses, micro-cracking leading to softening, fracture for both soils and interfaces with the same basic framework. It is found to account for the foregoing factors in a hierarchical manner, with smaller or the same number of parameters compared to other available models. The classical plasticity models such as von Mises, Mohr - Coulomb and Drucker - Prager do not allow adequately for the volumetric response, and for the existence of yielding before the ultimate (failure) surface is reached. Hence, their use is often limited for evaluation of failure or ultimate loads. In the critical state and cap models, the continuous hardening or yielding parameter is dependent only on the volumetric plastic strain.

However, in the Hierarchical Single-Surface (HISS) models, hardening is dependent on both volumetric and deviatoric plastic strain, respectively. The DSC allows for discontinuities experienced by a deforming material, that can often result in degradation or softening; it can also allow stiffening and healing in deforming materials. Because the DSC allows for the coupling between the relative intact (RI) and fully adjusted (FA) responses, it can avoid difficulties such as spurious mesh dependence that occurs in classical damage models. Also, if such a coupling is considered in the classical damage model by introducing additional enrichments, the resulting models may become complex. In the fracture mechanics approach, usually it is required to introduce cracks in advance of the loading. In contrast, the DSC does not need a priori introduction of cracks, initiation and growth of micro-cracking, fracture. The failure can be traced at appropriate locations depending upon geometry, loading and boundary conditions and on the basis of critical disturbance obtained from test results. The DSC allows identification, initiation and growth of micro - structural instability or liquefaction by using the critical disturbance.

The DSC/HISS models also possess the following advantages:

[1] The yielding in the HISS model is assumed to be dependent on total plastic strains or plastic work. Hence, in contrast to other models such as critical state and cap in which yielding is based on the volumetric strains, the HISS model includes the effect of plastic shear strains also.

[2] The yield surface allows for different strengths along different stress paths.

[3] Because of the continuous and special shape of the yield surface, it allows for dilatational strains before the peak stress, which can be common in many geomaterials.

[4] The DSC allows for degradation and softening, and it can allow also for stiffening or healing. Introduction of disturbance can account for (a part) the non - associative behavior, i.e., deviation of plastic strain increment from normality.

[5] The DSC allows intrinsically the coupling between RI and FA parts and the non - local effects. Hence, it is not necessary to add extra or special enrichments, e.g., micro - crack interaction and gradient.

[6] The DSC is general and can be used for a wide range of materials like geologic, concrete, asphalt, ceramics, metal, alloys and silicon, if appropriate test data is available and can also be used for repetitive loading which may involve a large number of loading cycles.

CHAPTER 6

CONCLUSIONS

6.1 General

The chapter enlists the conclusions derived from the results of model testing and numerical modeling of soil – nailed slopes with three different types of soil nails. It also incorporates some major conclusions based on comparison of results between model testing and numerical modeling.

6.2 Conclusions

Model testing of soil – nailed slopes with smooth soil nails, screw soil nails, helical soil nails have been carried out in the present work at three different slope angles of 45°, 60° and 90° using four different nail inclinations of 0°, 15°, 20° and 30° with horizontal. The numerical modeling of reinforced slope with three different types of soil nails at all slope angles and nail inclinations have been carried out using limit equilibrium based SLOPE/W and finite element based PLAXIS 2D. The pullout behavior of helical nail has also been investigated with 2D FE package PLAXIS 2D and 3D FE package ABAQUS/Explicit. Based on the results obtained from present work, following conclusions can be made:

1) The load carrying capacity of an unreinforced can be increased by reinforcing the slope with nails. The soil – nailed slopes undergo smaller slope deformation as compared to unreinforced slopes. The reinforcing action of helical nails and screw nails is greater than smooth nails depicted by maximum load carrying capacity for helical nails followed by screw nails and then smooth nails. However, it can also be concluded that slope deformation does not follow the same effect of reinforcement corresponding to these three types of nails.

2) The maximum load carrying capacity varies with slope angle (β) and nail inclination (i). For $\beta \leq 60°$, optimum nail inclination is i = 15°. For $\beta > 60°$, i = 0° gives the maximum load carrying capacity. Thus, it can be concluded that maximum reinforcing action of soil nails can be obtained between i = 0° to 15° and beyond i = 15°, effect of soil nailing on soil slopes with increasing slope angels from β = 45° to 90° is minimal. This pattern of soil nail reinforcement is common for all types of nails namely smooth, screw and helical soil nails.

3) The failure surface for a soil – nailed slope can be inferred as a circular slip failure for $\beta \leq 60°$ irrespective of the type of nail used for reinforcement. For $\beta = 90°$, slip surface is much complex to predict but is characterized by overturning of slope about the toe for all nail types. Moreover, soil – nailed failure mechanism will always include settlement of slope crest under surcharge loads and horizontal displacements of slope face for all nail types.

4) Limit equilibrium method and Finite element method can well predict the soil – nailed slope response. The critical slip surfaces obtained from LEM are similar to model testing whereas slope deformation behavior of soil – nailed slopes during failure are close to model testing as depicted by FEM.

5) LEM and FEM both can predict the limiting conditions namely pullout capacity, tensile capacity or the facing capacity in the load transfer mechanism of nails. The intersection of failure surface with nail length governs which condition has been mobilized. The results in LEM are dependent upon nail length and bond length. Slopes having longer nail bond length are more stable than those in which no bond lengths are mobilized. On the other hand, FEM is independent of the nail length. The analysis is dependent on nail bending stiffness; axial stiffness and soil - nail interaction. Thus, it can be concluded that higher bending stiffness and soil - nail interaction, better is the reinforcement action of nails and more stable the slope. FEM analysis depicts variation in FOS with changing interface strength, however no provision of interface strength is available in the LEM routine.

6) The factor of safety more than 1.5 for all nail types depicts that soil nailing of unreinforced slope provides stability against failure. However, better stability is obtained by using helical nails as compared to screw nails and smooth nails.

7) The load transfer mechanism of helical nails is different from that of screw nails and smooth nails. Helical nails derive its pullout resistance capacity from nail shaft friction and additional bearing from helical plates, whereas screw nails and smooth nails primarily depend upon interface friction between nail surface and surround soil to generate pullout resistance during failure.

8) The helical plate spacing, diameter, embedment ratio, length ratio and number of helical plates all affect the pullout capacity of helical soil nails. There is a critical s/D_h or s/D_c ratio of 3 and D_h/D_s or D_c/d_s ratio of 3 beyond which load transfer mechanism

of helical soil nails changes from deep global cylindrical failure to shallow local individual plate failure.

9) Maximum nail forces are generated at top row of nails for all slope angels using smooth, screw and helical nails. It can also be concluded that long soil nail lengths should be used at slope top and smaller nail lengths can be employed for slope stability at bottom row of nails.

10) The helical nails and screw nails more suitable than smooth nails as they provide ease of installation with minimum spoils and disturbance to surrounding soil. They also provide satisfactory performance in reinforcement of unstable slopes.

6.3 Scope for Future Work

The present research work has been limited to static analysis of soil – nailed slopes which leaves a research gap for dynamic analysis of soil slopes using smooth, screw and helical nails. Moreover, soil nailing has been carried out in same soil conditions of drained sandy soil has been used for all model testing and numerical modeling which can be further looked into by using a different type of soil such as cohesive soil or a c – ϕ soil. Further validation of this research work can be done by carrying out large scale field studies using similar types of soil nails as smooth, screw and helical.

REFERENCES

[1] Jewell R.A., "*Strength and deformation in reinforced soil design*", Proc. of the 4th Int. Conf. on Geotextiles, Geomembranes and Related Products, Rotterdam, Netherlands, May 29, pp. 913-946, 1990.

[2] Rabcewicz L.V., "*The new Austrian tunneling method*", Water Power, pp. 453-457, 1964.

[3] Stocker M.D., Korber G. W., Gassler G., Gudehus G., "*Soil nailing*", Int. Conf. on Soil Reinfocement, Paris, vol. 2, March 1979, pp. 469–474, 1979.

[4] Gassler G., Gudehus G., "*Soil Nailing - some aspects of a new technique*", Proc. 10th Int. Conf. Soil Mechanics and Foundation Engineering, Stockholm, Balkeema, Rotterdam, vol. 3, pp. 665-670, 1981.

[5] Plumelle C., "*Full scale experimental nailed soil retaining structures*", Revue Française de Geotechnique, vol. 40, pp. 45-50, 1986.

[6] Clouterre R., "*Soil nailing recommendation 1991*", An English translation of 'Recommendations CLOUTERRE — 1991, USA Report No. FHWA-SA-93-026, US Department of Transportation, Federal Highway Administration, 400 Seventh Street, Washington DC, 1991.

[7] Shen C. K., Bang S., and Herrman L. R., "*Ground movement analysis of earth support system*", J. of Geotech. and Geoenv. Engg., ASCE 107(GT12), pp. 1609-1624, 1981.

[8] Elias V., Juran I., "*Soil Nailing for Stabilization of Highway Slopes and Excavations*", Publication FHWA-RD-89-198, Washington D.C., Federal Highway Administration, 1991.

[9] FHWA, "*Soil Nailing Field Inspectors Manual - Soil Nail Walls*", Report No. FHWA-SA-93-068, Federal Highway Administration, Washington DC, 1994.

[10] Jewell R., Pedley M., "*Analysis for Soil Reinforcement with Bending Stiffness*", Journal of Geotechnical Engineering, vol. 118, no. 10, pp. 1505-1528, 1992.

[11] Ortigao J.A.R., Palmeira E.M., Zirlis A.C., "*Experience with soil nailing in Brazil: 1970-1994*", Proc. Int. Civil Engineer, Geotechnical Engineering, vol. 113, pp. 93-106, 1995.

[12] Hirano M., "*Actual status of the application of Soil Nailing to expressway cut slope construction in Japan*", Landmarks in earth reinforcement. Proc. of Int. Earth Reinf., Kyushu, Japan, pp. 919-934, 2001.

[13]Seto P., Won G.W., Choi, K.Y., "*Use of soil nailing in stabilization of a freeway embankment*", Earth Reinforcement Practice: Proc. of the Int. Symp. on Earth Reinforcement Practice, Fukuoka, Kyushu, Japan, pp. 11-13, 1992.

[14]Watkins A.T., Powell G.E., "*Soil nailing to existing slopes as landslip preventive works*", Hong Kong Eng, vol. 20, no. 3, pp. 20-27, 1992.

[15]Babu G.S., Singh V.P., "*Reliability analyses of soil nail walls*", Georisk, vol. 3, no. 1, pp. 44-54, 2009.

[16] Ortigao J.A., Palmeira E.M., "*Optimised design for soil nailed walls*", Proc. of the 3rd Int. Conf. on Ground Improvement Geosystems (GIGS), 10 April, 1997, pp. 368 – 374, 1997.

[17] Dai Z.H., Guo W.D., Zheng G.X., Ou Y., Chen Y.J., "*Moso Bamboo Soil-Nailed Wall and its 3D Nonlinear Numerical Analysis*", Int. J. of Geomech., vol. 16, no. 5, 2016.

[18] Tan Y.C., Chow C.M., "*Slope stabilization using soil nails: design assumptions and construction realities*", Malaysia – Japan Symposium on Geohazards and Geoenvironmental Engineering, Bangi, Malaysia, December, 2004, pp. 13-14, 2004.

[19] Gassler G., "*Stabilization of a cutting slope along a high-speed railway line using extremely long nails*", In the practice of soil reinforcing in Europe: Proceedings of the symposium, The practice of soil reinforcing in Europe, International Geosynthetics Society, Institution of Civil Engineers, Thomas Telford, London, 18 May, 1995, pp. 214 – 226, 1995.

[20]Warner M.F., Barley A.D., "*Cliff stabilization by soil nailing, Bouley Bay, Jersey, C. I*", Proc. of the 3rd Int. Conf. on Ground Improvement and Geosystem, Thomas Telford, London, 10 April, 1997, pp. 468 – 476, 1997.

[21]Lazarte C.A., Elias V., Espinoza R.D., Sabatini P.J., "*Geotechnical Engineering Circular No. 7: Soil Nail Walls*", Federal Highway Administration, Washington DC, March, 2003.

[22]Louis C., "*Theory and Practice in Soil Nailing Temporary or Permanent Works*", ASCE, Annual Conference, Boston, 1986.

[23]Gassler G., "*Soil nailing - theoretical basis and practical design*", Proc. of Int. Geotechnical Symposium on Theory and Practice of Earth Reinforcement, Fukuoka, Japan, Balkema, 1988, pp. 285 – 288, 1988.

[24]Myles B., “*New techniques for soil nailing slopes*”, Proc. of Int. Conf. on Landslides, Slope Stability and the Safety of Infra-structures, Malaysia, 1994, pp. 265-271, 1994.

[25]Hanna S., Juran I., Levy O., Benslimane A., “*Recent developments in Soil – Nailing - Design and practice*”, Soil Improvement for Big Digs, Geotechnical Special Publication No. 81, ASCE, pp. 259 – 284, 1998.

[26]Hubble Power Systems, Inc., “*Screw nailing retention earth structures*”, Soil Screw Design manual Edition 2, Chance™, 2015.

[27]Bruce D.A., Jewell R.A., “*Soil nailing: Application and Practice - Part 2*”, Ground Engineering, vol. 19, no. 8, pp. 21 – 33, Januray, 1987.

[28]Raju G.V.R., “*Behavior of nailed soil retaining structures*”, Ph.D. dissertation, Nanyang Technological University, Singapore, 1996.

[29]Cornforth D., “*Landslides in practice: Investigation, analysis, and remedial/preventative options in soils*”, John Wiley, New York, 25 February, 2005.

[30]Juran I., Elias V., “*Ground anchors and soil nails in retaining structures*”, Foundation engineering handbook, Springer US, pp. 868 – 905, 1991.

[31]Schlosser F., “*Behavior and design of soil nailing*”, Int. Symp. on Recent Development in Ground Improvement Techniques, pp.399 - 413, 1982.

[32]Juran I., “*Reinforced soil systems - application in retaining structures*”, Geotechnical Engineering, vol. 16, no. 1, pp. 39 - 82, 1985.

[33]Jewell R.A., Pedley M.J., "*Soil nailing design: the role of bending stiffness*", Ground Engineering, pp. 30 - 36, 1990.

[34]Jewell R.A., Pedley M.J., "*Analysis for Soil Reinforcement with Bending Stiffness*", Journal of Geotechnical Engineering, vol. 118, no.10, pp. 1505 - 1528, 1992.

[35]Bridle R.J., Davies M.C., “*Analysis of soil nailing using tension and shear: experimental observations and assessment*”, Proc. of the Institution of Civil Engineers-Geotechnical Engineering, vol. 125, no. 3, pp. 155 – 67, 1997.

[36]FHWA, “*Geotechnical Engineering Circular No. 7: Soil Nail Walls*”, Report No. FHWA0-IF-03- 017, Federal Highway Administration, Washington, USA, 2003.

[37]Luo S.Q., Tan S.A., Yong K.Y., "*Pull-out resistance mechanism of a soil nail reinforcement in dilative soils*", Soils and Foundations, vol. 40, no. 1, pp. 47 - 56, 2000.

[38]Hoyt R.M., Clemence S.P., "*Uplift Capacity of Helical Anchors in Soil*", Proc. of the 12th Int. Conf. on Soil Mechanics and Foundation Engineering, Rio de Janeiro, Brazil August 13, 1989, vol. 2, pp. 1019 - 1022, 1989.

[39]Juran I., Beech J., De Laure E., "*Experimental Study of the Behavior of nailed Soil Retaining Structures on Reduced Scale Models*", Proceedings of Int. Symp. on In Situ Soil and Rock Reinforcement, Paris, France, 1984.

[40]Juran I., and Elias V., "*Soil Nailed Retaining Structures, Analysis of Case Histories*", Geotechnical Special Publication No. 12, ASCE, New York, pp. 232 - 244, 1987.

[41]Gassler G., Gudehus G., "*Soil nailing statistical design*", Proc. of VIIIth ECSMFE, Helsinki, vol. 2, May 2, 1983, pp.491 – 494, 1983.

[42]Schwing E., Gudehus G., "*Soil – Nailing Design and Application to Modern and Ancient Retaining Walls*", Proc. of Int. Geotechnical Symp. on Theory and Practice of Earth Reinforcement, Fukuoka, Kyushu, Japan, 5 - 7 October, 1988, pp. 605 – 610, 1988.

[43]Kitamura T., Nagao A., Uehara S., "*Model Loading Test of Reinforced Slope with Steel Bars*", Proc. Int. Geotechnical Symp. On Theory and Practice of Earth Reinforcements, Kyushu, Japan, 5 - 7 October, 1988, pp. 311 - 316, 1988.

[44]Gutierrez V., Tatsuoka A.F., "*Role of Facing in Reinforcing Cohesion less Soil Slopes by Means of Metal Strips*", Proc. Int. Geotechnical Symp. on Theory and Practice of Earth Reinforcement, Kyushu, Japan, 5 - 7 October, 1988, pp. 289 - 294, 1988.

[45]Hayashi S, Ochiai H., Otani J., Umezaki I.T., Quan J.A., "*Mechanism and Design Method of Soil Reinforcement of Cut-off Slope with Steel Bars*", Proc. Int. Reinforced Soil Conf., Glasgov, pp. 201 – 205, 1990.

[46]Huang C.C., Tatsuoka F., Sato Y., "*Failure mechanisms of reinforced sand slopes loaded with a footing*", Soils and Foundations, vol. 34, no. 2, pp. 27 - 40, June 15, 1994.

[47]Kodaka T., Asaoka A., Pokharel G., "*Model tests and theoretical analysis of reinforced soil slopes with facing panels*", Soils and Foundations, vol. 35, no. 1, pp. 33 – 45, March, 1995.

[48] Kim D.S., Juran I., Nasimov R., Drabkin S., "*Model Study on the Failure Mechanism of Soil-Nailed Structure Under Surcharge Loading*", Geotechnical Testing Journal, vol. 18, no. 4, pp. 421 – 430, December, 1995.

[49] Nishida K., Nishigata T., "*Reaction on Reinforcing Force and Restrainment Effect on Soil Nailing*", Earth Reinforcement, Balkema, pp. 815 – 824, 1996.

[50] Rajagopal K., Ramesh G.V., "*Studies on the behavior of Soil Nailed Retaining Walls*", Int. Conf. on Civil Engineering, Bangalore, pp. 943 – 950, 2001.

[51] Pokharel S.K., Parsons R.L., Pierson M., Han J., Willems I., "*Use of Flexible Facing for Soil Nail Walls*" Univ. of Kansas, Civil, Environ. & Architectural Eng. Deptt., Kansas, Rep. No. K-TRAN: KU-10-6, Contract C1835, November, 2011.

[52] Jewell R.A., "*Some effects of reinforcement on the mechanical behavior of soils*", Doctoral dissertation, University of Cambridge, 1980.

[53] Tei K., Taylor N.R., Milligan G.W., "*Centrifuge model tests of nailed soil slopes*", Soils and Foundations, vol. 38, no. 2, pp. 165 - 177, Jun 15, 1998.

[54] Zhang J., Pu J., Zhang M., Qiu T., "*Model Tests by Centrifuge of Soil Nail Reinforcements*", Journal of Testing and Evaluation, vol. 29, no. 4, pp. 315-328, 2001.

[55] Hong Y.S., Chen R.H., Wu C.S., Chen J.R., "*Shaking table tests and stability analysis of steep nailed slopes*", Canadian Geotechnical Journal, vol. 42, no. 5, pp. 1264 - 1279, Oct 1, 2005.

[56] Huang C.C., Horng J.C., Charng J.J., "*Seismic stability of reinforced slopes: effects of reinforcement properties and facing rigidity*", Geosynthetics International, vol. 15, no. 2, pp. 107 - 118, April 1, 2008.

[57] Deepa V., Viswanadham B.V., "*Centrifuge model tests on soil - nailed slopes subjected to seepage*", Proc. of the Inst. of Civil Engineers - Ground Improvement, August, 2009, vol. 162, no. 3, pp. 133 – 144, 2009.

[58] Rotte V.M., Viswanadham B.V., "*Performance of 2V: 1H slopes with and without soil-nails subjected to seepage: Centrifuge study*", Geo Congress 2012: State of the Art and Practice in Geotechnical Engineering, pp. 643 – 652, 2012.

[59] Rotte V.M., Viswanadham B.V., "*Influence of nail inclination and facing material type on soil - nailed slopes*", Proc. of the Inst. of Civil Engineers - Ground Improvement, May, 2013, Vol. 166, No. 2, pp. 86 – 107, 2013.

[60] Rawat S., Zodinpuii R., Manna B., Sharma K.G., "*Investigation on failure mechanism of nailed soil slopes under surcharge loading: testing and analysis*", Geomechanics and Geoengineering, vol. 9, no. 1, pp. 18 - 35, Jan 29, 2014.

[61] Gottardi G., Simonini P., "*The viscoplastic behaviour of a geogrids reinforced model wall*", Geosynthetics International, vol. 10, pp. 34 – 46, 2003.

[62] Sanvitale N., Simonini P., Bisson A., Cola S., "*Role of the facing on the behavior of soil - nailed slopes under surcharge loading*", Proc. of the 18th Int. Conf. on Soil Mechanics and Geotech. Eng., Paris, pp. 2091- 2094, 2013.

[63] White D.J., Take W.A., Bolton M.D., "*Soil deformation measurement using particle image velocimetry (PIV) and photogrammetry*", Géotechnique, vol. 53, no. 7, pp. 619 – 631, 2003.

[64] Zhang G, Cao J., Wang L., "*Failure behavior and mechanism of slopes reinforced using soil nail wall under various loading conditions*", Soils and Foundations, vol. 54, no. 6, pp. 1175 – 1187, Dec 31, 2014.

[65] Chan C.M., Raman M.H., "*Screw - In Soil Nail for Slope Reinforcement against Slip Failure: A Lab - Based Model Study*", Int. Journal of Geomate, vol. 12, no. 29, pp. 148 – 155, Jan., 2017.

[66] Bruce D.A., Jewell R.A., "*Soil nailing: application and practice - part 1*", Ground Engineering, vol. 19, no. 8, pp. 10 - 15, Nov, 1986.

[67] Shen C.K., Herrmann L.R., Romstand K.M., Bang S., Kim Y.S., Denatale J.S., "*In situ Earth Reinforcement Lateral Support System*", Department of Civil Engineering, University of California, Davis, California, Report No. 81- 03, 1981a.

[68] Shen C.K., Bang S., Romstad J.M., Kulchin L., Denatale J.S., "*Field measurements of an earth support system*", Journal of the Geotech. Engg. Division, ASCE, vol. 107, no. GT-12, 1981b.

[69] Guilloux A., Notte G., Gonin H., "*Experiences on a Retaining Structure by Nailing in Moraine Soil*", Proc. of VIIIth ECSMFE, Helsinki, vol. 2, pp. 499 – 502, 1983.

[70] Nicholson P.J., Wycliffe – Jones P.T., "*Soil Nailing. An Earth Reinforcement System for Support of Excavation*", Int. Conf. on in - situ Soil and Rock Reinforcement, Paris, October, 1984.

[71] Long N.T., Livet J., Boutonnet M., Marchal J., Olivier G., Nabonne A., Plaut E., "*Repair of a Reinforced Earth Wall*", Int. Conf. on Case Histories in Geotechnical Engineering, pp. 335 - 339, 1984.

[72] Harmston J., Rhodes G.W., “*Soil Nailing Saves Distressed Timber Wall*”, Serviceability of Earth Retaining Structures, ASCE, pp. 130 – 136, 1994.

[73] Baker D.A., “*Soil nailing in Weathered Keuper Marl - a case history*”, Ground Engineering, vol. 27, no. 1, Jan, 1994.

[74] Cheng S.S., Hansen L.A., “*Design, construction and performance of a soil nailed wall in Puerto Rico*”, Serviceability of Earth Retaining Structures, ASCE, pp. 1 – 16, 1994.

[75] Unterreiner P., Schlosser F., Benhamida B., “*Calculation of the Displacement of a Full Scale Experimental Soil Nailed Wall – French Research Project Clouterre*”, The Practice of Soil Reinforcing in Europe, Thomas Telford, London, pp. 195 – 213, 1995.

[76] Drumm E.C., Tant C.R., Mauldon M., Berry R.M., “*Instrumentation and Monitoring of a Nailed Mine – Waste Slope*”, Earth Reinforcement, Balkema, pp. 741 – 752, 1996.

[77] Barley A.D., Maddison J.D., Jones D.B., “*The use of soil nails for the stabilization of a new cutting for the realignment of the A4059 at Lletty Turner Bends*”, Densification and Reinforcement: Proc. of the Third Int. Conf. on Ground Improvement Geosystems, Thomas Telford, London, 3 - 5 June, 1997, pp. 459 – 467, 1997.

[78] Benhamida B., Unterreiner P., Schlosser F., “*Numerical analysis of a full scale experimental soil nailed wall*”, Proc. of 3rd Int. Conf. on Ground Improvement Geosystems, London, pp. 452 – 458, 1997.

[79] Forth R.A., “*Soil nailing - a cost - effective way of improving the factor of safety of marginally stable slopes in Hong Kong*”, Densification and Reinforcement: Proc. of the Third Int. Conf. on Ground Improvement Geosystems, Thomas Telford, London, 3 - 5 June, 1997, pp. 383 – 388, 1997.

[80] Knochenmus G., Bretelle S., Schlosser F., “*TALREN Stability analysis program for the design of complex reinforced soil structures: important case histories*”, Densification and Reinforcement: Proc. of the Third Int. Conf. on Ground Improvement Geosystems, Thomas Telford, London, 3 - 5 June, 1997, pp. 390 – 397, 1997.

[81] Martin J., “*The Design and Installation of Soil Nail Slope Stabilization Schemes using Snail*”, Densification and Reinforcement: Proc. of the Third Int. Conf. on Ground

Improvement Geosystems, Thomas Telford, London, 3 - 5 June, 1997, pp. 399 – 406, 1997.

[82] Briaud J.L., Lim Y., "*Soil - nailed wall under piled bridge abutment: simulation and guidelines*", Journal of Geotechnical and Geoenvironmental Engineering, vol. 123, no. 11, pp. 1043 - 1050, Nov, 1997.

[83] Hanna S., Juran I., Levy O., Benslimane A., "*Recent developments in soil –nailing - Design and Practice*", Soil Improvement for Big Digs, Geotechnical Special Publication No. 81, ASCE, pp. 259 – 284, 1998.

[84] Khalil M., Rhodes M., Daly J., Ferris J., "*Soil Nail Walls in Residual Soils*", Soil Improvement for Big Digs, Geotechnical Special Publication No. 81, ASCE, pp. 214 - 225, 1998.

[85] Soliman N., Ro K., "*Monitoring the Performance of a Soil Nailed Wall*", Soil Improvement for Big Digs, Geotechnical Special Publication No. 81, ASCE, pp. 226 – 238, 1998.

[86] Turner J.P., Jensen W.G., "*Landslide stabilization using soil nail and mechanically stabilized earth walls: Case study*", Journal of Geotechnical and Geoenvironmental Engineering, vol. 131, no. 2, pp. 141- 150, Feb, 2005.

[87] Oral T., Sheahan T.C., "*The use of soil nails in soft clays*", Design and Construction of Earth Retaining Systems, Geotechnical Special Publication No. 83, ASCE, Reston, Va, pp. 26 – 40, 1998.

[88] His J., Taylor B., "*Application of Soil Nails in Urban Infrastructure Development*", Australian Geomechanics: Journal and News of the Australian Geomechanics Society, vol. 37, no. 3, pp. 61 – 80, June, 2002.

[89] Ann T.S., Cheang W., Hai, Tan D., "*Finite element analysis of a soil nailed slope - some recent experience*", In 3rd Asian Regional Conf. on Geosynthetics: Now and Future of Geosynthetics in Civil Engineering, Seoul, Korea, June, 2004, pp. 183 – 192, 2004.

[90] Sayão A.S., Lima A.P., Springer F.O., Nunes A.L., Dias P.H., Gerscovich D.M., "*Design and instrumentation aspects of a 40m high nailed slope*", Proc. of the Int. Conf. on Soil Mechanics and Geotech. Engg, Aa Balkema, vol. 16, no. 3, pp. 1409 – 1413, 2005.

[91] Turner J.P., Jensen W.G., "*Landslide stabilization using soil nail and mechanically stabilized earth walls: Case study*", Journal of Geotechnical and Geoenvironmental Engineering, vol. 131, no. 2, pp. 141 – 150, Feb, 2005.

[92] Liew S.S., Liong C.H., "*Two Case Studies on Soil Nailed Slope Failures*", Int. Conf. on Slopes, Malaysia, pp. 1 – 10, 2006.

[93] Durgunoglu H.T., Keskin H.B., Kulac H.F., Ikiz S., Karadayilar T., "*Performance of soil nailed walls based on case studies*", Proc. of the XIV European Conf. on Soil Mechanics and Geotech. Engg, Madrid, Spain 2007, pp. 559 – 564, 2007.

[94] Menkiti C.O., Long M., "*Performance of soil nails in Dublin glacial till*", Canadian Geotechnical Journal, vol. 45, no. 12, pp. 1685 - 1698, 9 Dec, 2008.

[95] Long M., Menkiti C.O., "*Geotechnical properties of Dublin boulder clay*", Géotechnique, vol. 57**,** no. 7, pp. 595 – 611, 2007.

[96] Skipper J., Follett B., Menkiti C.O., Long M., Clarke – Hughes J., "*The engineering geology and characterisation of Dublin Boulder Clay*", Quarterly Journal of Engineering Geology and Hydrogeology (QJEGH), vol. 38, pp. 171 – 187, 2005.

[97] Zolqadr E., Yasrobi S.S., Norouz Olyaei M., "*Analysis of soil nail walls performance- Case study*", Geomechanics and Geoengineering, vol. 11, no. 1, pp. 1 – 2, 2 Jan, 2016.

[98] Rabejac S., Toudic P., "*Construction of a retaining wall between Versailles-Chantiers and Versailles - Matelots*", Revue générale des chemins de fer, French railway review no. 93, pp. 232 – 237, 1974.

[99] Cartier G., and Gigan J.P., "*Experiments and observations on soil nailing structures*", Proc. of the Eight European Conf. on Soil Mechanics and Foundation Engineering, Helsinki, May, 1983, vol. 2, pp. 473 – 476, 1983.

[100] Ingold T.S., "*An application of ballistic soil nailing*", Proc. of the Symp. on the practice of soil reinforcing in Europe, Tenax Group, International Geosynthetics Society, Institution of Civil Engineers, Thomas Telford, 18 May, 1995, pp. 302 – 309, 1995.

[101] Ingold T.S., Miles B., "*Ballistic Soil Nailing*", Proc. of the Int. Symp. on Earth Reinforcement, pp. 765 – 770, 1996.

[102] Hall G.J., "*The joint use of ballistic soil nailing and reinforced soil in Huddersfield*", Proc. of the Symp. on the practice of soil reinforcing in Europe, Tenax Group,

International Geosynthetics Society, Institution of Civil Engineers, Thomas Telford, 18 May, 1995, pp. 227 – 240, 1995.

[103]Srinivasa Murthy B.R., Sivakumar Babu G.L., Srinivas A., "*Analysis of prototype soil - nailed retaining wall*", Proc. of the Institution of Civil Engineers-Ground Improvement, vol. 6, no. 3, pp. 129 – 136, 2002.

[104]Gosavi M.S., "*Behaviour of nailed open cuts*", Ph.D. thesis, Indian Institute of Technology, Roorkee, India, 2006.

[105]Smith J., Grapel C., Proskin S., Oad S., "*Use Of Launched Soil Nails To Stabilize Shallow Slope Failure On Urban Access Road 172*", In 2009 Annual Conf. and Exhibition of the Transportation Association of Canada - Transportation in a Climate of Change, Vancouver, British Columbia, 2009.

[106]Deardorff D., Moeller M., Walt E., "*Results of an Instrumented Helical Soil Nail Wall*", Earth Retention Conference 3, pp. 262 – 269, 2010.

[107]Upsall B.M., "*A study on the pullout capacity of the spiral nail groutless soil nailing system*", Master's Thesis, University of Washington, Seattle, Wash., 161 p. 2004.

[108]Upsall B.M, Aziz E., Holtz B., "*SR900 guardrail stabilization using the spiralnail groutless soil nailing system*", Foundation Drilling, vol. 27, no. 2, pp. 36 - 43, 2006.

[109]Stephens T.J., Holtz R.D., Aziz E.S., "*Construction and Initial Performance of a Full - Scale Excavation Supported by Spiral nail Groutless Soil Nails*", Sound Geotechnical Research to Practice: Honoring Robert D. Holtz II, pp. 525 – 538, 2013.

[110]Cheng Y.M., Au S.K., Yeung A.T., "*Laboratory and field evaluation of several types of soil nails for different geological conditions*", Canadian Geotechnical Journal, vol. 53, no. 4, pp. 634 – 645, Oct 15, 2015.

[111]Cheng Y.M., Wei W.B., "*Application of Innovative GFRP Pipe Soil Nail System in Hong Kong*", Key Engineering Materials, vol. 353 - 358, pp. 3006 – 3009, 2007.

[112]Cheng Y.M., Choi Y.K., Yeung A.T., Tham L.G., Au A.S., Wei W.B., Chen J., "*New soil nail material - Pilot study of grouted GFRP pipe nails in Korea and Hong Kong*", Journal of Materials in Civil Engineering, vol. 21, no. 3, pp. 93 - 102, March 21, 2009.

[113]Lindsay F.M., Mickovski S.B., Smith M.J., "*Testing of self - drilled hollow bar soil nails*", Proc. of the XVI European Conf. on Soil Mechanics and Geotech. Engg: Geotech. Engg. for Infrastructure and Development, pp. 2969 – 2974, 2015.

[114]Dywidag Systems International, "*DYWI Drill Hollow Bar brochure*", 2008.

[115]Dai Z.H., Guo W.D., Zheng G.X., Ou Y., Chen Y.J., "*Moso Bamboo Soil -Nailed Wall and Its 3D Nonlinear Numerical Analysis*", Int. J. of Geomechanics, vol. 16, no. 5, pp. 04016012(1-14), Feb 3, 2016.

[116]Juran I., "*Reinforced Soil Systems - Application in Retaining Structures*", Geotechnical Engineering, vol. 16, pp. 39 - 82, 1985.

[117]Bridle R.J., Davies M.C.R., "*Analysis of Soil Nailing Using Tension and Shear: Experiment Observations and Assessment*", Proc. Inst. Civil Engg. and Geotech. Engg, vol. 125, no. 3, pp.155 – 167, 1997.

[118]GEO. Geoguide 7, "*Guide to Soil Nail Design and Construction*", Geotechnical Engineering Office, Civil Engineering and Development Department, The Government of Hong Kong, Special Administrative Region, ISBN: 978-962-02-0375-6, GEO REPORT No. 197, 2008.

[119]Ingold T., "*Some observations on the Laboratory Measurement of Soil - Geotextile Bond*", Geotechnical Testing Journal, vol. 5, no. 3/4, pp. 57- 67, 1982.

[120]Pedley M.J., "*The Performance of Soil Reinforcement in Bending and Shear*", Ph.D. thesis, University of Oxford, 1990.

[121]Tei K., "*A study of soil nailing in sand*", Ph. D. thesis, Magdalen College, University of Oxford, 1993.

[122]Milligan G.W.E, Tei K., "*The Pull - out Resistance of Model Soil Nails*", Soils and Foundations, vol. 38, no. 2, pp. 179 - 190, 1998.

[123]Chu L.M., Yin J.H., "*Comparison of interface shear strength of soil nails measured by both direct shear box tests and pullout tests*", J. of Geotech. and Geoenv. Engg., vol. 131, no. 9, pp. 1097 – 107, Sept, 2005.

[124]Schlosser F., Guilloux A., "*Le frottement dans les sols*", Rev. Francaise Geotechnique, vol. 16, pp. 65 – 77, 1981.

[125]Morris J.D., "Physical and numerical modeling of grouted nails in clay." Ph.D. thesis, University of Oxford, 1999.

[126]Chang K.T., Milligan G.W., "*Effects of the transition zone in a nailed wall model test*", Earth reinforcement, Balkema, University of Oxford, UK, pp. 333 – 338, 1996.

[127]Milligan G.W., Chang K.T., Morris J.D., "*Pull - out resistance of soil nails in sand and clay*", Ground Improvement Geosystems: Densification and Reinforcement,

Proc. of the third Int. Conf. on Ground Improvement Geosystems, London, June 1997, pp. 3 – 5, 1997.

[128]Franzén G., "*Soil Nailing. A Laboratory and Field Study of Pullout Capacity*", Ph.D. Dissertation, Chalmers University of Technology, Goteberg, Sweden, 1998.

[129]Wang Z., Richwien W., "*A study of soil - reinforcement interface friction*", J. of Geotech. and Geoenv. Engg., vol. 128, no. 1, pp, 92 – 94, January, 2002.

[130]Hong Y.S., Wu C.S., Yang S.H., "*Pullout resistance of single and double nails in a model sandbox*", Canadian Geotech. J., vol. 40, no. 5, pp. 1039 – 1047, Oct 1, 2003.

[131]Hong Y.S., Chen R.S., "*Nonlinear analysis of model nail for pullout behaviour*", Proc. of the Conf. on Computer Applications in Civil and Hydraulic Engg., Taichung, Taiwan, Republic of China, 17 – 18 Feb, 2000, pp. 629 – 637, 2000.

[132]Junaideen S.M., Tham L.G., Law K.T., Lee C.F., Yue Z.Q., "*Laboratory study of soil nail interaction in loose, completely decomposed granite*", Canadian Geotech. J., vol. 41, no. 2, pp. 274 – 286, April 1, 2004.

[133]Hsu S.T., Liao H.J., "*Uplift behaviour of cylindrical anchors in sand*", Canadian Geotech. J., vol. 35, pp. 70 – 80, 1998.

[134]Chai X.J., Hayashi S., "*Effect of constrained dilatancy on pull-out resistance of nails in sandy clay*", Proc. of the Institution of Civil Engineers - Ground Improvement, July 1, 2005, vol. 9, no. 3, pp. 127 – 135, 2005.

[135]Pradhan B., Tham L.G., Yue Z.Q., Junaideen S.M., Lee C.F., "*Soil – nail pullout interaction in loose fill materials*", Int. J. of Geomechanics, vol. 6, no. 4, pp. 238 – 247, July, 2006.

[136]Heymann G., Rohde A.W., Schwartz K., Friedlaender E., "*Soil nail pullout resistance in residual soils*", Proc. of the Int. Symp. on Earth Reinforcement Practice, Kyushu, Japan, Nov 11, 1992, Vol. 1, pp. 487 – 492, 1992.

[137]Feijo R.L., Erhlich M., "*Nail pullout tests in residual soils in Rio De Janeiro – Brazil*", Proc., Soil - Rock America, pp. 2133 – 2138, 2003.

[138]Li J., "*Field study of soil nailed loose fill slope*", Ph.D. thesis, Univ. of Hong Kong, Hong Kong, 2003.

[139]Tan S.A., Ooi P.H., "*An Experiment study on rapid pullout test of soil nail in sand*", Ground Modification and Seismic Mitigation, pp. 199 – 206, 2006.

[140]Tan S.A., Ooi P.H., Park T.S., Cheang W.L., "*Rapid pullout test of soil nail*", J. of Geotech. and Geoenv. Engg., vol. 134, no. 9, pp. 1327 - 1338, Sept, 2008.

[141]Yin J.H., Su L.J., "*An innovative laboratory box for testing nail pull-out resistance in soil*", Geotech. Testing J., vol. 29, no. 6, pp. 1 – 11, 2006.

[142]Su L.J., Yin J.H., Zhou W.H., "*Influences of overburden pressure and soil dilation on soil nail pull-out resistance*", Computers and Geotechnics, vol. 37, no. 4, pp. 555 – 564, Jun 30, 2010.

[143]Gosavi M., Saran S., Mittal S., "*Evaluation of Apparent Co-efficient of Friction between Soil and Nails*", Proc. of the 12th Int. Conf. of the Int. Assoc. for Computer Methods and Advances in Geomechanics (IACMAG), Goa, Oct 1, 2008, pp. 1346 - 1354, 2008.

[144]Zhou W., "*Experimental and theoretical study on pullout resistance of grouted soil nails*", Doctoral dissertation, The Hong Kong Polytechnic University, 2008.

[145]Su L.J., "*Laboratory Pull-Out Testing Study on Soil Nails in Compacted Completely Decomposed Granite Fill*", Ph.D. Thesis, The Hong Kong Polytechnic University, 2006.

[146]Su L.J., Chan T.C.F., Shiu Y.K., Cheung T., Yin J.H., "*Influence of Degree of Saturation on Soil Nail Pull-Out Resistance in Compacted Completely Decomposed Granite Fill*", Canadian Geotech. J., vol. 44, no. 11, pp. 1314 – 1428, 2007.

[147]Yin J.H., Zhou W.H., "*Influence of grouting pressure and overburden stress on the interface resistance of a soil nail*", J. of Geotech. and Geoenv. Engg., vol. 135, no. 9, pp. 1198 - 1208, Aug 14, 2009.

[148]Akiş E., "*The Effect of Group Behavior on the Pull - Out Capacity of Soil Nails in High Plastic Clay*", Doctoral Dissertation, Middle East Technical University, 2009.

[149]Phear A., Dew C., Ozsoy B., Wharmby N.J., Judge J., Barley A.D., "*Soil nailing - best practice guidance*", no. C637, 2005.

[150] Seo H.J., Jeong K.H., Choi H., Lee I.M., "*Pullout resistance increase of soil nailing induced by pressurized grouting*", J. of Geotech. and Geoenv. Engg., vol. 138, no. 5, pp. 604 – 613, Aug 25, 2011.

[151]Hong C.Y., Yin J.H., Pei H.F., Zhou W.H., "*Experimental study on the pullout resistance of pressure - grouted soil nails in the field*", Canadian Geotech. J., vol. 50, no. 7, pp. 693 – 704, May 3, 2013.

[152]Bonaparte R., Schmertmann G.R., "*Reinforcement extensibility in reinforced soil wall design*", The application of polymeric reinforcement in soil retaining structures, Springer Netherlands, pp. 409 – 457, 1988.

[153]Wright S.G., Duncan J.M., "*Limit equilibrium stability analyses for reinforced slopes*", Transportation Research Record No. 1330, 1991.

[154]Huang C., Tatsuoka F., "*Stability analysis for footings on reinforced sand slopes*", Soils and Foundations, vol. 34, no. 3, pp. 21 – 37, Sept 15, 1994.

[155]Liang R.Y., Feng F.X., Vitton S.J., Lee S., "*Displacement - based stability analysis for anchor reinforced slope*", Soils and foundations, vol. 38, no. 3, pp. 27 - 39, Sept 15, 1998.

[156]Bang S.C., Chung Y.I., "*The effect of the nail skew angle of soil nailing wall*", KSCE J. of Civil Engg., vol. 3, no. 1, pp. 73 - 79, Mar 13, 1999.

[157]Luo S.Q., Tan S.A., Yong K.Y., "*Pull – out resistance mechanism of a soil nail reinforcement in dilative soils*", Soils and Foundations, vol. 40, no. 1, pp. 47 – 56, Feb 15, 2000.

[158]Bennis M., De Buhan P.A., "*A multiphase constitutive model of reinforced soils accounting for soil - inclusion interaction behaviour*", Mathematical and computer modelling, vol. 37, no. 5 – 6, pp. 469 – 475, Mar 1, 2003.

[159]Patra C.R., Basudhar P.K., "*Optimum design of nailed soil slopes*", Geotech. and Geological Engg., vol. 23, no. 3, pp. 273 – 296, Jun 1, 2005.

[160]Gosavi M., Saran S., Mittal S., "*Pseudo - Static Analysis of Soil Nailed Excavations*", Geotech. and Geological Engg., vol. 27, no. 4, pp. 571 - 583, Aug 1, 2009.

[161]Yin J.H., Hong C.Y., Zhou W.H., "*Simplified analytical method for calculating the maximum shear stress of nail-soil interface*", Int. J. of Geomechanics, vol. 12, no. 3, pp. 309 - 317, Jul 2, 2011.

[162]Hong C.Y., Yin J.H., Zhou W.H., Pei H.F., "*Analytical study on progressive pullout behavior of a soil nail*", J. of Geotech. and Geoenv. Engg., vol. 138, no. 4, pp. 500 – 507, Aug 5, 2011.

[163]Gurpersaud N., Vanapalli S.K., Sivathayalan S., "*Semi - empirical method for estimation of pullout capacity of grouted soil nails in saturated and unsaturated soil environments*", J. of Geotech. and Geoenv. Engg., vol. 139, no. 11, pp. 1934 - 1943, Jan 4, 2013.

[164]Zhang C.C., Xu Q., Zhu H.H., "*Evaluations of load - deformation behavior of soil nail using hyperbolic pullout model*", Geomechanics and Engineering, vol. 6, no. 3, pp. 277 – 292, 2014.

[165]Duncan J.M., "*State of the art: limit equilibrium and finite-element analysis of slopes*", J. of Geotech. Engg., vol. 122, no. 7, pp. 577 - 596, Jul, 1996.

[166]Ugai K., Leshchinsky D.O., "*Three - dimensional limit equilibrium and finite element analyses: a comparison of results*", Soils and Foundations, vol. 35, no. 4, pp. 1 - 7, Dec 15, 1995.

[167]Smith I.M., Su N., "*Three-dimensional FE analysis of a nailed soil wall curved in plan*", Int. J. for Numerical and Analytical Methods in Geomechanics, vol. 21, no. 9, pp. 583 - 597. Sep 1, 1997.

[168]Ng C.W., Lee G.T., "*A three - dimensional parametric study of the use of soil nails for stabilizing tunnel faces*", Computers and Geotechnics, vol. 29, no. 8, pp. 673 - 697, Dec 31, 2002.

[169]Xue L.K., "*Numerical modeling of anchor – soil interaction*", Doctoral dissertation, National University of Singapore, 2003.

[170]Eng L.C., "*Finite element study of 2D equivalence to 3D analysis of a discrete soil nail problem with applications to serviceability design*", Doctoral dissertation, National University of Singapore, 2003.

[171]Shaw-Shong L., "*Slope failures in tropical residual soils*", In Tropical Residual Soils Engg., Taylor & Francis, pp. 73 - 101, Jun 15, 2004.

[172]Harald W., Van Aller P.E., "*Sted Version 6.5, The smart editor for Pcstabl*", 1989.

[173]Alhabshi A., "*Finite Element Based Design Procedures for MSE/Soil - Nail Hybrid Retaining Wall Systems*", Doctoral dissertation, Texas Tech University, 2006.

[174]Zhou Y., Tham L.G., Li J., To C.Y., Xu K., "*Simplified numerical analysis of the strengthening effect of soil nails in a loose fill slope*", Proc. of the 12th Int. Conf. of Int. Assoc. for Computer Methods and Advances in Geomechanics (IACMAG), Oct 1 – 6, 2008, Goa, India, 2008.

[175]Wei W., "*Three dimensional slope stability analysis and failure mechanism*", Doctoral dissertation, The Hong Kong Polytechnic University, 2008.

[176]Wei W.B., Cheng Y.M., Li L., "*Three-dimensional slope failure analysis by the strength reduction and limit equilibrium methods*", Computers and Geotechnics, vol. 36, no. 1, pp. 70 – 80, Mar 31, 2009.

[177]Fan C.C., Luo J.H., "*Numerical study on the optimum layout of soil – nailed slopes*", Computers and Geotechnics, vol. 35, no. 4, pp. 585 – 599, Jul 31, 2008.

[178]Mohamed A.A., "*Design charts for soil nailing*", Doctoral dissertation, Benha University, 2010.

[179]Zhou Y.D., Cheuk C.Y., Tham L.G., "*An embedded bond-slip model for finite element modeling of soil–nail interaction*", Computers and Geotechnics, vol. 36, no. 6, pp. 1090 – 1097, Jul 31, 2009.

[180]Zhou Y.D., Cheuk C.Y., Tham L.G., "*Numerical modeling of soil nails in loose fill slope under surcharge loading*", Computers and Geotechnics, vol. 36, no. 5, pp. 837 – 850, Jun 30, 2009.

[181]Zhou Y.D., Xu K., Tang X., Tham L.G., "*Three-dimensional modeling of spatial reinforcement of soil nails in a field slope under surcharge loads*", J. of Applied Mathematics, vol. 2013, Sep 24, 2013.

[182]Chin K.H., Trongtham N., Wolschlag C., "*Design of permanent soil nail walls using numerical modeling techniques*", Earth Retention Conference 3, pp. 748 -755, 2010.

[183]Babu G.S., Singh V.P., "*Numerical analysis of performance of soil nail walls in seismic conditions*", ISET Journal of Earthquake Technology, vol. 45, no. 1-2, pp. 31-40, Mar – Jun, 2008.

[184]Ma L., Shen S.L., Du Y.J., Sun W.J., "*A case study of the behavior of soil–nail supported deep mixed wall in the soft deposit of Shanghai*", Lowland Technol. Int., Int. Assoc. Lowland Technol. (IALT), vol. 13, no. 2, pp. 1 – 8, Dec, 2011.

[185]Zhou W.H., Yin J.H., Hong C.Y., "*Finite element modeling of pullout testing on a soil nail in a pullout box under different overburden and grouting pressures*", Canadian Geotech. J., vol. 48, no. 4, pp. 557 – 567, Apr 12, 2011.

[186]Chen L., Zeng L., "*Numerical Analysis for the Effect of Soil Nailing to the Stress and Deformation Behavior of Foundation Pit*", Electronic J. of Geotech. Engg., vol. 17, pp. 1251 – 1259, 2012.

[187]Kim Y., Lee S., Jeong S., Kim K., "*The effect of pressure-grouted soil nails on the stability of weathered soil slopes*", Computers and Geotechnics, vol. 49, pp. 253 – 263, Apr 30, 2013.

[188]Lin H., Xiong W., Cao P., "*Stability of soil nailed slope using strength reduction method*", European J. of Env. and Civil Engg., vol. 17, no. 9, pp. 872 - 885, Oct 1, 2013.

[189]Devries B., “*LRFD Pullout Resistance Factor Calibration for Soil Nails Incorporating Survival Analysis and PLAXIS 2D*”, Masters Dissertation, University of Texas at Arlington, 2013.

[190]Xue X., Yang X., Liu E., “*Application of the modified Goodman model in soil nailing*”, Int. J. of Geomechanics, vol. 13, no. 1, pp. 41- 48, Aug 27, 2011.

[191]Asoudeh A., Oh E., “*Strength parameter selection in stability analysis of residual soil nailed walls*”, Int. J. of Geomate, vol. 7, no. 13, pp. 950 – 955, Sep 1, 2014.

[192]Al-Jubair H.S., Maki A.A., “*Numerical Modeling of Grouted Soil Nails*”, Int. J. of Engg. Research & Technol. (IJERT), vol. 4, no. 5, pp. 1640 – 1648, May, 2015.

[193]Das B.M., “*Earth anchors*”, Developments in Geotechnical Engineering, vol. 50, Amsterdam, Elsevier, 1990.

[194]Perko H.A., “*Helical piles: a practical guide to design and installation*”, John Wiley & Sons, 2009.

[195]Mitsch M.P., Clemence S.P., “*The uplift capacity of helix anchors in sand*”, Uplift Behavior of Anchor Foundations in Soil, ASCE, pp. 26 - 47, Oct, 1985.

[196]Kulhawy F.H., “*Uplift behavior of shallow soil anchors - An overview*”, Uplift Behavior of Anchor Foundations in Soil, ASCE, pp. 25, 1985.

[197]Ghaly A., Hanna A., Hanna M., “*Uplift behavior of screw anchors in sand. I: dry sand*”, J. of Geotech. Engg., vol. 117, no. 5, pp. 773 - 793, Mar, 1991.

[198]Kenny M.J., Canakci H., Andrawes K.Z., “*Densification of granular soils during CFA pile augering*”, Ground improvement geosystems: densification and reinforcement, Davies & Schlosser (eds.), Thomas Telford, London, pp. 134 - 140, Apr 10, 1997.

[199]Mooney J.S., Adamczak S., Clemence S.P., “*Uplift capacity of helical anchors in clay and silt*”, Uplift Behavior of Anchor Foundations in Soil, ASCE, pp. 48 – 72, 1985.

[200]Prasad V.Y., Rao S.N., “*Lateral capacity of helical piles in clays*”, J. of Geotech. Engg., vol. 122, no. 11, pp. 938 - 941, Nov, 1996.

[201]Ghaly A.M., “*Load-displacement prediction for horizontally loaded vertical plates*”, J. of Geotech. and Geoenv. Engg., vol. 123, no. 1, pp. 74 - 76, Jan, 1997.

[202]Merifield R.S., Sloan S.W., “*The ultimate pullout capacity of anchors in frictional soils*”, Canadian Geotech. J., vol. 43, no. 8, pp. 852 - 868, Aug 1, 2006.

[203]Merifield R.S., “*Ultimate uplift capacity of multiplate helical type anchors in clay*”, J. of Geotech. and Geoenv. Engg., vol. 137, no. 7, pp. 704 - 716, Nov 4, 2010.

[204]Livneh B., El Naggar M.H., “*Axial testing and numerical modeling of square shaft helical piles under compressive and tensile loading*”, Canadian Geotech. J., vol. 45, no. 8, pp. 1142 – 1155, Jul 31, 2008.

[205]Tappenden K., Sego D., Robertson P., “*Load Transfer Behavior of Full - Scale Instrumented Screw Anchors*”, Contemporary Topics in Deep Foundations, pp. 472 – 479, 2009.

[206]Lutenneger A.J., “*Behavior of multi - helix screw anchors in sand*”, Proc. of the 14th Pan - American Conf. on Soil Mechanics and Geotech. Engg., Toronto, Ont. [CD ROM], 2011.

[207]Sakr M., “*Installation and performance characteristics of high capacity helical piles in cohesionless soils*”, J. of the Deep Foundations Institute, vol. 5, no. 1, pp. 39 – 57, Jun 1, 2011.

[208]Papadopoulou K., Saroglou H., Papadopoulos V., “*Finite element analyses and experimental investigation of helical micropiles*”, Geotech. and Geol. Engg., vol. 32, no. 4, pp. 949 - 963, Aug 1, 2014.

[209]Knappett J.A., Brown M.J., Brennan A.J., Hamilton L., “*Optimising the compressive behaviour of screw piles in sand for marine renewable energy applications*”, Int. Conf. on Piling & Deep Foundations, Stockholm, Sweden, 21st - 23rd May, 2014.

[210]Demir A., Ok B., “*Uplift response of multi-plate helical anchors in cohesive soil*”, Geomechanics and Engineering, vol. 8, no. 4, pp. 615 - 630, Apr 1, 2015.

[211]Spagnoli G., Gavin K., “*Helical piles as a novel foundation system for offshore piled facilities*”, Abu Dhabi Int. Petroleum Exhibition and Conf., Society of Petroleum Engineers, Nov 9, 2015.

[212]Bagheri F., El Naggar M.H., “*Effects of installation disturbance on behaviour of multi-helix piles in structured clays*”, J. of the Deep Foundations Institute, vol. 9, no. 2, pp. 80 - 91, 2015.

[213]Hoyt R.M., Clemence S.P., “*Uplift capacity of helical anchors in soil*”, Proc. of the 12th Int. Conf. on Soil Mechanics and Foundation Engg., Rio de Janeiro, Brazil, Aug 13, 1989, vol. 2, pp. 1019 – 1022, 1989.

[214]Tokhi H.A., “*A study of new screw soil nail*”, Doctoral dissertation, RMIT University, Melbourne, 2016.

[215]Babu G.S., "*Case studies in soil nailing*", Proc. of Indian Geotech. Conf., Geotide, Guntur, India, pp. 582 – 585, 2009.

[216]IS: 2720, "*Determination of Grain Size Distribution by Seiving*", Part IV, 1985.

[217]IS: 2720, "*Determination of Specific Gravity – fine, medium and coarse grained soils*", Section – 2, Part III, 1992.

[218]IS: 2720, "*Determination of Water content – dry density relation using light compaction*", Part VII, 1992.

[219]Plumelle C., Schlosser F., "*A French National Research Project on Soil Nailing: CLOUTERRE",* Performance of Reinforced Soil Structures: Proc. of Int. Reinforced Soil Conf., Glassgow, pp. 219-223, 1990.

[220]Byrne R.J., Cotton D., Porterfield J., Wolschlag C., Ueblacker G., "*Manual for design and construction monitoring of soil nail walls*", No. FHWA-SA-96-069, 1996.

[221]SLOPE/W, "*A software package for slope stability analysis*", Ver. 5. GEO-SLOPE International, Calgary, Alta, 2001.

[222]Spencer E., "*A method of analysis of the stability of embankments assuming parallel inter-slice forces*", Geotechnique, vol. 17, No. 1, pp. 11-26, 1967.

[223]Morgenstern, N.R. and Price, V.E., "*The analysis of the stability of general slip surfaces*", Geotechnique, vol. 15, no. 1, pp. 79-93, 1965.

[224]Griffiths D.V., Lane P.A., "Slope stability analysis by finite elements", Geotechnique, vol. 49, no. 3, pp. 387-403, 1999.

[225]Brinkgreve R.B.J., Engin, E., Swolfs, W.M., "Plaxis 2D 2012 Manual." Plaxis bv, The Netherlands, 2012.

[226]Griffiths D.V., Smith I.M., Molenkamp F., "*Computer implementation of a double-hardening model for sand"*, Proc. IUTAM conf. on deformation and failure of granular materials, Delft, pp. 213-221, 1982.

[227]Fawaz A., Farah E., Hagechehade F., *"Slope stability analysis using numerical modelling"*, American Journal of Civil Engineering, vol. 2, no. 3, pp. 60-67, 2014.

[228]Shiu Y.K., Chang G.W.K., "*Effects of inclination, length pattern and bending stiffness of soil nails on behavior of nailed structures*", GEO Report No.197, Geotechnical Engineering Office, Hong Kong, 2006.

[229]Babu G.S., Singh V.P., "*Simulation of soil nail structures using PLAXIS 2D*", Plaxis Bulletin, Spring Issue No. 25, pp. 16-21, 2009.

[230] Ann T., Hai O. and Lum C., 2004, "*Simulation of soil nail's dynamic pullout response*", Plaxis Bulletin Issue, no. 15, pp. 10-12, 2004.

[231] Salhi L., Nait-Rabah O., Deyrat C., Roos C., "*Numerical Modelling of Single Helical Pile Behaviour under Compressive Loading in Sand*", Electronic Journal of Geotechnical Engineering, vol. 18, pp. 4319-4338, 2013.

[232] ASTM, "Annual Book of ASTM Standards", American Society for Testing and Materials, Pennsylvania, 2002.

[233] Hong C.Y., Yin J.H., Pei H.F., "*Comparative study on pullout behaviour of pressure grouted soil nails from field and laboratory tests*", Journal of Central South University, vol. 20, no. 8, pp. 2285– 2292, 2013.

[234] Niroumand H., Kassim K.A., Ghafooripour A., RamliNazir H.S., "*Performance of Helical Anchors in Sand*", Electronic Journal of Geotechnical Engineering, vol. 17, pp. 2683-2702, Jan 1, 2012.

[235] Perko H.A., "*Energy method for predicting installation torque of helical foundations and anchors*", New technological and design developments in deep foundations, pp. 342-352, 2000.

[236] HKIE, "*Soil Nails in Loose Fill Slopes. A Preliminary Study - Final Report*", The Hong Kong Institution of Engineers Geotechnical Division, no. 88, 2003.

[237] Dasari G.R., Soga K., "*A guide book for soil models and soil-pipe analysis using ABAQUS*", Report submitted to Tokyo Gas, 2000.

[238] Leung C.F., Lee F.H., Yet N.S., "*The role of particle breakage in pile creep in sand*", Canadian Geotechnical Journal, vol. 33, no. 6, pp. 888-898, 1997.

[239] ABAQUS. Hibbit D., Karlsson B., Sorensen P., "*ABAQUS v6.13 User's manuals*", Dassault Systems, Simulia Corp, Providence RI, USA, 2013.

[240] Lum C.W., "*Static pullout behaviour of soil nails in residual soil*", Doctoral dissertation, National University of Singapore, 2007.

[241] Krahn J., "*Stability modelling with SLOPE/W: An engineering methodology*", The 1th Edt. Canada, May, 2004.

[242] Mittal S., Biswas A.K., (2006) "*River bank erosion control by soil nailing*", Geotechnical & Geological Engineering, vol. 24, no. 6, pp. 1821-1833, 2006.

[243] Shiu Y.K., Chang G.W.K., "*Effects of inclination, length pattern and bending stiffness of soil nails on behaviour of nailed structures*", Geotechnical Engineering Office, Civil Engineering and Development Department, 2006.

[244] Kulhawy F.H., Peterson M.S., "*Behavior of sand-concrete interfaces*", Proc., 6th Pan-Am Conf. on Soil Mechanics and Foundation Engineering, vol. 8, pp. 225–236, 1979.

[245] Lutenegger A.J., "*Cylindrical shear or plate bearing?—Uplift behavior of multi-helix screw anchors in clay*", Contemporary Issues in Deep Foundations, vol. 185, pp. 456-463, 2009.

[246] Kurian N.P., Shah S.J., "*Studies on the behaviour of screw piles by the finite element method*". Canadian Geotechnical Journal, vol. 46, no. 6, pp. 627-638, 2009.

[247] Tokhi H., Ren G., Li J., "*Laboratory study of a new screw nail and its interaction in sand*", Computers and Geotechnics, vol. 78, pp. 144-154, 2016.

[248] Rao S.N., Prasad Y.V.S.N., Shetty M.D., "*The behaviour of model screw piles in cohesive soils*", Soils and Foundations, vol. 31, no. 2, pp. 35-50, 1991.

[249] Mittal S, Mukherjee S., "*Behavior of Group of Helical Screw Anchors under Compressive Loads*", Geotechnical and Geological Engineering, vol. 33, no. 3, pp. 575-592, 2015.

[250] Rowe R. K., David, H., "*The behavior of anchor plates in sand*", Geotechnique, vol. 32, no. 1, pp. 25-41, 1982.

PUBLICATIONS

Journal Publications

[1] Rawat S., Gupta A.K., "*An Experimental and Analytical Study of Slope Stability by Soil Nailing*", Electronic Journal of Geotechnical Engineering, vol. 21, no. 17, pp. 5577-5597, 2016. **[Scopus Indexed]**

[2] Rawat S., Gupta A.K., "*Analysis of a Nailed Soil Slope Using Limit Equilibrium and Finite Element Methods*", International Journal of Geosynthetics and Ground Engineering, vol. 2, no. 4, pp. 34, 2016. **[Springer Publication]**

[3] Rawat S., Gupta A.K., "*Numerical Modelling of Pullout of Helical Soil – Nail*", Journal of Rock Mechanics and Geotechnical Engineering, vol. 9, no. 4, August 2017. **[Scopus Indexed, Elsevier Publication]**

[4] Rawat S., Gupta A.K., "*Testing and Modelling of Screw Nailed Soil Slopes*", Indian Geotechnical Journal, pp. 1-20, 2017. doi:10.1007/s40098-017-0229-7. **[Scopus Indexed, Springer Publication]**

[5] Rawat S., Gupta, A.K., Dhiman A., "*Analysis of pullout behaviour of soil nail with circular discs*", Journal of Rock Mechanics and Geotechnical Engineering, vol. 9, no. 5, Oct 2017. **[Scopus Indexed, Elsevier Publication]**

Submission Info

SUBMISSION ID	820906299
SUBMISSION DATE	01-Jun-2017 11:09
SUBMISSION COUNT	1
FILE NAME	Final_Thesis_SAURABH...
FILE SIZE	24.06M
CHARACTER COUNT	438840
WORD COUNT	88317
PAGE COUNT	309

ORIGINALITY

OVERALL	11%
INTERNET	4%
PUBLICATIONS	10%
STUDENT PAPERS	1%

GRADEMARK

LAST GRADED	N/A
COMMENTS	0
QUICKMARKS	